Repeat Sequence Fluorene-Co-Methylene Polymers and Phosphorescent Mercury Sensors

by

Robert W. Walters

B.S. Chemistry, Pennsylvania State University, 1996

M.S. Chemistry, University of Pittsburgh, 2003

Submitted to the Graduate Faculty of

Chemistry in partial fulfillment

of the requirements for the degree of

Doctor of Philosophy

University of Pittsburgh

2009

UNIVERSITY OF PITTSBURGH

Department of Chemistry

This dissertation was presented

by

Robert W. Walters

It was defended on

July 30, 2009

and approved by

Stephane Petoud, Assistant Professor, Department of Chemistry

Alex Star, Assistant Professor, Department of Chemistry

Kacey Marra, Assistant Professor, Department of Surgery and Bioengineering

Thesis Advisor: Tara Y. Meyer, Associate Professor, Chemistry

Repeat Sequence Fluorene-Co-Methylene Polymers and Phosphorescent Mercury Sensors

Robert W. Walters, PhD

University of Pittsburgh, 2009

The synthesis of liquid crystalline alternating copolymers containing exact segment lengths of fluorene and methylene units is described. The copolymers were made by first assembling the 9,9-bis-(2-ethylhexyl)-flourene oligomers with repeat units of 3-8 followed by attachment of alkyl groups with terminal olefins capable of undergoing acyclic diene metathesis (ADMET) polymerization. The photophysical and thermal properties of these polymers were studied and are described. The absorption and emission maximums as well as the liquid crystalline transition temperatures are directly related to the number of repeat fluorene and methylene units contained in each segment.

Two different mercury sensors that use long lived luminescence as the detecting signal are described. The long lived emission allows for time resolved emission spectroscopy that can eliminate background noise that is problematic in detecting very low levels of mercury in samples. Both sensors use mercury coordinating species based upon thymine groups that are capable on binding mercury ions selectively over other metal ions that may be present in mercury containing samples. The two sensors differ greatly in the mechanism for the generation of long lived luminescence. One is based on phosphorescent 2-phenylpyridine iridium complexes and the other is based upon fluorene sensitized europium complexes. The two sensors both show the ability to detect mercury ions at 10^{-6} molar levels and it is believed that the detection level should be even lower when time resolved emission spectroscopy is used. The

iridium sensor shows a quenching of phosphorescence in the presence of mercury and the europium sensor shows an increase in the long lived luminescence but a decrease in fluorescence in the presence of mercury ions.

TABLE OF CONTENTS

PREFACE ..... **XVIII**

1.0 FLUORENE-*CO*-METHYLENE POLYMERS (PFMS) **1**

1.1 INTRODUCTION **1**

1.1.1 Overview and Relationship to Previous Work **1**

1.1.2 Repeating Sequence Copolymers (RSCs) **4**

1.1.3 Organic Electronics and Devices **6**

1.1.4 Fluorene Based Polymers and Oligomers as Electroactive Materials **8**

1.1.5 Liquid Crystalline Polymers **10**

1.2 SYNTHESIS OF PFMS **11**

1.2.1 Introduction **11**

1.2.2 Naming Conventions **15**

1.2.3 Synthesis of Monofluorene Intermediates **17**

1.2.4 Synthesis of Bifluorene Intermediates **19**

1.2.5 Synthesis of s(ehF$_3$M$_x$) Segmers **20**

1.2.6 Synthesis of s(ehF$_4$M$_x$) Segmers **21**

1.2.7 Synthesis of the s(ehF$_5$M$_x$) Segmers **22**

1.2.8 Synthesis of the s(ehF$_6$M$_{18}$) Segmer **23**

1.2.9 Synthesis of s(ehF$_7$M$_{18}$) Segmer **24**

1.2.10 Synthesis of s(ehF$_8$M$_{18}$) 25

1.2.11 Synthesis of s(F$_x$M$_x$) segmers 26

1.2.12 Synthesis of p(ehF$_x$M$_y$) polymers 26

1.2.13 NMR Spectroscopy of p(ehF$_x$M$_y$) RSCs 30

1.3 PHOTOPHYSICAL PROPERTIES OF POLYMERS 35

1.3.1 Absorption Spectroscopy 35

1.3.2 Emission Spectroscopy 36

1.4 PHYSICAL PROPERITES OF POLYMERS 39

1.5 CONCLUSIONS 45

1.6 EXPERIMENTAL 46

1.6.1 UV- Vis Spectroscopy 46

1.6.2 Emission Spectroscopy 46

1.6.3 Differential Scanning Calorimetry 47

1.6.4 Polarized Optical Microscopy 47

1.6.5 Synthetic Procedures 47

1.6.5.1 Synthesis of Oligomeric Fluorene Segmers 70

1.6.5.2 Synthesis of Polymethylene-*co*-Fluorenes 78

2.0 PHOSPHORESCENT MERCURY SENSORS 88

2.1 IRIDIUM COMPLEXES FOR MERCURY SENSING 91

2.1.1 Introduction 91

2.1.2 Design of the Mercury Sensing Iridium Complex 94

2.1.3 Synthesis of Iridium Based Mercury Sensor 97

2.1.4 Structure of Ir(ppy)$_2$(uppy) 99

2.1.4.1 NMR Spectroscopy 99
2.1.5 Crystal Structure 101
2.1.6 Photophysical Properties 103
2.1.7 Mercury Ion Sensing 106
2.1.8 Conclusions 108
2.1.9 Experimental 109
2.1.9.1 Photophysical Characterization 109
2.1.9.2 X-Ray Crystallography 109
2.1.9.3 Density Functional Calculations 109
2.1.9.4 Synthetic Methods and Equipment 110
3.0 LANTHANIDE BASED MERCURY SENSORS 116
3.1 INTRODUCTION 116
3.2 FLUORENE DTPA LANTHANIDE COMPLEXES 119
3.2.1 DTPA-Fluorene Synthesis 120
3.2.2 Photophysical Properties of the DTPA Fluorene Lanthanide Complexes 122
3.3 FLUORENE THYMINE COMPLEXES AS FLUORESCENT MERCURY SENSORS 124
3.4 FLUORENE AND LANTHANIDE BASED MERCURY SENSOR 126
3.4.1 Design and Synthesis Lanthanide Based Mercury Sensor 126
3.4.2 Photophysical Properties and Mercury Sensing 131
3.5 CONCLUSIONS 136
3.5.1 Experimental 137

3.5.1.1 Photophysical Characterization 137

(a) Synthetic Methods and Equipment 137

APPENDIX A 148

APPENDIX B 162

APPENDIX C 170

APPENDIX D 175

BIBLIOGRAPHY 191

LIST OF TABLES

Table 1.1. Summary of polymers prepared in the Copenhafer series. 2

Table 1.2. Summary of polymers from the series bearing branched substituents on the fluorene units. 3

Table 1.3: The synthesis and characterization data for the p(ehF$_x$M$_y$) series of RSCs. 29

Table 1.4. The absorption and emission maxima for the p(ehF$_x$M$_{18}$) series 36

Table 1.5. The nematic to isotropic phase transition for the segmers and polymers as measured by polarized optical microscopy and DSC 43

Table 2.1. HOMO and LUMO energy values from B3LYP Density Functional Theory calculations[a] for Ir(ppy)$_2$(uppy) and Ir(ppy)$_3$ 96

Table 2.2. The iridium containing bonds lengths of Ir(ppy)$_2$(uppy), *mer*-Ir(tpy)$_3$, and *fac*-Ir(ppy)$_3$. 103

Table 3.1. The luminescence lifetimes and quantum yields of emission of the 11-Eu and 12-Eu complexes. 123

LIST OF FIGURES

Figure 1.1. General structure of polymer series started by Jim Copenhafer and finished by the author of this dissertation, Robert Walters. F_x = number of repeat fluorene units and M_y = number of repeat methylene units. 2

Figure 1.2. General structure of the RSC series with enhanced liquid crystal behavior discussed in this work. 3

Figure 1.3. Examples of common architectures and comparison with the repeating sequence architecture. 4

Figure 1.4. Structure of repeating sequence copolymers made by Tetsuka and coworkers. 5

Figure 1.5. Poly(ethylene) based copolymers with exact segment control made by Wagener and coworkers.[19-21] 6

Figure 1.6. The structures of various conjugated polymers: (a) polyaniline, (b) polythiophene, (c) polycarbazole, and (d) polyfluorene. 7

Figure 1.7. A visual representation of the alignment of mesogens in the three most common liquid crystalline phases. 11

Figure 1.8. The numbering convention for fluorene. 11

Figure 1.9. Retro synthetic reaction scheme for the formation of the poly(fluorene-*co*-methylene) polymers. 12

Figure 1.10. The trimethyl silyl protection and deprotection of aryl halides. 13

Figure 1.11. ω-Alkenyl boranes used in this work and a representative alkyl-aryl Suzuki coupling reaction. 14

Figure 1.12. Grubbs I and II catalysts and a representative ADMET polymerization. 15

Figure 1.13. Examples of fluorene units with various substitution patterns provided to illustrate the naming convention. 15

Figure 1.14. Structures of the trifluorene segmers and polymers. 16

Figure 1.15. A typical GPC chromatograph of p(ehF_4M_{18}) performed in THF at RT. 28

Figure 1.16. The ^{1}H NMR spectra of (a) Si-ehF_4-Si and (b) I-ehF_4-I. 31

Figure 1.17. The ^{1}H NMR spectrum of s(ehF_4M_{18}). 32

Figure 1.18. ^{1}H NMR spectrum of the ADMET polymerization reaction mixture for s(ehF_4M_{18}). 32

Figure 1.19. ^{1}H NMR spectrum of p(ehF_4M_{18}) after hydrogenation. 33

Figure 1.20. ^{13}C NMR spectra of (a) I-ehF_4-I, (b) s(ehF_4M_{18}), and (c) p(ehF_4M_{18}). 34

Figure 1.21. Normalized absorption spectra of the p(ehF_xM_y) series of polymers in CH_2Cl_2 (~10^{-6} M). 35

Figure 1.22. Normalized solution emission intensity spectra of p(ehF_xM_y) series of polymers in CH_2Cl_2 (~10^{-6} M). 37

Figure 1.23. (A) The normalized thin film emission spectra of the p(ehF_xM_y) series of polymers drop cast from $CHCl_3$ on glass slides. (B) An expansion of selected spectra to highlight the small change in emission maximum wavelength. 38

Figure 1.24. Representation of the self assembled nematic and hexagonal phases of hairy rod polymers (a,b) drawn end on and (c,d) side on. Figure used without permission from reference 82..... 40

Figure 1.25. Polarized optical microscopy images of the mesophase textures of (a) p(ehF_4M_{18}) and (b) p(ehF_5M_{18}). 41

Figure 1.26: DSC trace of p(ehF_3M_{18}) with a scan rate of 10 ^oC per minute. 42

Figure 1.27. The N-I phase transition temperatures for p(ehF_3M_{10}) (circle), p(50% ehF_3M_{10} : 50% ehF_3M_{10}) (square), p(10% ehF_3M_{10} : 90% ehF_3M_{10}) (triangle), and p(ehF_5M_{10}) (diamond). 44

Figure 2.1. An illustration of time resolved emission spectroscopy. The phosphorescent emission can be measured during the gate time after the delay thereby eliminating the background fluorescence. 89

Figure 2.2. Two reported iridium based mercury sensors capable of detecting mercury by coordination through the sulfur atoms.[109, 110] 91

Figure 2.3. Previously reported fluorescent based mercury sensors that utilize thymine units for mercury coordination. [95, 105] 92

Figure 2.4. The crystal structure of a 2:1 complex of 1-methylthime and mercury. (Figure reproduced without permission from reference 132). 93

Figure 2.5. A well studied phosphorescent iridium complex, $Ir(ppy)_3$, and the mercury sensing iridium complex, $Ir(ppy)_2(uppy)$, made in this work. 94

Figure 2.6. The (a) LUMO, (b) LUMO +1, and (c) HOMO surfaces of $Ir(ppy)_2(uppy)$ as calculated using B3LYP Density Functional Theory. (d) An energy level diagram illustrating the lower energy π^* level of the uppy ligand compared to the unsubstituted ppy ligand. 95

Figure 2.7. The ^{1}H NMR spectra of (A) $Ir(ppy)_2(uppy)$, (B) *fac*-$Ir(ppy)_3$, and (C) *mer*-$Ir(ppy)_3$ (reproduced without permission).[143] 100

Figure 2.8. Structure of $Ir(ppy)_2(uppy)$. (Thermal ellipsoids drawn at 90% probability) 102

Figure 2.9. Illustration of the S_1 to T_1 transition for phosphorescent iridium complexes. 104

Figure 2.10. The absorption and emission spectra of $Ir(ppy)_2(uppy)$. 104

Figure 2.11. Emission spectrum of $Ir(ppy)_2(uppy)$ at a concentration of 1 μM with varying levels of mercury acetate in 50% ethylene glycol / 50% water. 106

Figure 2.12. The relative emission intensity of $Ir(ppy)_2(uppy)$ at a concentration of 1 μM with various metal ions at a concentration of 10 μM in 50% ethylene glycol / 50% water. 107

Figure 3.2. Lanthanide based zinc sensor where Ln^{3+} = Eu or Gd made by Hanaoka et al. [194] . 118

Figure 3.3. Upper: absorption spectra of both Eu^{3+} complexes formed with the mono 11 (blue line) and terfluorene 12 (red line) ligands in DMSO, 80 μM, 298 K. Lower: normalized steady-state emission spectra of both Eu^{3+} complexes formed with the mono 11 (purple line) and terfluorene 12 (black line) ligands in DMSO, 80 μM, 298 K. Lower inset: magnification of the Eu^{3+} signal on the spectrum of the Eu^{3+} complex formed with the terfluorene ligand 12 in DMSO, 80 μM, 298 K. Figure from reference 198. 122

Figure 3.4. The quenching of the fluorescent emission form the bis thymine fluorene 15 by ~1 equivalent of $Hg(OAc)_2$ in a 1:1 methanol:water solution. 125

Figure 3.5. The structure of the bifluorene europium compound 16 capable of coordinating mercury through the thymine units. 126

Figure 3.6. Absorption spectrum of 16 with and without mercury in a 1:1 methanol / water mixture at 10^{-5} M. 132

Figure 3.7. Fluorescent emission spectra of 16 with and without mercury in a 1:1 methanol / water solution..... 133

Figure 3.8. Bong lived luminescence spectra of 16 with and without 1 equivalent of mercury in a1:1 methanol / water mixture at 10^{-5} M..... 134

Figure 3.9. Phosphorescence excitation spectrum of 16 measured at an emission wavelength of 615 nm in a 1:1 methanol / water mixture at 10^{-5} M. 135

LIST OF SCHEMES

Scheme 1.1. Synthesis of monofluorene derivatives. 17

Scheme 1.2. Synthetic route to bifluorene building blocks. 19

Scheme 1.3. Synthesis of trifluorene segmers. 20

Scheme 1.4. Synthesis of the tetrafluorene segmers. 21

Scheme 1.5. Synthesis of pentafluorene segmers. 22

Scheme 1.6. Synthesis of hexafluorene segmer. 23

Scheme 1.7. Synthesis of heptafluorene segmer. 24

Scheme 1.8. Synthesis of octafluorene segmer. 25

Scheme 1.9. ADMET polymerization of s(ehF$_x$M$_{10}$) and subsequent hydrogenation. 27

Scheme 2.1. The synthesis of the uppy ligand. 97

Scheme 2.2. Synthesis of Ir(ppy)$_2$(acac). 99

Scheme 2.3. Synthesis of Ir(ppy)$_2$(uppy). 99

Scheme 3.1. Synthesis of monofluorene DTPA ligand (X=H) and terfluorene DTPA ligand (X=2-(9,9-dihexyl)-fluorene). 120

Scheme 3.2. The synthesis of a model compound to determine its ability to detect mercury by emission quenching. 124

Scheme 3.3. Synthesis of the mono fluorene DOTA precursor. 127

Scheme 3.4. Synthesis of mono fluorene *t*-butyl DOTA coupling partner. 128

Scheme 3.5. The synthesis of the mono fluorene thymine coupling partner 23. 129

Scheme 3.6. Suzuki coupling to form bis fluorene unit 24. 129

Scheme 3.7. Deprotection of t-butyl groups and formation of final europium complex. 131

PREFACE

After ten years as an industrial chemist working on a variety of projects at PPG Industries Inc., I returned to school to obtain my PhD in chemistry. I found the differences between industrial life and academic life to be great and I developed a new perspective of science in general. I would like to thank my advisor, Tara Y. Meyer, for accepting me in her research group helping me to remember that science should not based entirely on profits but should also focus on continuous learning and understanding the fundamentals of the different areas we researched. I have enjoyed my time working in her group on a variety of projects that have help to broaden my understanding of three very different areas of chemistry. I would also like to thank Dr. Stepháne for his work on our collaborations. Ryan Staysich and Ben Norris were also very insightful group members who were always there to talk about crazy ideas and to help out a new graduate student trying to use unfamiliar instruments or in other nuances of academic research.

I thank Dr. Alexander Star, Dr. Kacey Marra, and Dr. Stepháne Petoud for serving on my dissertation committe, Dr. Geoffry Hutchinson, Dr. Nathaniel Rosi, and Dr. David Waldeck for serving on my proposal committee, and Dr. Stepháne Petoud, Dr. Toby Chapman, and Dr. Tara Meyer for serving on my MS thesis committee.

I would also like to thank my wife, Lisa, for her support of my more hectic academic life. My three children, Seth, Morgan, and Rebecca, may not have been as supportive but they

enjoyed their infrequent Saturday trips to see where Dad worked more than I did. I owe a great deal of gratitude (and many more years of service) to PPG Industries, Inc. for their financial support and the time off to complete my research at the University of Pittsburgh.

Symbols and Abbreviations

ADMET	acyclic diene metathesis
b	broad
d	doublet
DOTA	1,4,7,10-tetraazacyclododecane-*N*-*N'*-*N''*-*N'''*-tetraacetic acid
DTPA	diethylenetriaminepentaacetic acid
m	multiplet
OLED	organic light emitting diode (or device)
OFET	organic field effect transistor
POM	polarized optical microscope
ppy	2-phenylpyridine
PFM	poly(fluorene-*co*-methylene)
RSC	Repeat Sequence Copolymer
t	triplet
TBABr	tetrabutylammonium bromide
T_g	glass transition temperature
uppy	4-uracil-2-phenylpyridine

1.0 FLUORENE-*co*-METHYLENE POLYMERS (PFMs)

1.1 INTRODUCTION

1.1.1 Overview and Relationship to Previous Work

An incomplete series of fluorene-*co*-methylene repeating sequence copolymers (RSCs) with similar structures to the polymers made and discussed in this work had been made by a previous Meyer group member (James Copenhafer). My initial work on this project began with the completion of the work on this project which included the synthesis of two new polymers (Figure 1.1 and Table 1.1) to complete the series and the repeat synthesis of a previously made polymer that had a very low molecular weight. I acquired the absorption and emission spectroscopic data for these three polymers and recollected the thin film emission spectra for all the polymers in this series for publication. Finally, I determined the thermal properties by DSC (differential scanning calorimetry) for a subset of these polymers. Since this work has been previously published[1] and discussed in Copenhafer's thesis, the experimental details for synthesis of these polymers are included in the experimental section but neither the synthetic schemes nor the spectroscopic data for these polymers will be discussed in detail herein. Instead, this chapter will focus on the synthesis of a new set of fluorene-*co*-methylene RSCs that were completely synthesized and characterized by me and have not yet been reported in the literature.

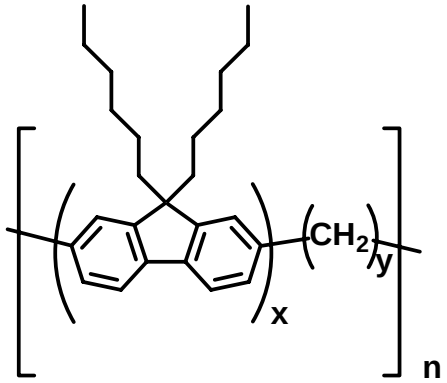

p(F_xM_y)

Figure 1.1. General structure of polymer series started by Jim Copenhafer and finished by the author of this dissertation, Robert Walters. F_x = number of repeat fluorene units and M_y = number of repeat methylene units.

Table 1.1. Summary of polymers prepared in the Copenhafer series.

Polymer[a]	Fluorene Repeat Units	Methylene Repeat Units	Synthesized By[b]
p(F_1M_{10})	1	10	J.C.
p(F_2M_{10})	2	10	J.C.
p(F_3M_{10})	3	10	J.C.
p(F_4M_{10})	4	10	R.W.
p(F_1M_{18})	1	18	J.C.
p(F_2M_{18})	2	18	J.C.
p(F_3M_{18})	3	18	J.C.
p(F_4M_{18})	4	18	J.C.
p(F_5M_{18})	5	18	R.W.
p(F_6M_{18})	6	18	R.W.
p(F_7M_{18})	7	18	J.C.
p(F_8M_{18})	8	18	J.C.

[a] F = fluorene units, M = methylene units

[b] J.C. = Jim Copenhafer; R.W. = Robert Walters.

The polymers discussed in this dissertation (Figure 1.2 and Table 1.2) differ from the Copenhafer materials in that they bear a 2-ethylhexyl substitution on the fluorene unit and as a consequence exhibit enhanced liquid crystalline properties. The enhancement of the liquid crystalline properties was important to our goal of correlating sequence with phase transition behavior. The repeating sequence structure of these polymers was characterized by NMR

spectroscopy and the photophysical properties and thermal properties of these polymers were also studied. We report herein on our findings that confirm that the photophysical properties and the transition temperatures of the liquid crystalline phases do, in fact, depend on the sequence of fluorene and methylene repeat units. The ability to control the photophysical and thermal properties of the polymers is of importance for their potential use in organic light emitting devices where control of the desired frequency of emission and stable thin film forming properties are necessary.

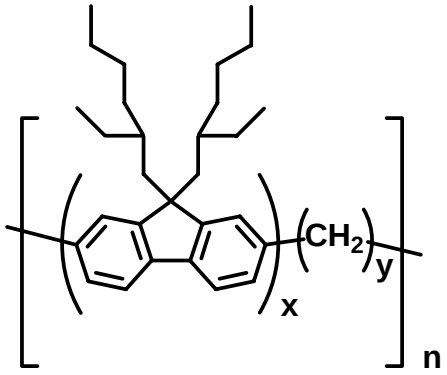

p(ehF$_x$M$_y$)

Figure 1.2. General structure of the RSC series with enhanced liquid crystal behavior discussed in this work.

Table 1.2. Summary of polymers from the series bearing branched substituents on the fluorene units.

Polymer[a]	Fluorene Repeat Units	Methylene Repeat Units
p(ehF$_3$M$_{10}$)	3	10
p(ehF$_3$M$_{18}$)	3	18
p(ehF$_4$M$_{10}$)	4	10
p(ehF$_4$M$_{18}$)	4	18
p(ehF$_5$M$_{10}$)	5	10
p(ehF$_5$M$_{18}$)	5	18
p(ehF$_6$M$_{18}$)	6	18
p(ehF$_7$M$_{18}$)	7	18
p(ehF$_8$M$_{18}$)	8	18

[a] ehF = 2-ethylhexyl fluorene; M = methylene

1.1.2 Repeating Sequence Copolymers (RSCs)

The fluorene-*co*-methylene polymers, whose preparation and characterization are discussed herein, belong to a unique architectural class of macromolecules known as repeating sequence copolymers (RSCs) (Figure 1.3). The study of copolymers with exact lengths of the repeating units is an interesting approach for the design of high performance polymers. It is hoped that by controlling the lengths and functionality between the linking groups the physical and photophysical properties of the polymers can be controlled to a greater extent than the randomly distributed polymers that are often made. For example, the fine tuning of the polymers physical properties could lead to improved performance of the polymers used in the medical and electronics fields.

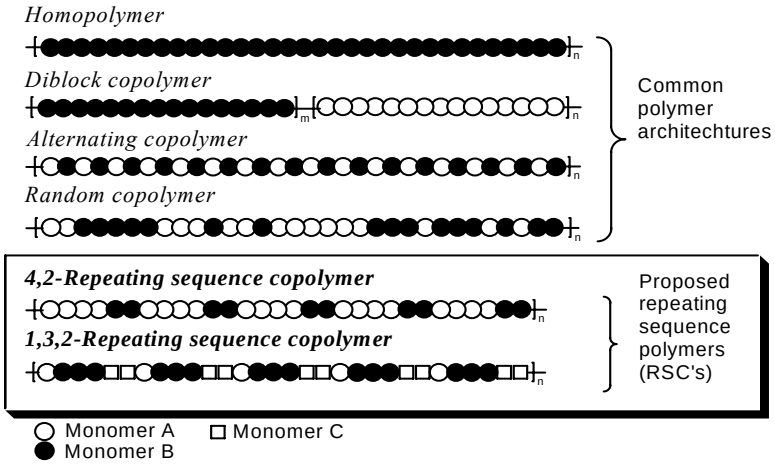

Figure 1.3. Examples of common architectures and comparison with the repeating sequence architecture.

Polyamides,[2] polyurethanes,[3] polyesters,[4, 5] etc. copolymers with exact segment lengths have properties that are dependent upon the sequence and the number of repeat units of the monomers. The hydrogen bonds that are formed between the urethane and amide linkages for example can control the melting and flow temperatures of the copolymers. Although examples

of copolymers with exact segments lengths have been demonstrated, most of the polymers with these common linkages have segments with inexact or oligomeric spacers. For example polyurethanes are typically made by reacting diisocyanates with oligomeric or polymer diols with repeating ether groups with imprecise segment lengths.[6-9]

Many main chain liquid crystalline polymers also have a repeating-sequence-like structure and the thermal properties of these polymers are often dependent upon the lengths of the spacing segment.[10] These copolymers usually contain aromatic mesogenic functionalities with alkyl, ether, or ester spacing groups. In most studies, only the segment length of the spacer group is changed and the mesogenic segment remains at a constant length. The inability to alter both of the repeating segments in these polymers limits the ability to have the control over the physical properties of the polymers that we desire in our work on RSCs.

Recently, biodegradable polymers with repeating ester groups[11] and combinations of ester and amide groups[12, 13] have been reported. The exact sequence control is of interest for controlling the degradation rates as well as the thermal and processing properties of the polymers. In particular the work by Tetsuka et al demonstrated a large number of polymers (Figure 1.4) with different numbers of methylene spacers between ester and amide linkages as well as varying number of oligoester repeat units.[12] The melting temperatures and tensile strength of the polymers were related to the spacing of the amide groups by both the methylene units and the oligoester groups.

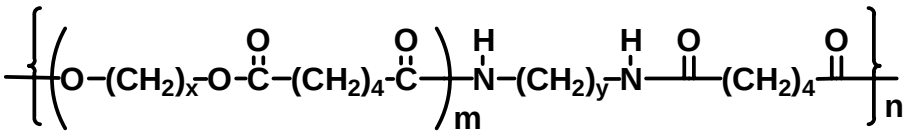

Figure 1.4. Structure of repeating sequence copolymers made by Tetsuka and coworkers.

Other studies of RSCs have shown the effect of branching[14-16] and of various substitutions[17-20] on polyethylene where the distance between substitutions is controlled (Figure 1.5). In most cases these model polymers were made to understand the relationship of random copolymers to copolymers with specific sequences. The model polymers were made by acyclic diene metathesis (ADMET) to mimic random polymers of ethylene copolymerized with halogen or alkyl substituted ethylene as well as copolymers of ethylene and acrylic acid. The thermal properties of the polymers were shown to be dependent of the exact sequence of the polymers when compared to the random copolymers.

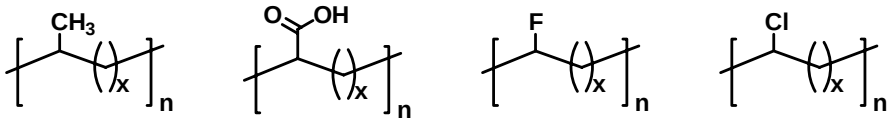

Figure 1.5. Poly(ethylene) based copolymers with exact segment control made by Wagener and coworkers.[19-21]

1.1.3 Organic Electronics and Devices

The fluorene segments in the RSCs discussed herein are of particular importance because polymers and oligomers that contain fluorene repeat units have been shown to exhibit conductive and emissive properties that make them suitable for applications in electronic devices.[22] The use of organic materials in electronic devices is an area of great focus in the fields of chemistry and materials science. The advantages of replacing traditional inorganic based materials with organic molecules, such as fluorene, include more economical manufacturing processes and the potential for improved performance. As such, organic electronic materials are being studied for use in organic field effect transistors (OFETs), organic light emitting devices (OLEDs), and solar cells.[23] The study of these materials for OLEDs is of importance because of their use as highly

efficient next generation displays and lighting applications. Organic solar cells can offer improved efficiencies of energy generation from solar radiation.[23-26]

The growing field of organic electronic materials can be traced to the original Nobel prize winning work on conducting polymers by MacDiarmid and coworkers.[27] Since their discovery of doped polyacetylenes, many conjugated polymers with conductive properties have been reported: polythiophenes,[28] polyaniline,[29] polycarbazoles,[30] and polyfluorenes[31] (Figure 1.6). Structural modification of the conductive polymers to improve the bulk packing of the conjugated groups has resulted in significant improvements in conductivities compared with the early generation polymers.

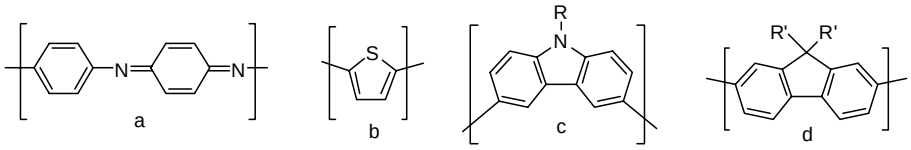

Figure 1.6. The structures of various conjugated polymers: (a) polyaniline, (b) polythiophene, (c) polycarbazole, and (d) polyfluorene.

Organic electronic materials, both polymers and small molecules, have been heavily studied due to their potential for use in next generation displays or in highly efficient lighting systems when incorporated into OLEDs.[31] The OLED structure in the simplest form contains an anode and cathode with an electroluminescent organic layer sandwiched between them. The recombination of the hole (radical cation) and the electron (radical anion) in the organic layer creates excitons or excited states that can then emit light.[32] The higher efficiency of light generation for OLEDs when compared to conventional lighting systems is appealing for obvious reasons. OLEDs high efficiencies are also of interest for hand held electronics where power consumption of the display and battery lifetimes are interrelated. Two different families of OLEDs are currently being developed. Small molecule OLEDs generally rely on the vapor

deposition of the multiple layers needed to create a high performance device. The high cost of vapor deposition makes this method less desirable than polymer OLEDs (or PLEDs) where the organic layers can be formed by ink jet printing.[33]

1.1.4 Fluorene Based Polymers and Oligomers as Electroactive Materials

The emission color of the polymer OLEDs is of one of the major factors in determining which polymers are most used. Blue, green, and red light are all necessary for the generation of a full color display or for the formation of white light. Materials such as poly(phenylenevinylene) and derivatives have been used as green emissive polymers. Polyfluorene is often doped with small molecule red emitting materials to generate the red light component by energy transfer from the wider band gap host to lower band gap emissive dopant material.[34]

The most important family of polymeric blue emitting materials is based upon polyfluorene, which is a widely studied conjugated polymer with a unique set of optical, electronic, and physical properties that make it appealing for a variety of applications including organic light emitting diodes (OLEDs) and organic field effect transistors (OFETs).[31] The polymer has a high quantum yield of blue emission necessary for full color or white OLEDs. Recent research on polyfluorene or oligofluorenes has focused on improving the emission color and efficiency[35-40] or the photo and electroluminescent stability[41-48] of the material. Additional work has focused on the liquid crystalline properties of the materials that allows for their alignment and subsequent generation of polarized blue light or improvement of conductive properties.[49] The polarization of the light is an area or interest in LCD technology where 50% of the light generated by the back plane is lost by the absorption of the cross polarized films. If

polarized OLEDs could be used as the back plane light source then the first polarized film could be removed and a theoretical increase of 50% in the efficiency of the display would be obtained.

Shorter chains of fluorenes have also proven useful because of their inherent tunability. The number of repeat units in an oligofluorene can be altered to directly control the emission color of the material.[22, 50-54] Thermal properties of these oligomers are also controlled by the number of repeat units. One limitation of these systems is the difficulty in making usable films for devices because of the potential for crystallization to occur during printing or spin casting techniques unless the oligomers have a large number of repeat units. The incorporation of the oligofluorenes into a polymer backbone separated by methylene spacing groups, such as the ones described herein, is one way to avoid film forming problems since polymers are know to be well behaved in the film forming process.

Many conjugated copolymers have been made with fluorene units and other aromatic optically active groups that alter the emissive and conductive properties of the polymer. The pure blue emission of oligofluorenes is often lost in these copolymers. The spacing of oligomeric fluorenes by optically inactive groups has been demonstrated prior to our work,[55, 56] but these examples used either ether or ester linking groups in the spacers which are potential sites of degradation in OLEDs.

In this report oligofluorene-*co*-methylene polymers with tunable emission properties and liquid crystalline phases are discussed. Previous work, initiated by James Copenhafer and continued by the author of this thesis, in the Meyer group has shown photophysical and thermal properties of oligomeric fluorenes with methylene spacers. The published initial results demonstrated that by spacing the conjugated oligofluorenes with an optically inactive and inert methylene spacer, the desirable properties of the oligofluorenes could be combined with the

desirable film forming and processing properties of the polymers.[1] The polymers did not exhibit any liquid crystalline properties and these previous results will be discussed only briefly in this report. None of the previous reports of block copolymers containing oligofluorenes as well as optically inactive spacer groups demonstrated liquid crystalline properties.[55, 56,1]

1.1.5 Liquid Crystalline Polymers

One of the properties that would be expected to respond strongly to changes in sequence in polymeric RSCs is liquid crystallinity. Many liquid crystalline main chain polymers have been studied and have been shown to have interesting thermal, physical, and optical properties.[57, 58] Main chain liquid crystals polymers have mesogenic units as part of the back bone of the polymer. These mesogenic groups can orient themselves into ordered phases that have both properties of both liquids and crystals. There are numerous phases possible for these materials and Figure 1.7 shows three of the more common phases seen. As can be seen in Figure 1.7, the nematic phase has less order than the smectic A phase since there is only orientation in one direction. Liquid crystalline polymers can have multiple phases that present themselves at different temperatures. The crystal to smectic to nematic to isotropic phases would appear as an increase in temperature causes more disorder in the system. The liquid crystalline phases can be examined by polarized optical microscopy. When the materials are in liquid crystalline phases they cause a twisting in the phase of the light. Cross polarized lenses are used and no light is passed through unless the sample causes a twist of the light. A sample in its isotropic or random phase appears dark but a nematic phase sample allows light though and gives the appearance of a distinctive texture.

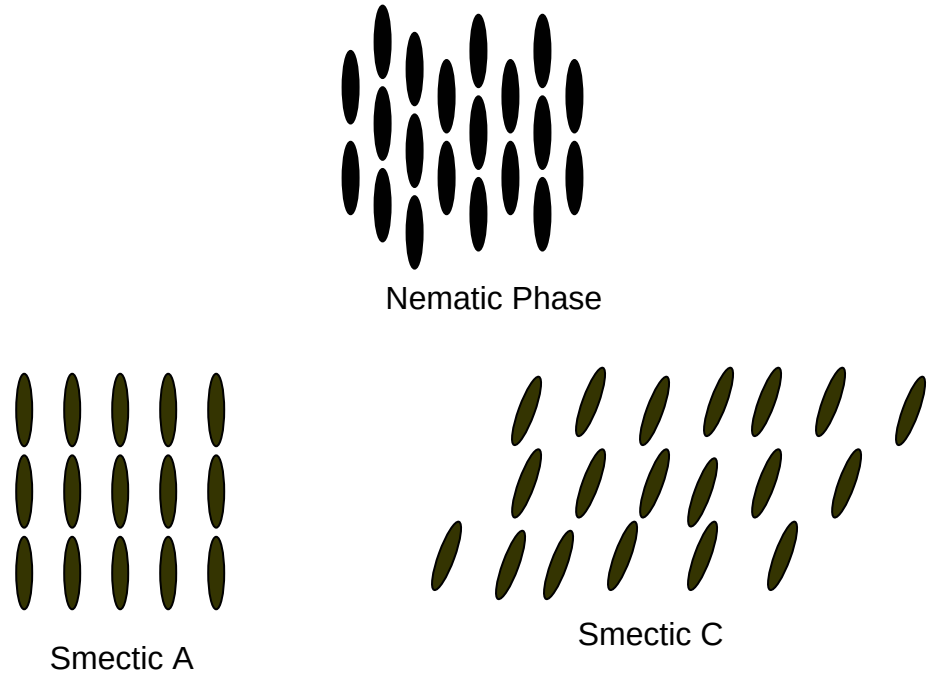

Figure 1.7. A visual representation of the alignment of mesogens in the three most common liquid crystalline phases.

1.2 SYNTHESIS OF PFMS

1.2.1 Introduction

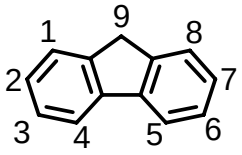

Figure 1.8. The numbering convention for fluorene.

Synthesis of fluorene-containing materials most often involves the reactions involving the 2-, 7-, and 9-positions of fluorene. Figure 1.8 illustrates the numbering scheme of fluorene. The 9-position is often substituted by deprotonation and subsequent quenching with an electrophile in a S_n2 reaction. The 2- and 7-positions are the sites where electrophilic aromatic substitutions are most likely to occur. Thus, the 9-position can be bis-substituted with a variety of alkyl groups and the 2- and 7- positions are often brominated or iodinated for further manipulation.

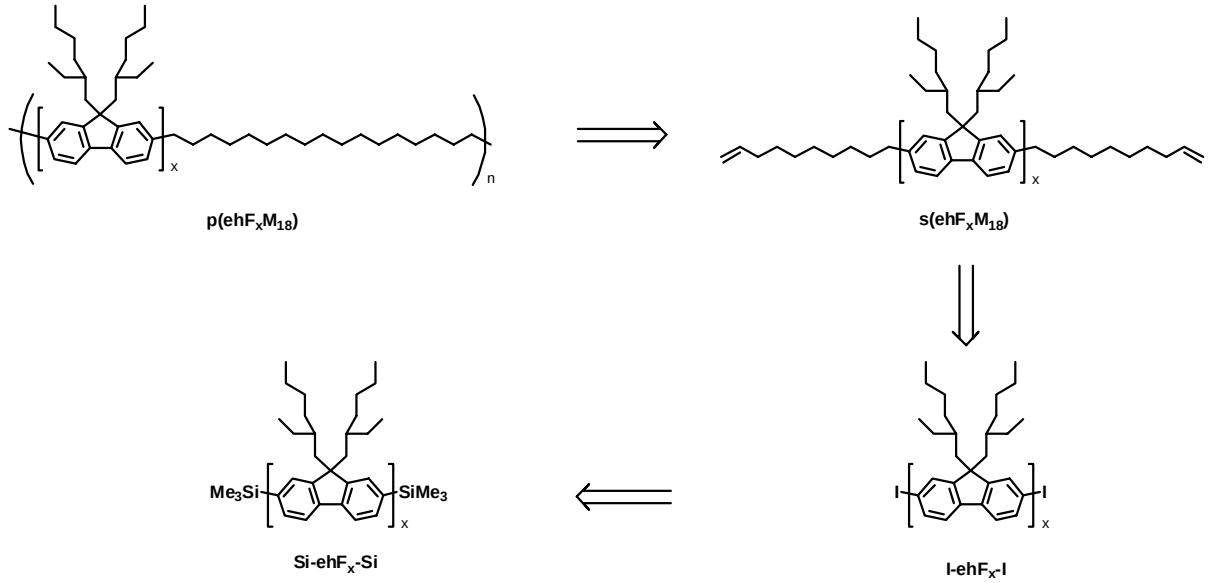

Figure 1.9. Retro synthetic reaction scheme for the formation of the poly(fluorene-*co*-methylene) polymers.

The general synthetic approach to the PFM RSCs is shown in Figure 1.9. The formation of **p(ehF$_x$M$_{18}$)** with varying fluorene repeat units and different alkyl substitutions was accomplished by ADMET polymerization of bis terminal olefin monomers **s(ehF$_x$M$_{18}$)**. The terminal olefin monomers were prepared from the bis iodo oligomers **I-ehF$_x$-I** through alkyl-aryl Suzuki couplings. Deprotection of the bis silyl groups **Si-ehF$_x$-Si** allowed for the formation of the bis iodo fluorene oligomers. The synthetic methodologies developed by Geng et al[53] were used for the synthesis of oligomeric fluorenes with either *n*-hexyl or 2-ethylhexyl alkyl side

chains at the 9-position. By incorporating a convergent/divergent methodology, many of the same synthetic intermediates were used in the synthesis of oligomers with different numbers of repeat units. The synthetic procedures also allowed for exact control over the number of repeat units in the oligomer.

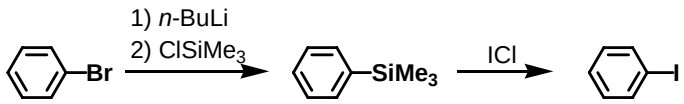

Figure 1.10. The trimethyl silyl protection and deprotection of aryl halides.

One of the most commonly used techniques in our synthetic approach used to prepare the RSC segmers is the protection and subsequent deprotection of aryl halogen groups (Figure 1.10). The use of trimethyl silyl groups as halogen protecting groups allows for the generation of the oligomers with only one challenging Suzuki coupling involving the mono substitution of 2,7-dibromofluorenes. This methodology was first developed for the synthesis of oligomeric phenylenes with precise control over the number of repeat units.[59, 60] Aryl trimethyl silyl groups were incorporated by lithium-halogen exchange and the subsequent quenching with chlorotrimethylsilane. The deprotection of the trimethyl silyl groups was accomplished with iodine monochloride to form iodo groups. The deprotection reaction is nearly quantitative which is necessary for the synthesis of higher oligomers where separation of starting materials and products is very difficult.

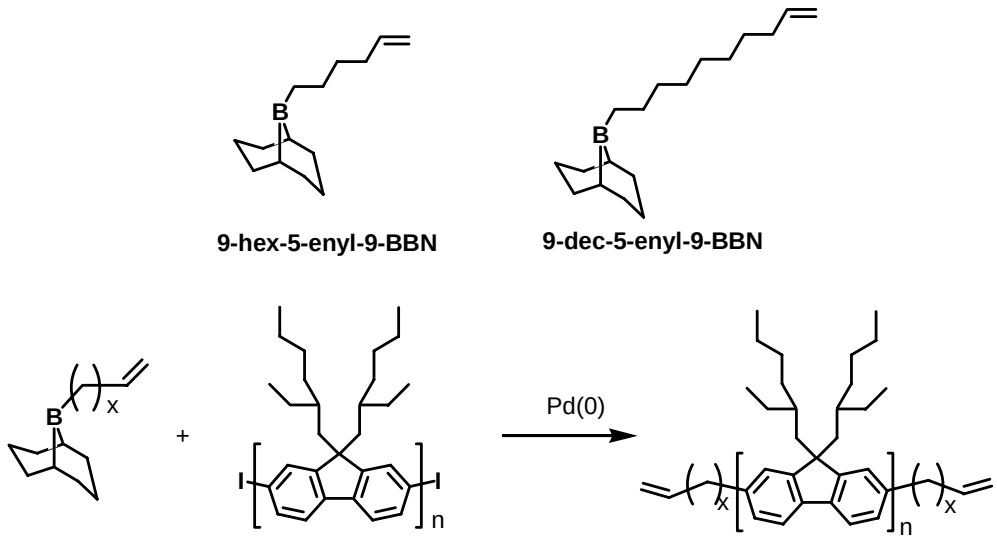

Figure 1.11. ω-Alkenyl boranes used in this work and a representative alkyl-aryl Suzuki coupling reaction.

Another important reaction in our synthetic approach is the Suzuki coupling reaction,[61] which is the methodology employed for the formation of aryl-aryl bonds and is used extensively in this reaction scheme to make exact fluorene segments. Suzuki methodology was also used for coupling of the aryl iodides with ω-alkenyl boranes to form the segmers that can then be polymerized with metathesis reactions.[62]

The key reaction in our synthetic scheme is the ADMET polymerization technique (Figure 1.12) originally developed by Wagener and coworkers using ruthenium based olefin metathesis catalysts.[63-66] The ADMET polymerization reaction is capable of making polymers with exact sequence control. The loss of ethylene, which is the only byproduct in the reaction, shortens the methylene chain by two carbon atoms relative to the starting material. Since the purification of the polymers is important for OLEDs, where impurities have been shown to be a cause of degradation, the lack of other by-products is a significant advantage.[67] ADMET is also attractive because Wagener has also shown that the disubstituted olefin formed in the ADMET

reaction can be hydrogenated by the same ruthenium catalyst when silica gel and hydrogen gas is added to the reaction.[66]

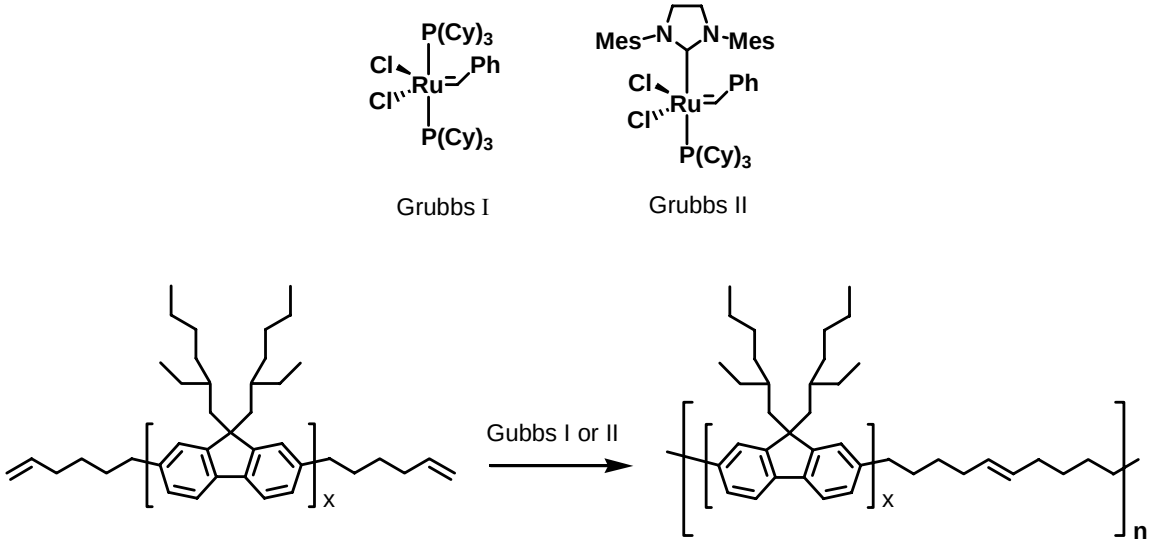

Figure 1.12. Grubbs I and II catalysts and a representative ADMET polymerization.

1.2.2 Naming Conventions

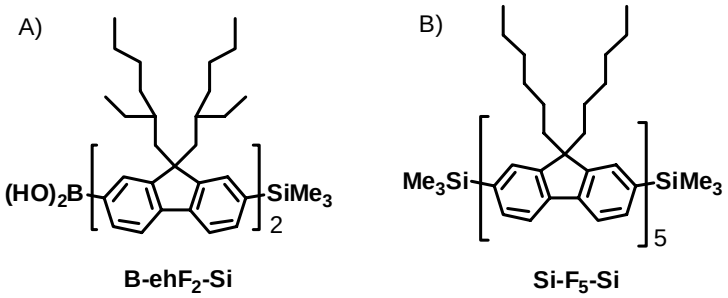

Figure 1.13. Examples of fluorene units with various substitution patterns provided to illustrate the naming convention**.**

Descriptive abbreviations for the intermediates and final polymer products will be used through the remainder of this chapter due to the complexity of the IUPAC names of such materials. Synthetic intermediates will be designated by the functional end groups as well as the alkyl substitution on the 9-position and the number fluorene units. For example the name **B-ehF$_2$-Si,** shown in Figure 1.13A**,** indicates a bifluorene unit with the 9-position being substituted with bis 2-ethylhexyl groups. The **B** indicates one end has a boronic acid functionality and the **Si** represents a trimethyl silyl group on the other end of the fluorene unit. The other end groups used in this work are **Br** for bromine and **I** for iodine. Fluorene units with *n*-hexyl substitutions at the 9-position are represented as a simple **F**. For example, **Si-F$_5$-Si** is the abbreviation for the material shown in Figure 1.13B.

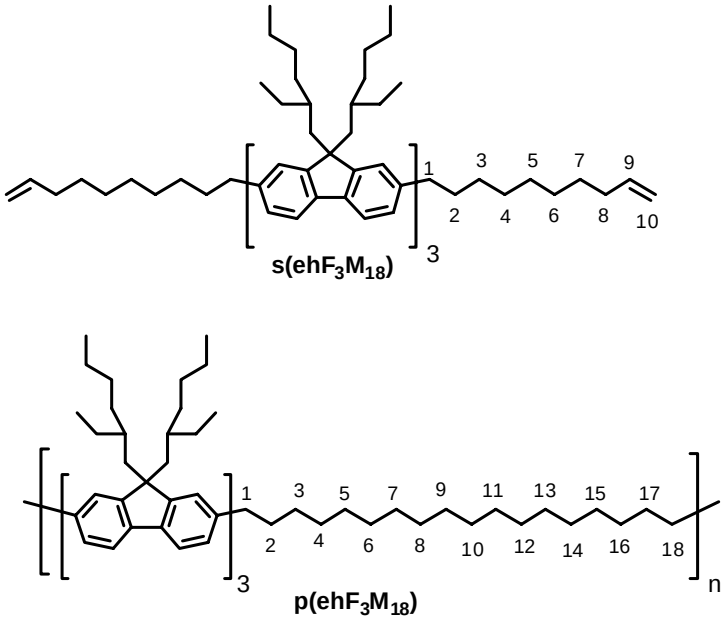

Figure 1.14. Structures of the trifluorene segmers and polymers.

Segmers and polymers are represented by a slightly different nomenclature (Figure 1.14). For example **s(ehF$_3$M$_{18}$)** represents a segmer with 3 fluorene repeat units and two 10-carbon terminal alkene arms. This segmer would then be used to make the polymer **p(ehF$_3$M$_{18}$)** via ADMET polymerization. One carbon from each terminal olefin arm is lost during ADMET creating an 18-methylene chain designated as **M$_{18}$**.

1.2.3 Synthesis of Monofluorene Intermediates

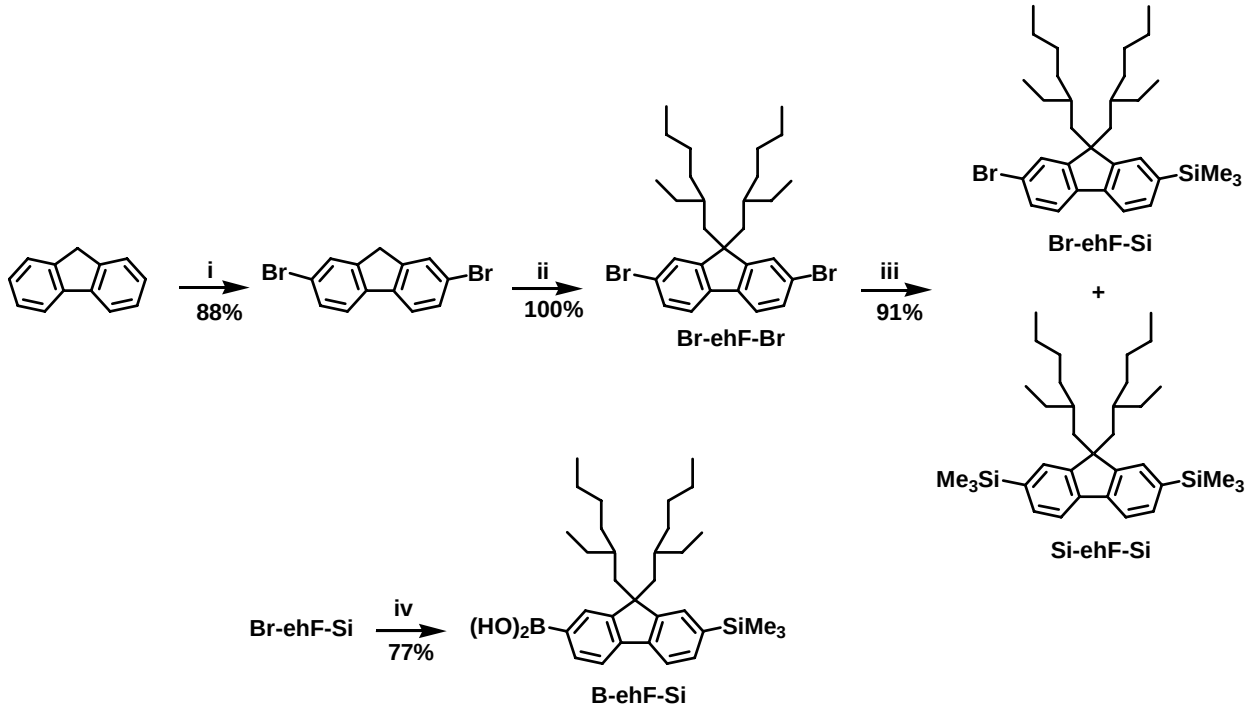

Scheme 1.1. Synthesis of monofluorene derivatives. (i) Br_2, $FeCl_3$, $CHCl_3$, 0 ^oC to RT. (ii) KOH, TBABr, 2-ethylhexyl bromide, toluene, water, 80^oC, 2 h. (iii) *n*BuLi, $ClSiMe_3$, THF, -78 ^oC to RT. (iv) *n*BuLi, $B(OiPr)_3$, THF, -78 ^oC to RT.

The monofluorene synthetic intermediates, 2,7-dibromofluoene**, Br-ehF-Br**, **Br-ehF-Si**, and **B-ehF-Si**, were prepared in multi-gram quantities using established methods (Scheme 1.1). The bromination of fluorene with bromine and $FeCl_3$, as the catalyst, produced 2,7-dibromofluorene in an 88% yield on a 100 g scale with recrystallization being the only purification step.[68] The alkylation of 2,7-dibromofluorene was performed with toluene, aqueous KOH, TBABr, and 2-ethylhexyl bromide at 80 ^oC for 2 h to produce **Br-ehF-Br** in a quantitative yield on a 100 g scale. These reaction conditions offer a significant advantage over the more commonly used alkylation in DMSO with KOH and 2-ethylhexyl bromide.[69] It was found that DMSO reaction was quite slow and purification was difficult.

The synthetic methods of Geng et al.[53] were used for the synthesis of **Br-ehF-Si** and **B-ehF-Si**. Lithium-halogen exchange with one of the bromo groups of the dibromo **Br-ehF-Br** with *n*-butyllithium at -78 ^oC followed by quenching with trimethyl silyl chloride gave **Br-ehF-Si** in a 91% yield. The reaction does not produce the desired product exclusively since both the starting material and the bis silyl **Si-ehF-Si** product, which are not separable by chromatography, are present in the crude mixture as determine by GC-MS. Although these impurities are inseparable at this stage, they are easily separated from the products formed in subsequent reactions with this mixture of compounds. The metal halogen exchange of the bromo group of **Br-ehF-Si** with *n*-butyllithium at -78 ^oC followed by quenching with triisopropyl borate and the subsequent hydrolysis gave the boronic acid **B-ehF-Si** in a 77% yield.

1.2.4 Synthesis of Bifluorene Intermediates

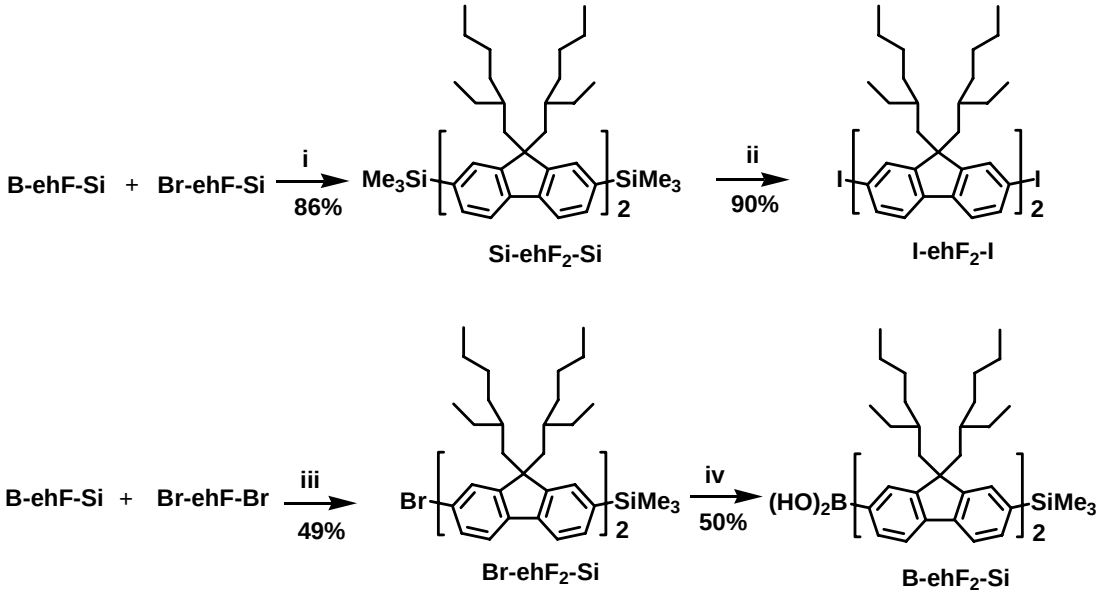

Scheme 1.2. Synthetic route to bifluorene building blocks. (i) $Pd(PPh_3)_4$, 2 M K_2CO_3, TBABr**,** Toluene, 75 ^oC, 24 h (ii) ICl, CH_2Cl_2, 0 ^oC to RT. (iii) $Pd(PPh_3)_4$, 2 M K_2CO_3, ethanol**,** toluene, reflux, 18 h. (iv) *n*BuLi, $B(O\textit{i}Pr)_3$, THF, -78 ^oC to RT.

The bifluorene units were assembled by aryl-aryl Suzuki coupling reactions of the monofluorene intermediates (Scheme 1.2). The coupling of the monobromo fluorene **Br-ehF-Si** and the fluorene boronic acid **B-ehF-Si**, with $Pd(PPh_3)_4$ as the catalyst, produced the bis silyl bifluorene **Si-ehF$_2$-Si** in an 86% yield. The oxidative deprotection of the trimethyl silyl groups with ICl gave the bis iodo bifluroene **I-ehF$_2$-I** in a 90% yield. The iodo groups were introduced to enable future Suzuki coupling reactions. The synthetically useful boronic acid **B-ehF$_2$-Si** was made by the Suzuki coupling of the dibromo fluorene **Br-ehF-Br** and the boronic acid **B-ehF-Si**. As there was no significant difference in the reactivities of the two aryl bromides in the reaction, a statistical mixture of starting material **Br-ehF-Br**, **Br-ehF$_2$-Si**, and **Si-ehF$_3$-Si** were present after workup. The ratio of **Br-ehF$_2$-Si** versus **Si-ehF$_3$-Si** can be improved by using excess **Br-ehF-Br.** **Br-ehF$_2$-Si** was formed in a 49% yield when 2 equivalents of the dibromo **Br-ehF-Br**

were used. Fortunately, the products and the starting materials are separable by chromatography. Boronation of **Br-ehF-Si** was accomplished by lithium-halogen exchange with *n*-butyllithium followed by quenching with triisopropyl borate and hydrolysis to yield the mono-boronated product in a 50% yield.

1.2.5 Synthesis of s(ehF$_3$M$_x$) Segmers

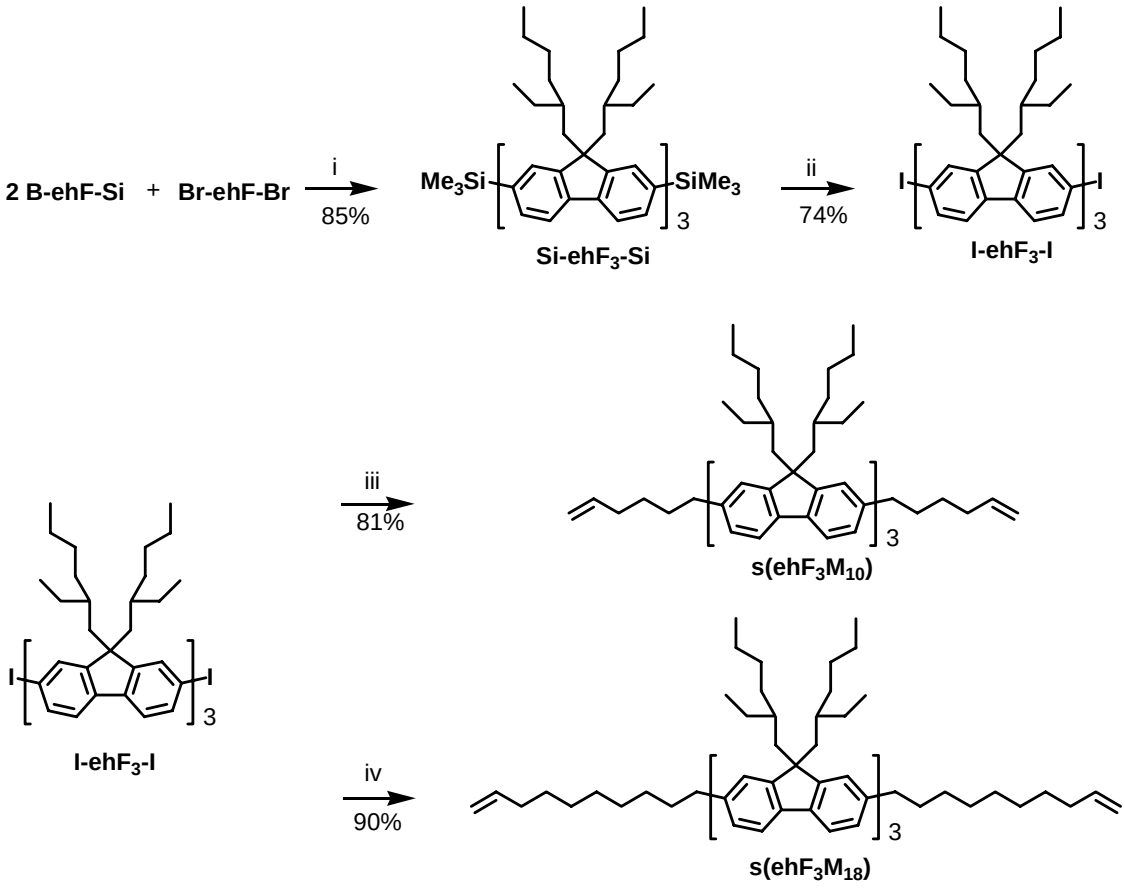

Scheme 1.3. Synthesis of trifluorene segmers. (i) $Pd(PPh_3)_4$, K_2CO_3, ethanol**,** toluene, reflux, 18 h. (ii) ICl, CH_2Cl_2, 0 ^oC to RT. (iii) 9-hex-5-enyl-9-BBN, $PdCl_2(PPh_3)_2$, 2 M K_2CO_3, TBABr, toluene, 45 ^oC, 20 h. (iv) 9-dec-5-enyl-9-BBN, $PdCl_2(PPh_3)_2$, 2 M K_2CO_3, TBABr, toluene, 45 ^oC, 18 h.

The trifluorene segmers (Scheme 1.3) were made by a Suzuki coupling of the dibromo **Br-ehF-Br** with the mono-boronated **B-ehF-Si** to yield the trimer **Si-ehF$_3$-Si** in an 85% yield.

The yield of this reaction is much higher than for the reactions to make **Br-ehF$_2$-Si** because a small excess of boronic acid was used and the reaction proceeded to completion. The conversion of the silyl groups to the iodo substituents of the trimer **I-ehF$_3$-I** in a 74% yield was then followed by alkyl-aryl Suzuki coupling reactions. The trimer **I-ehF$_3$-I** was coupled with the arm precursor **9-hex-5-enyl-9-BBN** using a palladium catalyst to yield the two armed **s(ehF$_3$M$_{10}$)** in an 81% yield. The **I-ehF$_3$-I** was also coupled with the longer arm precursor **9-dec-5-enyl-9-BBN** with a palladium catalyst to yield **s(ehF$_3$M$_{18}$)** in a 90% yield.

1.2.6 Synthesis of s(ehF$_4$M$_x$) Segmers

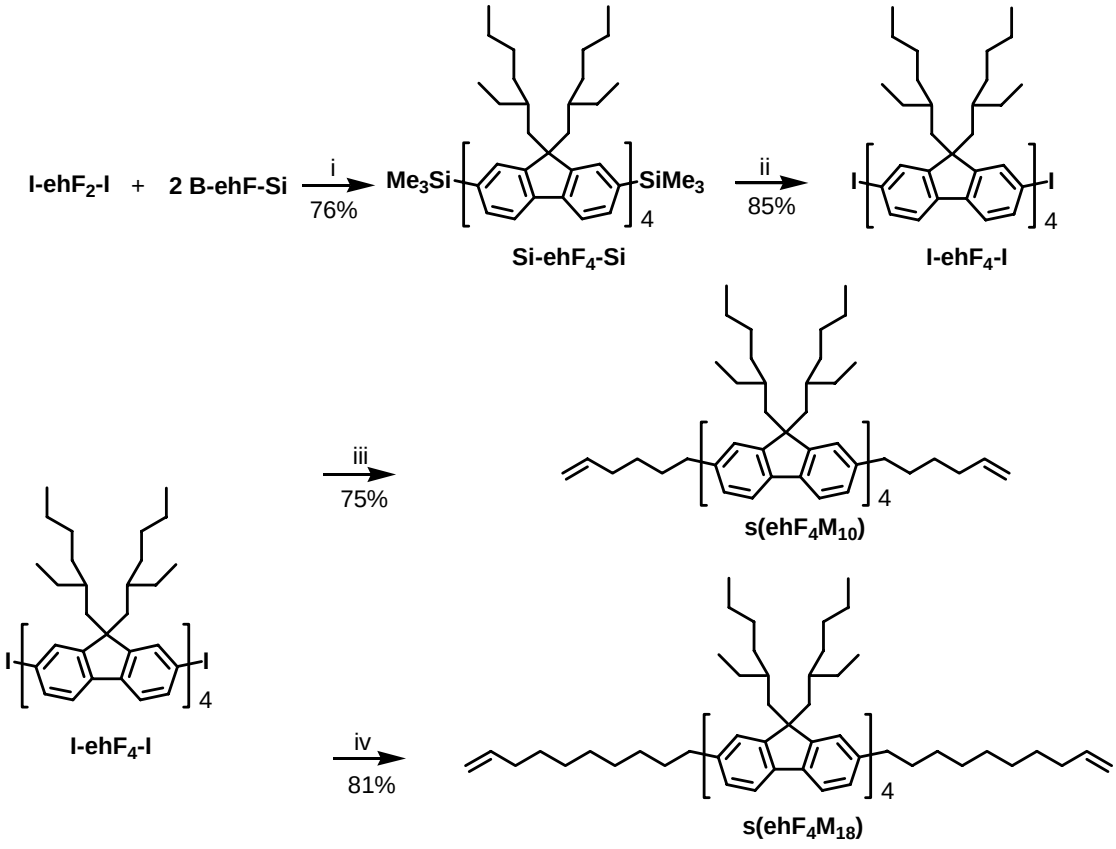

Scheme 1.4. Synthesis of the tetrafluorene segmers. (i) $Pd(PPh_3)_4$, 2 M K_2CO_3, TBABr**,** toluene, reflux, 18 h. (ii) ICl, CH_2Cl_2, 0 ^oC to RT. (iii) 9-hex-5-enyl-9-BBN, $PdCl_2(PPh_3)_2$, 2 M K_2CO_3, TBABr, toluene, 45 ^oC, 20 h. (iv) 9-dec-5-enyl-9-BBN, $PdCl_2(PPh_3)_2$, 2 M K_2CO_3, TBABr, toluene, 45 ^oC, 18 h.

The tetrafluorene oligomers were synthesized by the same procedures as the trifluorene oligomers (Scheme 1.4). The diiodo bifluorene **I-ehF$_2$-I** was reacted with excess of the boronic acid **B-ehF-Si** to form the bis silyl tetrafluorene **Si-ehF$_4$-Si** in a 76% yield. The **Si-ehF$_4$-Si** was reacted with ICl to form diiodo tetrafluorene **I-ehF$_4$-I** in an 85% yield. The Suzuki couplings with the 9-BBN derivatives and **I-ehF$_4$-I** produced **s(ehF$_4$M$_{10}$)** in a 75% yield and **s(ehF$_4$M$_{18}$)** in a 81% yield.

1.2.7 Synthesis of the s(ehF$_5$M$_x$) Segmers

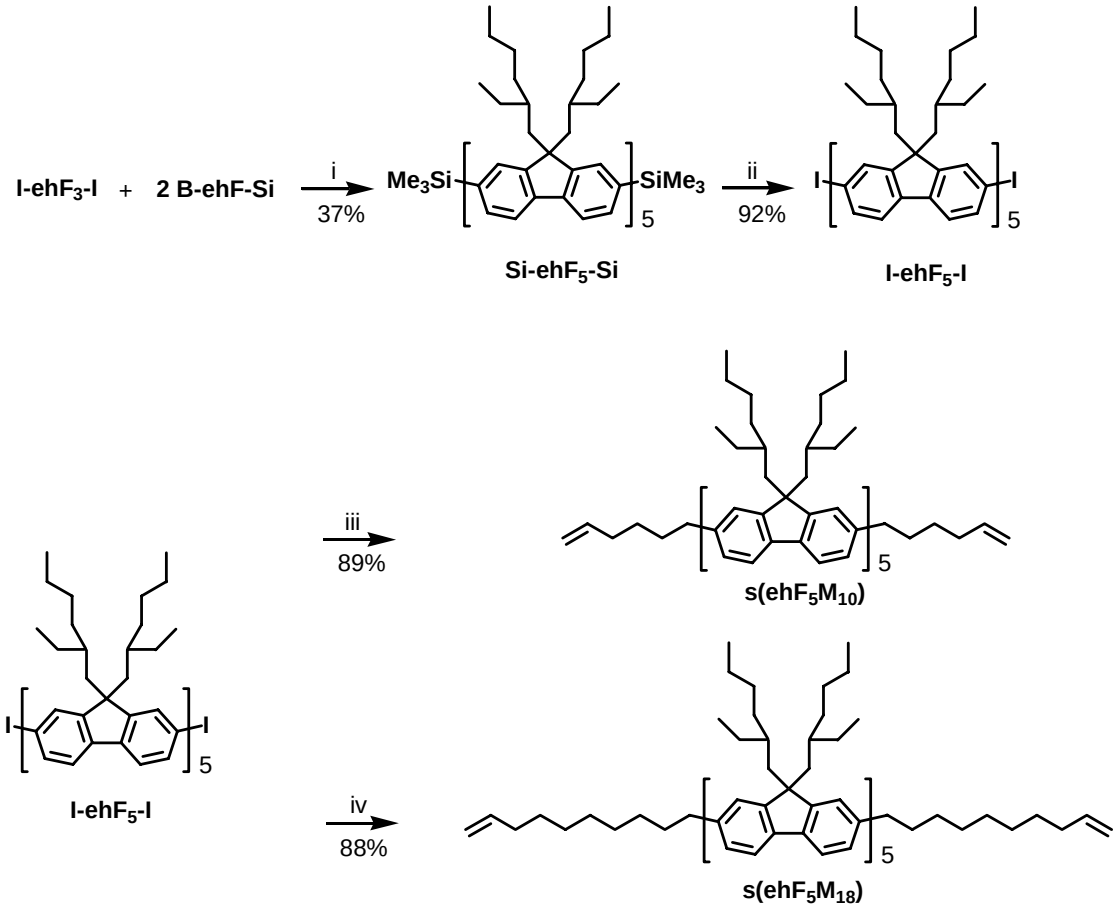

Scheme 1.5. Synthesis of pentafluorene segmers. (i) $Pd(PPh_3)_4$, K_2CO_3, TBABr**,** toluene, ethanol, reflux, 18 h. (ii) ICl, CH_2Cl_2, 0 ^oC to RT. (iii) 9-hex-5-enyl-9-BBN, $PdCl_2(PPh_3)_2$, 2 M K_2CO_3, TBABr, toluene, 45 ^oC, 18 h. (iv) 9-dec-5-enyl-9-BBN, $PdCl_2(PPh_3)_2$, 2 M K_2CO_3, TBABr, toluene, 45 ^oC, 20 h.

The pentafluorene segmers were prepared by coupling of the trimeric unit with two monomeric fluorene units (Scheme 1.5). The Suzuki coupling of the terfluorene **I-ehF$_3$-I** with 2 equivalents of the boronic acid **B-ehF-Si** only produced the desired pentamer **Si-ehF$_5$-Si** in a 37% yield. The reaction conditions here did not use TBABr (tetrabutylammonium bromide) as a phase transfer catalyst. The TBABr appears to be an important reagent for the Suzuki coupling of the very non polar fluorene units. Isolation of this product from starting materials is difficult as there is only a small change in polarity of the **Si-ehF$_5$-Si** and **I-ehF$_3$-I** by silica gel column chromatography. The conversion of the trimethyl silyl group to iodine works cleanly using ICl to generate **I-ehF$_5$-I** in a 92% yield. The Suzuki couplings of **I-ehF$_5$-I** with the 9-BBN derivatives produced **s(ehF$_5$M$_{10}$)** in an 89% yield and **s(ehF$_5$M$_{18}$)** in an 88% yield.

1.2.8 Synthesis of the s(ehF$_6$M$_{18}$) Segmer

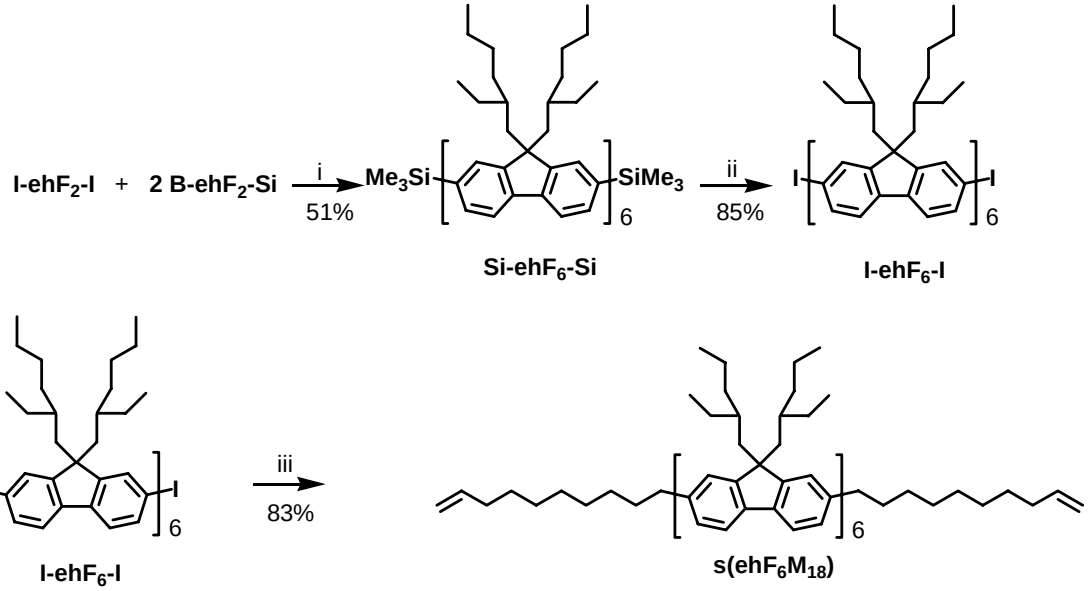

Scheme 1.6. Synthesis of hexafluorene segmer. (i) $Pd(PPh_3)_4$, 2 M K_2CO_3, TBABr**,** toluene, reflux, 24 h. (ii) ICl, CH_2Cl_2, 0 ^oC to RT. (iii) 9-dec-5-enyl-9-BBN, $PdCl_2(PPh_3)_2$, 2 M K_2CO_3, TBABr, toluene, 45 ^oC, 18 h.

The hexafluorene oligomer was made by first reacting diiodo bifluorene **I-ehF$_2$-I** with excess **B-ehF$_2$-Si** in a Suzuki coupling reaction with a Pd(0) catalyst to form **Si-ehF$_6$-Si** in a modest 51% yield (Scheme 1.6). The Suzuki coupling to form the higher oligomers proceeds in modest yields but purification of the product is facile when using the bifluorene boronic acid **B-ehF$_2$-Si** as the coupling partner. The oxidative deprotection with ICl to form the diiodo **I-ehF$_6$-I** proceeded in an 85% yield. The Suzuki coupling of **I-ehF$_6$-I** with 9-dec-5-enyl-9-BBN produces **s(ehF$_6$M$_{18}$)** in an 83% yield.

1.2.9 Synthesis of s(ehF$_7$M$_{18}$) Segmer

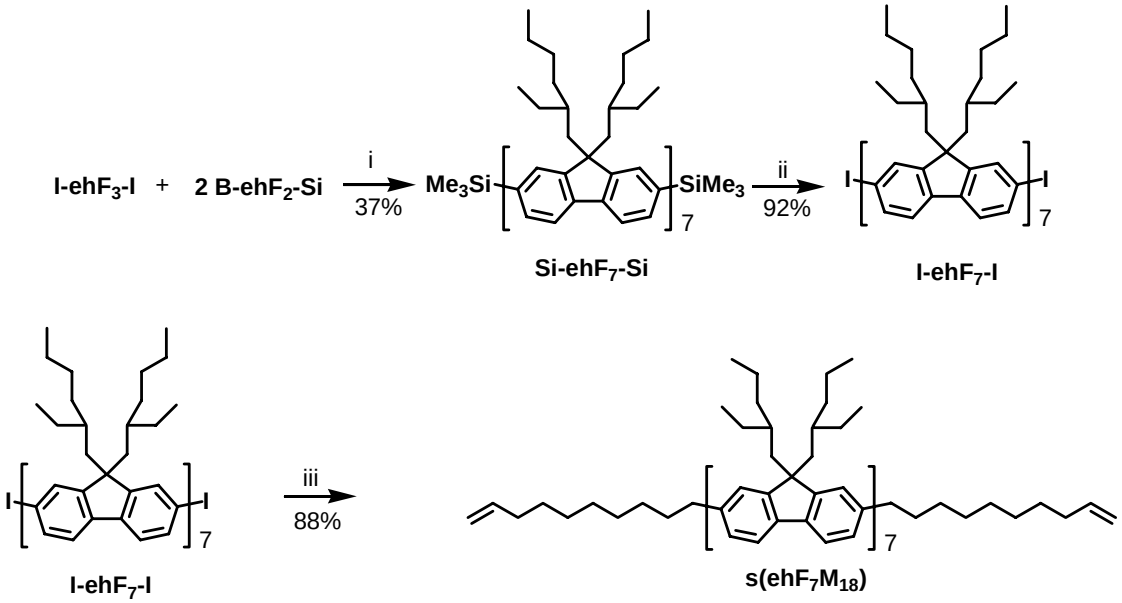

Scheme 1.7. Synthesis of heptafluorene segmer. (i) $Pd(PPh_3)_4$, 2 M K_2CO_3, TBABr**,** toluene, reflux, 24 h. (ii) ICl, CH_2Cl_2, 0 ^oC to RT. (iii) 9-dec-5-enyl-9-BBN, $PdCl_2(PPh_3)_2$, 2 M K_2CO_3, TBABr, toluene, 45 ^oC, 18 h.

The synthesis of the heptafluorene oligomer begins with the Suzuki coupling of the diiodo **I-ehF$_3$-I** with excess **B-ehF$_2$-Si** to form **Si-ehF$_7$-Si** in a 43% yield (Scheme 1.7). The deprotection to form the diiodo **I-ehF$_7$-I** proceeded in an 83% yield after purification. The

Suzuki coupling of this with **9-dec-5-enyl-9-BBN** was completed in a 73% yield. Again, the separation of the products of the previous two reactions from the starting materials is difficult with silica gel chromatography.

1.2.10 Synthesis of s(ehF$_8$M$_{18}$)

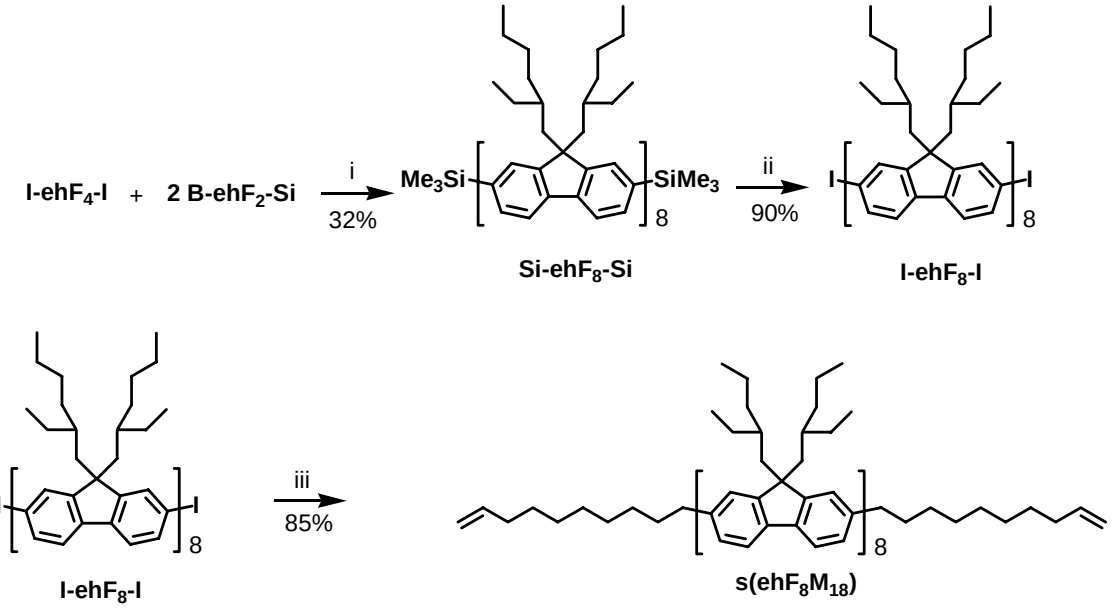

Scheme 1.8. Synthesis of octafluorene segmer. (i) $Pd(PPh_3)_4$, 2 M K_2CO_3, TBABr**,** toluene, reflux, 24 h. (ii) ICl, CH_2Cl_2, 0 ^oC to RT. (iii) 9-dec-5-enyl-9-BBN, $PdCl_2(PPh_3)_2$, 2 M K_2CO_3, TBABr, toluene, 45 ^oC, 18 h.

The synthesis of the octafluorene oligomer begins with the Suzuki coupling of the previously described **I-ehF$_4$-I** with excess **B-ehF$_2$-Si** to form **Si-ehF$_8$-Si** in a 32% yield (Scheme 1.8). The yields for the Suzuki coupling, to form the long oligomers, are poor but purification of the product can be accomplished easily with silica gel chromatography. The standard deprotection of **Si-ehF$_8$-Si** to form **I-ehF$_8$-I** proceeded in a 90% yield. The Suzuki coupling of **I-ehF$_8$-I** with 9-dec-5-enyl-9-BBN is completed in an 85% yield.

1.2.11 Synthesis of s(F_xM_x) segmers

The synthesis of the 9,9-bis (*n*-hexyl)fluorene segmers was performed in an analogous manner as their respective 2-ethylhexyl segmers. The synthesis of the **s(F_4M_{18})**, **s(F_5M_{18})**, and **s(F_6M_{18})** are described in more detail in the experimental section and in Copenhafer et al[1] where evaluation of the photophysical and thermal properties of the respective properties are also described. The alkyl group substitution does not alter the synthetic schemes or greatly affect the yields of the reactions.

1.2.12 Synthesis of p(ehF$_x$M$_y$) polymers

Two different methods (Scheme 1.9) were employed to carry out the polymerization of the segmers and subsequent hydrogenation. Method A followed the procedures developed by Wagener et al[66] and used Grubbs I as the catalyst and toluene with a small amount diphenyl ether as the solvent system. This method involved the slow removal of ethylene and toluene under vacuum at RT. The reaction is was heated to 45 ^oC and stirred under vacuum with the remaining non-volatile diphenyl ether keeping the reaction from gelling. The residual ruthenium catalysts from the polymerization were then used to hydrogenate the remaining internal olefins. The reaction was performed in toluene with silica gel under H_2 atmosphere at 80 ^oC. The polymer can then be purified by precipitation into acetone. Method B used the Grubbs II catalyst to perform the ADMET polymerization. The more active catalyst does not require the removal of ethylene under vacuum and the reaction was carried out in refluxing CH_2Cl_2. In this method, the hydrogenation was then performed using Wilkinson's catalyst under H_2 pressure in toluene. This

hydrogenation was also faster and more reliable than using the residual Grubbs I or II catalyst and silica gel that were used for method A.

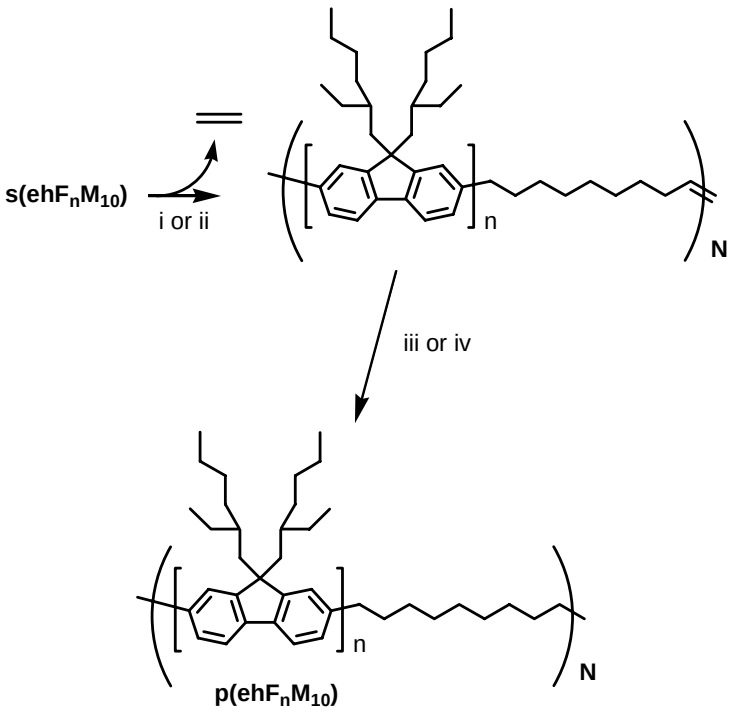

Scheme 1.9. ADMET polymerization of s(ehF$_x$M$_{10}$) and subsequent hydrogenation. (i) Grubbs I, diphenyl ether, toluene, vacuum, RT to 45 ^{o}C, (ii) Grubbs II, reflux CH_2Cl_2, (iii) Grubbs I, SiO_2, toluene, H_2 180 psi, 80 ^{o}C, (iv) Wilkinson's catalyst, toluene, 180 psi, 80 ^{o}C.

Gel permeation chromatography (GPC) was used to determine the relative molecular weights of the final polymers using polystyrene standards for calibration. A typical GPC chromatogram of **p(ehF$_4$M$_{18}$)** is show in Figure 1.15 and demonstrates the monomodal distribution of the majority of the polymers that were isolated. The results of the polymerizations and subsequent hydrogenations are shown in Table 1.3. The polymers have reasonable molecular weights but the degrees of polymerization are quite modest. The large segmers begin with high molecular weights and only a few repeat units are necessary to get a M_n

of greater than 20 K g/mol. The low degrees of polymerization are likely caused by impurities in the segmers that terminate the metathesis polymerization. Typically, the final three steps of the segmer synthesis result in products that are inseparable from the starting materials. For example, **Si-ehF$_4$-Si**, **I-ehF$_4$-I**, and **s(ehF$_4$M$_{18}$)** all have the same R_f on silica gel with all elution solvents that were tried. Therefore, some of the final segmers are likely to have some terminating end groups such as trimethyl silyl, iodo, or hydrogen instead of the desired 5-hexenyl or 9-decenyl alkene units.

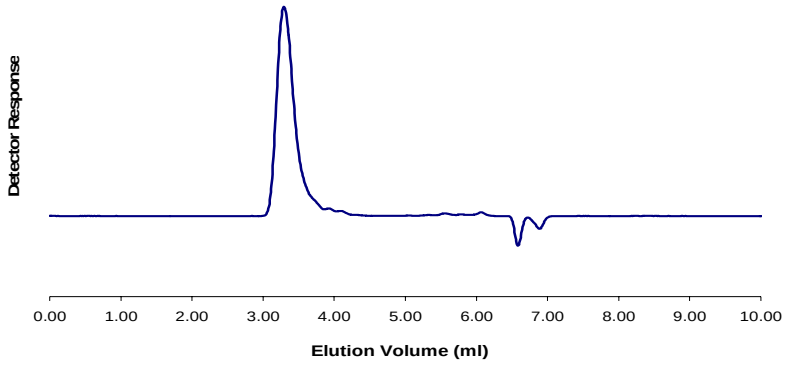

Figure 1.15. A typical GPC chromatograph of **p(ehF$_4$M$_{18}$)** performed in THF at RT.

It is well known that monomer purity is a major cause of low degrees of polymerization in condensation polymerizations. Previous work by Walba et al[70] showed that by switching from Grubbs I to Grubbs II could increase the degrees of polymerizations in ADMET systems dramatically. If impurities were the cause of the low degrees of polymerization then no change would be seen in the M_n when different catalysts were used. Since no change in M_n was seen for the polymerization of same **s(F$_5$M$_{18}$)** segmer with Grubbs I and Grubbs II, the impurities are therefore the likely cause of low degrees of polymerizations for most of the polymers that were made.

Table 1.3: The synthesis and characterization data for the **p(ehF$_x$M$_y$)** series of RSCs.

Polymer	Method[a]	Yield %	M_n[b] (10^3 g/mol)	M_w[c] (10^3 g/mol)	PDI[d]	DP[e]
p(ehF$_3$M$_{10}$)	B	73	22	39	1.8	12
p(ehF$_3$M$_{18}$)	A	60	22	29	1.3	15
p(ehF$_4$M$_{10}$)	A	80	20	28	1.4	12
p(ehF$_4$M$_{18}$)	A	90	42	54	1.3	23
p(ehF$_5$M$_{10}$)	B	66	25	33	1.3	12
p(ehF$_5$M$_{18}$)	A	90	27	40	1.5	12
p(ehF$_6$M$_{18}$)	A	66	32	40	1.3	12
p(ehF$_7$M$_{18}$)	A	86	49	57	1.2	15
p(ehF$_8$M$_{18}$)	A	75	25	32	1.3	8
50% p(ehF$_3$M$_{10}$) 50% p(ehF$_5$M$_{10}$)	B	58	25	34	1.4	---
10% p(ehF$_3$M$_{10}$) 90% p(ehF$_5$M$_{10}$)	B	71	33	46	1.4	----
p(F$_4$M$_{18}$)	A	90	25	36	1.4	16
p(F$_5$M$_{18}$)	A	69	25	37	1.5	13
p(F$_6$M$_{18}$)	A	66	23	33	1.4	10

[a]Method of polymerization (A) Grubbs I under vacuum or (B) Grubbs II in refluxing CH_2Cl_2. [b]The number average molecular weight from GPC with polystyrene standard. [c]The weight average molecular weight from GPC with polystyrene standard. [d]Polydispersity from M_n/M_w. [e]Degree of polymerization from M_n / monomer molecular weight.

The ADMET polymerization and hydrogenation results for two mixed copolymers that were made from mixtures of two different segmers are also included in Table 1.3. The two segmers were combined at different weight ratios in one reaction vessel and since the ADMET polymerization should not exhibit any reactivity difference between the monomers there should be a random distribution (not RSCs) of the trifluorene oligomers and the pentafluorene oligomers in the polymer backbone. The mixed copolymers were made at two different ratios of segmers, one is a 50:50 mole ratio mixture of the **s(ehF$_3$M$_{10}$)** and **s(ehF$_5$M$_{10}$)** and the other a 10:90 mole ratio mixture of **s(ehF$_3$M$_{10}$)** and **s(ehF$_5$M$_{10}$)**. These polymers were made to examine the copolymers made from mixed monomer systems and are further discussed in the physical properties section of the chapter.

1.2.13 NMR Spectroscopy of p(ehF$_x$M$_y$) RSCs

The structures of the intermediates and final polymer products were examined by ^{1}H and ^{13}C NMR spectroscopy and in this section is presented a detailed analysis of the spectra associated with an example polymer, **p(ehF$_4$M$_{18}$),** including selected intermediates on the synthetic pathway is presented. It should be noted that despite the broadness of peaks in the spectra and complexity of the ^{1}H NMR spectroscopy of these high MW species, this was the primary analytical method used to both to monitor the progress of certain reactions and to confirm the identity of the products. Mass spectroscopy did not prove useful as the high molecular weights precluded the use of most techniques and MALDI was not readily available. In addition, changes in polarity of the starting materials and products were often quite small making reaction monitoring via thin layer chromatography difficult.

The structure of the oligomers with trimethyl silyl groups and the subsequent replacement of these silyl end groups with iodo groups were verified with ^{1}H NMR spectroscopy. The protons of the trimethyl silyl groups (H_a) of **Si-ehF$_4$-Si** are clearly distinguishable as a singlet at 0.31 ppm (Figure 1.16a). The trimethyl silyl groups at 0.31 ppm, the protons of the alkyl carbon attached at the 9 position of fluorene (H_b) at 2.1 ppm, and the aryl region from 7.4 to 8.0 ppm integrated to ratios consistent with the proposed structure. The reaction of **Si-ehF$_4$-Si** with iodine monochloride replaces the trimethyl silyl groups with an iodo groups and the spectrum of the product is nearly identical to that of the precursor with the exception of the disappearance of the singlet at 0.31 ppm (Figure 1.16b).

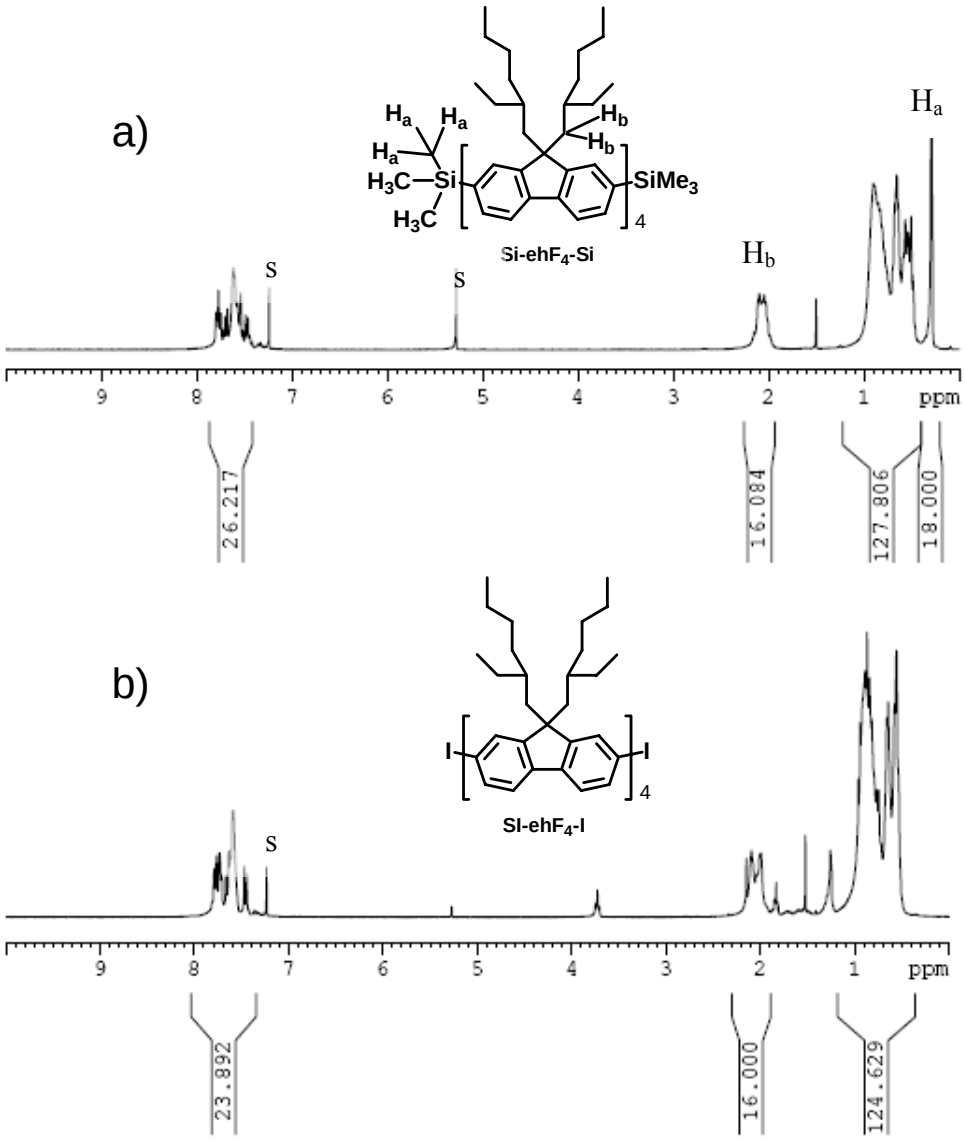

Figure 1.16. The ^{1}H NMR spectra of (a) **Si-ehF$_4$-Si** and (b) **I-ehF$_4$-I**.

The Suzuki coupling to graft the 9-decenyl groups to the tetramers was monitored by observation of the characteristic chemical shifts in the ^{1}H NMR spectrum for the newly formed benzylic groups and terminal olefins. The ^{1}H NMR spectrum of **s(ehF$_4$M$_{18}$)**, shown in Figure 1.17, exhibits a characteristic broad triplet at 2.8 ppm for the benzylic protons. The terminal olefin group's ^{1}H NMR signals are a multiplet for the external olefin (H_a) at 5.00 ppm and a

multiplet for the internal olefin protons at 5.85 ppm (H_b). The integration of the terminal olefin resonances with those from the fluorene unit is consistent with the desired bis-substitution.

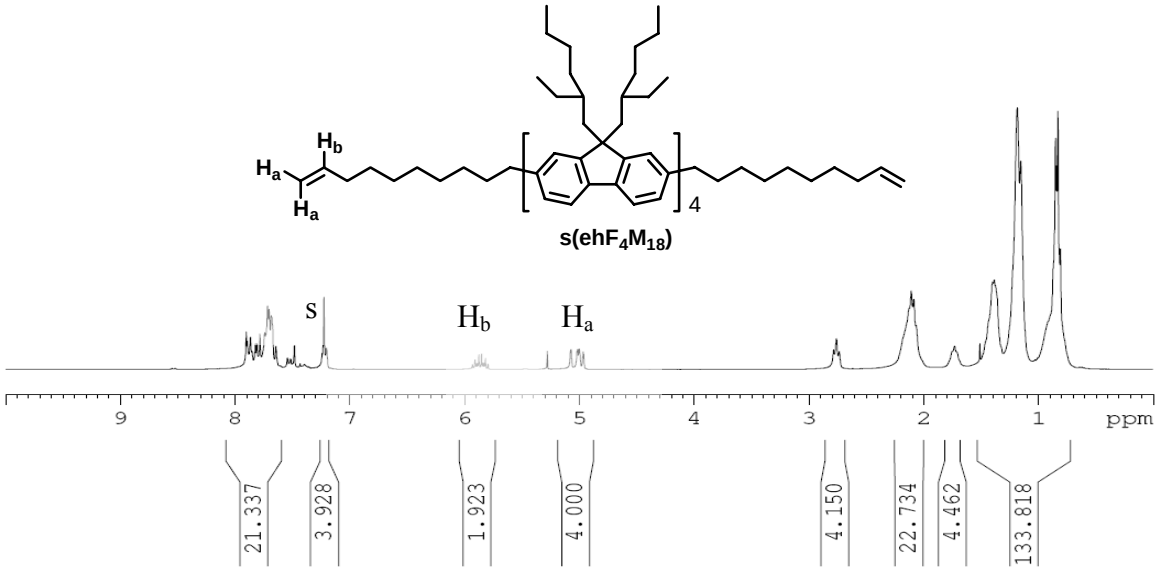

Figure 1.17. The ^{1}H NMR spectrum of **s(ehF$_4$M$_{18}$)**.

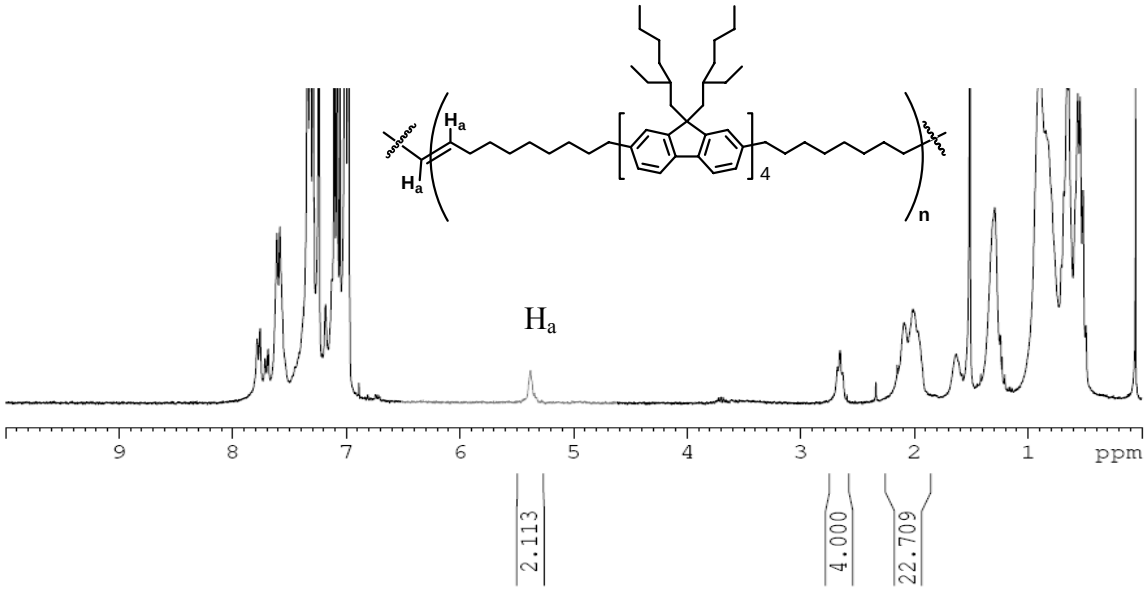

Figure 1.18. ^{1}H NMR spectrum of the ADMET polymerization reaction mixture for **s(ehF$_4$M$_{18}$)**.

The ADMET polymerization was monitored by ^{1}H NMR spectroscopy as well. The crude reaction mixture spectrum, shown in Figure 1.18, no longer shows resonances for the terminal olefin groups from the segmer but rather exhibits a signal at 5.35 ppm for new internal olefin peak (H_a) produced by metathesis. After hydrogenation, this internal olefin peak also disappears (not visible even after 100 scans of a 0.2 M sample), which suggests that the hydrogenation proceeds nearly quantitatively (Figure 1.19). The purified **p(ehF$_4$M$_{18}$)** ^{1}H NMR spectrum shows no remaining olefin protons and the expected ratios for the integration of aromatic, benzylic, and alkyl protons.

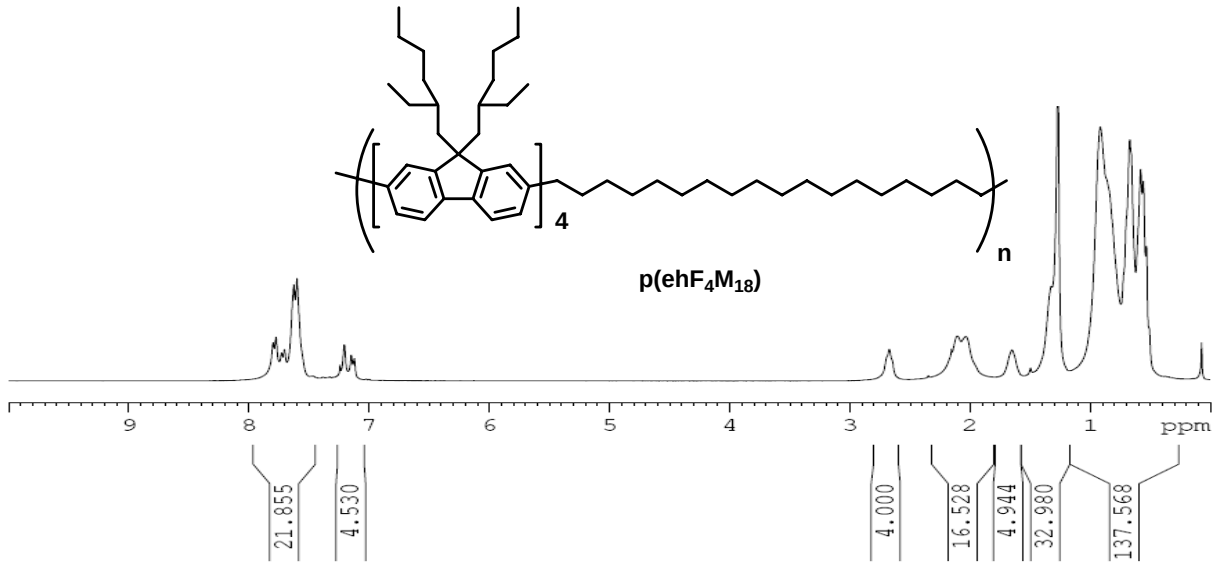

Figure 1.19. ^{1}H NMR spectrum of **p(ehF$_4$M$_{18}$)** after hydrogenation.

The ^{13}C NMR spectra of the compounds can also be used to verify the formation of the desired products. Figure 1.20 shows the spectra of the transformation of **I-ehF$_4$-I** (a) to **s(ehF$_4$M$_{18}$)** (b) and then to **p(ehF$_4$M$_{18}$)** (c). The presence of the iodo groups can be verified by the characteristic shift for the C-I group at 92 ppm. This peak disappears as the iodo group is transformed to the 9-decenyl group in the Suzuki coupling reaction. A new characteristic peak

for the RC=*C*H is now apparent at 114 ppm. The polymerization and subsequent hydrogenation of the segmer produces **p(ehF$_4$M$_{18}$)** with a ^{13}C spectrum where the RC=*C*H peak is no longer present.

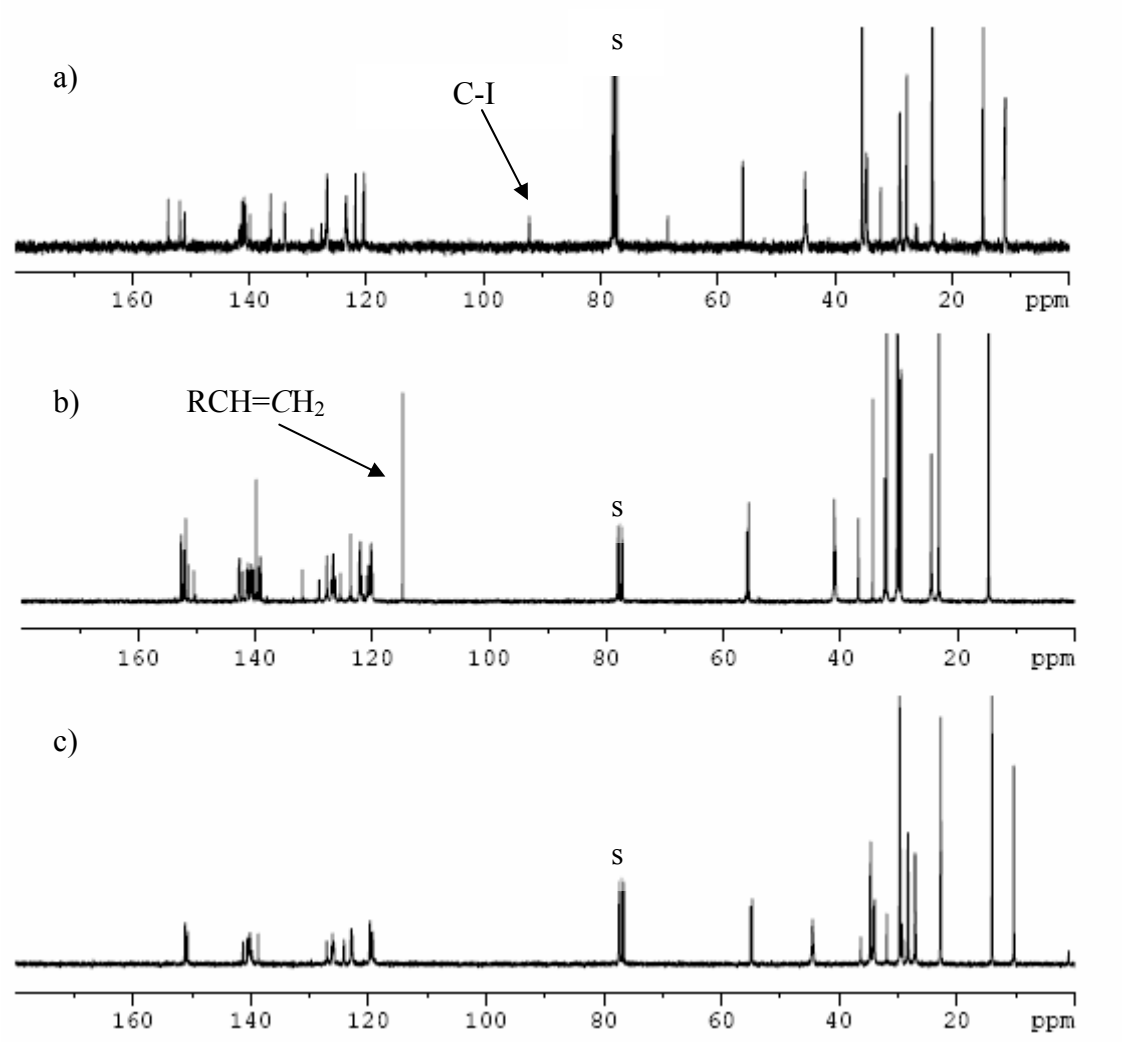

Figure 1.20. ^{13}C NMR spectra of (a) **I-ehF$_4$-I**, (b) **s(ehF$_4$M$_{18}$)**, and (c) **p(ehF$_4$M$_{18}$)**.

The NMR spectra for **p(ehF$_4$M$_{18}$)** and the precursors to this compound are typical of those found for other members of the series. Spectra for other members of this series can be found in Appendix A.

1.3 PHOTOPHYSICAL PROPERTIES OF POLYMERS

1.3.1 Absorption Spectroscopy

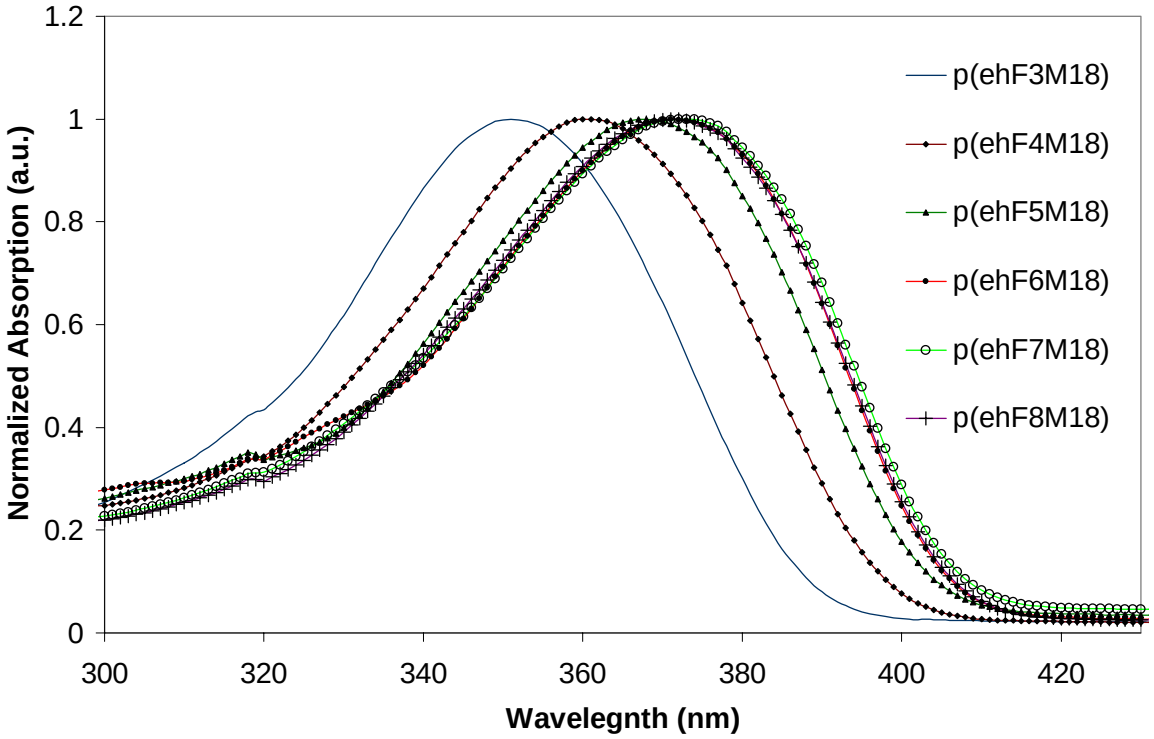

Figure 1.21. Normalized absorption spectra of the **p(ehF$_x$M$_y$)** series of polymers in CH_2Cl_2 (~10^{-6} M).

The absorption spectra the of the **p(ehF$_x$M$_y$)** series shows the expected trend of decreasing energy for the absorption maximum with increasing fluorene units. Figure 1.21 shows the normalized absorption spectra and Table 1.4 lists the absorption maximums of the polymers in CH_2Cl_2. The shift in wavelength of the maximum absorption begins to become smaller as the number of repeat units increases. For the change from **p(ehF$_3$M$_{18}$)** to **p(ehF$_4$M$_{18}$)** a 8 nm increase in absorption maximum is seen but for the change from to **p(ehF$_6$M$_{18}$)** to **p(ehF$_8$M$_{18}$)**

only a 1 nm increase in absorption maximum is seen. The effective conjugation length for the fluorene units appears be maximized at around 6 repeat units in the solution absorption spectrum. Previous work[50, 52, 71] has shown very similar results with respect to chain lengths of oligofluorenes in their absorption and emission spectra.

Table 1.4. The absorption and emission maxima for the **p(ehF$_x$M$_{18}$)** series.

Polymer	Solution Absorption[a] Max (nm)	Solution Emission[b] Max (nm)	Thin Film Emission[c] Max (nm)
p(ehF$_3$M$_{18}$)	351	397	400
p(ehF$_4$M$_{18}$)	360	406	409
p(ehF$_5$M$_{18}$)	368	410	416
p(ehF$_6$M$_{18}$)	371	412	417
p(ehF$_7$M$_{18}$)	373	412	419
p(ehF$_8$M$_{18}$)	373	412	419

[a]Absorption maximum measured in dilute CH_2Cl_2 solutions (~10^{-6} M). [b]The solution emission maximum measured in dilute CH_2Cl_2 solution (~10^{-6} M). [c]The thin film emission maximum. The films were dropcast onto quartz slides from a $CHCl_3$ solution.

1.3.2 Emission Spectroscopy

Due to their intense blue emission, fluorene based polymers and oligomers have been widely studied for use in OLEDs. The number of repeat units in the fluorene segment also controls the emission energy for the oligomer.[31] Increasing the number of fluorene repeat units increases the maximum emission wavelength in both solution and thin film emission.[54] Although the emission tunability has been shown previously for oligomeric fluorenes, the ability to control both the emission maximum and have a process-friendly polymer is a major advantage of the polymers discussed in this report.

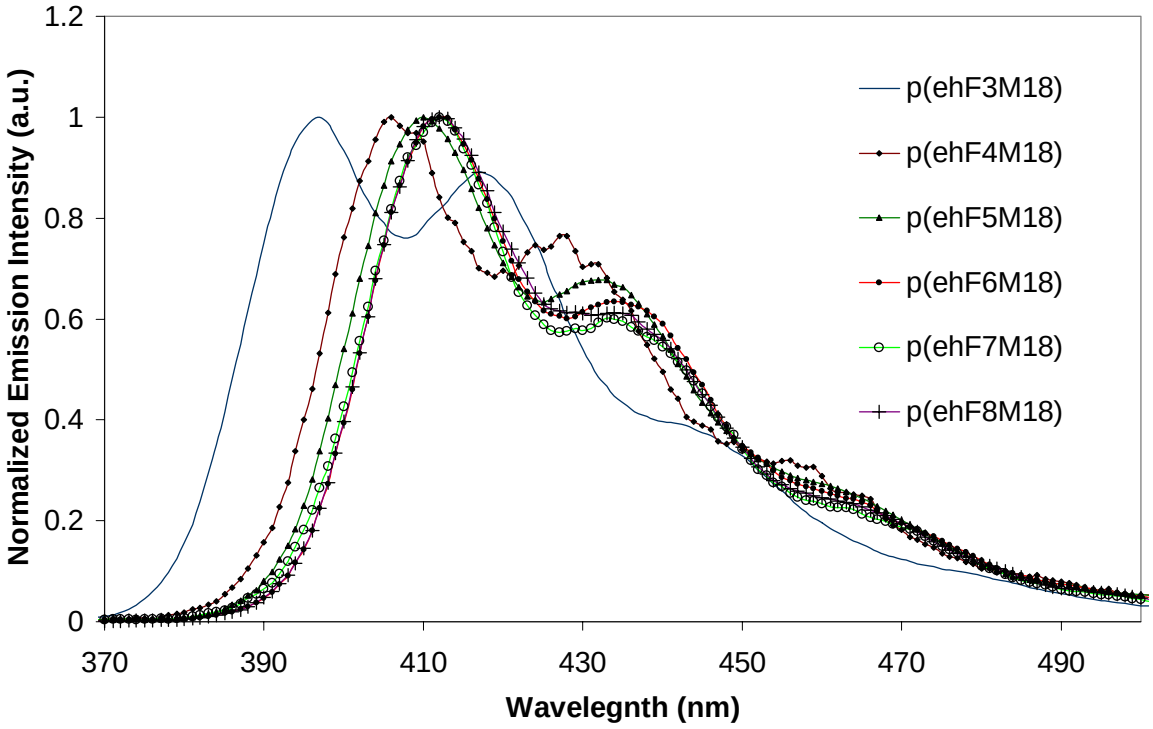

Figure 1.22. Normalized solution emission intensity spectra of **p(ehF$_x$M$_y$)** series of polymers in CH_2Cl_2 (~10^{-6} M).

The normalized solution emission of dilute mixtures of the polymers in CH_2Cl_2 is shown in Figure 1.22 and tabulated in Table 1.4. The effect of increasing the number of fluorene units becomes smaller as the number of repeat units is increased. This increase in emission and the leveling effect of the number of repeat fluorene units on emission matches what has been previously shown in the literature for fluorene oligomers by Yoon and coworkers.[54] The three emission bands of the fluorene can be assigned to the 0-0, 0-1, and 0-2 singlet emission bands.[72]

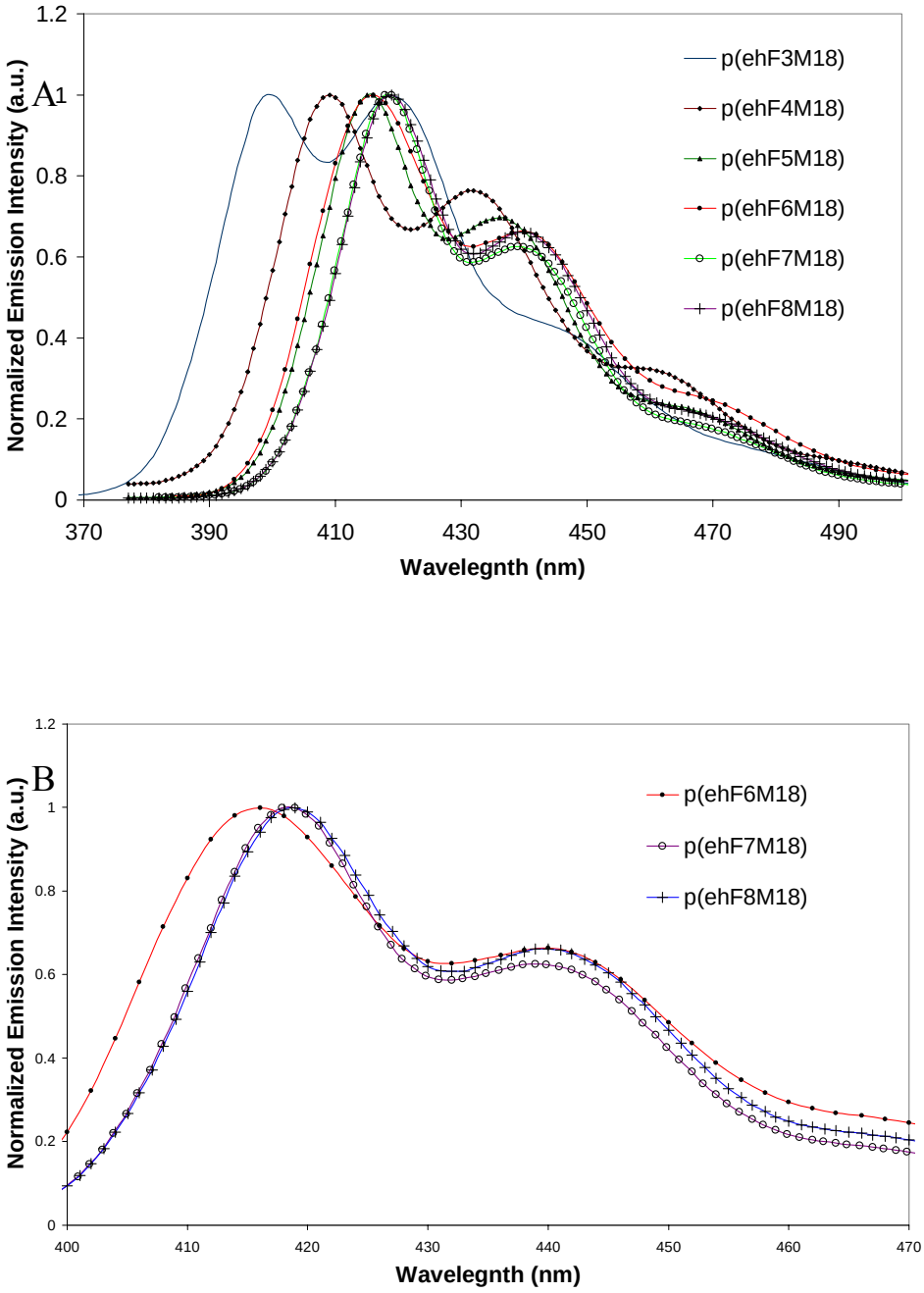

Figure 1.23. (A) The normalized thin film emission spectra of the **p(ehF$_x$M$_y$)** series of polymers drop cast from $CHCl_3$ on glass slides. (B) An expansion of selected spectra to highlight the small change in emission maximum wavelength.

The emission spectra of thin films of the polymers were also measured. The emission maximum wavelength of thin films of the polymers also begins to reach a maximum value as the

number of fluorene repeat units increases (Figure 1.23a and b). The thin film emission of the polymers is of importance since OLEDs are made by layering thin films of the organic materials. There is a small bathochromic (red) shift of the emission maximum in the thin film when compared to the solution emission. The interaction or aggregation between the closely packed fluorene groups is likely responsible for this shift although the polarity of the medium may have some effect on the emission maximum. Aggregation would cause a decrease in the band gap of the polymer through a stabilization of the ground state of the molecule. The solution emission was measured in methylene chloride which is likely to be a more polar environment than the solid polymer film. The polarity of the media may have an effect on the stabilization or destabilization of the excited states.

1.4 PHYSICAL PROPERITES OF POLYMERS

The fluorene-co-methylene RSCs made in this work have tunable liquid crystalline properties, as well as control of emission maximums. The ability of mesogenic fluorene containing polymers to be aligned and generate polarized emission is of interest for creating higher efficiency LCDs with OLEDs as back light. No previous work has demonstrated the control over the liquid crystalline phase temperatures and emission maximums combined with the good film forming properties of polymers that is demonstrated in this report.

In our work, the switch from *n*-hexyl groups to 2-ethylhexyl groups at the 9-position of fluorene unit resulted in polymers that exhibit mesophases in polarized optical microscopy. The alkyl groups of the fluorene units have been shown to have a significant effect on the mesophases of other fluorene polymers or oligomers. Changes are seen in the mesophase

behavior when the side chains are switched from *n*-hexyl, *n*-octyl, or 2-ethylhexyl groups in polyfluorene and chiral alkyl side chains have been used for the generation of circularly polarized emission in fluorene oligomers.[53] The structural properties of flourene based polymers and oligomers have been studied by different groups using a variety of techniques to determine how the structure affects the thermal and the optical properties.[73-81] The side chains help to space the conjugated backbones and eliminate the formation of aggregates caused by the close packing of conjugated groups.

The structure of polyfluorene with 2-ethylhexyl substituents has been evaluated and the mesophase is believed to have a hexagonal structure that is often seen in hairy rod polymer systems (Figure 1.24).[81-83] This structure is quite similar to the nematic phase in that it has only one degree of directional order. The mesophases of oligofluorenes may have similar solid state structures depending upon the number of fluorene units in the chain. The spacing, with methylene units, of the oligofluorene units in our polymers would likely disrupt such a structure form forming. Oligofluorenes with 2-ethylhexyl side chains are believed to exhibit a nematic phase but studies are still on going to determine the true mesophase.[54]

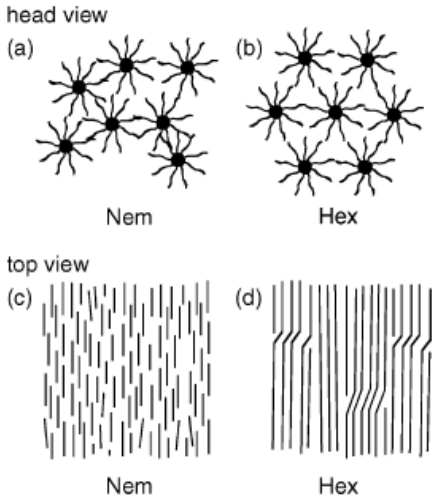

Figure 1.24. Representation of the self assembled nematic and hexagonal phases of hairy rod polymers (a,b) drawn end on and (c,d) side on. Figure used without permission from reference 82.

The **p(ehF$_x$M$_y$)** and **s(ehF$_x$M$_y$)** materials were studied by polarized optical microscopy with a hot stage to control temperatures of dropcast films on glass slides. Phase transitions were observed by changes in the appearance of the films as the temperature was varied. Some of the films formed by dropcasting started as amorphous glasses; others already showed some organization as determine by the appearance of a mesophase. Figure 1.25 shows the texture of the phases of two representative polymers studied here. The textures of these mesophases and the other polymers and segmers studied are consistent with nematic phases based on the Schlieren patterns. The nematic to isotropic phase change can be seen during both heating and cooling cycles. The values reported are the average of these temperatures. As can be seen the temperature of the nematic to isotropic phase is greatly affected by the number of fluorene units in the polymer of segmer. Increasing the number of fluorene units increases the rigidity of the polymer or segmer which increases the N-I (nematic to isotropic) transition temperature.

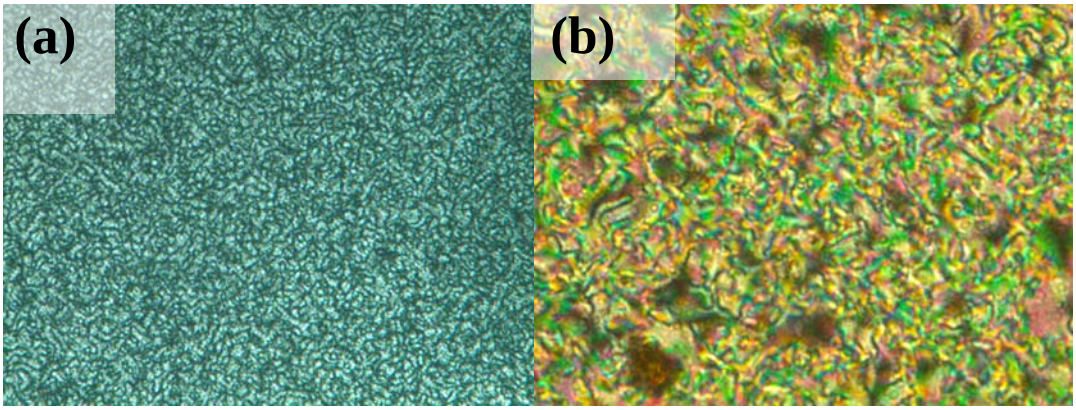

Figure 1.25. Polarized optical microscopy images of the mesophase textures of (a) **p(ehF$_4$M$_{18}$)** and (b) **p(ehF$_5$M$_{18}$)**.

A transition that is very close in temperature to what is observed for the N-I transition as determine by polarized optical microscope is easily observable in both the heating and cooling scan using differential scanning calorimetry (DSC). Figure 1.26 shows the DSC trace for **p(ehF$_3$M$_{18}$)** and Table 4 includes the transition temperature for the other polymers.

Unfortunately, no glass transitions are identifiable in the DSC traces for any of the polymers made in this work.

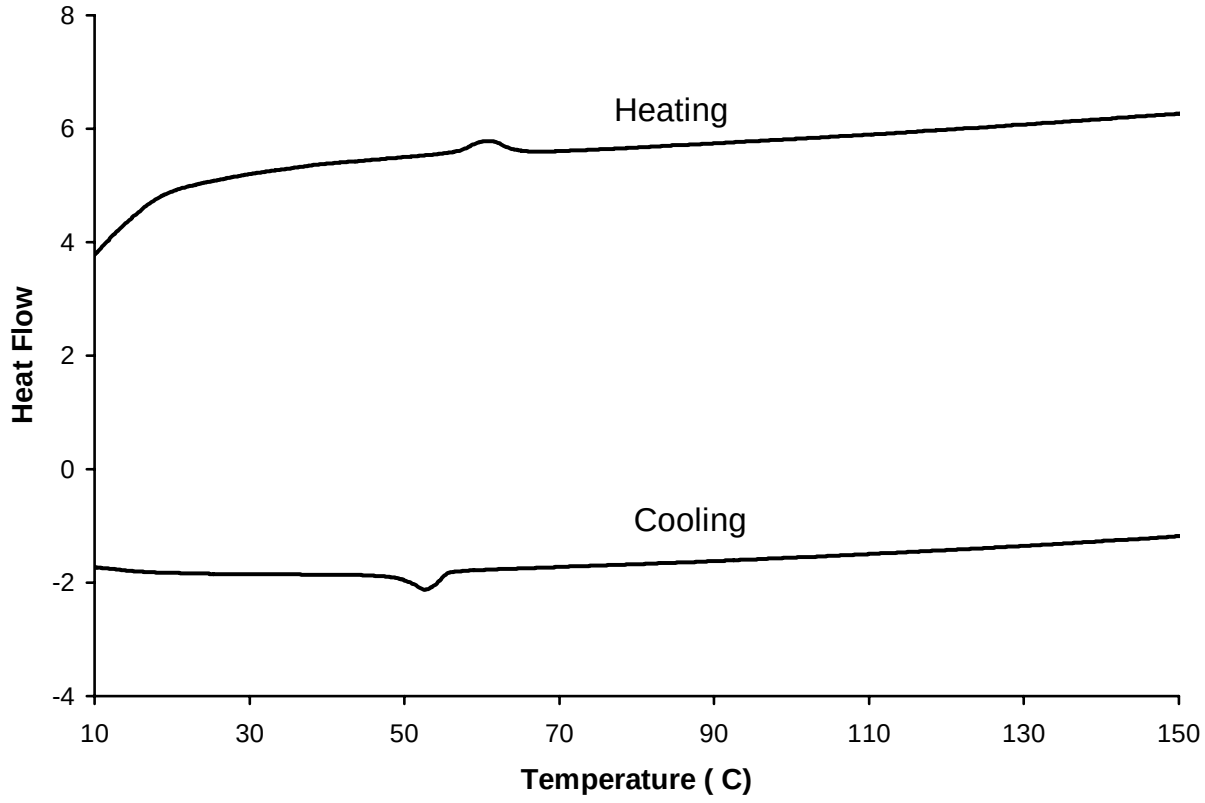

Figure 1.26: DSC trace of p(ehF$_3$M$_{18}$) with a scan rate of 10 ^{o}C per minute.

The difference in phase transition temperature between the segmers and polymers is affected by the number of fluorene repeat units. For longer the repeat fluorene units a smaller difference in N-I transition temperature between the segmer and the respective polymer is observed. Smaller fluorene repeat units show a greater effect from the polymerization of the segmer on the N-I transition. For example, the N-I transition temperature for **p(ehF$_4$M$_{18}$)** is nearly double that of **s(ehF$_4$M$_{18}$)** but the N-I transition temperature for **p(ehF$_6$M$_{18}$)** is less than 10% greater than that of **s(ehF$_6$M$_{18}$)**.

Table 1.5. The nematic to isotropic phase transition for the segmers and polymers as measured by polarized optical microscopy and DSC.

Repeat Unit	POM Segmer N-I (^oC)[a]	POM Polymer N-I (^oC)[b]	DSC Transition Polymer N-I (^oC)[c]
ehF_3M_{18}	RT	62	55
ehF_3M_{10}	65	83	81
ehF_4M_{18}	55	141	143
ehF_4M_{10}	80	151	147
ehF_5M_{18}	202	225	230
ehF_5M_{10}	230	242	247
ehF_6M_{18}	248	269	275
ehF_7M_{18}	> 300	> 300	---

[a]The nematic to isotropic transition temperature for the different lengths of segmers as measured by POM. [b,c]The nematic to isotropic transition temperatures of the polymers with different fluorene and methylene lengths as measured by POM[b] and DSC[c].

The methylene spacer length has a greater effect on the N-I transition temperature for polymers with shorter fluorene units than polymers with longer fluorene units. For **p(ehF$_3$M$_y$)**, a 25% increase in the N-I transition is observed when the methylene spacer is shortened from 18 to 10 carbons. For the **p(ehF$_5$M$_y$)** system, only a 8% increase in the N-I transition is observed when the methylene spacer is shortened from 18 to 10 carbons. The fluorene units are more rigid than the flexible methylene spacers and can have a dominate effect on the N-I transition temperature. The polymers and segmers with longer fluorene repeat units have a higher percentage of fluorenes relative to methylene groups and changes from 10 to 18 methylene units has only a small effect on the N-I transition temperature.

Two random mixed copolymers were also made and compared to RSC polymers to determine the effect of the specific sequence. Figure 1.27 shows the plot of the N-I temperature for pure **p(ehF$_3$M$_{10}$)** and **p(ehF$_5$M$_{10}$)**. The plot also includes the random mixed copolymers of the two segmers one with 10% **s(ehF$_3$M$_{10}$)** and 90% **s(ehF$_5$M$_{10}$)** and the other with 50%

s(ehF$_3$M$_{10}$) and 50% **s(ehF$_5$M$_{10}$)**. The nearly linear relationship indicates that there is no unusual effect on the N-I transition temperature caused by mixing the mesogens. Also, there is only one transition seen in the DSC data for these materials. These results are further proof that the mesophases are caused by the side chain groups and their interactions are not directly dependent on the segmer unit lengths. These results would also add further proof that the mesophase of the polymers is nematic in nature since a change in the mesogen length should cause a greater disruption of the more ordered smectic phase like a suppression in melting points of impure crystals. An advantage of this phenomena is that the N-I phase transition can be varied by mixing of different segmers to obtain a polymer with the desired transition temperatures for processing.

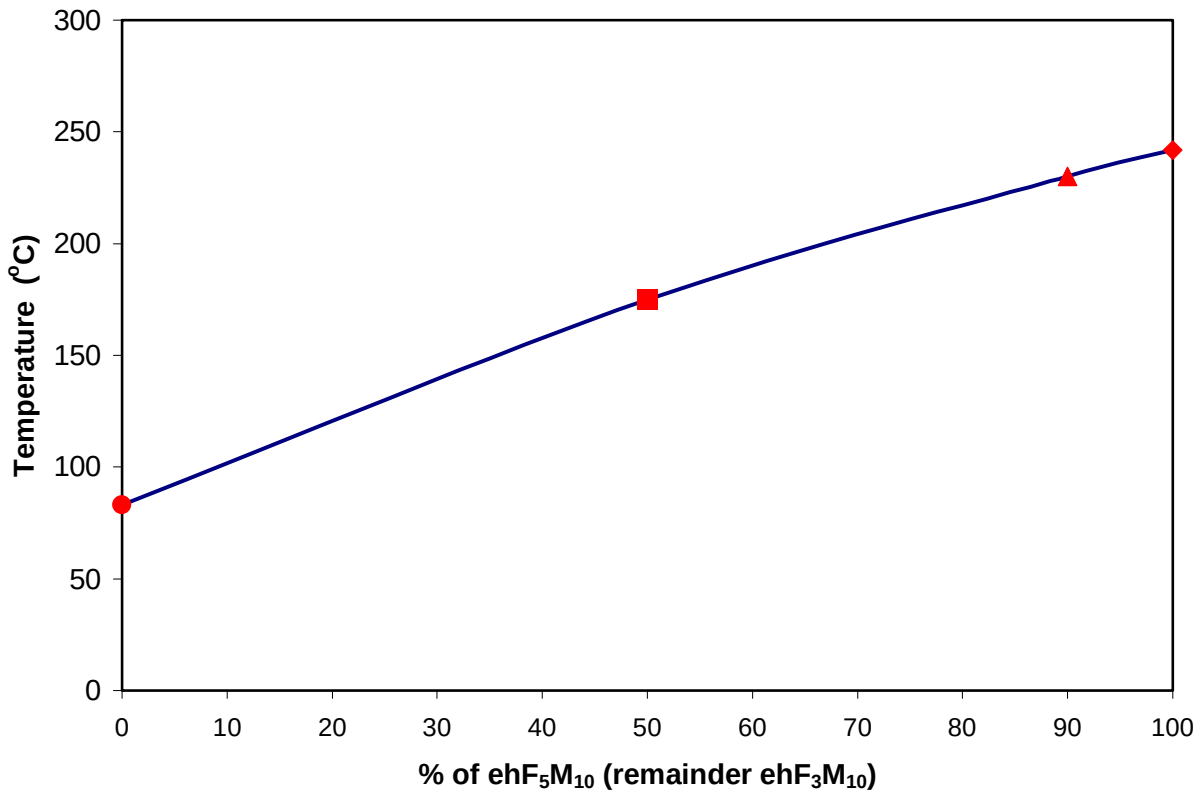

Figure 1.27. The N-I phase transition temperatures for **p(ehF$_3$M$_{10}$)** (circle), **p(50% ehF$_3$M$_{10}$: 50% ehF$_3$M$_{10}$)** (square), **p(10% ehF$_3$M$_{10}$: 90% ehF$_3$M$_{10}$)** (triangle), and **p(ehF$_5$M$_{10}$)** (diamond).

1.5 CONCLUSIONS

A series of 9,9-bis-(2-ethylhexyl)fluorene-co-methylene polymers have been synthesized by methods that allow for exact control over the segment lengths of the fluorene and methylene units independently. The synthesis involved the multi-step procedure to make the fluorene segments with 3-8 repeat units followed by the attachment of arms with terminal olefin groups. These monomers were then polymerized via ADMET and the remaining olefin groups were subsequently hydrogenated. The resulting polymers contained exact fluorene units connected by methylene linkers with exact lengths.

The change of the alkyl group at the 9-position of fluorene from *n*-hexyl to 2-ethylhexyl resulted in polymers that exhibit mesophases as determined by polarized optical microscopy and DSC. The mesophase of the polymers is believed to be nematic in nature based upon previous reports, the Schlieren texture of samples in the liquid crystalline phase, and the results of the polymers made by copolymerization of two different segmers.

The transition temperatures of the repeating sequence copolymers show an increase as the length of the fluorene units is increased and a decrease in transition temperatures are observed as the number of methylene units is increased. These results can be explained by the higher T_g or rigidity of fluorene segments compared to the methylene units. The structures of the RSCs could therefore be varied to fine tune the thermal properties that would be desirable for fabrication and operation of devices. No abnormal results, such as an odd-even effect, were observed for these materials and therefore the precise segment control of the RSCs has a minimal effect on the thermal properties of these polymers.

The exact segment control of the fluorene units allows for control of the absorption and emission maximum of the polymers. The increase in the number of fluorene units results in a

decrease in the both the absorption and emission energies as would be predicted from the increase in conjugation length. Amorphous films of these polymers exhibit emission maximum that can be tuned from 400 nm to 420 nm as the fluorene units are increased from 3 to 8. This control would allow for fine tuning of emission color of OLEDs made with these polymers.

1.6 EXPERIMENTAL

1.6.1 UV- Vis Spectroscopy

The absorption spectra for the **p(ehF$_x$M$_y$)** and **p(F$_x$M$_y$)** series of polymers were obtained in a dilute methylene chloride solution on a Perkin-Elmir UV/VIS/NIR Spectrometer Lamda 9 and analyzed using UV Winlab software.

1.6.2 Emission Spectroscopy

All emission spectra for the **p(ehF$_x$M$_y$)** and **p(F$_x$M$_y$)** series of polymers were made on a Varian Cary Eclipse Fluorescence Spectrophotometer. The solution emission spectra were obtained in dilute methylene chloride solutions and the thin film emission spectra were obtained by dropcasting a dilute solution of the polymer in chloroform onto a quartz slide and removal of solvent by heating at 60 ^{o}C.

1.6.3 Differential Scanning Calorimetry

Differential scanning calorimetry (DSC) was performed on a Perkin-Elmer Pyris 6 using ~10 mg samples. The samples were heated from 0 ^{o}C to typically 250 ^{o}C held for 5 min and then cooled back to 0 ^{o}C at 10 ^{o}C/min. This same heat cycle was repeated and the transition data is reported from the second heat cycle.

1.6.4 Polarized Optical Microscopy

The optical detection of the liquid crystal phase transitions were obtained on an Olympus BH-2 microscope with cross polarizers equipped with a Mettler FP52 hot stage connected to a Mettler FP5 temperature controller. The samples were prepared by dropcasting the sample from a dilute chloroform solution onto a glass slide.

1.6.5 Synthetic Procedures

Toluene was distilled under N_2 from sodium. THF (Fisher, HPLC grade) was passed through activated alumina using a SPS 400 (Innovative Technology). $Pd(PPh_3)_4$ (Strem), $Pd(Cl)_2(PPh_3)_2$ (Strem), and Grubbs I and Grubbs II catalysts (Aldrich) were commercially obtained and stored in a nitrogen-filled glove box. All other reagents were commercially obtained and used without further purification. ^{1}H- (300 MHz) and ^{13}C-NMR (75 MHz) spectra were recorded with Bruker spectrometers. Chemical shifts were referenced to residual ^{1}H or ^{13}C signals in deuterated solvents. Column chromatography was performed using Sorbent 60Å 40-63 μm standard grade silica. GC-MS was performed on a Hewlett Packard Series 5980 GC/5971 A MS with a Hewlett

Packard Series 1 column. GC was performed on a Hewlett Packard Series 6850 GC with a Hewlett Packard Series 1 methyl siloxane column. HRMS were obtained on a Fison VG Autospec in the Mass Spectral Facility of the University of Pittsburgh. GPC data were acquired in THF (HPLC grade, Fisher) on a Waters system equipped with a 515 pump, a U6K universal injector and a 2414 differential refractometer. Separations were achieved at 25° C on Jordi columns eluting at 0.5 mL/min. Elemental analysis was performed independently by Atlantic Microlab, Inc., Norcross, Georgia. Synthesis of Fluorene Intermediates

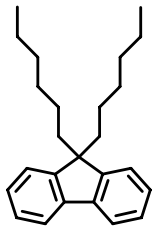

9,9-Dihexylfluorene *rwi1*: According to the methods of Ranger et al.,[84] fluorene (100 g, 0.301 mol) was dissolved in 500 ml of anhydrous THF and cooled to -78 ºC under an N_2 atmosphere. *n*-Butyllithium (2.5 M, 265 ml, 0.662 mol) was added dropwise. After the reaction was allowed to stir for an additional 60 min, 1-bromohexane (140 g, 0.72 mol) was added dropwise. After the reaction was allowed to warm to RT, the reaction was quenched with water. The mixture was washed with diethyl ether (2 x 200 ml). The combined organics were washed with brine, dried over magnesium sulfate, and the solvent removed by rotary evaporation. The product was crystallized from hexanes at -30 ºC to yield the product as colorless crystals (69.5 g, 70 %). ^{1}H (300 MHz, $CDCl_3$) δ 0.58 (b, 4 H), 0.72 (t, 6 H), 1.03 (b 12 H), 1.92 (m, 4 H), 7.28 (m, 6 H), 7.65 (m, 2 H). ^{13}C NMR (75 MHz, $CDCl_3$) δ 14.6, 23.2, 24.3, 30.3, 32.1, 41.0, 55.6, 120.2, 123.5, 127.3, 127.6, 141.7, 151.3. MS (EI) *m/z* 334 ($M^{\cdot+}$) 249, 179, 165.

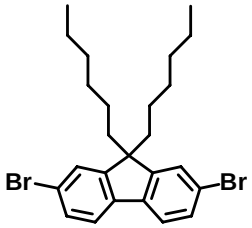

2,7-Dibromo-9,9-dihexylfluorene (Br-F-Br) *rwi3*: According to the methods of Price et al.,[68] 9,9-Dihexylfluorene (69.0 g, 0.207 mol) and $FeCl_3$ (0.5 g) were added to 400 ml $CHCl_3$. The mixture was cooled to 0 ºC and Br_2 (75.9 g, 0.475 mol) in 50 ml $CHCl_3$ was added dropwise over 60 min. The reaction was allowed to warm to RT and after 2 h the reaction was quenched with sodium thiosulfate solution. Water was added and the aqueous layer was washed with $CHCl_3$ (2 x 100 ml). The organic layers were combined and then washed with water, brine, and then dried over magnesium sulfate. The white solid **Br-F-Br** (75.1 g, 80%) was collected by crystallization from hexane at -30ºC. ^{1}H (300 MHz, $CDCl_3$) δ 0.58 (b, 4 H), 0.76 (t, 6 H), 1.04 (b, 12 H), 1.91 (m, 4H), 7.47 (m, 6 H). ^{13}C NMR (75 MHz, $CDCl_3$) δ 14.6, 23.2, 24.2, 30.2, 32.1, 40.8, 56.3, 121.7, 122.1, 126.8, 130.8, 139.7, 153.2.

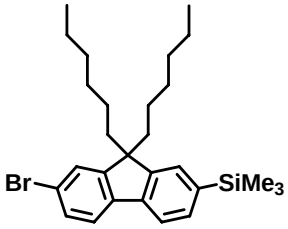

Br-F-Si *rwi2*: Adapting the method of Geng et al.,[53] 2,7-dibromo-9,9-dihexylfluorene (60.0 g, 0.122 mol) and 400 ml of anhydrous THFwere added to a flame dried flask and cooled to -78 ºC under an N_2 atmosphere. *n*-Butyllithium (2.5 M, 48.7 ml, 0.122 mol) was added dropwise and the reaction mixture was allowed to stir an additional 60 min before chlorotrimethylsilane (14.6 g, 0.134 mol) was added dropwise. After warming to RT, the reaction was quenched with water and the aqueous layer was washed with hexanes (3 x 100 ml). The organic layers were

combined, washed with brine, and dried over magnesium sulfate. The solvent was removed and the product was purified by Kugelrohr distillation at 200 ºC to yield **Br-F-Si** as a clear oil (57.1 g, 80%). ^{1}H (300 MHz, CDCl3) δ 0.31 (s, 9 H), 0.77 (m, 6H), 1.05 (b, 12 H), 1.92 (m, 4 H), 7.4-7.7 (m, 6H). ^{13}C NMR (75 MHz, $CDCl_3$) δ 14.6, 23.1, 23.2, 24.2, 24.3, 30.1, 30.2, 32.0, 32.1, 56.0, 119.6, 121.7, 126.8, 128.2, 130.5, 132.6, 140.2, 140.7, 141.3, 150.1, 153.8 MS (EI) *m/z* 486 ($M^{\cdot+}$), 471, 399, 315.

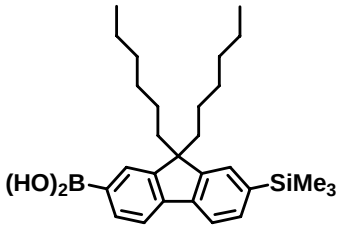

B-F-Si *rwi4*: Adapting the method of Geng et al.,[53] **Br-F-Si** (24.0 g, 49.4 mmol) and 150 ml of anhydrous THFwere added to a flame dried flask and cooled to -78 ºC under an N_2 atmosphere. *n*-Butyllithium (2.5 M 25.6 ml, 64 mmol) was added dropwise and the reaction was allowed to stir an additional 60 min before triisopropyl borate (13.0 g, 69.2 mmol) was added over 5 min. After warming to RT, the reaction was quenched with water and the aqueous layer was washed with diethyl ether (3 x 100 ml). The organic layers were combined, washed with brine, and dried over magnesium sulfate. The solvent was removed and the product was purified by column chromatography (silica gel, 100% hexanes then 40% ethyl acetate / hexanes as the eluent) to yield **B-F-Si** as a clear oil (19.1 g, 81%). ^{1}H (300 MHz, CDCl3) δ 0.36 (b, 9 H), 0.75 (t, 8 H), 1.11 (b, 12 H), 2.1 (t, 4 H), 7.56 (m, 3 H), 7.81 (d, 1 H), 7.91 (d, 1H), 8.25 (s, 1 H), 8.33 (pd, 2 H). ^{13}C NMR (75 MHz, $CDCl_3$) δ 14.6, 23.1, 23.2, 24.4, 30.2, 32.0, 40.8, 55.6, 120.0, 120.3, 128.4, 130.4, 132.5, 135.2, 140.8, 142.0, 146.2, 151.0, 151.4. MS (EI) *m/z* 406 (loss of $B(OH)_2$) ($M^{\cdot+}$) 391, 321, 235.

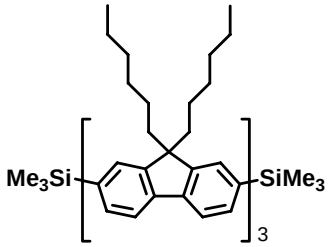

Si-F$_3$-Si *rwi5*: Adapting the method of Geng et al.,[53] **B-F-Si** (5.0 g, 10.2 mmol), **Br-F-Br** (11.4 g, 25.4 mmol), $Pd(PPh_3)_4$ (0.70 g, 0.61 mmol), K_2CO_3 (5.6 g, 41 mmol), 150 ml of toluene, and 50 ml ethanol were added to a Schlenk flask under an N_2 atmosphere. The mixture was heated to reflux for 20 h before water was added and the aqueous layer was washed with toluene (2 x 100 ml). The organic layers were combined, washed with brine, and dried over magnesium sulfate. The product was purified by column chromatography (Silica gel, 100% hexanes then 10% CH_2Cl_2/hexanes as the eluent) to yield **Si-F$_3$-Si** as a clear, glassy solid (10.8 g, 93%). ^{1}H (300 MHz, $CDCl_3$) δ 0.36 (b, 18 H), 0.75 (t, 25 H), 1.11 (b, 36 H), 2.1 (t, 12 H), 7.50-7.9 (m, 18 H). ^{13}C NMR (75 MHz, $CDCl_3$) δ 14.6, 23.1, 23.2, 24.4, 24.5, 30.2, 30.3, 32.0, 32.1, 40.8, 40.1, 55.7, 55.9, 119.6, 120.6, 120.6, 122.1, 126.6, 126.8, 128.3, 132.5, 139.6, 140.6, 140.9, 141.2, 141.3, 142.1, 150.8, 152.3, 152.4.

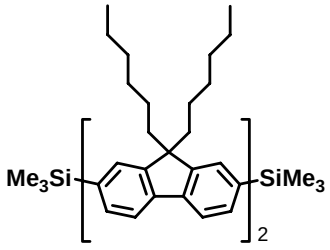

Si-F$_2$-Si *rwi7*: Adapting the method of Geng et al.,[53] **B-F-Si** (5.55 g, 12.3 mmol), **Br-F-Si** (5.0 g, 10.3 mmol), $Pd(PPh_3)_4$ (0.35 g, 0.311 mmol), K_2CO_3 (2,84 g, 2.06 mmol), 150 ml toluene, and 50 ml ethanol were added to a Schlenk flask under an N_2 atmosphere. The mixture was heated to reflux under a N_2 atmosphere for 20 h before water was added and aqueous layer was washed with toluene (3 x 50 ml). The organic layers were combined, washed with brine, and dried over

magnesium sulfate. The product was purified by column chromatography (Silica gel, 100% hexanes then 5% CH_2Cl_2/hexanes then 10% CH_2Cl_2/hexanes as the eluent) to yield **Si-F$_2$-Si** as a clear, glassy solid (5.5 g, 66%). ^{1}H (300 MHz, $CDCl_3$) δ 0.36 (b, 18 H), 0.75 (t, 25 H), 1.11 (b, 36 H), 2.1 (t, 12 H), 7.50-7.9 (m, 18 H). ^{13}C NMR (75 MHz, $CDCl_3$) δ 14.6, 23.1, 23.2, 24.3, 30.2, 30.3, 32.0, 32.1, 40.7, 55.7, 119.6, 120.5, 122.1, 126.6, 128.2, 132.4, 139.5, 140.6, 140.9, 141.2, 141.3, 142.0, 150.8, 152.3.

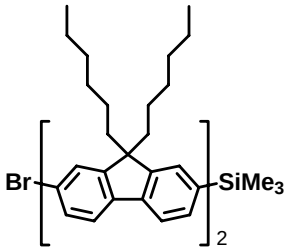

Br-F$_2$-Si *rwi8*: Adapting the method of Geng et al.,[53] **Br-F-Br** (5.0 g, 10.2 mmol), **B-F-Si** (3.4 g, 7.6 mmol), $Pd(PPh_3)_4$ (0.18 g, 0.15 mmol), K_2CO_3 (1.4 g, 10.2 mmol), 150 ml toluene, and 50 ml ethanol were added to a Schlenk flask under an N_2 atmosphere. The mixture was heated to reflux under a N_2 atmosphere for 24 h before water was added and the aqueous layer was washed with toluene (2 x 100 ml). The organic layers were combined, washed with brine and dried over magnesium sulfate. The product was purified by column chromatography (Silica gel, 100% hexanes then 10% CH_2Cl_2 / hexanes as the eluent) to yield **Br-F$_2$-Si** as a clear, glassy solid (2.7 g, 44%). ^{1}H (300 MHz, $CDCl_3$) δ 0.36 (b, 6 H), 0.83 (t, 18 H), 1.15 (b, 22 H), 2.1 (t, 8 H), 7.50-7.9 (m, 12 H). ^{13}C NMR (75 MHz, $CDCl_3$) δ 14.7, 23.2, 23.2, 24.2, 30.2, 30.3, 32.0, 32.1, 40.8, 41.0, 55.8, 56.2, 119.8, 120.7, 120.7, 121.7, 121.7, 122.1, 122.2, 126.7, 126.9, 127.0, 128.3, 130.7, 132.6 139.7, 139.9, 140.6, 141.1, 141.8, 142.1, 150.9, 151.8, 152.4, 153.9.

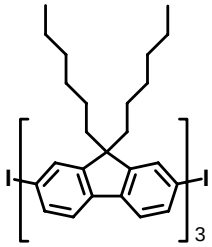

I-F$_3$-I *rwi9*: Adapting the method of Geng et al.,[53] **Si-F$_3$-Si** (10.0 g, 8.8 mmol) and CH_2Cl_2 (100 ml) were added to a round bottom flask and cooled in an ice bath. Iodine monochloride (2.84 g, 17.5 mmol) in CH_2Cl_2 (20 ml) was added dropwise over 10 min. After warming to RT, the reaction was quenched with a solution of sodium thiosulfate. The CH_2Cl_2 layer was washed with water, brine, and then dried over magnesium sulfate. The product was crystallized from CH_2Cl_2 and hexane mixture to yield **I-F$_3$-I** as a white solid (8.1 g, 73%) after filtration. ^{1}H (300 MHz, $CDCl_3$) δ 0.83 (t, 32 H), 1.15 (b, 36 H), 2.1 (m, 12 H), 7.50-7.9 (m, 18 H). ^{13}C NMR (75 MHz, $CDCl_3$) δ 14.2, 20.7, 22.6, 23.8, 29.6, 31.5, 40.3, 55.5, 92.5, 120.1, 121.4, 151.5, 126.2, 126.3, 132.1, 135.9, 139.3, 140.1, 140.4, 140.5, 141.2, 150.9, 151.8, 153.5.

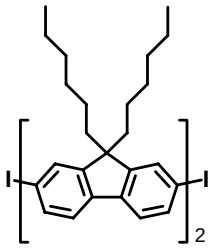

I-F$_2$-I *rwi10*: Adapting the method of Geng et al.,[53] **Si-F$_2$-Si** (5.4 g, 6.7 mmol) and CH_2Cl_2 (200 ml) were added to a round bottom flask and cooled in an ice bath. Iodine monochloride (2.16 g, 13.3 mmol) in CH_2Cl_2 (20 ml) was added dropwise over 10 min. After warming to RT, the reaction mixture was quenched with a solution of sodium thiosulfate. The CH_2Cl_2 layer was washed with water, brine, and then dried over magnesium sulfate. The product was crystallized from hexanes to yield **I-F$_2$-I** as a white solid (4.2g, 69%) after filtration. ^{1}H (300 MHz, CDCl3) δ 0.83 (t, 21 H), 1.15 (b, 25 H), 2.1 (m, 8 H), 7.50-7.9 (m, 12 H). ^{13}C NMR (75 MHz, $CDCl_3$) δ

14.6, 23.1, 24.3, 30.2, 32.0, 40.8, 56.1, 93.1, 120.7, 122.0, 122.1, 126.9, 132.7, 136.5, 140.0, 141.0, 141.6, 151.5, 154.0.

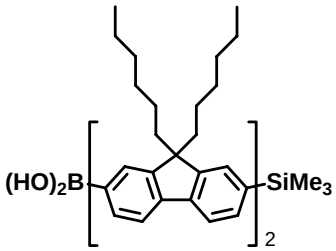

B-F$_2$-Si *rwi11*: Adapting the method of Geng et al,[53] **Si-F$_2$-Br** (3.6 g, 4.4 mmol) and 30 ml of anhydrous THF were added to a flame dried flask and cooled to -78 ºC in a N_2 atmosphere. *n*-Butyllithium (2.5 M 2.2 ml, 5.7 mmol) was added dropwise and the reaction was allowed to stir an additional 60 min before triisopropyl borate (13.0 g, 69.2 mmol) was added all at once. After warming to RT, the reaction was quenched with dilute hydrochloric acid and the aqueous layer was washed with diethyl ether (2 x 50 ml). The organic layers were combined, washed with brine, and then dried over magnesium sulfate. The solvent was removed and the product was purified by column chromatography (silica gel, 100% hexanes then 40% ethyl acetate / hexanes as the eluent) to yield **B-F$_2$-Si** as a clear oil (2.8 g, 82%). ^{1}H (300 MHz, $CDCl_3$) δ 0.33 (s, 9 H), 0.80 (b, 23 H), 1.11 (b, 29 H), 2.1 (t, 4 H), 2.2 (b, 4 H) 7.5-8.0 (m, 12 H), 8.25 (s, 1 H), 8.33 (d, 1 H). ^{13}C NMR (75 MHz, $CDCl_3$) δ -0.2, 14.6, 23.1, 23.2, 24.4, 24.5, 30.2, 30.4, 32.0, 32.1, 40.7, 41.0, 55.7, 55.8, 119.7, 120.0, 120.7, 121.3, 122.2, 126.7, 128.3, 128.4, 132.5, 132.4, 139.7, 140.5, 141.1, 142.0, 142.1, 145.9, 150.8, 151.6, 152.4, 153.0.

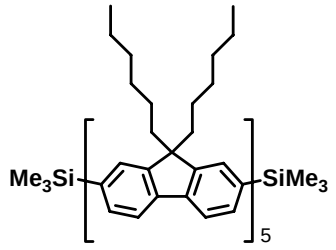

Si-F$_5$-Si *rwi13*: According the method of Geng et al.,[53] **B-F-Si** (3.0 g, 6.7 mmol), **I-F$_3$-I** (3.78 g, 3.0 mmol), $Pd(PPh_3)_4$ (0.10 g, 3 mol %), K_2CO_3 (5.6 g, 41 mmol), TBABr (0.29 g, 0.9 mmol), 50 ml of toluene, and 20 ml water were added to a Schlenk flask under N_2. The mixture was heated to reflux for 18 h under an N_2 atmosphere before water was added and the aqueous layer was washed with diethyl ether (3 x 50 ml). The organic layers were combined, washed with brine, and then dried over magnesium sulfate. The product was purified by column chromatography (Silica gel, 100% hexanes then 20% CH_2Cl_2 / hexanes as the eluent) to yield **Si-F$_5$-Si** as a clear, glassy solid (4.0 g, 74%). ^{1}H (300 MHz, $CDCl_3$) δ 0.33 (s, 18 H), 0.80 (b, 50 H), 1.11 (b, 60 H), 2.1 (b, 20 H), 7.5-8.0 (m, 30 H) ^{13}C NMR (75 MHz, $CDCl_3$) δ -0.2, 14.6, 23.1, 23.2, 24.4, 24.5, 30.2, 30.3, 32.0, 32.1, 40.8, 41.0, 55.7, 56.0, 119.6, 120.6, 122.2, 126.7, 126.8, 128.3, 132.5, 139.6, 140.7, 140.9, 141.1, 141.3, 142.1, 150.8, 152.3, 152.4.

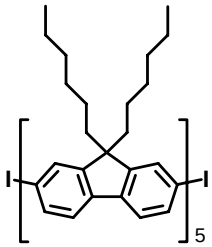

I-F$_5$-I *rwi15*: According the method of Geng et al.,[53] **Si-F$_5$-Si** (3.9 g, 2.2 mmol) and CH_2Cl_2 (30 ml) were added to a round bottom flask. After cooling in an ice bath, iodine monochloride (0.73 g, 4.5 mmol) in CH_2Cl_2 (10 ml) was added dropwise over 10 min. After warming to RT, the reaction was quenched with a solution of sodium thiosulfate and the aqueous layer was washed with CH_2Cl_2 (3 x 30 ml). The combined organic layers were washed with water, brine, and then dried over magnesium sulfate. The product was purified by column chromatography (Silica gel, 90% hexanes / CH_2Cl_2 as the eluent) to yield **I-F$_5$-I** as a clear, glassy solid (3.5 g, 85%). ^{1}H (300 MHz, $CDCl_3$) δ 0.8 (b, 50 H), 1.14 (b, 60 H), 2.1 (m, 20 H), 7.40-7.9 (m, 30 H). ^{13}C NMR (75

MHz, $CDCl_3$) δ 14.1, 22.6, 23.8, 23.9, 29.7, 31.5, 40.3, 40.4, 55.4, 55.5, 92.5, 120.0, 121.6, 126.2, 132.2, 135.9, 139.3, 140.0, 140.2, 140.3, 140.5, 140.6, 141.2, 151.0, 151.8, 153.5.

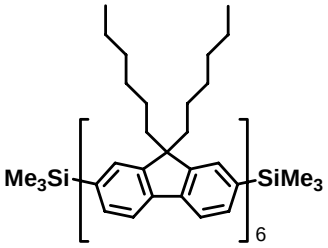

Si-F_6-Si *rwi17*: According the method of Geng et al,[53] **B-F_2-Si** (2.7 g, 3.5 mmol), **Br-F_2-Si** (1.44 g, 1.6 mmol), $Pd(PPh_3)_4$ (0.07 g, 4 mol%), K_2CO_3 (0.87 g, 6.3 mmol), TBABr (0.15 g, 30 mol%), 20 ml of toluene, and 10 ml water were added to a Schlenk flask under an N_2 atmosphere. The mixture was heated to reflux for 24 h before water was added and the aqueous layer was washed with diethyl ether (3 x 50 ml). The organic layers were combined and washed with brine and then dried over magnesium sulfate. The product was purified by column chromatography (silica gel, 100% hexanes then 20% CH_2Cl_2 / hexanes as the eluent) to yield **Si-F_6-Si** as a white solid (2.1 g, 62%). ^{1}H (300 MHz, $CDCl_3$) δ 0.36 (b, 18 H), 0.75 (b, 60 H), 1.11 (b, 72 H), 2.1 (b, 24 H), 7.50-7.9 (m, 36 H). ^{13}C NMR (75 MHz, $CDCl_3$) δ -0.2, 14.6, 23.1, 23.2, 24.3, 24.5, 30.2, 30.3, 32.0, 32.1, 40.7, 41.0.1, 55.7, 55.9, 119.6, 120.6, 122.1, 126.6, 126.8, 128.3, 132.5, 139.6, 140.6, 140.9, 141.2, 141.3, 142.0, 150.8, 152.4

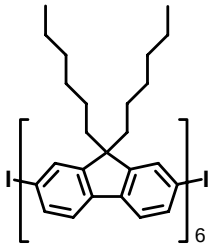

I-F_6-I *rwi19*: According the method of Geng et al.,[53] **Si-F_6-Si** (1.0 g, 0.5 mmol) and CH_2Cl_2 (10 ml) were to a round bottom flask. After cooling in an ice bath, iodine monochloride (1 M in CH_2Cl_2, 1.0 ml, 1.0 mmol) was added dropwise over 10 min before the reaction was allowed to

warm to RT. The reaction was then quenched with a solution of sodium thiosulfate and the aqueous layer was washed with CH_2Cl_2 (3 x 30 ml). The combined organic layers were washed with water, brine, and then dried over magnesium sulfate. The product was purified by column chromatography (silica gel, 90% hexanes / CH_2Cl_2 as the eluent) to yield **I-F_6-I** as a white solid (0.81 g, 81%). ^{1}H (300 MHz, $CDCl_3$) δ 0.81 (b, 60 H), 1.13 (b, 72 H), 2.1 (b, 24 H), 7.40-7.9 (m, 36 H). ^{13}C NMR (75 MHz, $CDCl_3$) δ 14.61, 22.6, 23.8, 23.9, 29.7, 31.5, 40.3, 40.4, 55.4, 55.5, 92.5, 120.0, 121.6, 126.2, 132.1, 135.9, 139.3, 139.9, 140.0, 140.2, 140.3, 140.5, 140.6, 141.2, 150.9, 151.8, 153.5

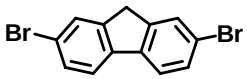

2,7-dibromofluorene *rwi59*: Adapting the method of Price et al.,[68] fluorene (100.0 g, 0.6 mol), $FeCl_3$ (100 mg), and 500 ml chloroform were added to a round bottom flask and cooled in an ice bath. Bromine (202 g, 1.26 mol) was added dropwise over 60 min and the reaction was allowed to warm RT. The reaction was then quenched with sodium thiosulfate and the aqueous layer was washed with chloroform (3 x 200 ml). The organic layers were combined and dried over magnesium sulfate before the solvent volume was reduced and hexane was added to induce crystallization. 2,7-dibromofluorene was collected as white crystals (170 g, 88%). ^{1}H (300 MHz, $CDCl_3$) δ 3.82 (s, 2 H) 7.3-7.7 (m, 6 H) ^{13}C NMR (75 MHz, $CDCl_3$) δ 31.2, 121.6, 121.8, 128.9, 130.8, 140.3, 145.4.

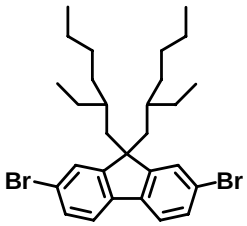

Br-ehF-Br *rwi62*: 2,7-dibromofluorene (50 g, 0.154 mol), 2-ethylhexyl bromide (89 g, 0.462 mol), KOH (64 g, 1.23 mol), TBABr (5 g, 15.4 mmol), 100 ml toluene, and 100 ml water were added to a Schlenk flask. The mixture was heated to 80 ºC under an N_2 atmosphere for 2 h. before water was added and the aqueous layer was washed with hexanes (2 x 100 ml). The combined organic layers were washed with brine and then dried over magnesium sulfate. **Br-ehF-Br** was purified by column chromatography (silica gel, 100% hexanes as the eluent) to yield a clear solid (85 g, 100%). ^{1}H (300 MHz, $CDCl_3$) δ 0.4-0.6 (m, 8 H), 0.6-1.0 (b, 22 H), 1.92 (d, 4 H, J = 5.4 Hz), 7.3-7.5 (m, 6 H). ^{13}C NMR (75 MHz, $CDCl_3$) δ 10.3, 14.0, 22.7, 27.1, 28.0, 28.1, 33.6, 34.7, 44.4, 55.4, 120.9, 127.3, 127.5, 130.1, 139.2, 152.5.

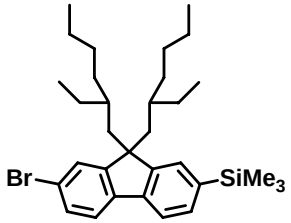

Br-ehF-Si *rwi63*: According to the method of Geng et al,[53] **Br-ehF-Br** (100 g, 0.182 mol) and 300 ml of anhydrous THFwere added to a flame dried flask and cooled to -78 ºC under an N_2 atmosphere before *n*-Butyllithium (1.6 M, 114 ml, 0.182 mol) was added dropwise. After the reaction was allowed to stir an additional 60 min, chlorotrimethylsilane (23.7 g, 0.218 mol) was added dropwise. After warming to RT and the reaction was quenched with water and the aqueous layer was washed with hexanes (2 x 100 ml). The organic layers were combined, washed with brine, and dried over magnesium sulfate. The product was purified by column chromatography (silica gel, 100% hexanes as the eluent) to yield **Br-ehF-Si** as a clear solid (90 g, 91%). ^{1}H (300 MHz, $CDCl_3$) δ 0.30 (s, 9 H), 0.4-0.6 (m, 8 H), 0.6-1.0 (b, 22 H), 1.97 (m, 4 H), 7.4-7.6 (m, 6 H). ^{13}C NMR (75 MHz, $CDCl_3$) δ -0.5, 10.9, 14.6, 23.3, 27.7, 27.8, 28.8, 29.0,

34.4, 34.8, 35.0, 35.2, 35.3, 44.6, 44.9, 55.7, 119.5, 121.1, 121.2, 127.9, 128.0, 128.1, 129.6, 130.4, 132.4, 132.5, 139.4, 140.9, 141.4, 149.5, 153.5.

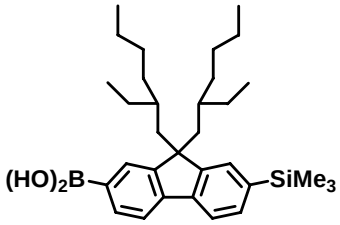

B-ehF-Si *rwi65*: According to the method of Geng et al,[53] **Br-ehF-Si** (80 g, 0.140 mol) and 300 ml of anhydrous THF were added to a flame dried flask and cooled to -78 ºC under an N_2 atmosphere. *n*-Butyllithium (1.6 M, 105 ml, 0.168 mol) was added dropwise over 30 min. After the reaction was allowed to stir an additional 60 min, triisopropyl borate (38.4 g, 0.196 mol) was added over 5 min. After warming to RT and the reaction was quenched with dilute hydrochloric acid and the aqueous layer was washed with diethyl ether (2 x 100 ml). The organic layers were combined, washed with brine, and dried over magnesium sulfate. The product was purified by column chromatography (silica gel, 100% hexanes then 50% ethyl acetate / hexanes as the eluent) to yield **B-ehF-Si** as a clear solid (60 g, 77%). ^{1}H (300 MHz, $CDCl_3$) δ 0.30 (s, 9 H), 0.4-0.6 (m, 30 H), 1.97 (m, 4 H), 7.4-8.0 (m, 6 H), 8.29 (m, 2 H). ^{13}C NMR (75 MHz, $CDCl_3$) δ -1.0, 10.3, 14.0, 22.6, 22.8, 27.1, 27.2, 28.3, 34.1, 34.1, 34.3, 34.7, 34.9, 44.2, 44.4, 54.9, 119.3, 119.6, 129.2, 131.2, 131.7, 134.4, 139.3, 141.7, 145.7, 149.9, 150.3.

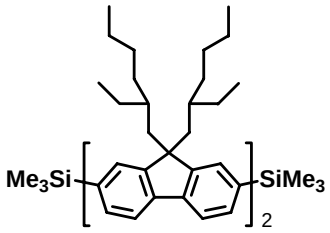

Si-ehF$_2$-Si *rwi64*: According to the method of Geng et al,[53] **Br-ehF-Si** (9.5 g, 17.5 mmol), **B-ehF-Si** (10.6 g, 21 mmol), K_2CO_3 (2 M, 35 ml, 70 mmol), $Pd(PPh_3)_4$ (0.41, 2 mol%), TBABr

(1.7 g, 5.3 mmol) and 100 ml of toluene were added to a Schlenk flask under an N_2 atmosphere. The mixture was heated to 75 ºC for 24 h before water was added and the aqueous layer was washed with hexane (2 x 100 ml). The organic layers were combined, washed with brine, and dried over magnesium sulfate. The product was purified by column chromatography (silica gel, 100% hexanes then 10% CH_2Cl_2 / hexanes as the eluent) to yield **Si-ehF$_2$-Si** as a clear solid (15.5 g, 86%). ^{1}H (300 MHz, $CDCl_3$) δ 0.31 (s, 18 H), 0.4-1.2 (m, 60 H), 2.06 (m, 8 H), 7.4-7.8 (m, 12 H). ^{13}C NMR (75 MHz, $CDCl_3$) δ -0.4, 10.9, 14.6, 14.7, 23.4, 23.4, 27.6, 27.6, 27.8, 28.9, 29.0, 34.7, 34.8, 35.0, 35.3, 44.8, 55.6, 119.4, 119.5, 120.5, 123.5, 123.5, 123.6, 123.7, 126.7, 126.8, 129.6, 132.2, 132.3, 132.4, 138.6, 141.0, 141.2, 142.4, 150.2, 151.7.

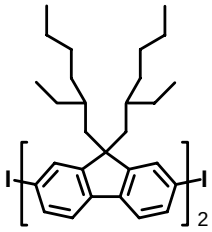

I-ehF$_2$-I *rwi66*: According to the method of Geng et al.,[53] Added **Si-ehF$_2$-Si** (14.2 g, 13.8 mmol) and CH_2Cl_2 (200 ml) to a round bottom flask and cooled in an ice bath before iodine monochloride (4.9 g, 30.3 mmol) in CH_2Cl_2 (50 ml) were added dropwise over 10 min. After warming to RT and the reaction was quenched with a solution of sodium thiosulfate, the CH_2Cl_2 layer was washed with water then brine and then dried over magnesium sulfate. The product was purified by column chromatography (silica gel, 100% hexanes then 10% CH_2Cl_2 / hexanes as the eluent) to yield **I-ehF$_2$-I** as a clear solid (12.8 g, 90%). ^{1}H (300 MHz, $CDCl_3$) δ 0.4-1.2 (b, 60 H), 2.06 (m, 12 H), 7.4-7.8 (m, 12H). ^{13}C NMR (75 MHz, $CDCl_3$) δ 10.3, 10.5, 14.0, 14.2, 22.7, 22.8, 27.1, 27.2, 28.1, 28.2, 33.8, 34.0, 34.7, 44.2, 44.4, 55.2, 91.7, 120.0, 121.3, 122.7, 122.8, 122.8, 122.9, 126.1, 126.3, 126.4, 127.2, 128.8, 133.3, 133.4, 135.8, 139.4, 140.6, 140.8, 140.9, 150.4, 150.5, 153.2.

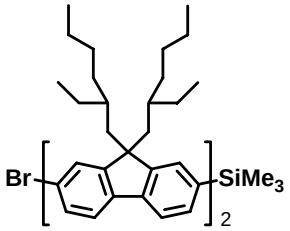

Br-ehF$_2$-Si *rwi70*: According to the method of Geng et al.,[53] **Br-ehF-Br** (5.0 g, 9.1 mmol), **B-ehF-Si** (2.3 g, 4.6 mmol), K_2CO_3 (2.53 g, 18.4 mmol), $Pd(PPh_3)_4$ (0.16 g, 3 mol%), 20 ml of toluene, and 10 ml ethanol were added to a Schlenk flask under N_2. The mixture was heated to reflux for 18 h before water was added and the aqueous layer was washed with hexane (2 x 50 ml). The organic layers were combined, washed with brine, and dried over magnesium sulfate. The product was purified by column chromatography (silica gel, 100% hexanes then 10% CH_2Cl_2 / hexanes as the eluent) to yield **Br-ehF$_2$-Si** as a clear solid (2.05 g, 49%). ^{1}H (300 MHz, $CDCl_3$) δ 0.30 (s, 9 H), 0.4-1.0 (b, 60 H), 2.02 (m, 8 H), 7.4-7.7 (m, 12 H). ^{13}C NMR (75 MHz, $CDCl_3$) δ -1.0, 10.3, 10.4, 14.0, 22.7, 27.1, 27.2, 28.1, 28.2, 28.4, 31.6, 33.8, 33.9, 34.0, 34.2, 34.4, 34.7, 44.2, 44.6, 55.0, 55.3, 118.8, 118.9, 119.9, 120.4, 120.9, 122.8, 123.0, 125.9, 126.0, 126.3, 126.4, 127.4, 127.5, 129.0, 131.7, 138.1, 139.2, 140.1, 140.6, 140.8, 141.0, 141.7, 149.6, 150.6, 151.1, 153.0.

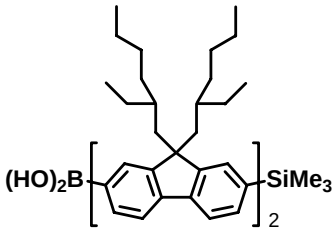

B-ehF$_2$-Si *rwi29*: According to the method of Geng et al.,[53] **Br-ehF$_2$-Si** (3.1 g, 3.3 mol) and 50 ml of anhydrous THF were added to a flame dried flask and cooled to -78 ºC under a N_2 atmosphere. *n*-Butyllithium (1.6 M, 2.5 ml, 4 mmol) was added dropwise. After the reaction was allowed to stir an additional 60 min, triisopropyl borate (0.88 g, 4.7 mmol) was added over 5

min. After warming to RT, the reaction was quenched with dilute hydrochloric acid and the aqueous layer was washed with diethyl ether (3 x 100 ml). The organic layers were combined, washed with brine, and dried over magnesium sulfate. The product was purified by column chromatography (silica gel, 100% hexanes then 50% ethyl acetate / hexanes as the eluent) to yield a clear solid (1.5 g, 50%). ^{1}H (300 MHz, $CDCl_3$) δ 0.0.31 (s, 9 H), 0.66-1.00 (m, 60 H), 2.06-2.24 (b, 8 H), 7.48-7.92 (m, 10 H), 8.32 (m, 2 H). ^{13}C NMR (75 MHz, $CDCl_3$) δ 10.3, 10.5, 14.0, 22.7, 22.8, 27.0, 27.2, 28.1, 28.4, 34.0, 34.4, 34.6, 44.2, 54.9, 118.9, 119.2, 119.9, 120.5, 123.1, 126.1, 128.3, 129.0, 131.1, 131.7, 134.6, 138.1, 140.0, 140.3, 140.6, 141.2, 141.7, 145.5, 149.6, 150.0, 151.1, 152.0.

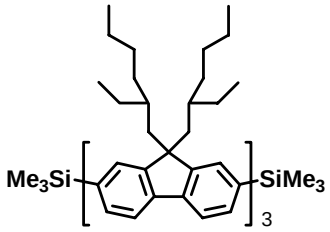

Si-ehF$_3$-Si *rwi54*: According to the method of Geng et al.,[53] **Br-ehF-Br** (10.0 g, 18.3 mmol), **B-ehF-Si** (23.7 g, 44 mmol), K_2CO_3 (10.1 g, 73 mmol), $Pd(PPh_3)_4$ (1.27 g, 6 mol%), 100 ml of toluene, and 50 ml ethanol were added to a Schlenk flask under N_2. The mixture was heated to reflux for 18 h before water was added and the aqueous layer was washed with hexane (3 x 50 ml). The organic layers were combined, washed with brine, and dried over magnesium sulfate. The product was purified by column chromatography (silica gel, 100% hexanes then 10% CH_2Cl_2 / hexanes as the eluent) to yield **Si-ehF$_3$-Si** as a clear solid (20.2 g, 85%). ^{1}H (300 MHz, $CDCl_3$) δ 0.31 (s, 18 H), 0.4-1.2 (b, 90 H), 2.06 (m, 12 H), 7.4-7.8 (m, 18H). ^{13}C NMR (75 MHz, $CDCl_3$) δ -0.4, 10.9, 14.6, 23.4, 27.6, 27.8, 29.0, 32.2, 34.8, 35.0, 35.3, 44.3, 55.5, 55.7, 119.5, 120.4, 123.5, 123.6, 126.6, 129.6, 132.3, 138.6, 140.7, 141.0, 142.4, 150.2, 151.8.

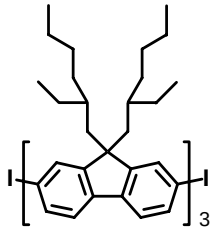

I-ehF$_3$-I *rwi56*: According to the method of Geng,[53] **Si-ehF$_3$-Si** (25.0 g, 19 mmol) and CH_2Cl_2 (200 ml) were added to a round bottom flask and cooled in an ice bath. Iodine monochloride (1 M in CH_2Cl_2, 42 ml, 42 mmol) was added dropwise over 30 min. After warming to RT, the reaction was quenched with a solution of sodium thiosulfate. The CH_2Cl_2 layer was washed with water, brine, and then dried over magnesium sulfate. The product was purified by column chromatography (silica gel, 100% hexanes then 5% CH_2Cl_2 / hexanes as the eluent) to yield **I-ehF$_3$-I** as a clear solid (20.1 g, 74%). ^{1}H (300 MHz, $CDCl_3$) δ 0.4-1.2 (b, 90 H), 2.06 (b, 12 H), 7.4-7.8 (m, 18H). ^{13}C NMR (75 MHz, $CDCl_3$) δ 11.5,14.0, 14.2, 22.8, 26.9, 27.1, 28.1, 28.2, 28.3, 31.6, 33.9, 34.0, 34.7, 44.1, 44.4, 55.0, 55.1, 55.2, 91.6, 199.6, 119.9, 120.0, 121.3, 122.7, 122.9, 124.1, 126.1, 126.3, 126.4, 126.8, 133.3, 133.4, 135.8, 139.3, 140.0, 140.1, 140.2, 140.7, 140.9, 141.0, 150.4, 151.0, 151.2, 153.2

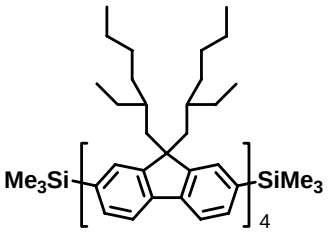

Si-ehF$_4$-Si *rwi71*: According to the method of Geng et al.,[53] **I-ehF$_2$-I** (6.0 g, 5.8 mmol), **B-ehF-Si** (6.5 g, 12.8 mmol), K_2CO_3 (2 M, 12 ml, 23 mmol), $Pd(PPh_3)_4$ (0.20, 3 mol%), TBABr (0.56 g, 1.7 mmol) and 50 ml of toluene were added to a Schlenk flask under N_2. The mixture was heated to 80 ºC for 24 h before water was added and the aqueous layer was washed with hexane (2 x 100 ml). The organic layers were combined, washed with brine, and dried over magnesium

sulfate. The product was purified by column chromatography (silica gel, 100% hexanes then 10% CH_2Cl_2 / hexanes as the eluent) to yield **Si-ehF$_4$-Si** as a clear solid (7.5 g, 76%). ^{1}H (300 MHz, $CDCl_3$) δ 0.31 (s, 18 H), 0.4-1.2 (b, 130 H), 2.06 (b, 16 H), 7.4-7.8 (m, 26 H). ^{13}C NMR (75 MHz, $CDCl_3$) δ -0.4, 10.9, 14.6, 23.4, 27.7 27.8, 29.0, 34.7, 34.9, 35.3, 44.8, 45.2, 55.6, 55.7, 119.5, 120.4, 123.5, 123.6, 126.6, 127.5, 127.7, 129.3, 129.6, 132.3, 138.6, 140.8, 141.0, 142.4, 150.2, 151.8.

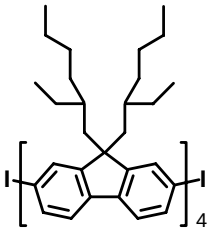

I-ehF$_4$-I *rwi78*: According to the method of Geng et al.,[53] **Si-ehF$_4$-Si** (7.0 g, 4.0 mmol) and CH_2Cl_2 (100 ml) were added to a round bottom flask and cooled in an ice bath before iodine monochloride (1 M in CH_2Cl_2, 9 ml, 9 mmol) was added dropwise over 30 min. After warming to RT, the reaction was quenched with a solution of sodium thiosulfate and the aqueous layer was washed with CH_2Cl_2 (2 x 100 ml). The combined organics were washed with water, brine, and then dried over magnesium sulfate. The product was purified by column chromatography (silica gel, 10% CH_2Cl_2 / hexanes as the eluent) to yield **I-ehF$_4$-I** as a clear solid (6.1 g, 85%). ^{1}H (300 MHz, $CDCl_3$) δ 0.4-1.2 (b, 120 H), 2.06 (b, 16 H), 7.4-7.8 (m, 24 H). ^{13}C NMR (75 MHz, $CDCl_3$) δ 10.9, 11.0, 14.6, 14.7, 23.3, 23.4, 26.2, 27.7, 28.8, 28.9, 32.2, 34.5, 34.7, 35.4, 45.1, 55.7, 55.8, 68.6, 92.2, 120.5, 121.9, 123.5, 126.7, 126.9, 127.7, 133.9, 134.0, 136.4, 139.9, 140.6, 140.7, 140.9, 141.3, 141.6, 151.0, 151.8, 153.8.

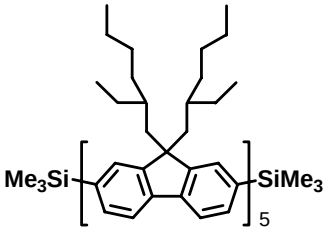

Si-ehF$_5$-Si *rwi57*: According to the method of Geng et al.,[53] **I-ehF$_3$-I** (15.7 g, 11.1 mmol), **B-ehF-Si** (12.3 g, 24.0 mmol), K_2CO_3 (6.1 g, 44 mmol), $Pd(PPh_3)_4$ (0.38 g, 3 mol%), 200 ml of toluene, and 100 ml ethanol were added to a Schlenk flask under N_2. The mixture was heated to 80 ºC for 24 h. Water was added and the aqueous layer was washed with hexane (2 x 100 ml). The organic layers were combined, washed with brine, and then dried over magnesium sulfate. The product was purified by column chromatography (silica gel, 100% hexanes then 10% CH_2Cl_2 / hexanes as the eluent) to yield **Si-ehF$_5$-Si** as a clear solid (8.5 g, 37%). ^{1}H (300 MHz, $CDCl_3$) δ 0.31 (s, 18 H), 0.4-1.2 (b, 150 H), 2.06 (b, 20 H), 7.4-7.8 (m, 30 H). ^{13}C NMR (75 MHz, $CDCl_3$) δ -0.4, 11.0, 14.6, 23.4, 27.7, 27.8, 29.0, 34.7, 34.8, 35.0, 35.3, 44.8, 45.1, 55.6, 55.7, 119.5, 120.4, 123.4, 123.6, 126.6, 126.7, 126.9, 129.6, 140.8, 141.0, 142.4, 151.8.

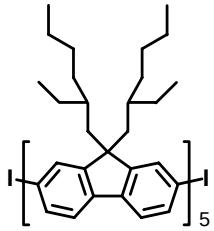

I-ehF$_5$-I *rwi86*: According to the method of Geng et al.,[53] **Si-ehF$_5$-Si** (2.5 g, 1.20 mmol) and CH_2Cl_2 (30 ml) were added to a round bottom flask and cooled in an ice bath before iodine monochloride (1 M in CH_2Cl_2, 4.8 ml, 4.8 mmol) was added dropwise over 30 min. After warming to RT, the reaction was quenched with a solution of sodium thiosulfate and the aqueous layer was washed with CH_2Cl_2 (2 x 50 ml). The combined organics were washed with water, brine, and then dried over magnesium sulfate. The product was purified by column

chromatography (silica gel, 10% CH_2Cl_2 / hexanes as the eluent) to yield **I-ehF$_5$-I** as a clear solid (2.4 g, 92%). ^{1}H (300 MHz, $CDCl_3$) δ 0.4-1.2 (b, 150 H), 2.06 (b, 20 H), 7.49 (m, 2 H), 7.6-7.8 (m, 28 H). ^{13}C NMR (75 MHz, $CDCl_3$) δ 11.0, 11.1, 14.7, 14.8, 14.9, 21.4, 23.4, 23.5, 26.0, 27.6, 27.9, 28.9, 29.0, 32.3, 34.5, 34.8, 34.9, 35.2, 35.4, 44.4, 45.2, 55.6, 55.8, 55.9, 92.3, 120.5, 122.0, 123.6, 126.8, 127.0, 134.0, 134.1, 136.5, 140.0, 140.6, 140.8, 140.9, 141.0, 141.4, 141.6, 141.8, 151.0, 151.1, 151.9, 153.9.

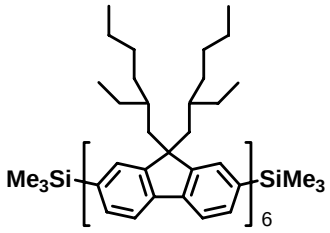

Si-ehF$_6$-Si *rwi31*: According to the method of Geng et al.,[53] **I-ehF2-I** (0.73 g, 0.71 mmol), **B-ehF$_2$-Si** (1.4 g, 1.57 mmol), K_2CO_3 (2 M, 1.7 ml, 3.6 mmol, $Pd(PPh_3)_4$ (0.03 g, 4 mol%), TBABr (0.069 g, 0.2 mmol) and 20 ml of toluene were added to a Schlenk flask under N_2. The mixture was heated to 80 ºC for 24 h before water was added and the aqueous layer was washed with hexane (2 x 15 ml). The organic layers were combined, washed with brine, and dried over magnesium sulfate. The product was purified by column chromatography (silica gel, 5% CH_2Cl_2/hexanes then 10% CH_2Cl_2 / hexanes as the eluent) to yield **Si-ehF$_6$-Si** as a clear solid (0.9 g, 51%). ^{1}H (300 MHz, $CDCl_3$) δ 0.31 (s, 18 H), 0.4-1.2 (b, 180 H), 2.06 (b, 24 H), 7.4-7.8 (m, 36 H). ^{13}C NMR (75 MHz, $CDCl_3$) δ -1.0, 10.4, 14.0, 22.8, 27.2, 28.4, 34.1, 34.2, 34.4, 34.8, 44.3, 44.6, 55.0, 55.1, 118.9, 119.8, 122.8, 123.0, 126.0, 126.2, 129.0, 131.7, 140.2, 140.5, 141.8, 149.6, 151.1, 151.2.

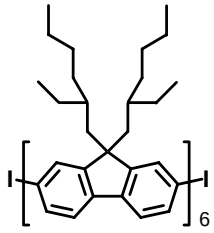

I-ehF$_6$-I *rwi39*: According to the method of Geng et al.,[53] **Si-ehF$_6$-Si** (0.40 g, 0.16 mmol) and CH_2Cl_2 (10 ml) were added to a round bottom flask and cooled in an ice bath before iodine monochloride (1 M in CH_2Cl_2, 0.35 ml, 0.35 mmol) was added dropwise over 30 min. After warming to RT, the reaction was quenched with a solution of sodium thiosulfate and the aqueous layer was washed with CH_2Cl_2 (2 x 15 ml). The combined organics were washed with water, brine, and then dried over magnesium sulfate. The product was purified by column chromatography (silica gel, 10% toluene / hexanes as the eluent) to yield **I-ehF$_6$-I** as a clear solid (0.35 g, 85%). ^{1}H (300 MHz, $CDCl_3$) δ 0.4-1.2 (b, 180 H), 2.06 (b, 24 H), 7.4-7.8 (m, 36 H). ^{13}C NMR (75 MHz, $CDCl_3$) δ 10.4, 14.0, 22.8, 27.2, 28.4, 34.1, 34.2, 34.4, 34.8, 44.3, 44.6, 55.0, 55.1, 91.1, 119.2, 121.0, 122.8, 123.0, 126.0, 126.2, 129.0, 131.7, 140.2, 140.5, 141.8, 149.6, 151.1, 151.2.

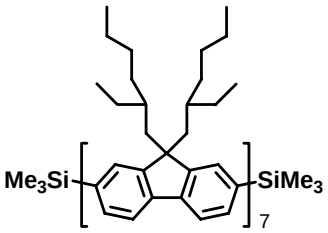

Si-ehF$_7$-Si *rwi88*: According to the method of Geng et al.,[53] **I-ehF$_3$-I** (2.8 g, 1.97 mmol), **B-ehF$_2$-Si** (4.23 g, 4.7 mmol), K_2CO_3 (2 M, 4.0 ml, 7.9 mmol), $Pd(PPh_3)_4$ (0.09, 4 mol%), TBABr (0.20 g, 0.6 mmol), and 30 ml of toluene were added to a Schlenk flask under N_2. The mixture was heated to 80 ºC for 24 h before water was added and the aqueous layer was washed with hexane (2 x 50 ml). The organic layers were combined, washed with brine, and dried over

magnesium sulfate. The product was purified by column chromatography (silica gel, 5% CH_2Cl_2 / hexanes then 10% CH_2Cl_2 / hexanes as the eluent) to yield **Si-ehF$_7$-Si** as a clear solid (2.4 g,, 43%). ^{1}H (300 MHz, $CDCl_3$) δ 0.31 (s, 18 H), 0.4-1.2 (b, 210 H), 2.06 (b, 28 H), 7.4-7.8 (m, 42 H). ^{13}C NMR (75 MHz, $CDCl_3$) δ -1.0, 10.4, 14.0, 20.7, 22.7, 22.8, 25.3, 27,2, 28.4, 31.6, 34.1, 34.2, 34.4, 34.8, 44.2, 44.6, 55.0, 55.1, 118.9, 119.8, 119.5, 122.7, 122.8, 122.9, 123.0, 126.1, 126.2, 126.3, 129.0, 131.7, 138.0, 140.2, 140.4, 140.5, 141.8, 149.6, 151.1, 151.2.

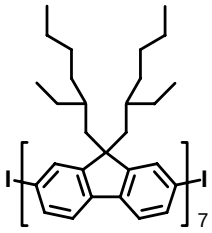

I-ehF$_7$-I *rwi90*: According to the method of Geng et al,[53] **Si-ehF$_7$-Si** (1.2 g, 0.42 mmol) and CH_2Cl_2 (10 ml) were added to a round bottom flask and cooled in an ice bath before iodine monochloride (1 M in CH_2Cl_2, 1.0 ml, 1.0 mmol) was added dropwise over 30 min. After warming to RT, the reaction was quenched with a solution of sodium thiosulfate and aqueous layer was washed with CH_2Cl_2 (2 x 15 ml). The combined organics were washed with water, brine, and then dried over magnesium sulfate. The product was purified by column chromatography (silica gel, 10% CH_2Cl_2 / hexanes as the eluent) to yield **I-ehF$_7$-I** as a clear solid (1.0 g, 83%). ^{1}H (300 MHz, $CDCl_3$) δ 0.4-1.2 (b, 210 H), 2.06 (b, 28 H), 7.48 (m, 2 H) 7.6-7.9 (m, 38 H). ^{13}C NMR (75 MHz, $CDCl_3$) δ 11.0, 11.1, 12.1, 14.7, 14.8, 21.4, 23.4, 26.0, 27.8, 28.9, 29.0, 29.7, 32.3, 34.6, 34.7, 34.9, 35.2, 35.4, 44.8, 45.2, 55.7, 55.8, 92.3, 120.5, 122.0, 123.6, 126.8, 126.9, 134.0, 134.1, 136.5, 140.0, 140.6, 140.8, 140.9, 141.0, 141.4, 141.6, 141.8, 151.0, 151.9, 153.7.

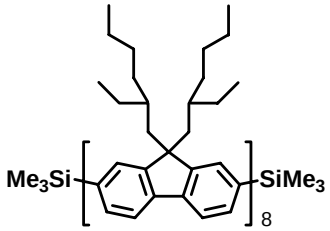

Si-ehF$_8$-Si *rwi81*: According to the method of Geng et al.,[53] **I-ehF$_4$-I** (2.5 g, 1.38 mmol), **B-ehF$_2$-Si** (2.73 g, 3.05 mmol), K_2CO_3 (2 M, 2.7 ml, 5.5 mmol), $Pd(PPh_3)_4$ (0.06, 4 mol%), TBABr (0.13 g, 0.41 mmol) and 15 ml of toluene were added to a Schlenk flask under N_2. The mixture was heated to 80 ºC for 24 h before water was added and the aqueous layer was washed with hexane (2 x 100 ml). The organic layers were combined, washed with brine, and dried over magnesium sulfate. The product was purified by column chromatography (silica gel, 5% CH_2Cl_2 / hexanes then 15% CH_2Cl_2 / hexanes as the eluent) to yield **Si-ehF$_8$-Si** as a clear solid (1.4 g, 32%). ^{1}H (300 MHz, $CDCl_3$) δ 0.31 (s, 18 H), 0.4-1.2 (b, 240 H), 2.06 (b, 32 H), 7.4-7.8 (m, 48 H). ^{13}C NMR (75 MHz, $CDCl_3$) δ -0.3, 11.0, 14.7, 21.3, 23.4, 25.9, 27.8, 29.0, 32.2, 34.7, 34.8, 35.0, 35.4, 44.9, 45.2, 55.6, 55.7, 119.5, 120.5, 123.5, 123.6, 126.7, 127.8, 129.4, 129.7, 132.4, 138.6, 140.8, 141.1, 142.4, 150.2, 151.7, 151.9.

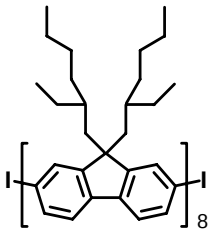

I-ehF$_8$-I *rwi84*: According to the method of Geng et al.,[53] Added **Si-ehF$_8$-Si** (1.4 g, 0.43 mmol) and CH_2Cl_2 (20 ml) to a round bottom flask and cooled in an ice bath before iodine monochloride (1 M in CH_2Cl_2, 1 ml, 1.0 mmol) was added dropwise over 30 min. After warming to RT, the reaction was quenched with a solution of sodium thiosulfate and the aqueous layer was washed with CH_2Cl_2 (2 x 20 ml). The combined organics were washed with water,

brine, and then dried over magnesium sulfate. The product was purified by column chromatography (silica gel, 15% CH_2Cl_2 / hexanes as the eluent) to yield **I-ehF$_8$-I** as a clear solid (1.3 g, 90%). %). ^{1}H (300 MHz, $CDCl_3$) δ 0.4-1.2 (b, 240 H), 2.06 (b, 32 H), 7.3-7.8 (m, 48 H). ^{13}C NMR (75 MHz, $CDCl_3$) δ 10.3, 10.4, 11.4, 14.0, 14.2, 20.7, 22.8, 25.3, 27.2, 28.3, 28.6, 29.1, 29.7, 31.6, 33.9, 34.1, 34.2, 34.7, 44.5, 55.0, 55.2, 91.6, 119.8, 120.9, 121.3, 122.9, 123.0, 124.1 126.1, 126.3, 126.8, 127.1, 128.7, 133.3, 133.4, 135.8, 139.0, 139.3, 139.9, 140.2, 140.3, 140.7, 140.9, 141.1, 150.4, 150.6, 151.3, 153.2.

1.6.5.1 Synthesis of Oligomeric Fluorene Segmers

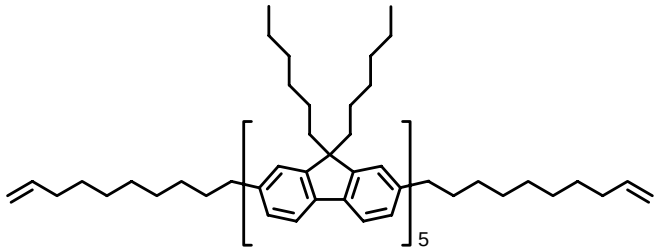

s(F$_5$M$_{18}$) *rwi35*: Adapting the method of Thiem et al.,[85] **I-F$_5$-I** (1.45 g, 0.76 mmol), TBABr (0.07 g, 0.23 mmol), K_2CO_3 (2 M, 7.6 ml, 15.2 mmol), and 20 ml of toluene were added to a Schlenk flask and thoroughly degassed. 9-dec-5-enyl-9-BBN (1.2 g, 4.6 mmol) and $PdCl_2(PPh_3)_2$ (16 mg, 3 mol%) were added under an N_2 atmosphere. The reaction mixture was heated to 45 ºC for 18 h before water was added and the aqueous layer was washed with hexanes (2 x 20 ml). The combined organic layers were washed with brine and then dried over magnesium sulfate. The product was purified by column chromatography (silica gel, 85% hexanes / CH_2Cl_2 as the eluent) to yield **s(F$_5$M$_{18}$)** as a clear solid (1.0 g, 68%). ^{1}H (300 MHz, $CDCl_3$) δ 0.79 (b,56 H), 1.0-1.5 (b, 94 H), 1.67 (b, 4 H) 2.1 (b, 24 H), 2.71 (m, 4 H), 4.96 (m, 4H), 5.83 (m, 2 H),7.17 (m, 4 H), 7.50-7.9 (m, 26 H). ^{13}C NMR (75 MHz, $CDCl_3$) δ 14.6, 23.2, 24.5, 29.6, 29.8, 29.8, 30.1, 30.3,

32.1, 32.4, 34.4, 36.9, 41.0, 55.6, 55.9, 114.7, 120.1, 120.6, 122.1, 123.7, 126.6, 126.8, 127.7, 128.8, 139.0, 139.8, 140.5, 140.6, 141.2, 141.3, 142.6, 151.8, 152.1, 152.4.

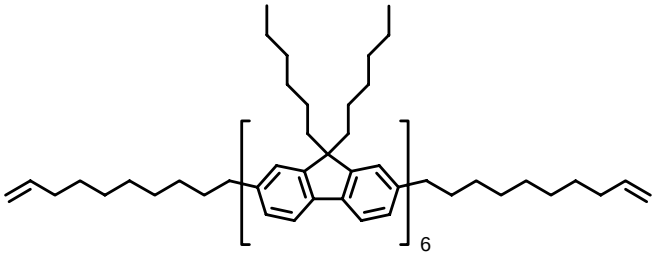

s(F_6M_{18}) *rwi30*: Adapting the method of Thiem et al.,[85] **I-F_6-I** (0.70 g, 0.31 mmol), TBABr (0.03 g, 30 mol%), K_2CO_3 (2 M, 3.1 ml, 6 mmol), and 20 ml of toluene were added to a Schlenk flask and thoroughly degassed. 9-dec-5-enyl-9-BBN (0.32 g, 1.3 mmol) and $PdCl_2(PPh_3)_2$ (6 mg, 3 mol%) were added under an N_2 atmosphere. The reaction mixture was heated to 45 ºC for 18 h before water was added and the aqueous layer was washed with hexanes (2 x 20 ml). The combined organic layers were washed with brine and then dried over magnesium sulfate. The product was purified by column chromatography (silica gel, 100% hexanes to 90% hexanes / CH_2Cl_2 as the eluent) to yield **s(F_6M_{18})** as a clear solid (0.30 g, 43%). ^{1}H (300 MHz, $CDCl_3$) δ 0.79 (b, 80 H), 1.0-1.5 (b, 120 H), 1.67 (b, 4 H) 2.1 (b, 28 H), 2.70 (t, 4 H), 4.96 (m, 4H), 5.83 (m, 2 H) 7.16 (b, 4 H), 7.50-7.9 (m, 32 H). ^{13}C NMR (75 MHz, $CDCl_3$) δ 14.0, 22.5, 23.8, 28.9, 29.1, 29.2, 29.5, 29.7, 31.4, 31.8, 33.8, 36.3, 40.4, 55.0, 55.3, 114.1, 119.4, 119.5, 119.9, 121.5, 123.0, 125.9, 126.1, 127.0, 138.4, 139.2, 139.8, 139.9, 140.0, 140.5, 140.6, 142.0, 151.1, 151.4, 151.8.

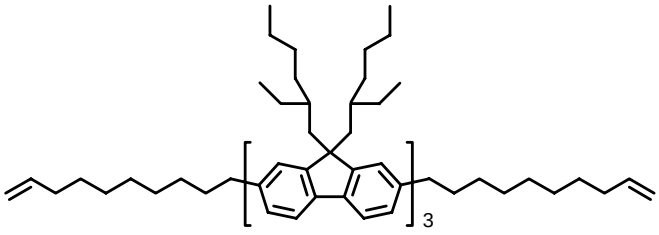

s(ehF$_3$M$_{18}$) *rwi75*: Adapting the method of Thiem et al,[85] **I-ehF$_3$-I** (1.0 g, 0.71 mmol), TBABr (0.07 g, 0.21 mmol), K_2CO_3 (2 M, 7.0 ml, 14.1 mmol), and 15 ml of toluene were added to a Schlenk flask and thoroughly degassed. 9-dec-5-enyl-9-BBN (1.1 g, 4.2 mmol) and $PdCl_2(PPh_3)_2$ (15 mg, 3 mol%) were added under an N_2 atmosphere. The reaction mixture was heated to 45 ºC for 18 h before water was added and the aqueous layer was washed with hexanes (2 x 20 ml). The combined organic layers were washed with brine and then dried over magnesium sulfate. The product was purified by column chromatography (silica gel, 5% CH_2Cl_2 / hexanes then 10% CH_2Cl_2 / hexanes as the eluent) to yield **s(ehF$_3$M$_{18}$)** as a clear solid (0.9 g, 90%). ^{1}H (300 MHz, $CDCl_3$) δ 0.4-1.2 (b, 90 H), 1.3 (b, 16 H), 1.65 (b, 4 H), 2.06 (b, 16 H), 2.67 (t, 4 H, J = 7.5 Hz), 4.96 (m, 4 H), 5.82 (m, 2 H), 7.13 (m, 4 H), 7.5-7.8 (m, 16H). ^{13}C NMR (75 MHz, $CDCl_3$) δ 10.3,14.0, 22.8, 27.0, 27.1, 28.3, 28.9, 29.2, 29.1, 29.5, 29.6, 31.9, 33.8, 33.9, 34.0, 34.1, 34.6, 34.7, 36.3, 44.5, 54.8, 54.9, 55.0, 114.1, 119.3, 119.4, 119.6, 119.7, 122.8, 122.9, 124.1, 124.2, 125.8, 125.9, 126.0, 127.1, 138.7, 139.2, 139.9, 140.1, 140.3, 140.6, 141.3, 150.7, 150.9, 151.2.

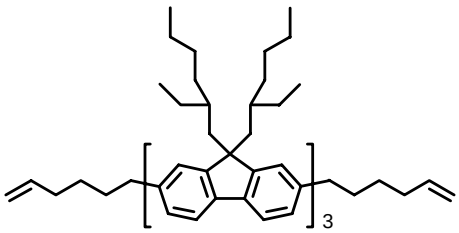

s(ehF$_3$M$_{10}$) *rwii54*: Adapting the method of Thiem et al.,[85] **I-ehF$_3$-I** (3.6 g, 2.5 mmol), TBABr (0.24 g, 0.75 mmol), K_2CO_3 (2 M, 25 ml, 50 mmol), and 20 ml of toluene were added to a Schlenk flask and thoroughly degassed. 9-hex-5-enyl-9-BBN (3.1 g, 15 mmol) and $PdCl_2(PPh_3)_2$ (50 mg, 3 mol%) were added under an N_2 atmosphere. The reaction mixture was heated to 45 ºC for 20 h before water was added and the aqueous layer was washed with hexanes (2 x 50 ml). The combined organic layers were washed with brine and then dried over magnesium sulfate.

The product was purified by column chromatography (Silica gel, 5% CH_2Cl_2 / hexanes then 10% CH_2Cl_2 / hexanes as the eluent) to yield **s(ehF$_3$M$_{10}$)** as a clear solid (3.3, 94%). ^{1}H (300 MHz, $CDCl_3$) δ 0.4-1.2 (b, 90 H), 1.3 (m, 4 H), 1.65 (m, 4 H), 2.06 (b, 16 H), 2.68 (t, 4 H, J = 7.2 Hz), 4.96 (m, 4 H), 5.82 (m, 2 H), 7.16 (m, 4 H), 7.5-7.8 (m, 14 H). ^{13}C NMR (75 MHz, $CDCl_3$) δ 10.4, 14.1, 22.9, 27.1, 27.2, 28.4, 28.6, 28.8, 31.4, 33.8, 34.0, 34.2, 34.7, 34.8, 36.2, 44.6, 53.4, 54.9, 55.1, 114.5, 119.4, 119.8, 122.8, 124.2, 125.9, 126.0, 126.2, 126.3, 127.2, 138.9, 139.9, 140.0, 140.2, 140.4, 140.5, 140.6, 141.1, 150.8, 150.9, 151.2.

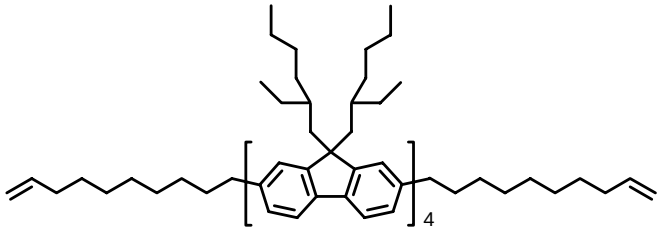

s(ehF$_4$M$_{18}$) *rwi83*: Adapting the method of Thiem et al.,[85] **I-ehF$_4$-I** (1.6 g, 1.0 mmol), TBABr (0.10 g, 0.30 mmol), K_2CO_3 (2 M, 10.0 ml, 20 mmol), and 20 ml of toluene were added to a Schlenk flask and thoroughly degassed. 9-dec-5-enyl-9-BBN (1.6 g, 6.0 mmol) and $PdCl_2(PPh_3)_2$ (20 mg, 3 mol%) were added under an N_2 atmosphere. The reaction mixture was heated to 45 ºC for 18 h before water was added and the aqueous layer was washed with hexanes (2 x 15 ml). The combined organic layers were washed with brine and then dried over magnesium sulfate. The product was purified by column chromatography (silica gel, 5% CH_2Cl_2 / hexanes as the eluent) to yield **s(ehF$_4$M$_{18}$)** as a clear solid (1.3 g, 81%). ^{1}H (300 MHz, $CDCl_3$) δ 0.4-1.2 (b, 120 H), 1.65 (b, 4 H), 2.06 (b, 20 H), 2.67 (t, 4 H, J = 7.5 Hz), 4.96 (m, 4 H), 5.82 (m, 2 H), 7.20 (m, 4 H), 7.5-7.8 (m, 20 H). ^{13}C NMR (75 MHz, $CDCl_3$) δ 10.3,14.0, 22.8, 27.0, 27.1, 28.3, 28.9, 29.2, 29.1, 29.5, 29.6, 31.9, 33.8, 33.9, 34.0, 34.1, 34.6, 34.7, 36.3, 44.5, 54.8, 54.9, 55.0, 114.1, 119.3, 119.4, 119.6, 119.7, 122.8, 122.9, 124.1, 124.2, 125.8, 125.9, 126.0, 127.1, 138.7, 139.2, 139.9, 140.1, 140.3, 140.6, 141.3, 150.7, 150.9, 151.2.

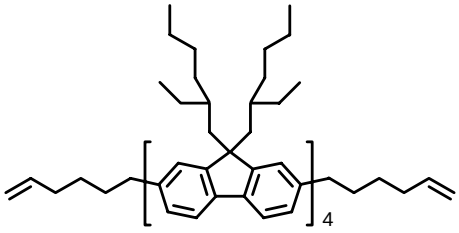

s(ehF$_4$M$_{10}$) *rwi101*: Adapting the method of Thiem et al.,[85] **I-ehF$_4$-I** (0.6 g, 0.38 mmol), TBABr (0.04 g, 0.11 mmol), K_2CO_3 (2 M, 4.0 ml, 8 mmol), and 20 ml of toluene were added to a Schlenk flask and thoroughly degassed. 9-hex-5-enyl-9-BBN (0.46 g, 2.3 mmol) and $PdCl_2(PPh_3)_2$ (8.0 mg, 3 mol%) were added under a N_2 atmosphere. The reaction mixture was heated to 45 ºC for 18 h before water was added and the aqueous layer was washed with hexanes (2 x 20 ml). The combined organic layers were washed with brine and then dried over magnesium sulfate. The product was purified by column chromatography (silica gel, hexanes then 10% CH_2Cl_2 / hexanes as the eluent) to yield **s(ehF$_4$M$_{10}$)** as a clear solid (0.45 g, 75%). ^{1}H (300 MHz, $CDCl_3$) δ 0.4-1.2 (b, 120 H), 1.3 (b, 4 H), 1.65 (b, 4 H), 2.06 (b, 20 H), 2.68 (t, 4 H, J = 7.5 Hz), 4.96 (m, 4 H), 5.82 (m, 2 H), 7.13 (m, 4 H), 7.5-7.8 (m, 20 H). ^{13}C NMR (75 MHz, $CDCl_3$) δ 10.4, 14.0, 22.8, 27.0, 27.1, 28.3, 28.6, 28.7, 31.3, 33.7, 34.0, 34.2, 34.7, 34.8, 36.2, 44.6, 54.8, 55.1, 114.4, 119.3, 119.8, 123.0, 124.2, 124.2, 125.9, 126.0, 126.3, 127.2, 128.7, 138.9, 139.8, 139.9, 140.1, 140.2, 140.4, 140.6, 141.1, 150.8, 150.9, 151.2.

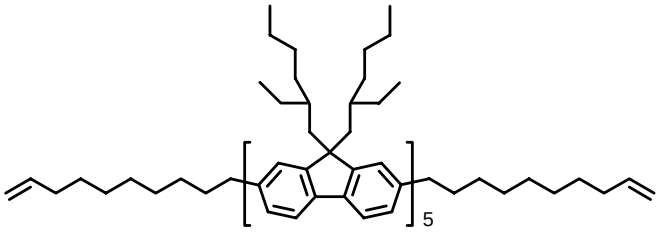

s(ehF$_5$M$_{18}$) *rwi98*: Adapting the method of Thiem et al.,[85] **I-ehF$_5$-I** (0.8 g, 0.36 mmol), TBABr (0.04 g, 0.11 mmol), K_2CO_3 (2 M, 3.6 ml, 7.2 mmol), and 20 ml of toluene were added to a Schlenk flask and thoroughly degassed. 9-dec-5-enyl-9-BBN (0.56 g, 2.2 mmol) and

$PdCl_2(PPh_3)_2$ (7.5 mg, 3 mol%) were added under an N_2 atmosphere. The reaction mixture was heated to 45 ºC for 18 h before water was added and the aqueous layer was washed with hexanes (2 x 20 ml). The combined organic layers were washed with brine and then dried over magnesium sulfate. The product was purified by column chromatography (silica gel, 10% CH_2Cl_2 / hexanes as the eluent) to yield **s(ehF$_5$M$_{18}$)** as a clear solid (0.7 g, 88%). ^{1}H (300 MHz, $CDCl_3$) δ 0.4-1.2 (b, 150 H), 1.65 (b, 4 H), 2.06 (b, 24 H), 2.67 (t, 4 H, J = 7.8 Hz), 4.94 (m, 4 H), 5.82 (m, 2 H), 7.13-7.20 (m, 4 H), 7.5-7.8 (m, 26 H). ^{13}C NMR (75 MHz, $CDCl_3$) δ 10.3, 14.0, 22.8, 27.1, 28.3, 29.0, 29.2, 29.3, 29.5, 29.6, 31.9, 33.8, 34.0, 34.1, 34.6, 34.7, 36.3, 44.5, 54.8, 55.1, 114.1, 119.3, 119.4, 119.8, 123.0, 124.2, 126.1, 126.3, 127.1, 138.7, 139.2, 140.0, 140.2, 140.6, 141.3, 150.7, 150.9, 151.2.

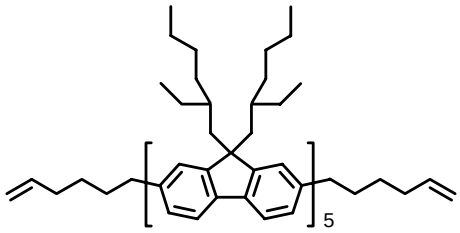

s(ehF$_5$M$_{10}$) *rwii56*: Adapting the method of Thiem et al.,[85] **I-ehF$_5$-I** (0.95 g, 0.43 mmol), TBABr (0.04 g, 0.13 mmol), K_2CO_3 (2 M, 4.3 ml, 8.6 mmol), and 20 ml of toluene were added to a Schlenk flask and thoroughly degassed. 9-hex-5-enyl-9-BBN (0.53 g, 2.6 mmol) and $PdCl_2(PPh_3)_2$ (9.1 mg, 3 mol%) were added under an N_2 atmosphere. The reaction mixture was heated to 45 ºC for 20 h before water was added and the aqueous layer was washed with hexanes (2 x 25 ml). The combined organic layers were washed with brine and then dried over magnesium sulfate. The product was purified by column chromatography (Silica gel, 10% CH_2Cl_2 / hexanes as the eluent) to yield **s(ehF$_5$M$_{10}$)** as a clear solid (0.8 g, 89%). ^{1}H (300 MHz, $CDCl_3$) δ 0.4-1.2 (b, 150 H), 1.3 (b, 4 H), 1.65 (b, 4 H), 2.06 (b, 26 H), 2.68 (t, 4 H, J = 7.2 Hz), 4.96 (m, 4 H), 5.82 (m, 2 H), 7.13 (m, 4 H), 7.5-7.8 (m, 25 H). ^{13}C NMR (75 MHz, $CDCl_3$) δ

10.4, 14.1, 22.8, 27.1, 27.2, 28.4, 28.6, 28.7, 31.4, 33.8, 34.1, 34.2, 34.1, 34.2, 34.7, 34.8, 36.2, 44.6, 54.9, 55.1, 114.5, 119.4, 119.8, 122.7, 122.9, 123.0, 124.2, 125.9, 126.0, 126.2, 126.3, 127.2, 138.9, 139.9, 140.0, 140.1, 140.2, 140.3, 140.4, 140.6, 141.1, 141.2, 150.8, 150.9, 151.3.

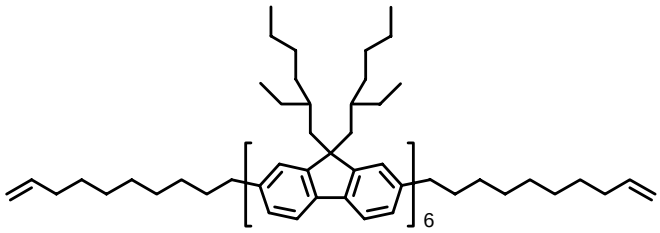

s(ehF$_6$M$_{18}$) *rwi41*: Adapting the method of Thiem et al.,[85] **I-ehF$_6$-I** (0.30 g, 0.12 mmol), TBABr (0.011 g, 0.035 mmol), K_2CO_3 (2 M, 1.2 ml, 2.3 mmol), and 15 ml of toluene were added to a Schlenk flask and thoroughly degassed. 9-dec-5-enyl-9-BBN (0.18 g, 0.70 mmol) and $PdCl_2(PPh_3)_2$ (2.4 mg, 3 mol%) were added under an N_2 atmosphere. The reaction mixture was heated to 45 ºC for 18 h before water was added and the aqueous layer was washed with hexanes (2 x 10 ml). The combined organic layers were washed with brine and then dried over magnesium sulfate. The product was purified by column chromatography (silica gel, 10% toluene / hexanes as the eluent) to yield **s(ehF$_6$M$_{18}$)** as a clear solid (0.25 g, 83%). ^{1}H (300 MHz, $CDCl_3$) δ 0.4-1.2 (b, 180 H), 1.65 (b, 4 H), 2.06 (b, 28 H), 2.67 (t, 4 H, J = 6.9 Hz), 4.94 (m, 4 H), 5.82 (m, 2 H), 7.13-7.20 (m, 4 H), 7.5-7.8 (m, 32 H). ^{13}C NMR (75 MHz, $CDCl_3$) δ 10.3, 14.0, 22.8, 27.1, 28.3, 29.0, 29.2, 29.6, 31.9, 33.8, 34.0, 34.6, 34.7, 44.5, 55.1, 114.1, 119.8, 123.0, 124.2, 126.1, 140.2, 151.2.

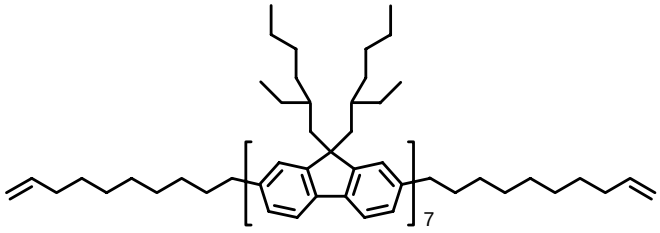

s(ehF$_7$M$_{18}$) *rwi92*: Adapting the method of Thiem et al.,[85] **I-ehF$_7$-I** (1.1 g, 0.33 mmol), TBABr (32 mg, 0.10 mmol), K_2CO_3 (2 M, 3.3 ml, 6.6 mmol), and 20 ml of toluene were added to a Schlenk flask and thoroughly degassed. 9-dec-5-enyl-9-BBN (0.51 g, 2.0 mmol) and $PdCl_2(PPh_3)_2$ (6.9 mg, 3 mol%) were added under an N_2 atmosphere. The reaction mixture was heated to 45 ºC for 18 h before water was added and the aqueous layer was washed with hexanes (2 x 20 ml). The combined organic layers were washed with brine and then dried over magnesium sulfate. The product was purified by column chromatography (silica gel, 10% CH_2Cl_2 / hexanes as the eluent) to yield **s(ehF$_7$M$_{18}$)** as a clear solid (0.8 g, 73%). ^{1}H (300 MHz, $CDCl_3$) δ 0.4-1.2 (b, 210 H), 1.65 (b, 4 H), 2.06 (b, 32 H), 2.67 (m, 4 H), 4.98 (m, 4 H), 5.87 (m, 2 H), 7.13-7.20 (m, 4 H), 7.5-8.0 (m, 38 H). ^{13}C NMR (75 MHz, $CDCl_3$) δ 10.3, 14.1, 14.2, 20.7, 22.7, 22.8, 25.3, 27.2, 28.4, 28.9, 29.1, 29.2, 29.3, 29.5, 29.6, 29.8, 31.7, 31.9, 33.9, 34.1, 34.2, 34.6, 34.7, 34.8, 36.4, 44.6, 54.8, 55.1, 114.2, 119.5, 119.9, 123.0, 124.2, 126.2, 127.2, 138.8, 139.1, 139.8, 140.1, 140.2, 140.4, 140.6, 141.3, 150.7, 150.9, 151.2.

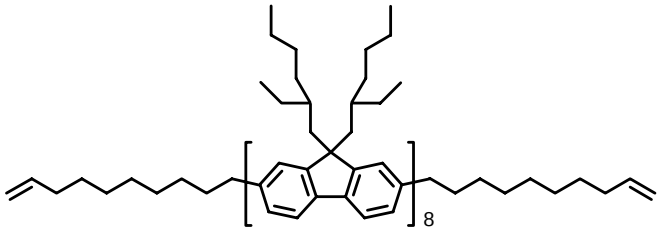

s(ehF$_8$M$_{18}$) *rwi96*: Adapting the method of Thiem et al.,[85] **I-ehF$_8$-I** (1.3 g, 0.39 mmol), TBABr (40 mg, 0.10 mmol), K_2CO_3 (2 M, 4.0 ml, 8.0 mmol), and 20 ml of toluene were added to a Schlenk flask and thoroughly degassed. 9-dec-5-enyl-9-BBN (0.60 g, 2.3 mmol) and

$PdCl_2(PPh_3)_2$ (8.0 mg, 3 mol%) were added under an N_2 atmosphere. The reaction mixture was heated to 45 ºC for 18 h under before water was added and the aqueous layer was washed with hexanes (2 x 20 ml). The combined organic layers were washed with brine and then dried over magnesium sulfate. The product was purified by column chromatography (silica gel, 10% CH_2Cl_2 / hexanes as the eluent) to yield **s(ehF$_8$M$_{18}$)** as a clear solid (1.1 g, 85%). ^{1}H (300 MHz, CDCl3) δ 0.4-1.2 (b, 240 H), 1.65 (b, 4 H), 2.06 (b, 32 H), 2.67 (m, 4 H), 4.98 (m, 4 H), 5.87 (m, 2 H), 7.13-7.20 (m, 4 H), 7.5-8.0 (m, 38 H). ^{13}C NMR (75 MHz, CDCl3) δ 10.3, 14.1, 14.2, 20.7, 22.7, 22.8, 25.3, 27.2, 28.4, 28.9, 29.1, 29.2, 29.3, 29.5, 29.6, 29.8, 31.7, 31.9, 33.9, 34.1, 34.2, 34.6, 34.7, 34.8, 36.4, 44.6, 54.8, 55.1, 114.2, 119.5, 119.9, 123.0, 124.2, 126.2, 127.2, 138.8, 139.1, 139.8, 140.1, 140.2, 140.4, 140.6, 141.3, 150.7, 150.9, 151.2.

1.6.5.2 Synthesis of Polymethylene-*co*-Fluorenes.

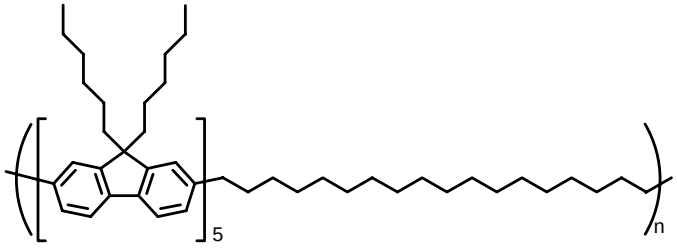

p(F$_5$M$_{18}$) *rwi37*: Adapting the method of Watson et al.,[66] **s(F$_5$M$_{18}$)** (0.53 g, 0.26 mmol), Grubbs 1 (4 mg, 2 mol%), 0.50 g of phenyl ether, and 10 ml of toluene were added to a Schlenk flask under a N_2 atmosphere. The ethylene by-product and toluene were slowly removed under vacuum before the reaction mixture was heated to 45 ºC for 18 h under vacuum. The mixture was dissolved in 10 ml of toluene and transferred to a stainless steel reaction vessel. Silica gel (0.2 g) was added and the vessel was charged to 180 psi with H_2. The mixture was heated to 80 ºC for 20 h. After cooling to RT, the silica gel was filtered and the toluene was removed under reduced pressure. The polymer was dissolved in a small amount of CH_2Cl_2 and precipitated into

acetone to yield **p(F_5M_{18})** (0.35 g, 69%) as a tan powder. ^{1}H NMR (300 MHz, $CDCl_3$) δ 0.76 (b, 64 H), 1.10-1.32 (b, 104 H), 1.52-1.65 (b, 5 H), 2.09 (b, 22 H), 2.68 (b, 4 H), 7.14 (b, 4 H), 7.59-7.83 (b, 24 H). ^{13}C NMR (75 MHz, $CDCl_3$) 14.0, 22.6, 23.9, 29.3, 29.7, 29.8, 30.9, 31.5, 31.9, 36.3, 40.4, 55.0, 55.3, 119.4, 119.5, 120.0, 121.5, 123.1, 126.0, 126.2, 127.1, 138.4, 139.9, 140.0, 140.6, 140.7, 142.1, 151.2, 151.5, 151.8.

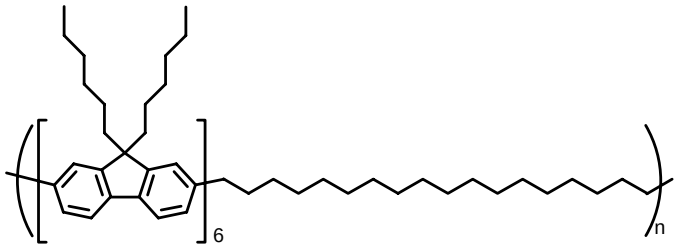

p(F_6M_{18}) *rwi32*: Adapting the method of Watson et al.,[66] **s(F_6M_{18})** (0.25 g, 0.11 mmol), Grubbs 1 (2 mg, 2 mol%), 0.45 g of phenyl ether, and 10 ml of toluene were added to a Schlenk flask under a N_2 atmosphere. The ethylene by-product and the toluene were slowly removed under vacuum before the reaction mixture was heated to 45 ºC for 18 h under vacuum. The mixture was dissolved in 10 ml of toluene and transferred to a stainless steel reaction vessel. Silica gel (0.5 g) was added and the vessel was charged to 180 psi with H_2. The mixture was heated to 80 ºC for 20 h. After cooling to RT, the silica gel was filtered and the toluene was removed under reduced pressure. The polymer was dissolved in a small amount of CH_2Cl_2 and precipitated into acetone to yield **p(F_6M_{18})** (0.20 g, 80%) as a tan powder. ^{1}H NMR (300 MHz, $CDCl_3$) δ 0.76 (b, 76 H), 1.10-1.32 (b, 120 H), 1.52-1.65 (b, 4 H), 2.09 (b, 24 H), 2.68 (b, 4 H), 7.14 (b, 4 H), 7.59-7.83 (b, 336 H). ^{13}C NMR (75 MHz, $CDCl_3$) 14.0, 22.6, 23.9, 29.3, 29.7, 31.5, 31.8, 40.4, 55.0, 55.4, 119.5, 120.0, 121.6, 123.1, 126.2, 127.1, 138.4, 140.0, 140.6, 142.1, 151.2, 151.5, 151.8.

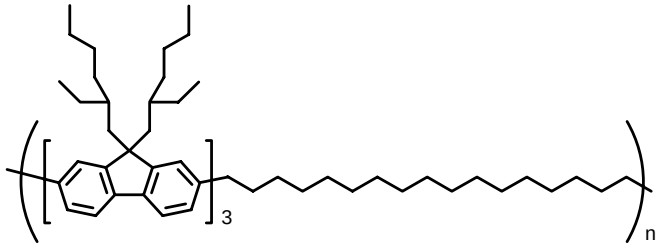

p(ehF$_3$M$_{18}$) *rwi77*: Adapting the method of Watson et al.,[66] **s(ehF$_3$M$_{18}$)** (0.5 g, 0.35 mmol), Grubbs 1 (6 mg, 2 mol%), 0.7 g of phenyl ether, and 10 ml of toluene were added to a Schlenk flask under a N_2 atmosphere. The ethylene by-product and the toluene were slowly removed under vacuum before the reaction mixture was heated to 45 ºC for 18 h under vacuum. The mixture was dissolved in 10 ml of toluene and transferred to a stainless steel reaction vessel. Silica gel (0.5 g) was added and the vessel was charged to 180 psi with H_2. The mixture was heated to 80 ºC for 20 h. After cooling to RT, the silica gel was filtered and the toluene was removed under reduced pressure. The polymer was dissolved in a small amount of CH_2Cl_2 and precipitated into acetone to yield **p(ehF$_3$M$_{18}$)** (0.3 g, 60%) as a white very viscous tar. ^{1}H (300 MHz, $CDCl_3$) δ 0.4-1.2 (b, 90 H), 1.3 (b, 28 H), 1.65 (b, 4 H), 2.06 (b, 12 H), 2.67 (t, 4 H, J = 7.5 Hz), 7.13 (m, 4 H), 7.5-7.8 (m, 16H). ^{13}C NMR (75 MHz, $CDCl_3$) δ 10.3, 14.0, 22.8, 27.1, 28.3, 29.2, 29.3, 29.5, 29.7, 31.9, 34.0, 34.1, 34.6, 34.7, 36.4, 44.5, 54.8, 55.1, 119.3, 119.4, 119.8, 123.0, 124.2, 126.0, 127.1, 138.7, 139.7, 140.0, 140.2, 140.6, 141.3, 150.7, 150.9, 151.2.

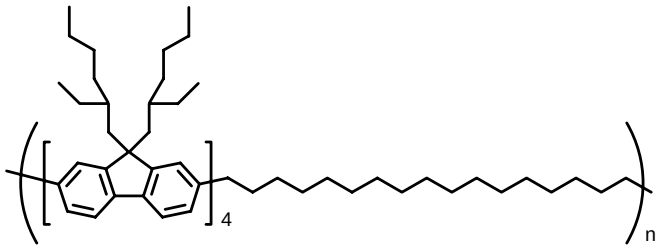

p(ehF$_4$M$_{18}$) *rwi93*: Adapting the method of Watson et al.,[66] **s(ehF$_4$M$_{18}$)** (0.45 g, 0.27 mmol), Grubbs 1 (4.5 mg, 2 mol%), 0.5 g of phenyl ether, and 10 ml of toluene were added to a Schlenk flask under a N_2 atmosphere. The ethylene by-product and the toluene were slowly removed

under vacuum before the reaction mixture was heated to 45 ºC for 18 h under vacuum. The mixture was dissolved in 15 ml of toluene and transferred to a stainless steel reaction vessel. Silica gel (0.5 g) was added and the vessel was charged to 180 psi with H_2. The mixture was heated to 80 ºC for 24 h. After cooling to RT, the silica gel was filtered and the toluene was removed under reduced pressure. The polymer was dissolved in a small amount of CH_2Cl_2 and precipitated into acetone to yield **p(ehF$_4$M$_{18}$)** (0.4 g, 90%) as a gummy, white solid. ^{1}H (300 MHz, $CDCl_3$) δ 0.4-1.2 (b, 120 H), 1.3 (b, 28 H), 1.65 (b, 4 H), 2.06 (b, 16 H), 2.67 (b, 4 H), 7.13 (m, 4 H), 7.5-7.8 (m, 10H). ^{13}C NMR (75 MHz, $CDCl_3$) δ 10.3, 14.0, 22.8, 27.0, 27.1, 28.3, 29.2, 29.3, 29.5, 29.7, 31.9, 34.0, 34.1, 34.6, 34.7, 36.3, 44.5, 54.8, 55.1, 119.3, 119.4, 119.8, 122.9, 124.2, 125.3, 126.0, 126.1, 127.1, 138.7, 139.8, 140.0, 140.2, 140.3, 140.6, 141.3, 150.7, 150.9, 151.1.

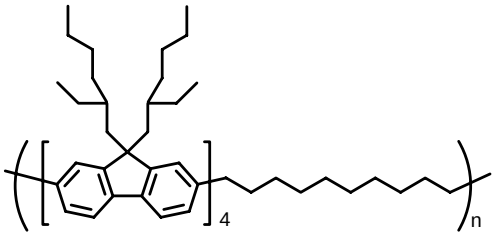

p(ehF$_4$M$_{10}$) *rwi102*: Adapting the method of Watson et al.,[66] **s(ehF$_4$M$_{10}$)** (1.0 g, 0.58 mmol), Grubbs 1 (10 mg, 2 mol%), 0.5 g of phenyl ether, and 10 ml of toluene were added to a Schlenk flask under a N_2 atmosphere. The ethylene by-product and the toluene were slowly removed under vacuum before the reaction mixture was heated to 45 ºC for 18 h under vacuum. The mixture was dissolved in 20 ml of toluene and transferred to a stainless steel reaction vessel. Silica gel (1.0 g) was added and the vessel was charged to 180 psi with H_2. The mixture was heated to 80 ºC for 24 hours. After cooling to RT, the silica gel was filtered and the toluene was removed under reduced pressure. The polymer was dissolved in a small amount of CH_2Cl_2 and precipitated into acetone to yield **p(ehF$_4$M$_{10}$)** (0.8 g, 80%) as a gummy, white solid. ^{1}H (300

MHz, $CDCl_3$) δ 0.4-1.2 (b, 120 H), 1.3 (b, 12 H), 1.65 (b, 4 H), 2.06 (b, 16 H), 2.67 (b, 4 H, 7.13 (m, 4 H), 7.5-7.8 (m, 20 H). ^{13}C NMR (75 MHz, $CDCl_3$) δ 11.0, 14.7, 23.4, 27.7, 28.9, 29.8, 30.0, 32.6, 34.6, 34.8, 35.3, 35.4, 37.0, 45.3, 55.4, 55.7, 119.9, 120.0, 120.4, 123.6, 124.8, 126.6, 126.7, 126.9, 127.7, 139.4, 140.7, 140.8, 141.0, 141.2, 141.9, 151.4, 151.5, 151.8.

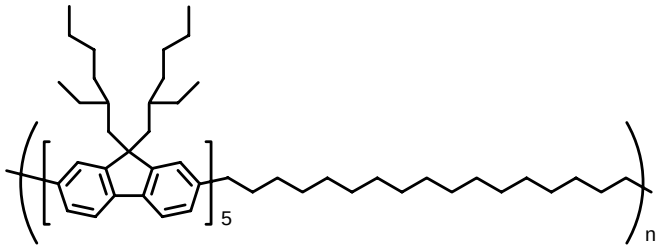

p(ehF$_5$M$_{18}$) *rwi100*: Adapting the method of Watson et al.,[66] **s(ehF$_5$M$_{18}$)** (0.45 g, 0.27 mmol), Grubbs 1 (4.5 mg, 2 mol%), 0.5 g of phenyl ether, and 10 ml of toluene were added to a Schlenk flask under a N_2 atmosphere. The ethylene by-product and the toluene were slowly removed under vacuum before the reaction mixture was heated to 45 ºC for 18 h under vacuum. The mixture was dissolved in 15 ml of toluene and transferred to a stainless steel reaction vessel. Silica gel (0.5 g) was added and the vessel was charged to 180 psi with H_2. The mixture was heated to 80 ºC for 24 h. After cooling to RT, the silica gel was filtered and the toluene was removed under reduced pressure. The polymer was dissolved in a small amount of CH_2Cl_2 and precipitated into acetone to yield **p(ehF$_5$M$_{18}$)** (0.4 g, 90%) as a gummy, white solid. ^1H (300 MHz, $CDCl_3$) δ 0.4-1.2 (b, 150 H), 1.3 (b, 28 H), 1.65 (b, 4 H), 2.06 (b, 20 H), 2.67 (b, 4 H), 7.13 (m, 4 H), 7.5-7.8 (m, 26H). ^{13}C NMR (75 MHz, $CDCl_3$) δ 10.3,14.0, 22.8, 27.0, 27.1, 28.3, 28.9, 29.2, 29.1, 29.5, 29.6, 31.9, 33.8, 33.9, 34.0, 34.1, 34.6, 34.7, 36.3, 44.5, 54.8, 54.9, 55.0, 114.1, 119.3, 119.4, 119.6, 119.7, 122.8, 122.9, 124.1, 124.2, 125.8, 125.9, 126.0, 127.1, 138.7, 139.2, 139.9, 140.1, 140.3, 140.6, 141.3, 150.7, 150.9, 151.2.

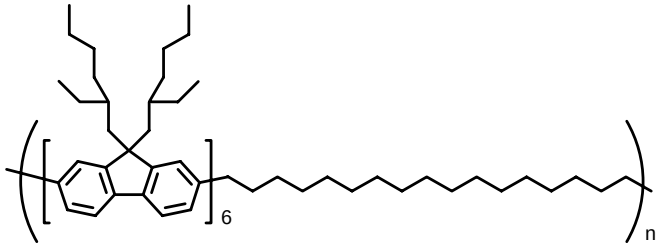

p(ehF$_6$M$_{18}$) *rwi43*: Adapting the method of Watson et al.,[66] **s(ehF$_6$M$_{18}$)** (0.30 g, 0.12 mmol), Grubbs 1 (2 mg, 2 mol%), 0.5 g of phenyl ether, and 10 ml of toluene were added to a Schlenk flask under a N_2 atmosphere. The ethylene by-product and the toluene were slowly removed under vacuum before the reaction mixture was heated to 45 ºC for 18 h under vacuum. The mixture was dissolved in 15 ml of toluene and transferred to a stainless steel reaction vessel. Silica gel (0.5 g) was added and the vessel was charged to 180 psi with H_2. The mixture was heated to 80 ºC for 24 h. After cooling to RT, the silica gel was filtered and the toluene was removed under reduced pressure. The polymer was dissolved in a small amount of CH_2Cl_2 and precipitated into acetone to yield **p(ehF$_6$M$_{18}$)** (0.20 g, 66%) as a gummy, white solid. . ^{1}H (300 MHz, $CDCl_3$) δ 0.4-1.2 (b, 180 H), 1.3 (b, 28 H), 1.65 (b, 4 H), 2.06 (b, 24 H), 2.67 (b, 4 H), 7.13 (m, 4 H), 7.5-7.8 (m, 32 H). ^{13}C NMR (75 MHz, $CDCl_3$) δ 10.4, 14.0, 22.8, 27.2, 28.4, 29.2, 29.4, 29.7, 31.9, 34.1, 34.7, 34.8, 36.4, 44.6, 54.8, 55.1, 119.4, 119.8, 123.0, 124.2, 126.1, 127.1, 138.8, 139.8, 139.9, 140.0, 140.2, 140.6, 141.3, 150.8, 150.9, 151.2.

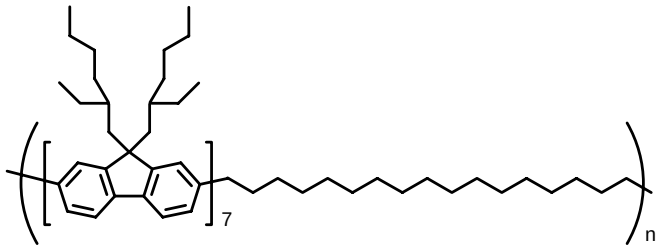

p(ehF$_7$M$_{18}$) *rwi94*: Adapting the method of Watson et al.,[66] **s(ehF$_7$M$_{18}$)** (0.70 g, 0.21 mmol), Grubbs 1 (3.4 mg, 2 mol%), 0.7 g of phenyl ether, and 15 ml of toluene were added to a Schlenk flask under a N_2 atmosphere. The ethylene by-product and the toluene were slowly removed

under vacuum before the reaction mixture was heated to 45 ºC for 18 h under vacuum. The mixture was dissolved in 15 ml of toluene and transferred to a stainless steel reaction vessel. Silica gel (0.5 g) was added and the vessel was charged to 180 psi with H_2. The mixture was heated to 80 ºC for 24 h. After cooling to RT, the silica gel was filtered and the toluene was removed under reduced pressure. The polymer was dissolved in a small amount of CH_2Cl_2 and precipitated into acetone to yield **p(ehF$_7$M$_{18}$)** (0.60 g, 86%) as a gummy, white solid. ^{1}H (300 MHz, $CDCl_3$) δ 0.4-1.2 (b, 210 H), 1.3 (b, 28 H), 1.65 (b, 4 H), 2.06 (b, 20 H), 2.67 (b, 4 H), 7.13 (m, 4 H), 7.5-7.8 (m, 38 H). ^{13}C NMR (75 MHz, $CDCl_3$) δ 10.3, 14.0, 22.8, 27.0, 27.1, 28.3, 29.2, 29.3, 29.5, 29.7, 31.9, 34.0, 34.1, 34.6, 34.7, 36.3, 44.5, 54.8, 55.1, 119.3, 119.4, 119.8, 122.9, 124.2, 125.8, 126.0, 126.1, 126.2, 127.1, 138.7, 139.8, 140.0, 140.2, 140.6, 141.3, 150.7, 150.9, 151.2.

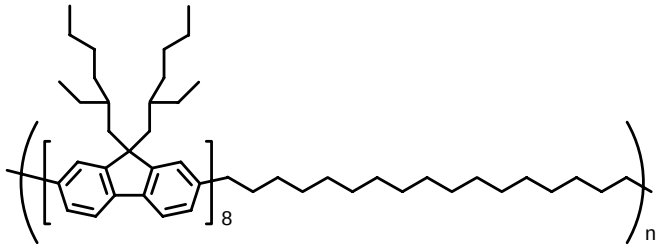

p(ehF$_8$M$_{18}$) *rwi97*: Adapting the method of Watson et al.,[66] **s(ehF$_8$M$_{18}$)** (0.40 g, 0.12 mmol), Grubbs 1 (2 mg, 2 mol%), 0.5 g of phenyl ether, and 10 ml of toluene were added to a Schlenk flask under a N_2 atmosphere. The ethylene by-product and the toluene were slowly removed under vacuum before the reaction mixture was heated to 45 ºC for 18 h under vacuum. The mixture was dissolved in 15 ml of toluene and transferred to a stainless steel reaction vessel. Silica gel (0.5 g) was added and the vessel was charged to 180 psi with H_2. The mixture was heated to 80 ºC for 24 h. After cooling to RT, the silica gel was filtered and the toluene was removed under reduced pressure. The polymer was dissolved in a small amount of CH_2Cl_2 and precipitated into acetone to yield **p(ehF8M$_{18}$)** (0.30 g, 75%) as a gummy, white solid. ^{1}H (300

MHz, $CDCl_3$) δ 0.4-1.2 (b, 210 H), 1.3 (b, 28 H), 1.65 (b, 4 H), 2.06 (b, 20 H), 2.67 (b, 4 H), 7.13 (m, 4 H), 7.5-7.8 (m, 38 H). ^{13}C NMR (75 MHz, $CDCl_3$) δ 10.3, 14.0, 22.8, 27.0, 27.1, 28.3, 29.2, 29.3, 29.5, 29.7, 31.9, 34.0, 34.1, 34.6, 34.7, 36.3, 44.5, 54.8, 55.1, 119.3, 119.4, 119.8, 122.9, 124.2, 125.8, 126.0, 126.1, 126.2, 127.1, 138.7, 139.8, 140.0, 140.2, 140.6, 141.3, 150.7, 150.9, 151.2.

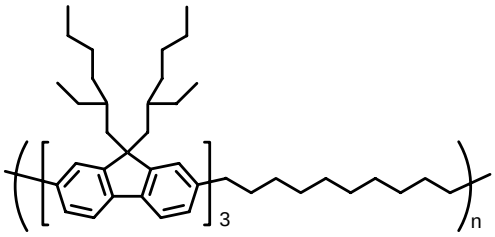

p(ehF$_3$M$_{10}$) *rwii55*: According to the method of Galli et al.,[86] **s(ehF$_3$M$_{10}$)** (0.15 g, 0.11 mmol), Grubbs 2 (2 mg, 2 mol %), and 3 ml CH_2Cl_2 were added to a round bottom flask and heated to reflux under N_2 atmosphere for 20 h. The reaction was quenched with ethyl vinyl ether and the solvent was removed under vacuum. The polymer was dissolved in 10 ml toluene and transferred to a stainless steel reaction vessel. Wilkinson's catalyst (10 mg) was added and the mixture was stirred for 18 h under an H_2 atmosphere. The polymer was dissolved in a small amount of CH_2Cl_2 and precipitated into acetone to yield **p(ehF$_3$M$_{10}$)** (0.11 g, 73%) as a gummy, white solid. ^1H (300 MHz, $CDCl_3$) δ 0.53-0.88 (b, 90 H), 1.3 (b, 12 H), 1.62 (b, 4 H), 2.06 (b, 12 H), 2.64 (t, 4 H, J = 7.5 Hz) 7.09-7.17 (m, 4 H), 7.5-7.8 (m, 14 H).

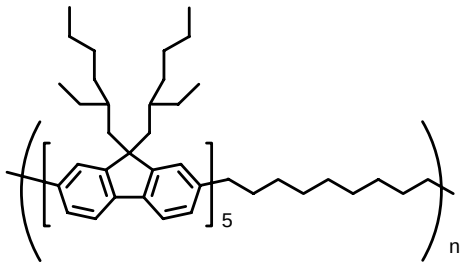

p(ehF$_5$M$_{10}$) *rwii63*: According to the method of Galli et al.,[86] **s(ehF$_5$M$_{10}$)** (0.15 g, 0.07 mmol), Grubbs 2 (1.2 mg, 2 mol%), and 5 ml CH_2Cl_2 were added to a round bottom flask and heated to reflux under N_2 atmosphere for 20 h. The reaction was quenched with ethyl vinyl ether and the solvent was removed under vacuum. The polymer was dissolved in 10 ml toluene and transferred to a stainless steel reaction vessel. Wilkinson's catalyst (10 mg) was added and the mixture was stirred for 18 h under a H_2 atmosphere. The polymer was dissolved in a small amount of CH_2Cl_2 and precipitated into acetone to yield **p(ehF$_5$M$_{10}$)** (0.10 g, 66%) as a white solid. . ^{1}H (300 MHz, $CDCl_3$) δ 0.53-0.88 (b, 150 H), 1.3 (b, 12 H), 1.62 (b, 4 H), 2.06 (b, 20 H), 2.64 (b, 4 H) 7.09-7.17 (m, 4 H), 7.5-7.8 (m, 26 H). ^{13}C NMR (75 MHz, $CDCl_3$) δ 10.3, 14.0, 22.8, 27.1, 28.3, 29.4, 31.9, 34.1, 34.7, 36.4, 44.6, 54.8, 55.1, 119.3, 119.8, 123.0, 124.2, 126.1, 127.1, 138.8, 140.0, 140.2, 140.6, 141.3, 150.8, 151.2.

50% p(ehF$_3$M$_{10}$) / 50% p(ehF$_5$M$_{10}$) *rwii66*: According to the method of Galli et al.,[86]**s(ehF$_3$M$_{10}$)** (0.10 g, 0.075 mmol) **s(ehF$_5$M$_{10}$)** (0.16 g, 0.075 mmol), Grubbs 2 (2.6 mg, 2 mol%), and 3 ml CH_2Cl_2 were added to a round bottom flask and heated to reflux under N_2 atmosphere for 20 h. The reaction was quenched with ethyl vinyl ether and the solvent was removed under vacuum. The polymer was dissolved in 10 ml toluene and transferred to a stainless steel reaction vessel. Wilkinson's catalyst (10 mg) was added and the mixture was stirred for 18 h under a H_2 atmosphere. The polymer was dissolved in a small amount of CH_2Cl_2 and precipitated into acetone to yield the copolymer (0.15 g, 58%) as a white solid.

10% p(ehF$_3$M$_{10}$) / 90% p(ehF$_5$M$_{10}$) *rwii66*: According to the method of Galli,[86]**s(ehF$_3$M$_{10}$)** (0.014 g, 0.011 mmol) **s(ehF$_5$M$_{10}$)** (0.20 g, 0.095 mmol), Grubbs 2 (2.6 mg, 2 mol%), and 5 ml

CH_2Cl_2 were added to a round bottom flask and heated to reflux under N_2 atmosphere for 20 h. The reaction was quenched with ethyl vinyl ether and the solvent removed. The polymer was dissolved in 10 ml toluene and transferred to a stainless steel reaction vessel. Wilkinson's catalyst (10 mg) was added and the mixture was stirred for 18 h under a H_2 atmosphere. The polymer was dissolved in a small amount of CH_2Cl_2 and precipitated into acetone to yield the copolymer (0.15 g, 71%) as a white solid.

2.0 PHOSPHORESCENT MERCURY SENSORS

The detection of toxic metal ions, such as mercury, in environmental samples is of great importance for the health of humankind. Mercury, in particular, is especially hazardous. The EPA has set limits of 2 ppb in drinking water due to its toxicity and potential for causing health issues such as birth defects.[87-89] Detection of low levels of mercury ions in aqueous samples, where other metal ions may also be present at high levels, is therefore an area of much current interest in the scientific research community.

Mercury detecting systems generally use absorption,[43, 90-94] emission,[95-106] or dual channels[107-110] as the reporting signal for mercury detection and, of these different detectors, fluorescent sensors are the most widely studied due to the sensitivity of the emission measurement. Fluorescent mercury sensors usually exhibit an increase or a decrease in the intensity of the emission in the presence of mercury because of a perturbation of the chromophore or an energy transfer that affects the photophysics. Many of the fluorescent mercury sensors are capable of detecting concentrations of mercury on an equal molar level as the sensor and can generally detect mercury ions at concentrations down to 10^{-6} M.[111] For example a 10^{-6} M solution of the sensor is capable of measuring a 10^{-6} M concentration of mercury in the solution. Therefore, the limit for mercury detection is determined by the sensitivity of the instrument used to measure the emission and any background fluorescence from other emitting materials in the sample which may mask the signal from the fluorescent

sensor. As the sensor's fluorescence becomes weaker because of dilution, the background fluorescence from other materials in the sample becomes more and more troublesome in the measurement.

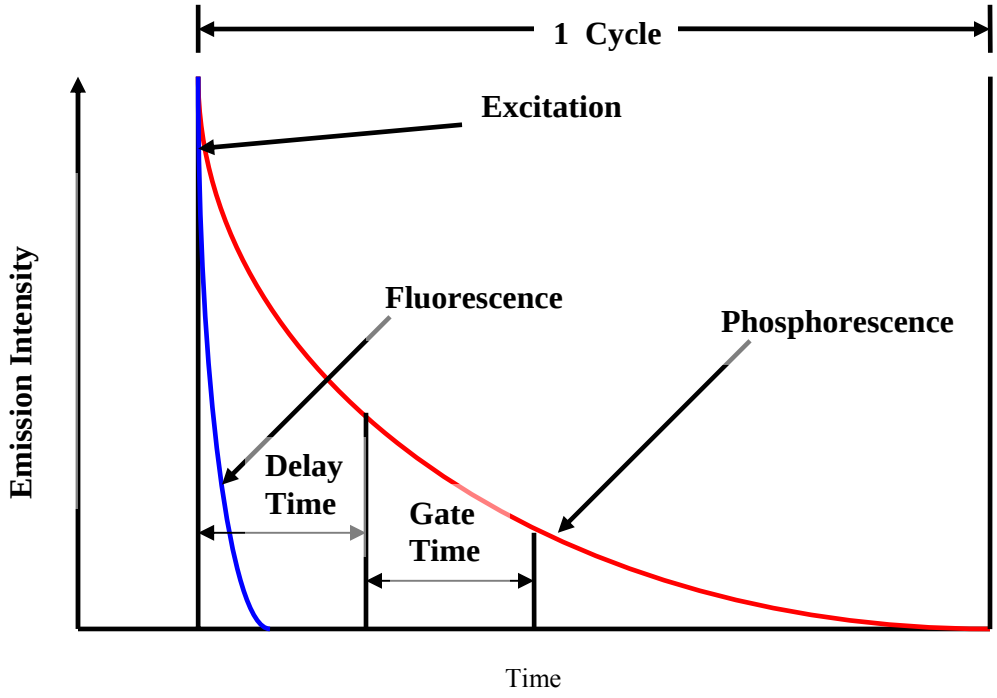

Figure 2.1. An illustration of time resolved emission spectroscopy. The phosphorescent emission can be measured during the gate time after the delay thereby eliminating the background fluorescence.

Time resolved emission measurements of phosphorescent based sensors, the methodology that we exploit in the systems described herein, can circumvent the problem of background fluorescence that limits the detection of very low levels of the metal ions in many fluorescent sensors of metal ions. Phosphorescent or other materials with long lived luminescence generally have excited state lifetimes (> 1 μs) considerably longer than fluorescent materials (< 200 ms). Time resolved emission spectroscopy (Figure 2.1) allows for the for background fluorescence to be eliminated from the collected spectra. After excitation of the sample with a light source there is a delay before the measurement of the of the longer lived

luminescence. This delay time is longer than any fluorescence emitted from the sample which eliminates any background fluorescence from the emission spectrum. The gate time is the only period during which the emission spectrum is collected. This cycle of emission data collection can be repeated and combined for many cycles thereby increasing the signal of the phosphorescent material. The accumulation of the time resolved emission cycles allows for the acquisition of spectrum with no background noise even from weakly emitting phosphorescent samples. Only a few examples of phosphorescent detection systems for mercury have reported in the literature.[108-110, 112, 113]

A coordinating species capable of binding mercury selectively is a key component in the design of selective phosphorescent and fluorescent mercury sensors. This coordinating species must have a high binding constant for mercury and a low binding constant for other metals such as iron and zinc that may be present at high levels in environmental samples. The binding of mercury must also be capable of causing a change in the photophysical properties of the sensor and therefore proper connectivity of the binding ligand to the emitting chromophore is also critical in the mercury sensor design.

Herein, is presented the preparation and characterization of two different phosphorescent mercury sensors. The sensors use either a thymine or the similar uracil functionality as the mercury coordinating species. The first sensor, discussed in this chapter, is based on iridium complexes with substituted 2-phenylpyridines as ligands. The second mercury sensor, discussed in Chapter 3, is a combination of fluorene chemistry discussed in Chapter 1 and lanthanide ions that have long luminescent properties. Both systems show sensitivity to mercury salts with selectivity for mercury over other metal ions.

2.1 IRIDIUM COMPLEXES FOR MERCURY SENSING

2.1.1 Introduction

Our first sensing system exploits the well-known phosphorescent properties of iridium bearing cyclometalated 2-phenylpyridine (**ppy**) derivatives as ligands. The use of iridium complexes as emissive materials has been extensively studied due their potential application in OLEDs where high quantum yields of emission and radiative decay from the triplet state are desired features.[114-119] Complexes bearing **ppy** ligands have well studied photophysical properties and it is known that these ligand systems can be easily modified to tune the photophysical and electrochemical properties. Compounds in this class also have good chemical stability as well as the high degree of photostability that is necessary for OLEDs. These properties make this family of compounds attractive for use as sensors. Although the excited state lifetimes of iridium complexes are relatively short (<5 μs) for phosphorescent materials, time resolved emission measurements of a fluoride anion sensing iridium complex has been demonstrated with proper equipment.[120] Iridium complexes with derivatives of 2-phenylpyridine have been used as sensors for a variety of species such as oxygen,[121-123] fluorine anions,[120, 124] assorted metal cations,[125] and homocystine.[126]

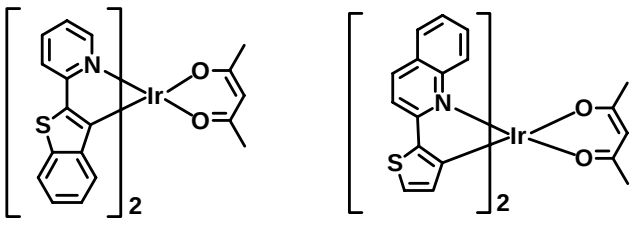

Ir(btp)$_2$(acac) **Ir(thq)$_2$(acac)**

Figure 2.2. Two reported iridium based mercury sensors capable of detecting mercury by coordination through the sulfur atoms.[109, 110]

Two iridium complexes capable of detecting mercury have been reported and these complexes use ligands with thiophene or benzothiophene groups (Figure 2.2) which can coordinate mercury with a sulfur atom.[109, 110] The complexes show a change in both absorption and emission energy as well as a change in the oxidation potentials of the complexes in the presence of mercury ions. These iridium compounds also demonstrate some selectivity for mercury over other metal ions in the absorption spectrum but show emission quenching when some other metal ions, notably iron, are present. This possibility of the sulfur atom binding to a variety of metal ions is problematic for the use of this mercury binding motive in selective metal ion sensors.

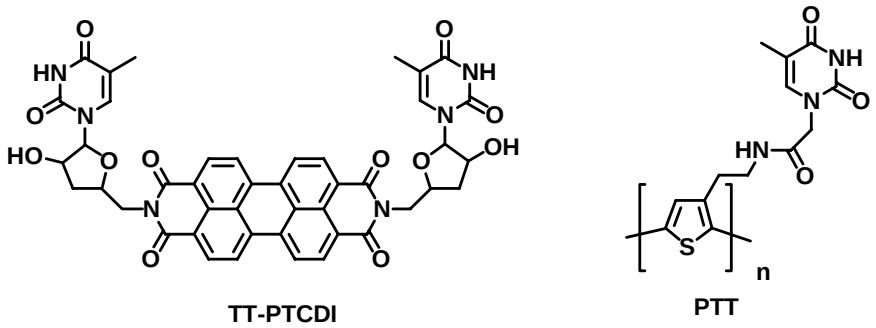

Figure 2.3. Previously reported fluorescent based mercury sensors that utilize thymine units for mercury coordination. [95, 105]

The use of the thymine functionality as a mercury ion coordinating species in fluorometric[95, 105, 127-131] and calometric[93] mercury ion sensors has been recently been exploited by several groups. The thymine group has been shown to be highly selective in coordinating mercury in DNA strands as well as small molecules and polymers containing thymine functionalities. The fluorescent mercury sensors with the thymine functional groups shown in Figure 2.3 use aggregation as the quenching mechanism since the mercury ions prefer bind to two thymine units.[95, 105] The aggregation causes the chromophores attached to the thymine units into close proximity with another chromophore causing quenching through π-stacking or energy

transfer. These sensors have been shown to be highly sensitive toward mercury and show no effect of other metal ions in competing ion studies.

The reversible binding of mercury to DNA was first discovered in 1952 and the crystal structures of 2:1 complexes of 1-methylthymine to mercury atoms have been studied.[132] The 1-methylthymine-mercury complex was formed by reacting mercury oxide with 1-methylthymine in methanol at neutral pH. The complex shows a coordination of mercury to the 3-nitrogen position of the two 1-methylthymine ligands (Figure 2.4).

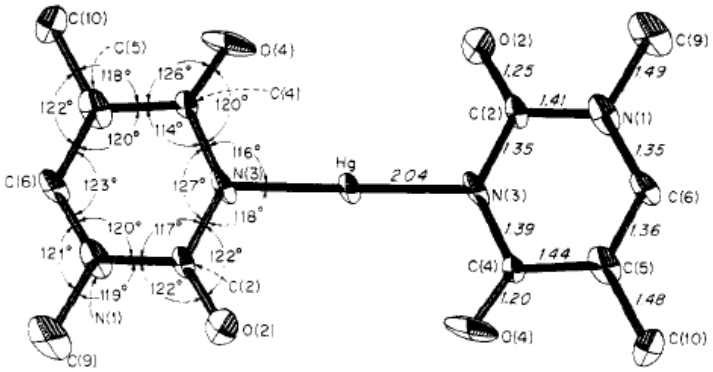

Figure 2.4. The crystal structure of a 2:1 complex of 1-methylthime and mercury. (Figure reproduced without permission from reference 132).

In this report, we describe the conjugated attachment of the uracil, which differs from thymine in that is has no 1-methyl group, directly to the 2-phenylpyridine ligand of an iridium complex and the study of its potential as a selective, phosphorescent, turn-off mercury sensor. The uracil group has a similar mercury coordinating environment as thymine and should also be useful as a mercury coordinating ligand for mercury detection. The commercial availability of 5-iodouracil makes the direct linking of the emissive chromophore to the double bond of uracil via Suzuki couplings an attractive technique for creating mercury sensors. This linkage incorporates the mercury coordination site into the emissive chromophore creating a system where the

electronic effects of mercury binding could cause changes in the emissive properties of the chromophore system.

2.1.2 Design of the Mercury Sensing Iridium Complex

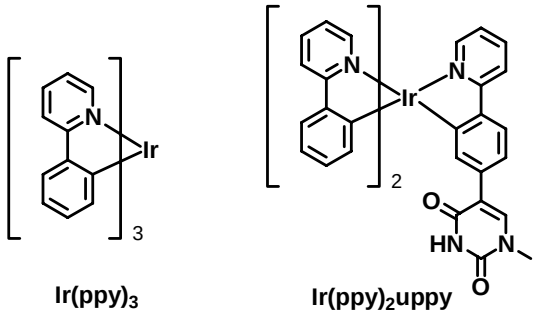

Figure 2.5. A well studied phosphorescent iridium complex, **Ir(ppy)$_3$**, and the mercury sensing iridium complex, **Ir(ppy)$_2$(uppy)**, made in this work.

The iridium complex, **Ir(ppy)$_2$(uppy)** (**uppy** = uracil-phenylpyridine) (Figure 2.5), was designed to exploit the known proclivity of cyclometalated iridium compounds of this type to emit from phosphorescent ^{3}MLCT states. It is also know from this literature that the modification of the ligands can be used to tune the emission energy by manipulating the HOMO-LUMO gap of the molecule. In the case of heteroleptic derivatives, the emission of complexes with different photoactive ligands is dominated by the lowest energy ligands.[133-136] Figure 2.5 shows the previously reported and well studied homoleptic complex **Ir(ppy)$_3$** and the mercury sensing derivative, **Ir(ppy)$_2$(uppy)**, that is the focus of this work. In **Ir(ppy)$_2$(uppy)**, the uracil group is conjugated through the 2-phenylpyridine group that is coordinated to the iridium atom.

Concerns about the complexation of the uracil group to iridium as well as the **uppy** ligand's more challenging synthesis were both factors in our decision to prepare a heteroleptic cyclometalated iridium complex. Smaller amounts of the uracil containing ligand are needed

for the synthesis of the heteroleptic complex and there is less probability for coordination of the uracil group to iridium. Previous groups have shown that the coordination of uracil and similar functional groups through the 1-nitrogen position with platinum to be facile and concerns over the potential coordination of the uracil group on the **uppy** ligand to iridium and subsequent interference with the cyclometalation reaction lead to the heteroleptic design.[137, 138]

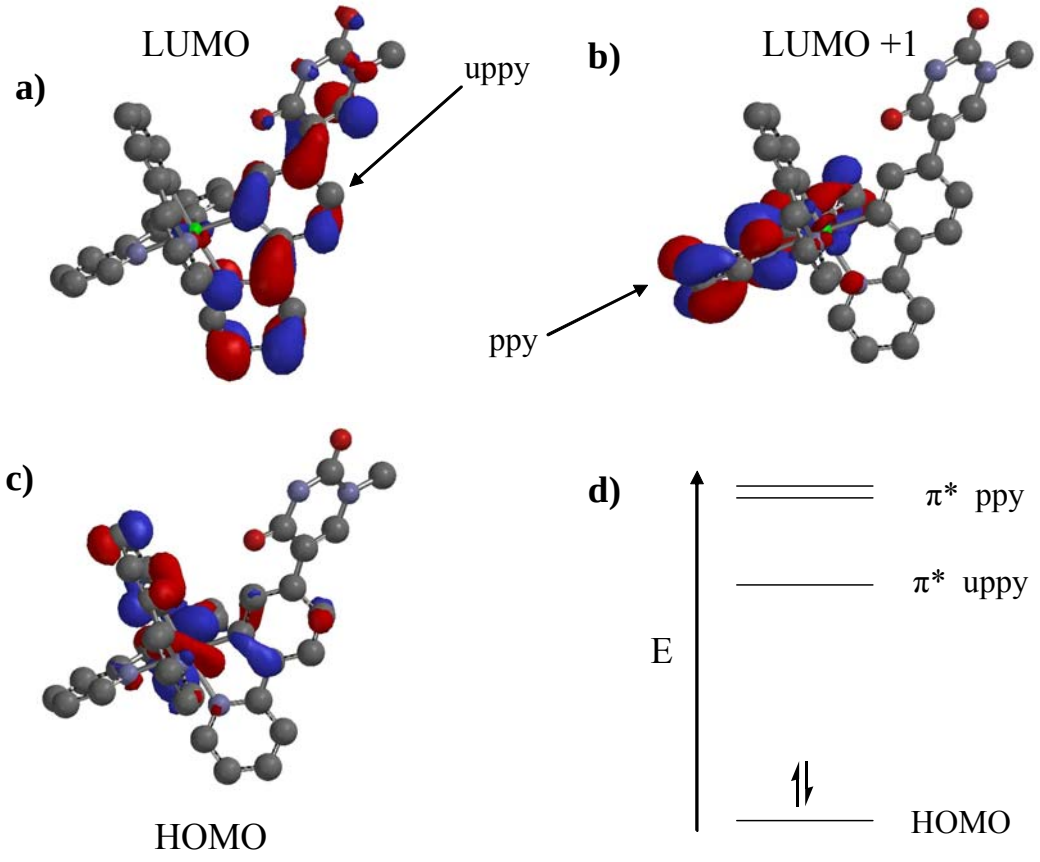

Figure 2.6. The (a) LUMO, (b) LUMO +1, and (c) HOMO surfaces of **Ir(ppy)$_2$(uppy)** as calculated using B3LYP Density Functional Theory. (d) An energy level diagram illustrating the lower energy π^* level of the uppy ligand compared to the unsubstituted ppy ligand.

Table 2.1. HOMO and LUMO energy values from B3LYP Density Functional Theory calculations[a] for **Ir(ppy)$_2$(uppy)** and **Ir(ppy)$_3$** .

	Energy (eV)	
	Ir(ppy)$_2$(uppy)	**Ir(ppy)$_3$**
LUMO	-1.35	-1.20
HOMO	-4.83	-4.84

[a]Calculated by Spartan (Wavefunction, Inc.) software package

As the electronic spectra of the **Ir(ppy)$_2$(uppy)** will be of primary importance to the function of the complex as a phosphorescent sensor, a discussion of the electronic structure is relevant. One would expect that the increase in the conjugation of the **uppy** ligand as compared to the **ppy** ligand decreases the band gap of **Ir(ppy)$_2$(uppy)** due to the lower lying LUMO of the **uppy** ligand relative to **ppy**. Since the HOMO energy of the complex should remain nearly the same, the band gap of the complexes would be expected to decrease. To examine this hypothesis, Density Functional Theory (DFT) calculations using a 6-31G* basis set were performed on **Ir(ppy)$_3$** and **Ir(ppy)$_2$(uppy)** using the Spartan (Wavefunction, Inc.) software package. The HOMO and LUMO energies are shown in Table 2.1 and the HOMO, LUMO, and LUMO^{+1} surfaces of **Ir(ppy)$_2$(uppy)**are shown in Figure 2.6. The LUMO surface shown in Figure 2.6 clearly resides on the **uppy** ligand with the HOMO residing mainly on the iridium atom. The most likely MLCT transition would occur from the iridium to the **uppy** ligand in this complex. The linking of the uracil group to the 2-phenylpyrdine through the double bond increases the conjugation of this ligand and lowers the LUMO energy of the complex by 0.15 eV when compared to **Ir(ppy)$_3$**. It was hoped that the coordination of mercury by the uracil group would then perturb the photophysics either by the shifting of the emission color or by quenching

of the emission. Aggregation of the complexes in solution could potentially cause a quenching of the emission intensity as well.

2.1.3 Synthesis of Iridium Based Mercury Sensor

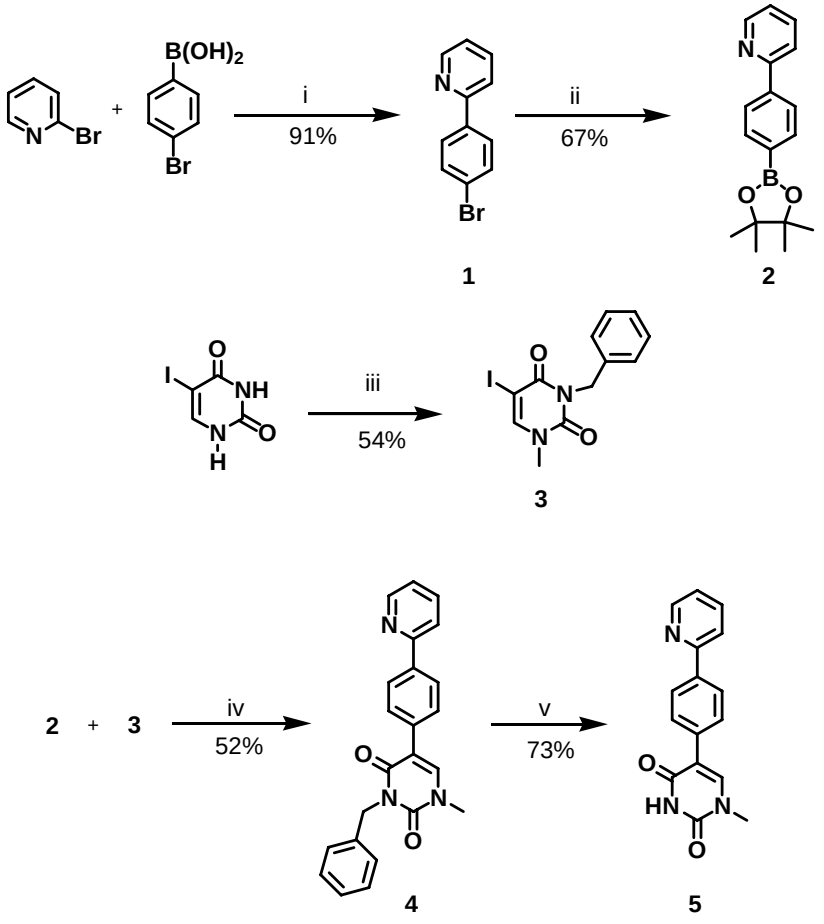

Scheme 2.1. The synthesis of the **uppy** ligand. (i) $Pd(PPh_3)_4$, K_2CO_3, toluene, ethanol, 80 ^oC. (iii) bis-(pinacolato)-diboron, $PdCl_2dppf$, KOAc, dioxane, 70 ^oC, 20 h. (iii)) MeI, K_2CO_3, DMSO, RT then BnBr, K_2CO_3, DMSO, RT. (iv) $PdCl_2dppf$, K_2CO_3, THF, 60 ^oC, 6 h. (v) $AlCl_3$, benzene, reflux, 3 h.

The synthetic strategy for incorporation of the uracil functionality into the 2-phenylpyridine ligand exploited two Suzuki couplings (Scheme 2.1). The high reactivity of 2-bromopyridine in Suzuki coupling conditions allowed for the selective coupling of 4-bromophenylboronic acid with 2-bromopyridine to give 2-(4-bromophenyl)pyridine **1** in very good yields. The conversion of the bromide **1** to the boronic pinacolate ester **2** by the Miyura reaction worked well with reasonable yields. An earlier attempt to convert bromide **1** to the boronic acid via lithium-halogen exchange and subsequent quenching with triisopropylborate was unsuccessful.

The uracil coupling partner **3** was produced by protection of the 3-nitrogen of 5-iodouracil with a benzyl group and alkylation of the 1-nitrogen with iodomethane. This two step reaction took advantage of the higher reactivity of the 3-nitrogen position in S_n2 reactions over that of the 1-nitrogen which allowed for selective 3-methyl and 1-benzyl substitution.

Suzuki coupling of protected uracil **3** and the boron pinacolate **2** proceeded rapidly to give product **4** in with a satisfactory yield.[139, 140] Deprotection of the benzylic group with aluminum chloride[141, 142] in benzene proceeded in high yields to produce the desired **uppy** ligand **5**.

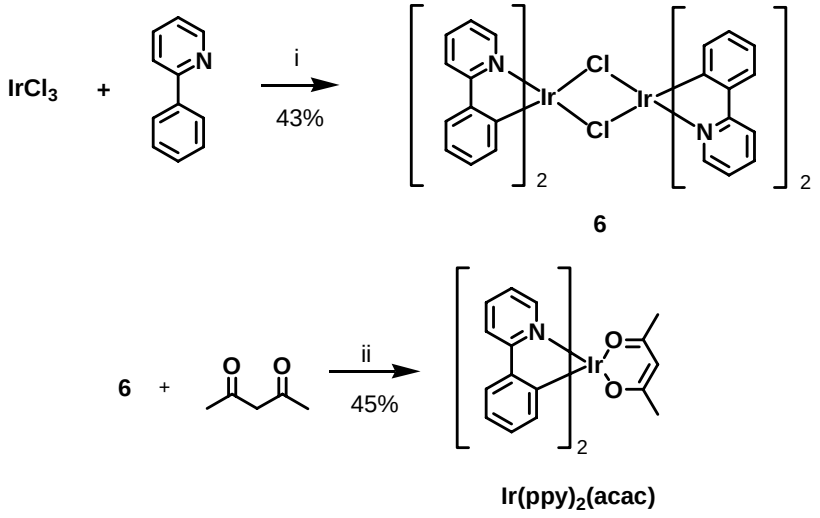

Scheme 2.2. Synthesis of **Ir(ppy)$_2$(acac)**. (i) 2-methoxyethanol, water, 90 ^{o}C, 20 h. (ii) K_2CO_3, 2-methoxyethanol, 80 ^{o}C. 20 h.

The cyclometalation reaction of 2-phenylpyridine with iridium chloride to form the chloro-bridged dimer **6** and the subsequent reaction of this chloro-bridged dimer with 2,4-pentanedione to form **Ir(ppy)$_2$(acac)** were accomplished by literature methods (Scheme 2.2).[115, 116] Previous reports have shown that the **acac** ligand can be displaced by substituted 2-phenylpyridine ligands.[143] Replacement of the **acac** ligand by the **uppy** ligand (Scheme 2.3) in refluxing ethylene glycol followed by purification by column chromatography and crystallization produced **Ir(ppy)$_2$(uppy)** in acceptable yields.

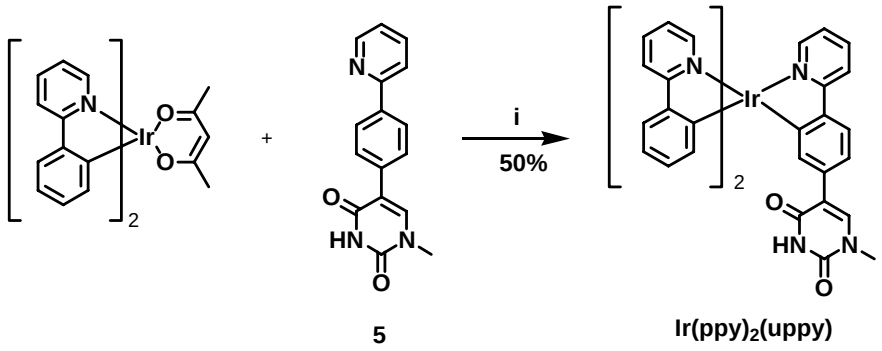

Scheme 2.3. Synthesis of **Ir(ppy)$_2$(uppy)**. (i) Ethylene glycol, reflux, 6 h.

2.1.4 Structure of Ir(ppy)$_2$(uppy)

2.1.4.1 NMR Spectroscopy

The simplicity of the ^{1}H NMR spectra of **Ir(ppy)$_2$(uppy)** is consistent with a pseudo facial arrangement of the ligands when compared to literature results for ***mer***- and ***fac***-**Ir(ppy)$_3$** (Figure 2.7). The integration of the doublet H_a at 8.15 ppm integrates to 3 protons which is consistent

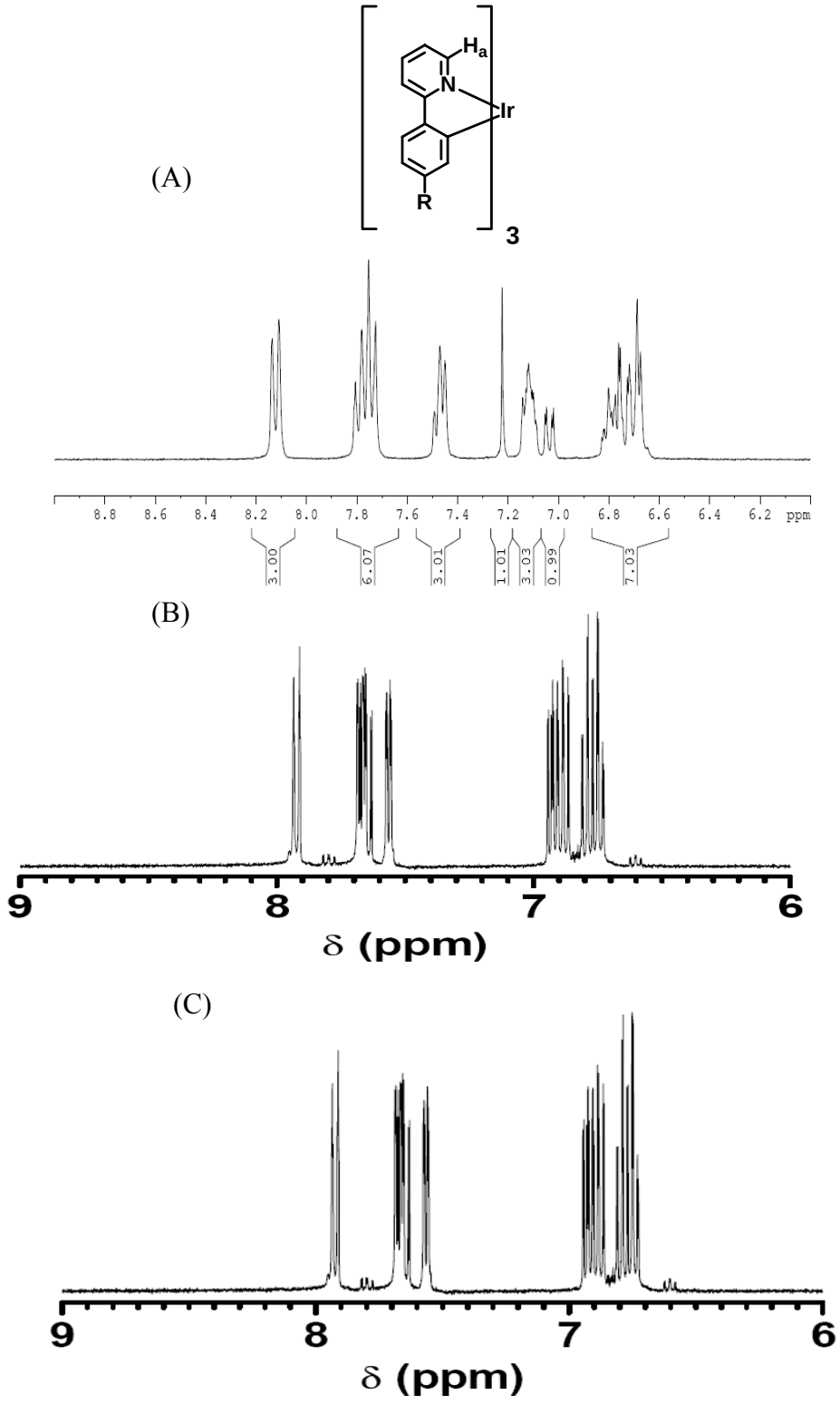

Figure 2.7. The ^{1}H NMR spectra of (A) **Ir(ppy)$_2$(uppy)**, (B) ***fac*-Ir(ppy)$_3$,** and **(C) *mer*-Ir(ppy)$_3$** (reproduced without permission).[143]

with the pseudo *fac* isomer of **Ir(ppy)$_2$(uppy)** where the *mer* isomer should have two different H_a species and should not integrate to 3 protons. Interestingly, only one doublet is observed at 8.15 ppm for H_a of **Ir(ppy)$_2$(uppy)** even though there are two different ligands and potentially two different H_a signals. It is likely that the close proximity of these protons to the iridium atom dominates their chemical shift. Based on these results the structure of the complex is assigned as a facial orientation.

2.1.5 Crystal Structure

Although the NMR spectra of **Ir(ppy)$_2$(uppy)** are consistent with a pseudo facial arrangement of the ligand the x-ray crystal structure of the complex shows the ligands in a meridional orientation. Single crystals of the complex were grown from slow diffusion of hexane into a concentrated solution of **Ir(ppy)$_2$(uppy)** in CH_2Cl_2. The structure shows that the complex has the three pyridine rings in an equatorial or meridonal orientation (Figure 2.8). The facial isomer has been shown to be the more stable thermodynamically stable isomer compared to the meridional isomer for tris substituted 2-phenylpyridine iridium complexes as the meridional isomers can be converted to the facial isomers thermally or by photoconversion with UV light.[143] The relatively high reaction temperature (180 ^oC) to form the complex generally produces the facial isomer of homoleptic tris 2-phenylpyridine complexes. It is possible that the sample that the crystals were isolated from contained small amounts of meridional complex in the bulk of the solution or that a different synthesis of the complex contained higher amounts of the meridional isomer than the samples that were analyzed by NMR spectroscopy.

The bond lengths for the iridium containing bonds of **Ir(ppy)$_2$(uppy)** are also consistent with the bonds lengths of ***mer*-Ir(tpy)$_3$** (4-tolylpyridine) (Table 2.2). **Ir(ppy)$_2$(uppy)** has bond

lengths that are comparable to those for the corresponding bonds of ***mer*-Ir(tpy)$_3$** whereas the bond lengths of the carbon to iridium and nitrogen to iridium bonds of ***fac*-Ir(ppy)$_3$** are all of nearly equal lengths.[143,144] Meridonal complexes exhibit longer nitrogen to iridium bonds for the pyridine rings that are *trans* to the phenyl ring when compared to the nitrogen to iridium bonds of pyridine rings that are trans to each other. This longer bond length is possibly the reason that the meridonal isomers have been shown to be less thermodynamically stable than the facial isomers of this family of 2-phenylpyridine iridium complexes.

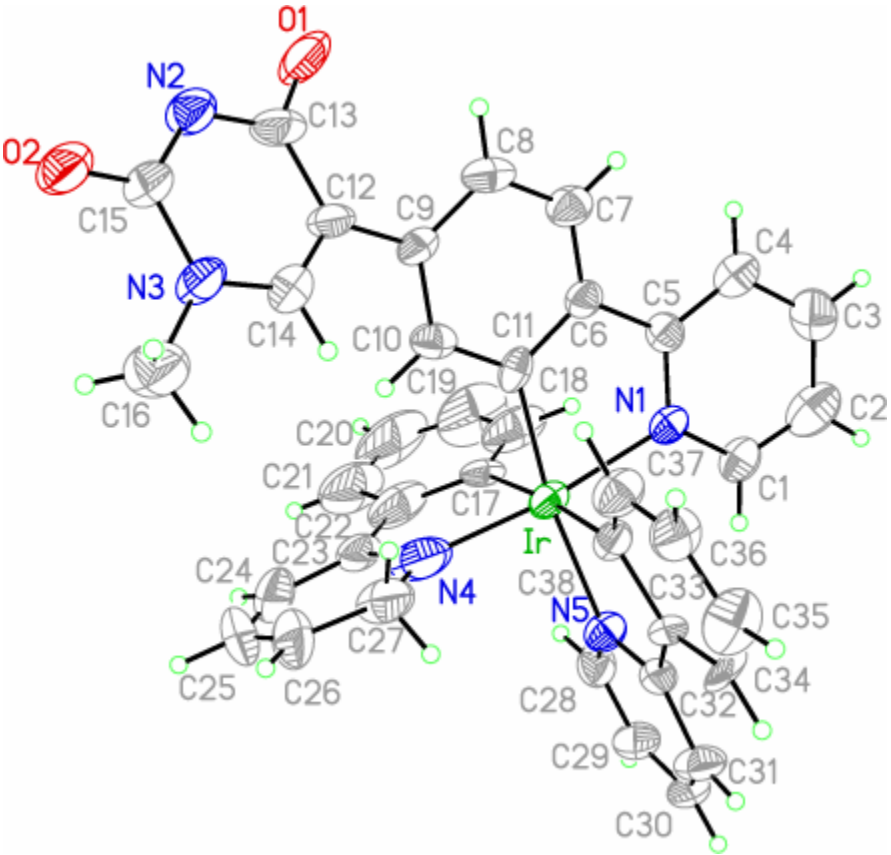

Figure 2.8. Structure of **Ir(ppy)$_2$(uppy)**. (Thermal ellipsoids drawn at 90% probability)

Table 2.2. The iridium containing bonds lengths of **Ir(ppy)$_2$(uppy)**, ***mer*-Ir(tpy)$_3$**, and ***fac*-Ir(ppy)$_3$**.

Bond Type	Bond Distance (Å)		
	Ir(ppy)$_2$(uppy)	*mer*-Ir(tpy)$_3$[a]	*fac*-Ir(ppy)$_3$[b]
Ir-C(11)	1.994	2.020	2.006
Ir-C(38)	2.015	2.076	
Ir-C(17)	2.095	2.086	
Ir-N(4)	2.034	2.044	2.088
Ir-N(1)	2.108	2.065	
Ir-N(5)	2.144	2.151	

[a]From reference 144. [b] From reference 145,

2.1.6 Photophysical Properties

The focus compound belongs to a family of phosphorescent iridium compounds whose photophysical properties are suitable for sensing applications. The heavy atom effect of iridium creates interesting changes in the photophysical properties of this family of iridium compounds when compared to many other transition metal complexes. The heavy atom effect and strong spin orbital coupling creates efficient intersystem crossing from the spin paired singlet state to the spin unpaired triplet state as illustrated in Figure 2.9. The radiative decay from this triplet state back to the ground state is an allowed transition and the quantum yields of emission for iridium complexes of this type in degassed solutions can be greater than 50%. The excited state lifetimes of the compounds are longer than fluorescent materials and are generally in the 1-100 μs range in degassed solutions. In air-saturated solutions the excited state lifetimes and quantum yields of emission are shortened due to the reaction of the triplet excited state with oxygen which generates singlet oxygen.

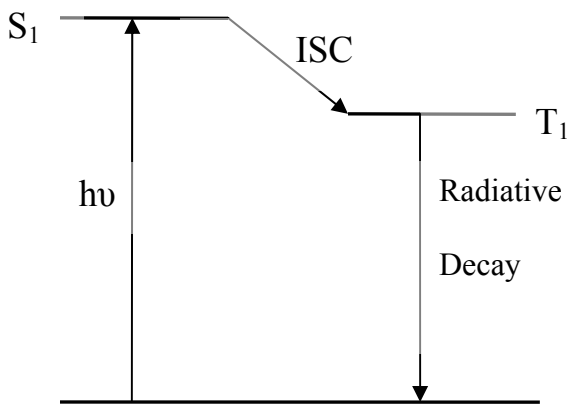

Figure 2.9. Illustration of the S_1 to T_1 transition for phosphorescent iridium complexes.

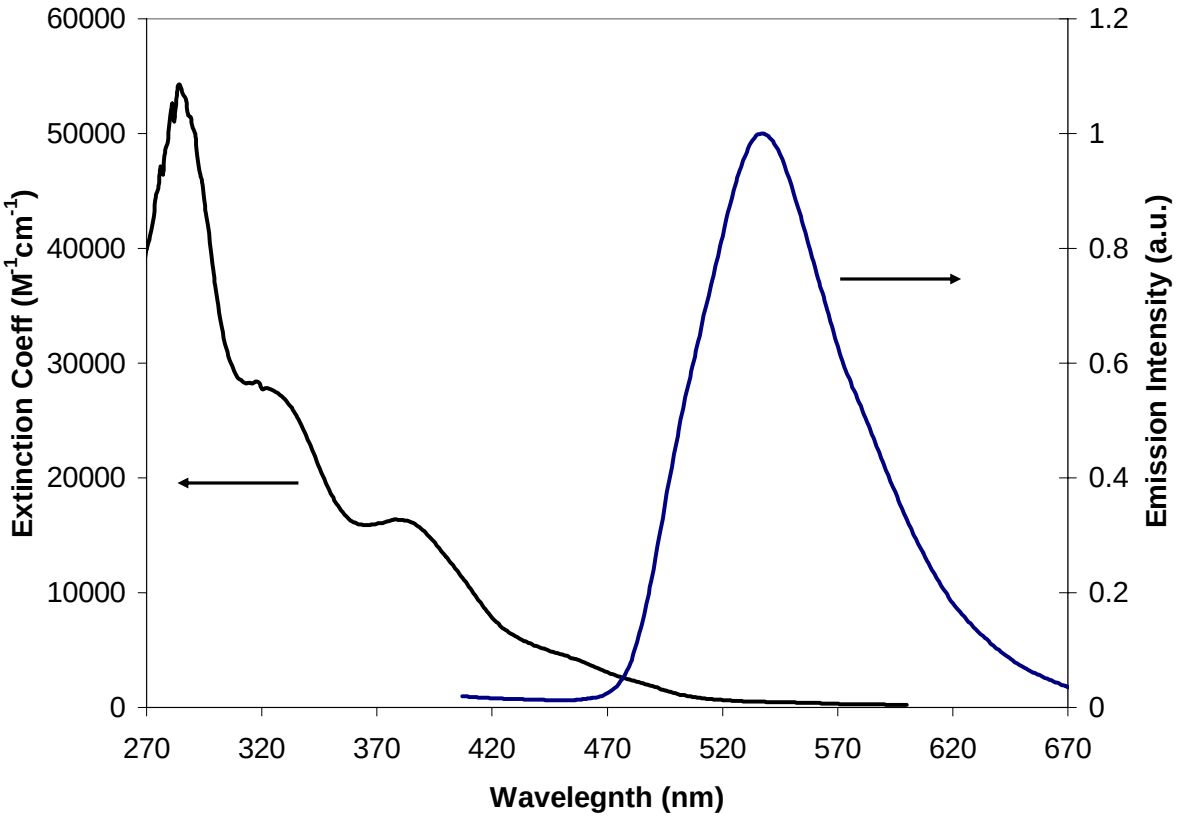

Figure 2.10. The absorption and emission spectra of **$Ir(ppy)_2(uppy)$**.

Although similar in overall behavior to **$Ir(ppy)_3$** and **$Ir(ppy)_2(acac)$**, the new uracil containing 2-phenylpyridine ligand changes the photophysics of the complex to a small degree

(Figure 2.10). The intense π-π^* band at 300 nm with extinction coefficient of 28000 $M^{-1}cm^{-1}$ is shifted to lower energy compared to **Ir(ppy)$_3$**. Weaker, less defined bands are seen at lower energies where the metal to ligand charge transfers are complicated due to the two potential ligands of different LUMO energies. The assignment of the weaker bands for ^{1}MLCT near 440 nm and the ^{3}MLCT bands near 440 m with extinction coefficients of 5000 $M^{-1}cm^{-1}$ and 2400 $M^{-1}cm^{-1}$ respectively is consistent with previous literature values for similar compounds. The similar extinction coefficients for the triplet and singlet MLCT bands shows the strong spin orbital coupling caused by iridium for the spin forbidden triplet excited states

The maximum emission peak at 537 nm of the complex is also shifted to lower energy by 20 nm when compared to **Ir(ppy)$_3$** or **Ir(ppy)$_2$(acac)** due to of the incorporation of the uracil group. This yellowish green emission has an excited state lifetime of 2.5 μs in an oxygen free 1:1 ethylene glycol to water solution which is comparable to **Ir(ppy)$_3$**. This family of compounds is significantly quenched by triplet oxygen and the excited state lifetimes become very short in the presence of oxygen.

2.1.7 Mercury Ion Sensing

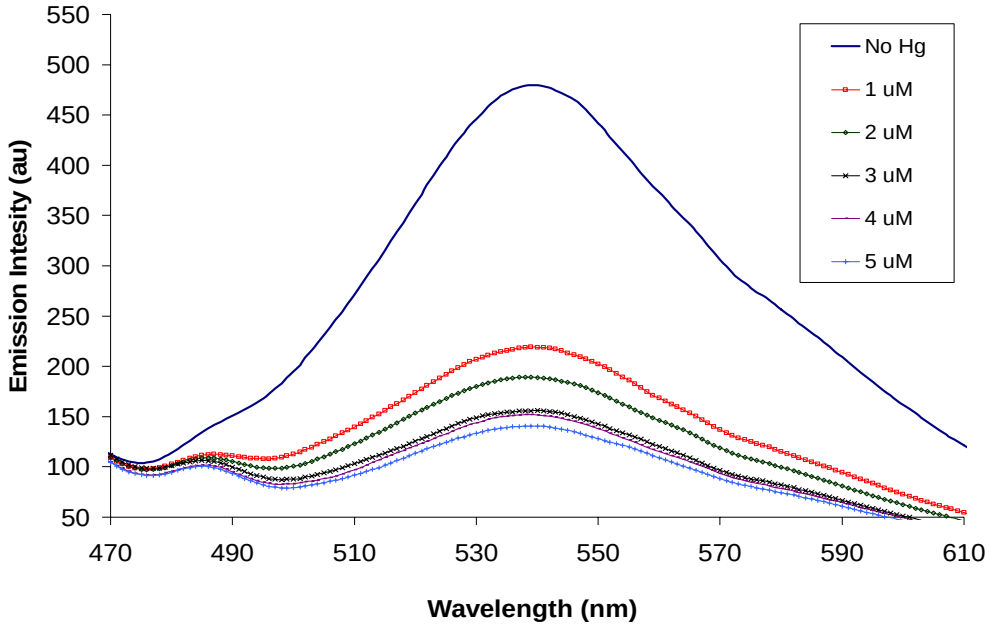

Figure 2.11. Emission spectrum of **Ir(ppy)$_2$(uppy)** at a concentration of 1 μM with varying levels of mercury acetate in 50% ethylene glycol / 50% water.

Ir(ppy)$_2$(uppy) exhibits the targeted mercury-sensing behavior as would be expected given the properties of the components. Although the complex is not completely soluble in water, it is soluble at 10^{-6} M in a 1:1 ethylene glycol: water solution. The emission and absorption of **Ir(ppy)$_2$(uppy)** was measured with varying levels of mercury ions present in the 1:1 ethylene glycol to water solutions. As shown in Figure 2.11, the compound is quenched by about 55% when 1 equivalent of mercury is present. Less significant decreases are seen as more equivalents are added. No spectral shift in emission is seen in the spectrum and only quenching

of emission is seen in a neutral solution. No change in the excited state lifetime is observed in the presence of mercury. In addition, there are very little spectral changes in the absorption spectrum in the mercury containing solutions.

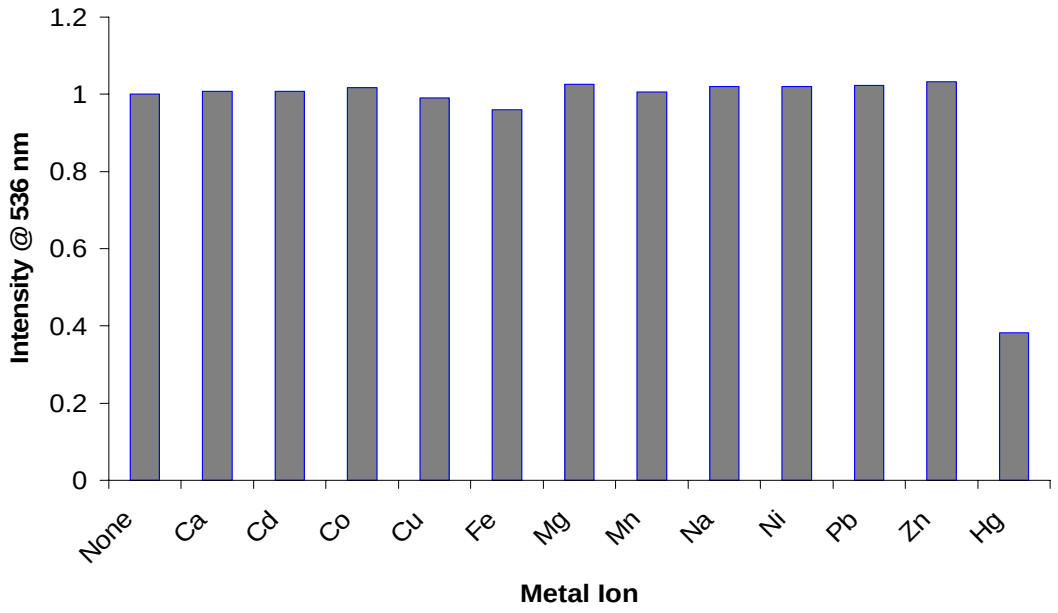

Figure 2.12. The relative emission intensity of **Ir(ppy)$_2$(uppy)** at a concentration of 1 μM with various metal ions at a concentration of 10 μM in 50% ethylene glycol / 50% water.

To determine the compound's ability to detect mercury ions selectively, the emissive properties of **Ir(ppy)$_2$(uppy)** were measured in presence of other common metal ions that could be present in environmental samples (Figure 2.12). The bar graph shows the emissive response of the compound to various metal ions (10 equivalents) when measured at 536 nm in a 1:1 ethylene glycol to water solution. No spectral shift is seen for any of the other ions and only significant quenching is seen for the mercury ions. This finding is not surprising given the previous work establishing the selectivity of the thymine functionality for binding mercury.

The formation of aggregates of the complex is the most likely cause of the decrease in emission of the complex in the presence of mercury. Although the mercury binding site of the

complex is conjugated into the emitting chromophore, this replacement of a proton with mercury does not seem to alter the photophysical properties of the complex dramatically. The lack of change in the absorption and shape of the emission bands does not indicate a major perturbation of the HOMO or LUMO of the complex at neutral pH. The coordination of mercury to the thymine groups has been studied and it has been shown that a complex with a 2:1 ratio of the ligand to mercury is formed. The similarity of thymine and uracil would suggest a 2:1 ligand to mercury complex would also be preferred for our complex. The formation of such an aggregate would be expected to quench the phosphorescent emission. In addition, it has been shown that increasing the concentration of iridium complexes in films and solution generally lowers the quantum yields of emission due to aggregation quenching.[145-152] Such aggregates can be difficult to identify since, in many cases, only small changes in the wavelength and shape of the emission spectrum is observed. Generally, the emission maximum shifts to slightly lower energy and a broadening of the emission spectrum is also observed.

2.1.8 Conclusions

An iridium complex with an uracil functionality for mercury binding was designed, synthesized, and the photophysical properties including its mercury sensing capabilities were measured. The complex showed the potential for mercury detection by phosphorescence quenching at 10^{-6} M levels as well as the selectivity for detecting mercury over other common metal ions that may be present in environmental samples. The sensitivity of the complex may be improved by use of time resolved emission spectroscopy on an appropriate instrument. The complex has reasonable solubility in water and ethylene glycol solutions that should be compatible with environmental

samples and similar materials have been proven to have a robust structure for long term studies making **Ir(ppy)$_2$(uppy)** potentially useful as a phosphorescent mercury sensor.

2.1.9 Experimental

2.1.9.1 Photophysical Characterization

The UV-Visible spectra were recorded on a Perkin-Elmer UV/VIS/NIR Spectrometer Lambda in DMSO at 10^{-5} M concentration. The steady state emission spectra were determined using a Varian Cary Eclipse Fluorescence Spectrophotometer in DMSO at 10^{-5} M. The mercury ion and competitive ion study was performed at 10^{-6} M in a non-degassed 50% ethylene glycol aqueous solution using the Varian Cary Eclipse Fluorescence Spectrophotometer. The relative emission intensity of the metal ions is the ratio of the metal containing sample versus the non metal containing solution.

2.1.9.2 X-Ray Crystallography

The single crystal X-ray structure was collected and solved by Dr. Steven Geib at the University of Pittsburgh. The data was collected at 203(2) K on a Bruker Smart Apex CCD diffactometer with graphite-monochromated MoKα (λ = 0.71073 Å) radiation.

2.1.9.3 Density Functional Calculations

The Density Functional Calculations were performed at the B3LYP/6-31G* level using the Spartan software package (Wavefunction, Inc.). The HOMO and LUMO energies and surfaces were calculated from minimized singlet geometries to approximate the ground state.

2.1.9.4 Synthetic Methods and Equipment

$Pd(PPh_3)_4$ (Strem), and $Pd(Cl)_2$dppf (Strem), were commercially obtained and stored in a nitrogen-filled glove box. All other reagents were commercially obtained and used without further purification. ^{1}H- (300 MHz) and ^{13}C-NMR (75 MHz) spectra were recorded with Bruker spectrometers. Chemical shifts were referenced to residual ^{1}H or ^{13}C signals in deuterated solvents. Column chromatography was performed using Sorbent 60Å 40-63 μm standard grade silica. GC-MS was performed on a Hewlett Packard Series 5980 GC/5971 A MS with a Hewlett Packard Series 1 column. GC was performed on a Hewlett Packard Series 6850 GC with a Hewlett Packard Series 1 methyl siloxane column. HRMS were obtained on a Fison VG Autospec in the Mass Spectral Facility of the University of Pittsburgh.

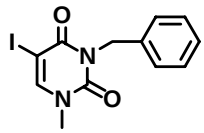

3

3-benzyl-5-iodo-1-methyl-uracil (3) *rwiii90*: 5-iodouracil (2.0 g, 8.4 mmol), iodomethane (1.31 g, 9.0 mmol), and K_2CO_3 (1.24 g, 9.0 mmol) were added to 30 ml of DMSO and stirred at RT for 4 h. Benzyl bromide (1.86 g, 11.0 mmol) and K_2CO_3 (1.39 g, 0.010 mmol) were then added and the mixture was allowed to stir for 16 h. Water (200 ml) was added and aqueous layer was washed with ethyl acetate (3 x 50ml). The organic layers were combined, washed with brine, and dried over magnesium sulfate. The solvent was removed and the product was purified by column chromatography (silica gel, 10% ethyl acetate in CH_2Cl_2 as the eluent) to yield a white solid (1.56 g, 54%). ^{1}H (300 MHz, $CDCl_3$) δ 0.3.38 (s, 3 H), 5.14 (s, 2 H), 7.25 (m, 3 H), 7.43 (d, 2 H, J = 7.5 Hz), 7.56 (s, 1 H). ^{13}C NMR (75 MHz, $CDCl_3$) δ 37.2, 46.1, 67.5, 127.9, 128.5, 129.5, 136.3, 147.6, 151.4, 160.3. MS (EI) *m/z* 342 ($M^{\cdot+}$), 233, 154. HRMS calcd for $C_{12}H_{11}IN_2O_2$: 341.9848. Found 341.9865.

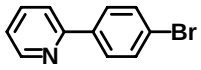

1

2-(4-bromophenyl)-pyridine (1) *rwii94*: 2-bromopyridine (5.93 g, 37.5 mmol), 4-bromophenyl boronic acid (3.0 g, 15 mmol), $Pd(PPh_3)_4$ (0.34 g, 2 mol%), and potassium carbonate (8.3 g, 60 mmol) were added to 30 ml toluene and 20 ml of ethanol under N_2. After the reaction was heated to 80 ºC for 20 h, water was added and the aqueous layer was washed with ethyl acetate (2 x 50 ml). The combined organic layers were washed with brine and dried over magnesium sulfate. The excess 2-bromopyridine was removed under vacuum and the product was purified by column chromatography (silica gel, CH_2Cl_2 as the eluent) to yield a white solid (3.2 g, 91%). ^1H (300 MHz, $CDCl_3$) δ 7.27 (m, 1), 7.64 (d, 2 H, J = 8.1 Hz), 7.77 (m, 2 H), 7.88 (d, 2 H, J=8.7), 8.7 (d, 1 H, J = 4.8 Hz). ^{13}C NMR (75 MHz, $CDCl_3$) δ 120.3, 122.4, 123.5, 128.5, 131.9, 136.9, 138.3, 149.8, 156.3. MS (EI) *m/z* 234 ($M^{\cdot+}$), 154, 127, 119, 101. HRMS calcd for $C_{11}H_8BrN$: 232.9840. Found 232.9838.

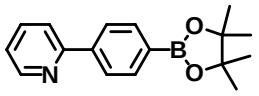

2

2-[4-(4,4,5,5-Tetramethyl-[1,3,2]dioxaborolan-2-yl)-phenyl]-pyridine (2) *rwii95*: Under an N_2 atmosphere, 2-(4-bromophenyl)-pyridine **1**, bis-(pinacolato)-diboron (1.63, 64 mmol), $PdCl_2dppf$ (0.10, 3 mol%), and potassium acetate (1.7 g, 17.2 mmol) were dissolved in 15 ml of 1,4-dioxane. The mixture was sparged with N_2 for 20 min and then the reaction was heated to 70 ºC for 20 h. The solvent was removed under reduced pressure and the solids were extracted with CH_2Cl_2 and water. The organics were washed with brine, dried over magnesium sulfate. The product was purified by column chromatography (silica gel, 40% ethyl acetate / hexanes as the eluent) to yield a white solid (0.81 g, 67%). ^1H (300 MHz, $CDCl_3$) δ 1.35 (s, 16 H), 7.25 (m, 1

H), 7.7-7.9 (m, 4 H), 8.0 (d, 2 H, J = 6.3 Hz), 8.67 (d, 1 H, J = 1 Hz). ^{13}C NMR (75 MHz, $CDCl_3$) δ 24.7, 83.9, 120.5, 122.4, 126.0, 135.0, 136.7, 149.7 MS (EI) *m/z* 281 (M^{+}), 266, 239 HRMS calcd for $C_{17}H_{20}BNO_2$: 281.1578. Found 281.1587.

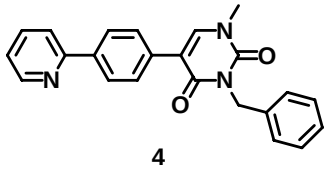

4

3-Benzyl-1-methyl-5-(4-pyridin-2-yl-phenyl)-uracil (4) *rwii92*: The boron pinacolate **2** (0.36 g, 1.3 mmol), 3-benzyl-5-iodo-1-methyl-uracil **3** (0.44 g, 1.3 mmol), $PdCl_2$dppf (0.05 g, 5 mol%), K_2CO_3 (2.6 ml, 2 M, 5.2 mmol), were added to 10 ml THF. After the reaction was heated to 60 ºC for 6 h under an N_2 atmosphere, water was added and the aqueous layer was extracted with ethyl acetate (2 x 20 ml) The combined organic layers were washed with brine and dried over magnesium sulfate. The product was purified by column chromatography (silica gel, 20% ethyl acetate / CH_2Cl_2 as the eluent) to yield a white solid (0.25 g, 52%). ^{1}H (300 MHz, CD_2Cl_2) δ 3.42 (s, 3 H), 5.18 (s, 2 H), 7.28 (m, 4 H), 7.40 (s, 1 H), 7.63 (d, 2 H, J = 3.9 Hz), 7.77 (m, 2 H), 8.04 (d, 2 H, J = 6.3 Hz), 8.66 (d, 1 H, J = 1 Hz). ^{13}C NMR (75 MHz, CD_2Cl_2) δ 24.6, 37.0, 44.6, 113.6, 120.2, 122.2, 126.7, 127.4, 128.3, 128.5, 128.7, 133.9, 136.7, 137.3, 138.6, 141.1, 149.7, 156.5, 162.0. MS (EI) *m/z* 369 (M^{+}), 235, 208 HRMS calcd for $C_{23}H_{19}N_3O_2$: 369.1479. Found 369.1477.

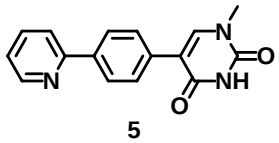

5

1-Methyl-5-(4-pyridin-2-yl-phenyl)-uracil (5) *rwiii93*: 3-Benzyl-1-methyl-5-(4-pyridin-2-yl-phenyl)-uracil **4** (0.20 g, 0.54 mmol) and aluminum chloride (0.35 g, 2.7 mmol) were added to 5 ml of benzene and the mixture was heated to reflux for 3 h. The reaction was quenched into

water and the aqueous layer was extracted with $CHCl_3$. The aqueous layer was adjusted to pH = 9 with potassium carbonate and this aqueous solution was extracted $CHCl_3$ (3 x 50 ml). The combined organics were washed with brine and dried over magnesium sulfate. The solvent was removed to yield a white solid product (0.11 g, 73%). ^{1}H (300 MHz, d_6-DMSO) δ 3.45 (s, 3 H), 7.33 (t, 1 H, J = 6.6 Hz), 7.72 (d, 2 H, J = 8.4 Hz), 7.86 (t, 1 H, 7.5 Hz), 7.96 (d, 1 H, J = 7.5 Hz), 8.07 (m, 3 H), 8.65 (d, 1H, J = 4.5 Hz), 11.74 (s, 1 H). ^{13}C NMR (75 MHz, d_6-DMSO) δ 35.9, 55.4, 112.0, 120.6, 123.0, 126.6, 128.4, 134.1, 137.6, 137.7, 145.0, 150.0, 151.2, 156.1, 163.2 MS (EI) *m/z* 279 ($M^{\cdot+}$) 256, 235, 230. HRMS calcd for $C_{16}H_{13}N_3O_2$: 279.1008. Found 279.0994.

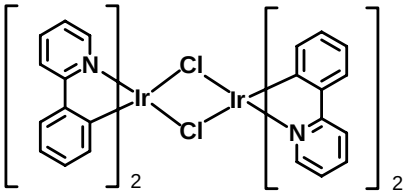

6

$[(ppy)_2Ir(\mu\text{-}Cl)]_2$ (6) *rwii14*: According to the methods of Lamansky et al,[115, 116] 2-phenylpyridine (1.04 g, 6.7 mmol) and $IrCl_3$ (1.0 g, 3.3 mmol) were added to 2-methoxyethanol (8 ml) and water (2 ml) under N_2. The mixture was heated to 90 ºC for 24 h during which a yellow precipitate was formed. The precipitate was filtered and washed with methanol to yield a yellow solid (1.5 g, 43%) ^{1}H (300 MHz, d_6-DMSO) δ 3.45 (s, 3 H), 7.51 (t, 1 H), 7.72 (d, 2 H), 7.85 (t, 1 H), 7.96 (m, 3 H), 8.65 (d, 1H), 11.74 (s, 1 H).

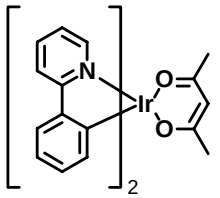

$Ir(ppy)_2(acac)$

$Ir(ppy)_2(acac)$ *rwii19*: According to the methods of Lamansky et al,[115, 116] $[(ppy)_2Ir(\mu\text{-}Cl)]_2$ **6** (0.50 g, 0.46 mmol), 2,4-pentanedione (0.19g, 1.9 mmol) and K_2CO_3 (0.26 g, 1.9 mmol) were

added to 10 ml of 2-methoxyethanol and heated to 80 ºC for 20 h. After the solvent was removed under reduced pressure, water was added and the aqueous layer was washed with CH_2Cl_2 (2 x 20 ml). The combined organics were washed with brine and dried over magnesium sulfate. The product was purified by column chromatography (silica gel, CH_2Cl_2 as the eluent) and crystallized from CH_2Cl_2 and hexanes to yield a yellow solid (0.25 g, 45%). ^{1}H (300 MHz, $CDCl_3$) δ 1.81 (s, 6 H), 6.23 (dd, 2 H, J=7.5, 0.9 Hz) 6.70 (td, 2H J=7.4, 1.5 Hz), 6.86 (td, 2H J=7.4, 1.5 Hz), 7.19 (td, 2 H, J=5.7, 1.5) 7.59 (dd, 2H, J=7.5, 1.2), 7.78 (td, 2 H, J=7.5, 1.5), 7.88 (d, 2 H, J=8.1), 8.51 (d, 2 H, J=5.7) ^{13}C NMR (75 MHz, $CDCl_3$) δ 26.3, 100.3, 118.5, 120.8, 121.8, 123.8, 128.8, 133.1, 137.1, 145.1, 147.4, 148.2, 168.2, 184.7. MS (TOF ES) *m/z* 623. HRMS calcd for $C_{27}H_{23}N_2O_2IrNa$: 623.1204. Found 623.1287.

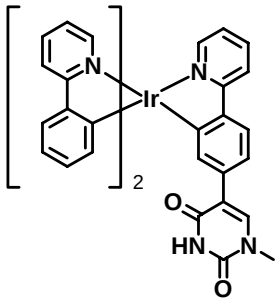

Ir(ppy)$_2$(uppy)

Ir(ppy)$_2$(uppy) *rwii19*: **Ir(ppy)$_2$(acac)** (0.13 g, 0.22 mmol) and **uppy 5** (0.06g, 0.22 mmol) were added to 5 ml of ethylene glycol and heated to reflux for 6 h under N_2. Water was added and the aqueous layer was washed twice with CH_2Cl_2. The combined organics were washed with brine and dried over magnesium sulfate. The product was purified by column chromatography (silica gel, 40% ethyl acetate / CH_2Cl_2 as the eluent) and crystallized from CH_2Cl_2 and hexanes to yield a yellow solid (0.08 g, 50%). ^{1}H (300 MHz, d_6-DMSO) δ 3.31 (s, 3 H), 6.6-6.8 (m, 8 H), 7.06 (dd, 1 H, J = 8.4 Hz, J = 1.8 Hz), 7.13 (b, 3 H), 7.22 (s, 1 H), 7.47 (m, 3 H) 7.76 (m, 7 H), 8.12 (d, 3 H, J = 7.8 Hz), 11.19 (s, 1 H). ^{13}C NMR (75 MHz, d_6-DMSO)

δ 35.7, 114.1, 119.6, 120.0, 120.5, 123.2, 124.1, 124.6, 129.6, 133.8, 135.6, 136.9, 137.3, 143.4, 143.6, 144.3, 147.2, 151.0, 160.6, 161.1, 162.9, 165.8, 166.1, 166.2 MS (TOF ES) *m/z* 802. HRMS calcd for $C_{38}H_{28}N_5O_2Ir$: 802.1700. Found 802.1770.

3.0 LANTHANIDE BASED MERCURY SENSORS

3.1 INTRODUCTION

In this chapter the development of a mercury sensor that is based on a combination of fluorene chemistry (discussed in Chapter 1) and lanthanide ions that are capable of long live luminescence is presented. The fluorene units were substituted so that they are capable of coordinating and photosensitizing lanthanide ions as well as including mercury binding thymine groups. Different ideas were explored for the development of the mercury sensor and these ideas were tested to determine the feasibility of the concept. The design of the proper ligand structure for the binding of the lanthanide ions and the proper linking of thymine groups to fluorene, for mercury coordination, were explored independently before being combined to make the final mercury sensor. A general introduction to mercury sensors is included at the beginning of Chapter 2 and will not be discussed in detail in this chapter.

The long excited state lifetimes of lanthanide complexes make them useful in applications, such as biological imaging,[153-160] where background fluorescence can be problematic and time resolved imaging is necessary to eliminate background noise. Many lanthanide containing complexes exhibit luminescent lifetimes on the order of 100's of microseconds to milliseconds.[161] Due of these long excited state lifetimes, the emission from these lanthanide complexes is easy to measure with time resolved emission spectroscopy.

Lanthanide complexes with a variety of different ligands have been widely studied for these special luminescent properties.

Due to the weak f-f transitions associated with the lanthanide ions, organic chromophores that are capable of sensitizing the lanthanide emission by energy transfer are often used as ligands or they are attached by a spacer to the coordinating species. The organic chromophores have much higher extinction coefficients than the lanthanide f-f transitions increasing the probability of the complex absorbing a photon. The S_1 excited state of the organic chromophore, formed after absorption of a photon, can undergo intersystem crossing to the T_1 state and then transfer energy to the lanthanide ion as shown in Figure 3.1.[162-171] The sensitization of the lanthanide has been performed with a variety of organic chromophores and the S_1 and T_1 energy levels of the organic chromophore can be tuned to alter the amount of energy transfer to the lanthanide ion.

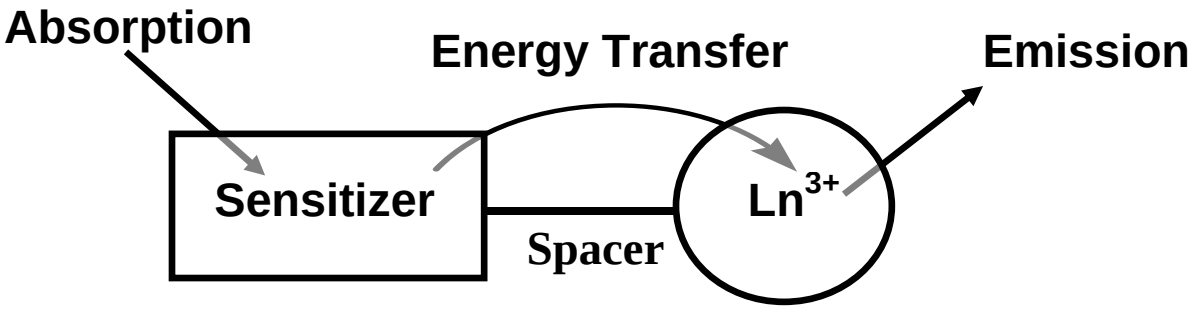

Figure 3.1. Illustration of the energy transfer mechanism of organic sensitizers to lanthanide ions.

The long lived luminescence of lanthanide complexes has been used as a reporter for the sensing a variety of species and this phenomenon has been discussed in several reviews.[172-178] The lanthanide complexes have been used as sensors for anions,[179-187] pH,[188-190] proteins,[191, 192] and transition metal ions.[193-196] These lanthanide based sensors have used a variety of techniques for the detection of different materials. One type of sensor relies on the displacement of labile solvent ligands with an incoming anionic ligand that changes the coordination environment of

the lanthanide ion.[174] The complexes can detect the presence of different anions such as acetate, fluoride, and chloride which can displace weakly bond solvent ligands. This displacement of solvent ligands can greatly affect the photophysical properties of the lanthanide ion and in some cases greatly increases the quantum yield of emission.

Other sensors rely of the complexing of anions or metal ions with a coordinating species attached to the organic chromophore that affects the sensitization of the lanthanide ion. The change in the sensitization of the lanthanide results in a detectable change in the phosphorescent emission. This type of sensor has been used to detect alkali cations, changes in pH, and metal ions such as zinc and copper. An increase in the long lived luminescence was observed for the compound shown in Figure 3.2 when zinc was present although there was no discussion of the mechanism for the phosphorescent enhancement.[194] There have been are no reports of lanthanide complexes being used as mercury sensors.

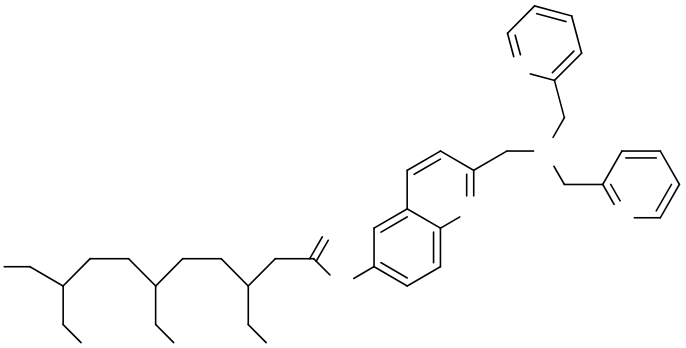

Figure 3.2. Lanthanide based zinc sensor where Ln^{3+} = Eu or Gd made by Hanaoka et al. [194]

In this report, a europium complex with a combination of mercury coordinating thymine groups and a bifluorene sensitizing groups will be discussed. The coordination of mercury to the thymine group causes a decrease in fluorescent emission from the bifluorene unit as well as an

increase in the long lived luminescence form the europium ion. Prior to the synthesis of the mercury sensing compound, a series of fluorene based DTPA lanthanide complexes were made to determine the ability of fluorene to sensitize lanthanide ions and will be discussed briefly. The design and synthesis of the mercury sensing lanthanide complex was performed by the author of this thesis and the photophysical testing, which is not yet complete, is being undertaken by our collaborators, Stephane Petoud and Hyounsoo Uh. Dr. Harry Edenborn from the National Energy Technology Laboratory (NETL) is also a collaborator on this project.

3.2 FLUORENE DTPA LANTHANIDE COMPLEXES

Our initial work focused on demonstrating the ability of fluorene to act as a sensitizer for lanthanides.[197] In this first generation, no mercury binding unit was installed. Since the phosphorescent mercury sensors were to be based on fluorene sensitizing groups and lanthanide ions, it was desirable to determine the potential for fluorene units to transfer energy to the lanthanide ion and generate long lived luminescence before undergoing more extensive synthesis to incorporate mercury binding units. The ability to tune the emission energy of fluorene oligomers by the number of repeat units and examine the effect that the sensitizer's excited state energy has on the energy transfer to the lanthanide ion was another interesting feature of these complexes.

Fluorene monomers and trimers were shown to be lanthanide sensitizing units by incorporating lanthanide binding units linked to fluorene at the 9,9-position (compounds **11-14** in Scheme 3.1). The lanthanide was coordinated by a DTPA based macrocyclic ligand that has been shown to exhibit high affinities for lanthanide guests. This work showed the ability of the

fluorene units to sensitize phosphorescent emission of lanthanide ions but the observed tendency of the system to self-polymerize made characterization and isolation of pure materials difficult. The synthetic work on these complexes was started by James Copenhafer in the Meyer group and D. Samuel Oxley from the Petoud group and continued by the author of this thesis. D. Samuel Oxley performed the photophysical measurements for these complexes. A significant portion of this investigation has been recently published.[197]

3.2.1 DTPA-Fluorene Synthesis

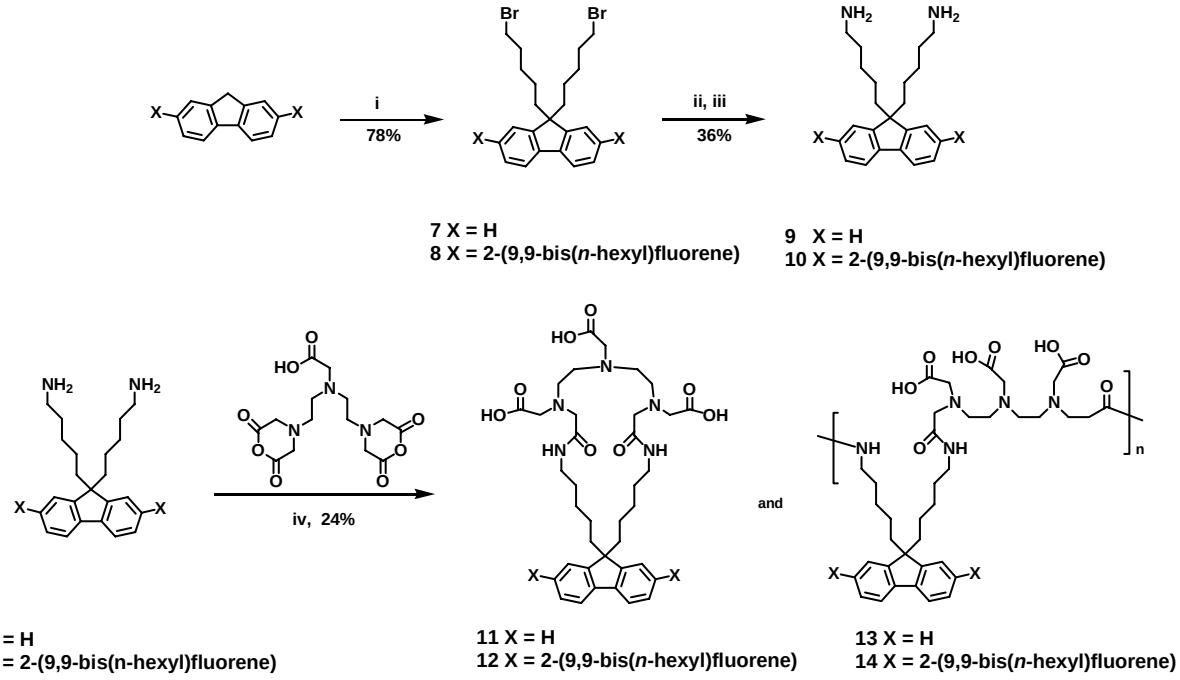

Scheme 3.1. Synthesis of monofluorene DTPA ligand (X=H) and terfluorene DTPA ligand (X=2-(9,9-dihexyl)-fluorene). (i) 1,6-dibromohexane, TBABr, KOH, toluene, H_2O, 75 ^oC, 15 min. (ii) NaN_3, DMF, 80 ^oC, 24 h. (iii) $LiAlH_4$, THF, 0 ^oC to RT. (iv) DBU, DMSO, RT.

James Copenhafer and D. Samuel Oxley prepared the ligand system shown in Scheme 3.1 as compounds **12** and **14**.[197] The synthesis of the ligands **11** and **13,** which were made by the author

of this thesis, begins with the alkylation of fluorene with an excess of 1,6-dibromohexane to yield bis(6-bromohexyl)fluorene **7** in a 78% yield. Dibromo **7** is converted to the bis(6-aminohexyl)fluorene in a two-step process. Reaction with sodium azide gives the bis azide compound which is then reduced with lithium aluminum hydride to yield the diamino **9** in a 36% yield overall.

The attachment of the DTPA proved difficult to control. The goal was to react both of the amine functional groups with a single DTPA to give a macrocyclic product. To achieve this configuration, diamino fluorene **9**, was treated with DTPA anhydride under very dilute conditions in DMSO with DBU as the base. The product of the reaction was poorly soluble and did not give interpretable GPC or MALDI data. James Copenhafer did obtain an elemental analysis of the ligand, however, which established a 1:1 ratio of DTPA to fluorene unit.[197] Based on these data we conclude that the product is likely a mixture of the desired macrocyclic product **11** and the polymeric species **13** as depicted in Scheme 3.1. The difficulty in forming the desired macrocycle can be explained by the known tendency of the alkyl arms attached at the 9,9-position of the fluorene have been shown to wrap back over the plane of the fluorene. This conformation would be expected to inhibit the formation of the macrocycle. The lanthanide ion was introduced by reacting the ligands **11** and **13** with 1 equivalent of the lanthanide chloride salt and 1.5 equivalents of sodium carbonate in DMSO. The DMSO was removed and the complex was evaluated without further purification.

3.2.2 Photophysical Properties of the DTPA Fluorene Lanthanide Complexes

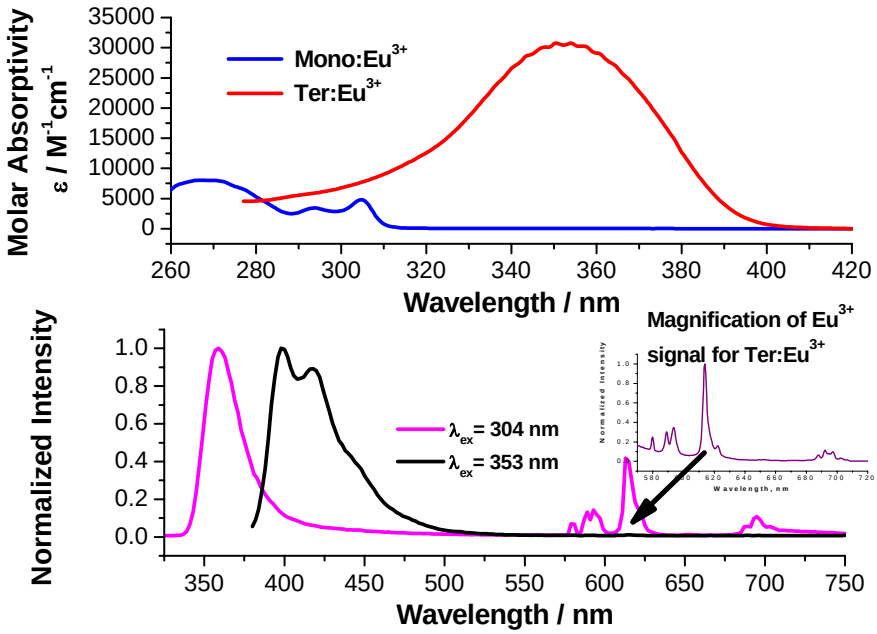

Figure 3.3. Upper: absorption spectra of both Eu^{3+} complexes formed with the mono **11** (blue line) and terfluorene **12** (red line) ligands in DMSO, 80 μM, 298 K. Lower: normalized steady-state emission spectra of both Eu^{3+} complexes formed with the mono **11** (purple line) and terfluorene **12** (black line) ligands in DMSO, 80 μM, 298 K. Lower inset: magnification of the Eu^{3+} signal on the spectrum of the Eu^{3+} complex formed with the terfluorene ligand **12** in DMSO, 80 μM, 298 K. Figure from reference 198.

The lanthanide complexes made with the fluorene-DTPA ligands showed the expected sensitization behavior, although the transfer of energy from fluorene to lanthanide is incomplete. Figure 3.3 shows the absorption and emission spectrum of the compounds as measured by D. Samuel Oxley.[197] The long lived luminescence of the europium ion is clearly visible in 600 nm range. The fluorescence from the fluorene units remains strong, however, establishing that the energy transfer from the lanthanide ions is not complete. The quantum yields of the fluorene

units and the europium ion as well as the excited state lifetimes of the europium centered emission are shown in Table 3.1 The quantum yield of europium long lived luminescence and the fluorescence from the fluorene sensitizer is much higher for the terfluorene unit compared to the monofluorene unit. The increase in quantum yield for the terfluorene demonstrates the ability to tune the energy transfer from the sensitizer to the lanthanide by altering the energy level of the organic chromophore. A multi-component excited state lifetime is observed for the long lived luminescence of both complexes indicative of multiple coordination environments for the europium ion. This multi-component excited state lifetime may be caused by the different coordinating environments of the monomeric (**11**,**12)** and polymeric ligand systems (**13**,**14**). These results show the potential for sensitization of europium by fluorene units and proved that these types of complexes may have potential for mercury sensing with the proper design.

Table 3.1. The luminescence lifetimes and quantum yields of emission of the **11-Eu** and **12-Eu** complexes.

Complex	Luminescence Lifetimes (ms)[a]	Quantum Yield	
		Eu3+-centered[b]	Fluorene-centered[c]
11-Eu^{3+}	1.44 ± 0.01 0.51 ± 0.03	0.010 ± 0.002	0.036 ± 0.005
12-Eu^{3+}	1.46 ± 0.01 0.61 ± 0.01	0.067 ± 0.006	0.84 ± 0.08

[a] λ_{ex}= 266 nm for **11**-Eu^{3+}, RT; λ_{ex} = 355 nm for **12**-Eu^{3+}, RT. [b]TbH22IAM used as reference.[198] [c]Quinine sulfate in 0.1 N H_2SO_4 used as reference (φ = 0.546). λ_{ex} = 300 nm for **11**-Eu^{3+} and λ_{ex} = 350 nm for **12**-Eu^{3+}.

3.3 FLUORENE THYMINE COMPLEXES AS FLUORESCENT MERCURY SENSORS

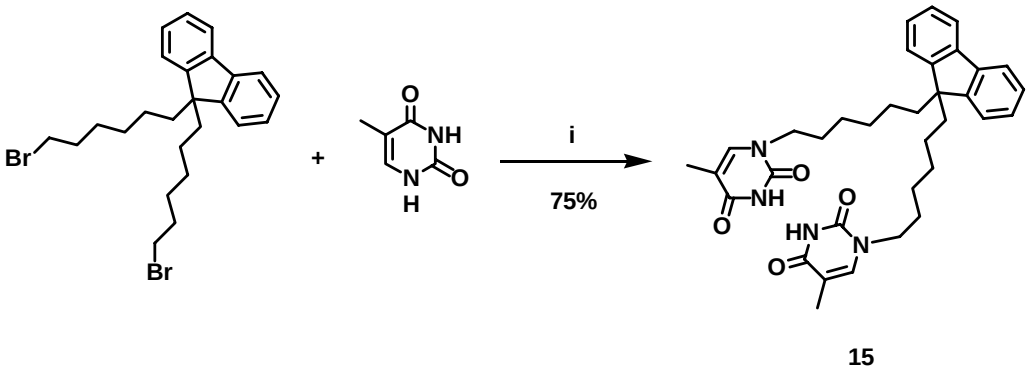

15

Scheme 3.2. The synthesis of a model compound to determine its ability to detect mercury by emission quenching. (i) K_2CO_3, KI, DMSO, RT.

As we planned to use the thymine group to coordinate the mercury in our final sensing molecule, a model compound, **15,** was prepared to test the potential for fluorene groups with thymine functional groups to detect mercury was made and quickly evaluated. A background discussion of the mercury binding ability of thymine is included in Chapter 2. The attachment of thymine groups to the fluorene unit was accomplished in a similar manner to the synthesis of the DTPA fluorene compounds (Scheme 3.2). Thus, the bis(6-bromohexyl)fluorene **7** was reacted with thymine in DMSO with potassium carbonate as the base. The desired regio-isomer, with the thymine linked at its 3-nitrogen position, was found to be preferred at low temperatures with a very high yield (~90%) of the desired isomer being formed at room temperature. Simple qualitative experiments with this compound showed its ability to sense mercury ions with emission spectroscopy (Figure 3.4). The emission intensity of the bis thymine **15** was found to

be quenched significantly in the presence of approximately one equivalent of mercury. This change in the excited state properties of this material in the presence of mercury was encouraging in that sensitization of lanthanides and the resulting long lived luminescence would also likely be affected if fluorene units containing thymines and lanthanide groups were combined.

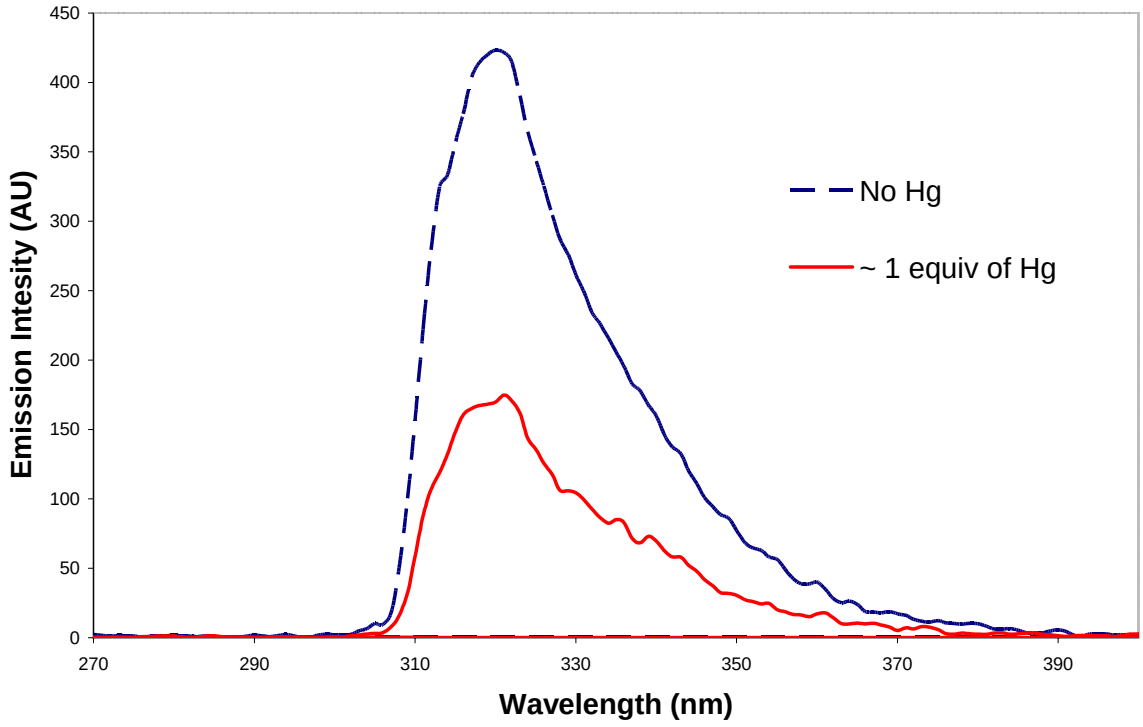

Figure 3.4. The quenching of the fluorescent emission form the bis thymine fluorene **15** by ~1 equivalent of $Hg(OAc)_2$ in a 1:1 methanol:water solution.

3.4 FLUORENE AND LANTHANIDE BASED MERCURY SENSOR

3.4.1 Design and Synthesis Lanthanide Based Mercury Sensor

Based upon the previous results of the fluorene DTPA lanthanide complexes (**11** and **12**) and the thymine-fluorene conjugate **15** capable of sensing mercury, a bifluorene unit **16** was designed in which one fluorene unit would have thymine units capable of coordinating mercury and the other fluorene unit would contain a ligand capable of binding lanthanide ions (Figure 3.5). Although the designed molecule appears complex, the two fluorene units could made independently and the convergent synthesis would utilize a Suzuki coupling to link the two fluorene units together to make a bifluorene unit. Although all the methods needed for the synthesis were well know difficulties in purification and problems with the compatibility of different functional groups had to be over come.

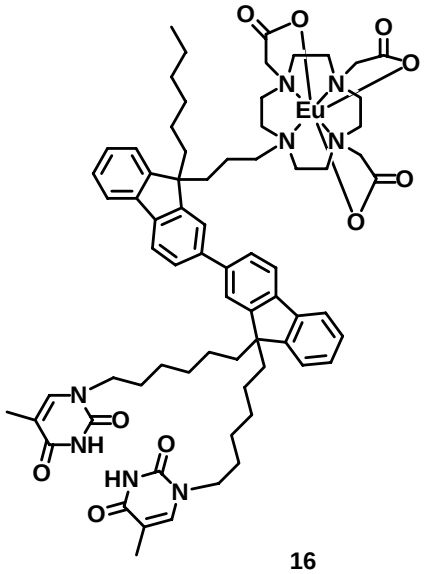

16

Figure 3.5. The structure of the bifluorene europium compound **16** capable of coordinating mercury through the thymine units.

Due to the difficulties in forming the desired DTPA fluorene lanthanide complex, another approach using a more hydrolytically stable lanthanide binding ligand based on DOTA (1,4,7,10-tetraazacyclododecane-*N*-*N'*-*N''*-*N'''*-tetraacetic acid) was selected for the mercury sensing complex.[167, 199] The improved stability of the lanthanide coordination is also advantageous due to the intention of exposing the complexes to environmental samples that might otherwise cause displacement of the lanthanide. It was particularly important that the synthesis of DOTA containing fluorene units could be designed to only produce the desired monomeric species.

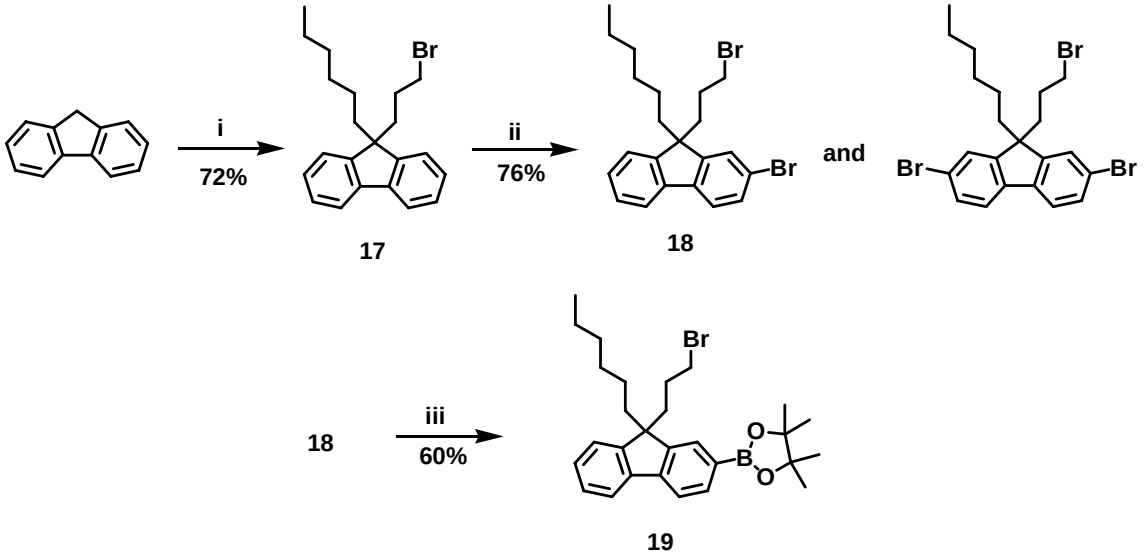

Scheme 3.3. Synthesis of the mono fluorene DOTA precursor. (i) *n*-BuLi, THF, -78 °C, 1 h, 1-bromohexane, -78 °C to RT, *n*-BuLi, THF, -78 °C, 1 h, 1,3 dibromopropane, -78 °C to RT. (ii) Bromine, $CHCl_3$, reflux, 18 h. (iii)) bis-(pinacolato)-diboron, $PdCl_2$dppf, KOAc, dioxane, 70 °C, 20 h.

The incorporation of the DOTA ligand onto a fluorene unit required development of a synthetic procedure to make a precursor, such as the monobromo fluorene **17,** that was capable of being mono substituted with DOTA. This was accomplished by alkylation of fluorene at the 9,9-position with a two step reaction to form compound **17** (Scheme 3.3). Fluorene was deprotonated with one equivalent of *n*-butyllithium and the anion was quenched with one equivalent of 1-bromohexane. This mono hexyl fluorene was then deprotonated with *n*-butyllithium and the anion was quenched with an excess of 1,3-dibromopropane to give **17**. The

overall yield for the two step reaction was 72%. The mono bromo **17** was then converted to the 2-bromo fluorene **18** the reaction with Br_2 in refluxing $CHCl_3$. The reaction was non-selective and a mixture of starting material, mono-brominated **18** and di-brominated products were obtained. These three materials were not separable by standard techniques but the reaction of this mixture with pinacolate borate using palladium as a catalyst produced the desired mono boron pinacolate **19** that was easily isolated by column chromatography in a 60% yield.

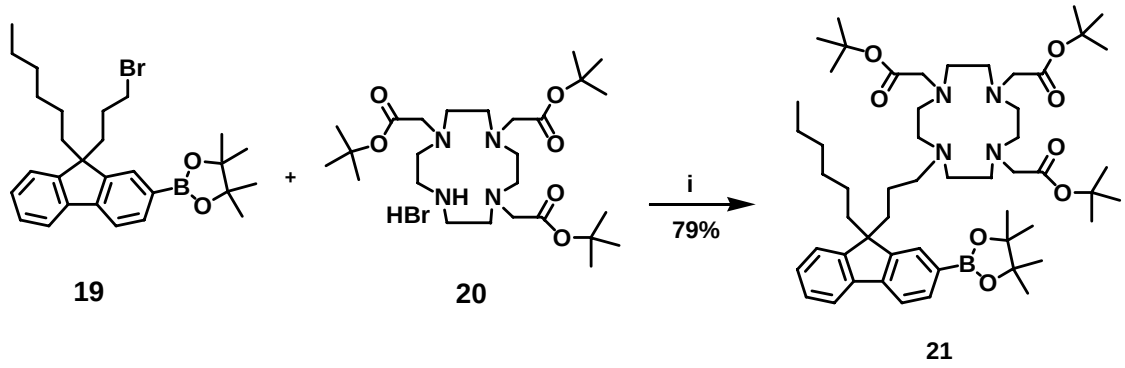

19 **20** **21**

Scheme 3.4. Synthesis of mono fluorene *t*-butyl DOTA coupling partner. (i) $CsCO_3$, acetonitrile, RT, 24 h.

The *t*-butyl protected DOTA fragment **20** was attached to the fluorene unit **19** by a S_n2 reaction to yield the *t*-butyl DOTA fluorene 23 in a 79% yield (Scheme 3.4). Attempts were made to incorporate the *t*-butyl DOTA fragment before the Miyura coupling to make the boron pinacolate group but separation of the product from the starting material proved to be difficult. It was also envisioned that the boron pinacolate monobromo alkyl compound **19** could be Suzuki coupled with a thymine fragment for ease of purification but the potential for thymine groups to react with the alkyl bromide in Suzuki coupling conditions precluded this approach.

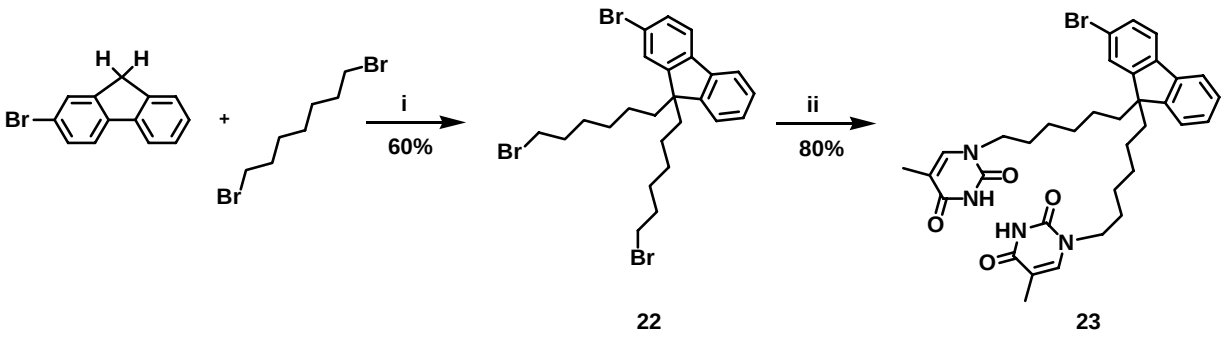

Scheme 3.5. The synthesis of the mono fluorene thymine coupling partner **23**. (i) 1,6-dibromohexane, KOH aqueous, TBABr, toluene, 80 ^{o}C, 2 h. (ii) thymine, K_2CO_3, KI, DMSO, RT, 24 h.

Thymine units were chosen as the mercury binding functionality and can be incorporated into the fluorene units through the alkyl substitutions at the 9-position as shown in an analogous manner to Scheme 3.2. In this case 2-bromofluorene was used as the starting material since the alkylation reaction with KOH as the base does not reacted with aryl halide group (Scheme 3.5). Thus bis-bromohexyl fluorene **22** was made in one step with a 60% yield. The terminal alkyl bromides were then reacted with thymine at room temperature to form the bis-thymine fluorene **23** in an 80% yield.

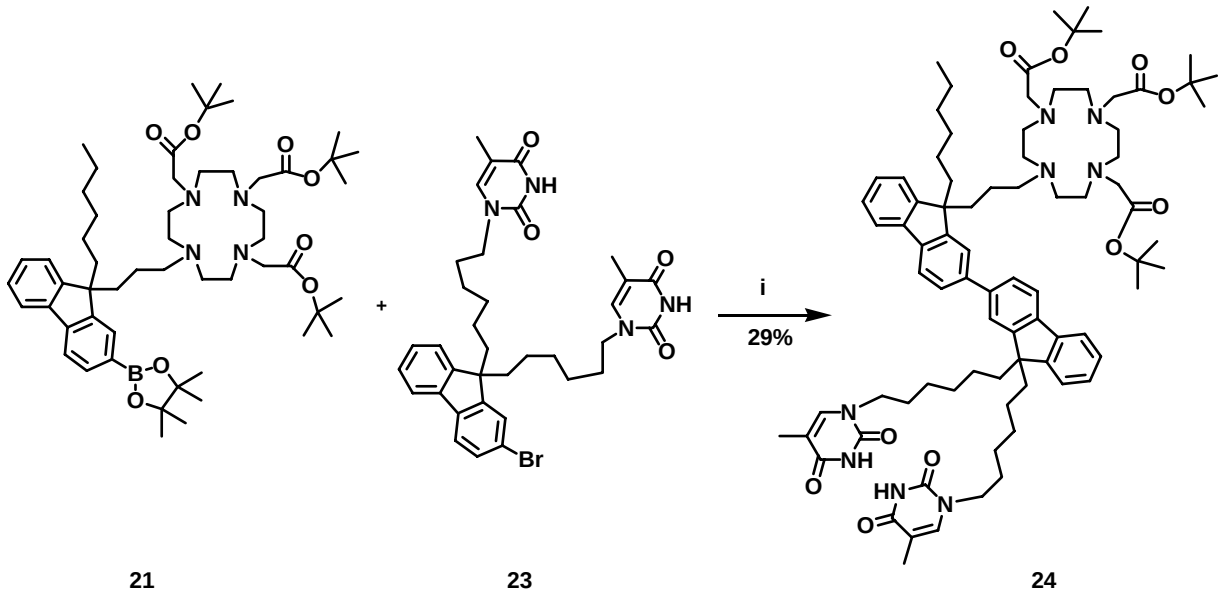

Scheme 3.6. Suzuki coupling to form bis fluorene unit **24**. (i) $PdCl_2$dppf, Na_2CO_3, DMF, water, 90 ^{o}C, 24 h.

The Suzuki coupling of the thymine fluorene unit and the *t*-butyl DOTA fragment was accomplished using $PdCl_2$(dppf) as the catalyst to form the *t*-butyl DOTA bis thymine bifluorene **24** in a 29% yield (Scheme 3.6). It was found that the bidentate ferrocene based phosphine ligand was necessary for the coupling to proceed in high yields. The coupling in the presence of thymine groups and the DOTA species was a concern because of there potential for binding to the palladium catalyst. Purification of the product was more challenging since the DOTA fluorene starting material and the product were inseparable by silica gel chromatography. Preparative HPLC was attempted but the poor solubility of the product in water rendered this technique ineffective. Purification was accomplished by first chromatography on silica gel followed by chromatography on basic alumina oxide.

The *t*-butyl groups can then be removed from **24** with trifluoroacetic acid to form the free acid **25** in a quantitative yield (Scheme 2.7). The high yield of the deprotection step was important as the free acid product is difficult to purify by standard methods. After the deprotection of the *t*-butyl groups with trifluoroacetic acid, the solvent and excess acid need only to be removed under reduced pressure. The deprotected DOTA ligand was now ready for coordinating lanthanide ions and the free acid **25** was reacted with $EuCl_3$ in a DMSO and water mixture with NaOH as the base. The europium complex **17** was purified by precipitation into water and was isolated in a 44% yield.

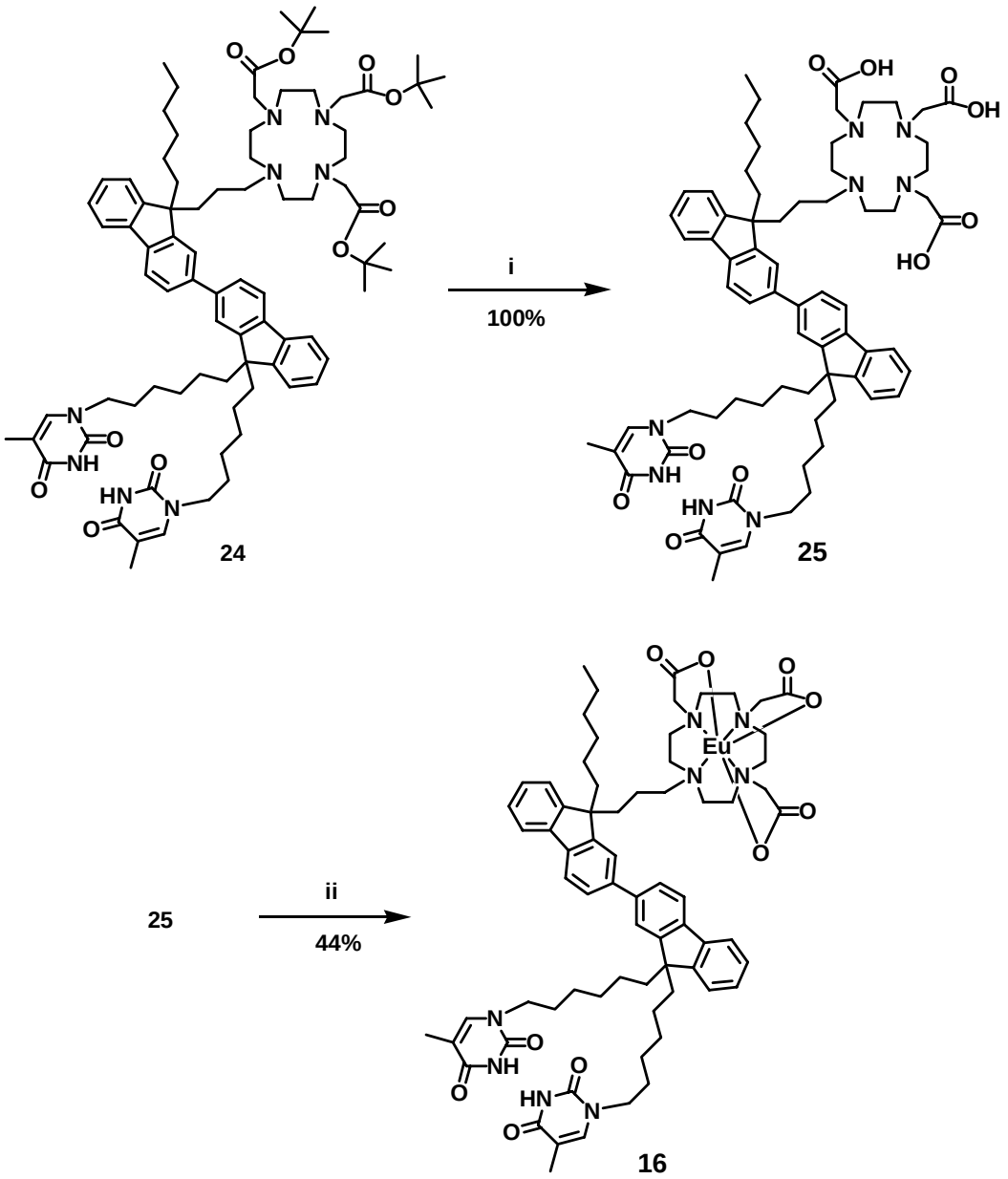

Scheme 3.7. Deprotection of t-butyl groups and formation of final europium complex. (i) Trifluoroacetic acid, CH_2Cl_2, RT, 24 h. (ii) $EuCl_3{\cdot}(H_2O)_6$, K_2CO_3, DMSO, 90 ^oC, 24 h

3.4.2 Photophysical Properties and Mercury Sensing

After some initial screening by the author of this thesis to show that the europium ion in compound **16** is sensitized by the fluorene dimer chromophore and that the compound does show

changes in the emission properties when mercury was present, the final compound **16** was further evaluated by Hyounsoo Uh in the Petoud group. A discussion of his initial photophysical measurements is included in this thesis.

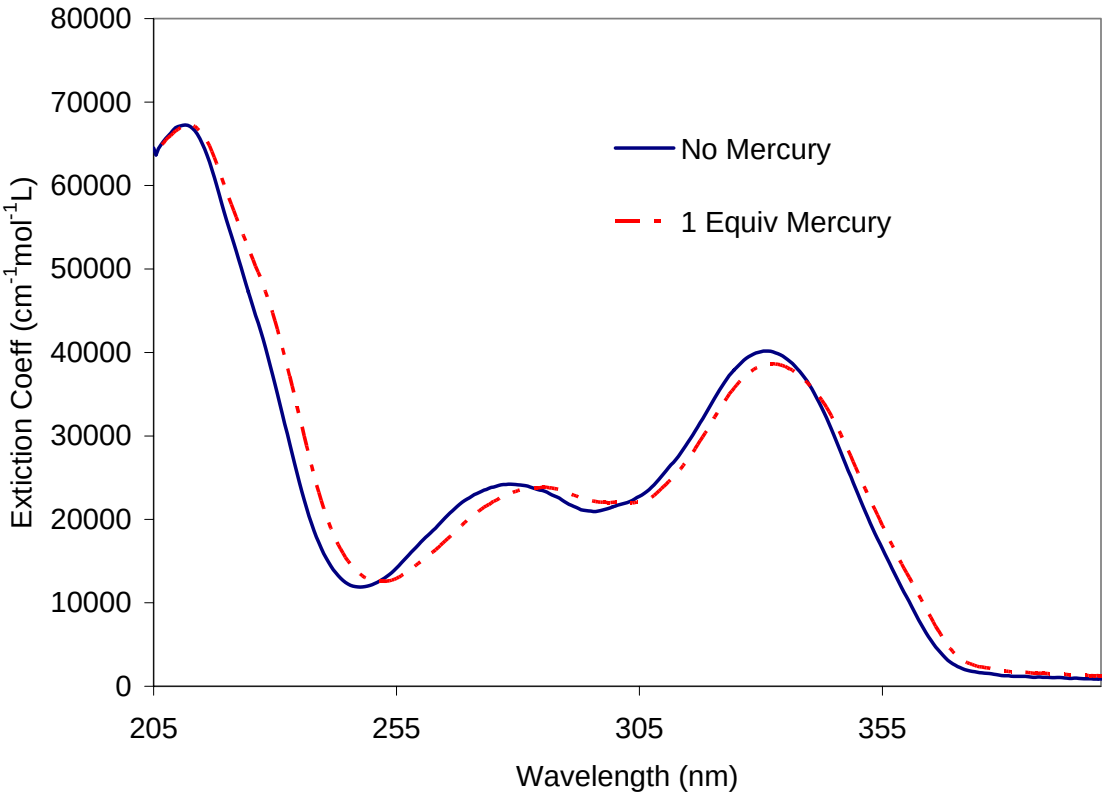

Figure 3.6. Absorption spectrum of **16** with and without mercury in a 1:1 methanol / water mixture at 10^{-5} M.

A small shift to lower energy is observed in the absorption spectrum of the mercury sensing compound **16** when mercury is present. The absorption spectrum of the europium complex is shown in Figure 3.6 with no mercury present and with one equivalent of mercury present. The extinction coefficient of the π-π* transition of the complex is similar to what has been reported for other π-π* transitions bifluorene chromophores.[54] The small decrease in intensity for the mercury containing sample may be within experimental error but the slight bathochromic shift appears to be a real phenomena. This shift is likely to be caused by some

aggregation of the chromophores due to the coordination of different bifluorene thymine units to the same mercury ion. The bathochromic shift in absorption has been reported for the aggregation of many different chromophores. [145, 149]

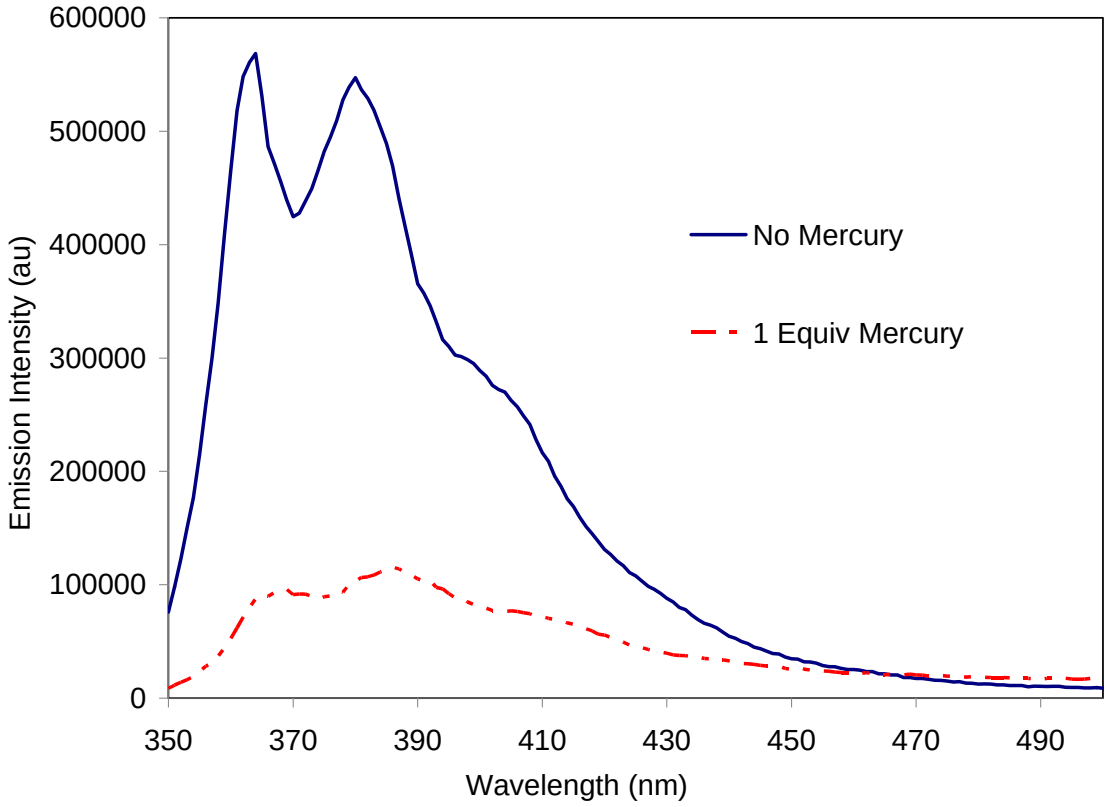

Figure 3.7. Fluorescent emission spectra of **16** with and without mercury in a 1:1 methanol / water solution at 10^{-5} M.

A dramatic decrease in the in the fluorescent emission intensity of the mercury sensor **16** is seen when one equivalent of mercury is present. The fluorescence emission spectrum of the complex with and without mercury is shown in Figure 3.7. This decrease can also be explained by an aggregation of the sensor molecules in the presence of mercury. The aggregation of the chromophores can cause energy transfer to occur before emission thereby decreasing the quantum yield of emission. This decrease in emission intensity by thymine containing

fluorescent mercury sensors has been reported by others and determined to be caused by the aggregation of the chromophores.[95, 105]

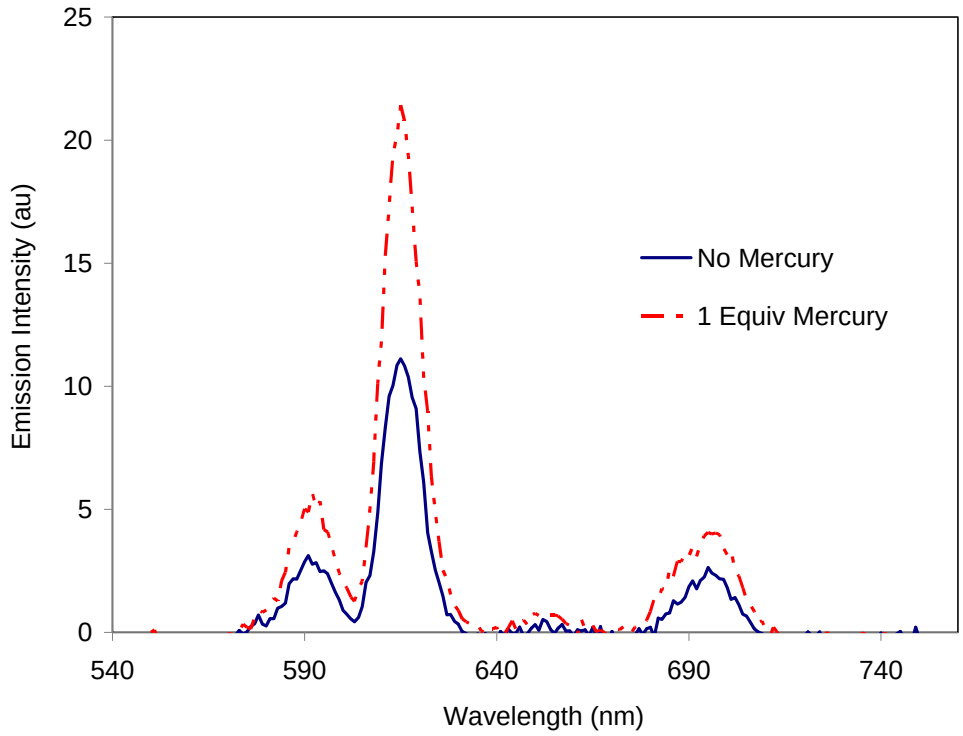

Figure 3.8. Bong lived luminescence spectra of **16** with and without 1 equivalent of mercury in a1:1 methanol / water mixture at 10^{-5} M.

Interestingly the intensity of the long lived luminescence of the europium ion in the mercury sensor **16** increased in the presence of mercury (Figure 3.8). The long lived luminescence excitation spectrum also shows an increase in intensity when mercury is present (Figure 3.9). Since no major change in the absorption spectrum is seen when mercury is added the increase in long lived luminescence is likely attributed to an increase in energy transfer from the fluorene unit to the europium ion. The reason for this increase is not completely understood. One possible explanation is that the increase in long lived luminescence is caused by a heavy metal effect from the mercury ion which could increase intersystem crossing of the bifluorene

excited state leading to an increase in triplet state formation and an increase in energy transfer to the europium ion. It has been shown that the energy transfer to lanthanide complexes occurs from the triplet state of the sensitizing chromophore.[200] An increase in the triplet state population of the sensitizer would then lead to more efficient energy transfer to the europium ion.

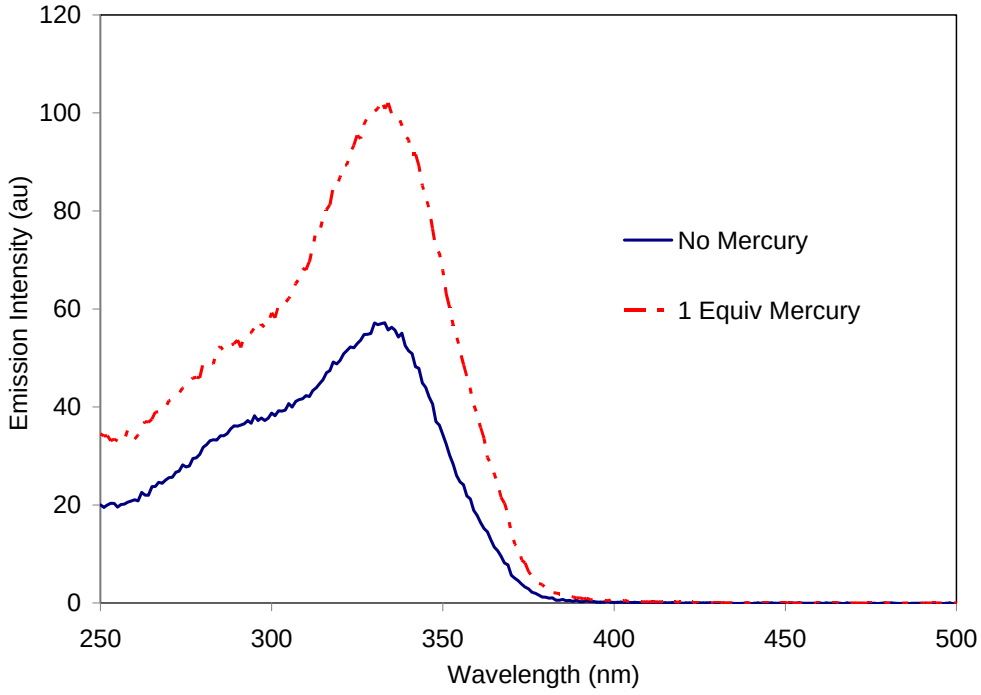

Figure 3.9. Phosphorescence excitation spectrum of **16** measured at an emission wavelength of 615 nm in a 1:1 methanol / water mixture at 10^{-5} M.

Another possible cause for the increase in long lived luminescence is that longer excited state lifetimes caused by aggregation of the fluorescent bifluorene chromophore increases energy transfer to the europium. A longer excited state lifetime would increase the probability of intersystem crossing to the triplet state which would increase energy transfer to the europium ion or potentially the longer excited state singlet lifetime would have more chance for energy transfer. Another potential theory is the thymine chromophore is capable of transferring energy

to the europium ion when mercury is present. Further photophysical studies should help to help to find the true cause of the increase in long lived luminescence. Whatever the cause of this increase in long lived luminescence intensity, the combination of a fluorescence decrease and a long lived luminescence increase is a new phenomenon for mercury sensing.

3.5 CONCLUSIONS

A novel multi-signal mercury sensor that shows a decrease in fluorescence and an increase in phosphorescence has been developed. The dual reporting signals of the sensor should make the detection of mercury more reliable as well as more qualitative and the different signals may also make the system more selective for the detection of mercury. The complex, based upon thymine functionalized fluorene ligands capable of binding europium and mercury, was made by a challenging convergent synthesis of two different functionalized fluorene units. Many synthetic methods and purification techniques were explored during the development of the ultimately successful synthetic method. The compound is capable of detecting mercury at a 10^{-6} M level and it is expected that the sensitivity will be even greater when proper time resolved measurements are made. The thymine groups have been show to be very selective in mercury binding over other ions and it is expected that this new mercury sensing complex will be selective in detecting mercury.

3.5.1 Experimental

3.5.1.1 Photophysical Characterization

The UV-Visible spectra were recorded on a Perkin-Elmer UV/VIS/NIR Spectrometer Lambda. The steady state emission spectra were determined using a Varian Cary Eclipse Fluorescence Spectrophotometer.

(a) Synthetic Methods and Equipment

$Pd(PPh_3)_4$ (Strem), and $Pd(Cl)_2$dppf (Strem), were commercially obtained and stored in a nitrogen-filled glove box. All other reagents were commercially obtained and used without further purification. ^{1}H- (300 MHz) and ^{13}C-NMR (75 MHz) spectra were recorded with Bruker spectrometers. Chemical shifts were referenced to residual ^{1}H or ^{13}C signals in deuterated solvents. Column chromatography was performed using Sorbent 60Å 40-63 μm standard grade silica. GC-MS was performed on a Hewlett Packard Series 5980 GC/5971 A MS with a Hewlett Packard Series 1 column. GC was performed on a Hewlett Packard Series 6850 GC with a Hewlett Packard Series 1 methyl siloxane column. HRMS were obtained on a Fison VG Autospec in the Mass Spectral Facility of the University of Pittsburgh.

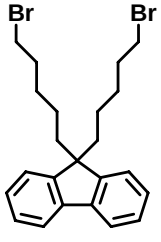

7

9,9-(6,6-Dibromohexyl)-fluorene 7: Adapting the method of Liu,[201] fluorene (1.7 g 10.2 mmol), 1,6-dibromohexane (20 g, 82 mmol), 75 ml of a 50% KOH_{aq} solution, and tetrabutylammonium bromide (0.65 g 2 mmol) were added to a round bottom flask and stirred at 70 ºC for 60 min. The reaction mixture was cooled to RT and extracted with diethyl ether (3 x 50 ml). The organic fractions were combined, washed with brine, dried over magnesium sulfate. The excess 1,6-dibromohexane was removed by vacuum distillation and the product was purified by column chromatography (silica gel, 10% CH_2Cl_2 / hexane) to yield a clear, viscous oil (4.6 g, 78%). ^1H (300 MHz, $CDCl_3$) δ 0.58 (m, 4 H), 0.99-1.24 (m, 8 H), 1.62 (p, 4 H), 1.95 (m, 4 H), 3.25 (t, 4 H) 7.24-7.34 (b, 6 H), 7.69 (b, 2 H). ^{13}C NMR (75 MHz, $CDCl_3$) δ 23.5, 27.8, 29.1, 32.7, 33.9, 40.2, 54.9, 119.7, 122.8, 126.9, 127.1, 141.1, 150.3.MS (EI) *m/z* 492 ($M^{\cdot+}$) 327

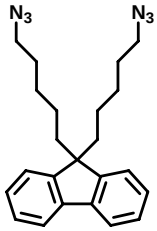

9,9-(6,6-azidohexyl)-fluorene: To a round bottom flask, 9,9-(6,6-dibromohexyl)-fluorene **7** (3.6 g, 7.3 mmol), sodium azide (1.14 g, 17.5 mmol), to 30 ml of DMF were added After heating at 80 ºC for 24, water was added (100 ml) and the aqueous layer was extracted with hexane (3 x 100ml). The combined organic layers were then washed with water, brine, and then dried over magnesium sulfate. The product was purified by column chromatography (silica gel, 50% $CHCl_3$ / hexanes as the eluent) to yield a clear oil (2.1 g, 68%). ^1H (300 MHz, $CDCl_3$) δ 0.62 (m, 4 H), 0.99-1.08 (b, 8 H), 1.37 (m, 4 H), 1.95 (m, 4 H), 3.10 (t, 4 H) 7.24-7.34 (b, 6 H), 7.69 (b, 2 H). ^{13}C NMR (75 MHz, $CDCl_3$) δ 23.5, 26.3, 28.7, 29.4, 40.2, 51.4, 119.7, 122.8, 126.9, 127.1, 141.1, 150.3. MS (EI) *m/z* 416 ($M^{\cdot+}$) 262

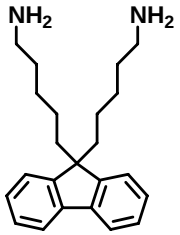

9

9,9-(6,6-aminohexyl)-fluorene 9: A round bottom flask was charger with 9,9-(6,6-azidohexyl)-fluorene (2.0 g, 4.8 mmol) and 30 ml of anhydrous THF. After cooling to 0 ºC, $LiAlH_4$ (19.2 ml, 1 M in diethyl ether, 19.2 mmol) was added dropwise and the reaction was stirred 1 h. The reaction was quenched by slow addition of ethanol followed by water. The aqueous layer was extracted with diethyl ether (3x100ml) and the combined organics were then washed with brine and dried over magnesium sulfate. The solvent was removed under vacuum to yield product as clear, viscous oil (0.9 g, 52%). ^{1}H NMR (300 MHz, $CDCl_3$) δ 0.62 (m, 4 H), 0.99-1.08 (b, 8 H), 1.37 (m, 4 H), 1.95 (m, 4 H), 3.10 (t, 4 H) 7.24-7.34 (b, 6 H), 7.69 (b, 2 H). ^{13}C NMR (75 MHz, $CDCl_3$) δ 23.5, 26.3, 28.7, 29.4, 40.2, 51.4, 119.7, 122.8, 126.9, 127.1, 141.1, 150.3. MS (EI) *m/z* 364 ($M^{\cdot+}$) 279, 265

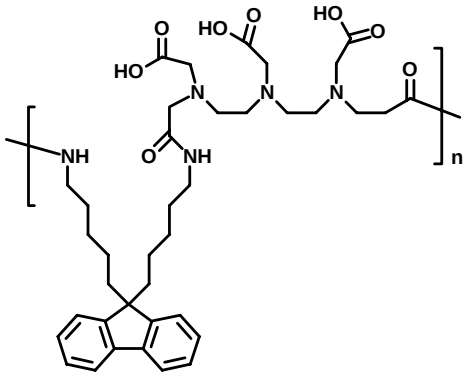

11,13

Fluorene DTPA Ligand 11,13: 9,9-(6,6-aminohexyl)-fluorene **9** (1.06 g, 29 mmol) and diethylenetriaminepentaacetic acid bisanhydride (1.04 g, 29 mmol), and 2 ml of DBU were

added to 200 ml of DMSO. After stirring at RT for 24 h, the DMSO was removed under reduced pressure at 40 ºC. The reaction was adjusted to neutral pH with acetic acid and the product was precipitated into water. The crude product was dissolved in DMSO and then precipitated into THF to yield 0.5 g of white solid. ^{1}H (300 MHz, $CDCl_3$) δ 0.46 (b, 4 H), 0.94 (b, 8 H), 1.14 (m, 4 H), 1.91 (b, 4 H), 2.6-3.6 (b, 28 H) 7.3-7.5 (b, 6 H), 7.75 (b, 2 H), 7.91 (b, 2h).

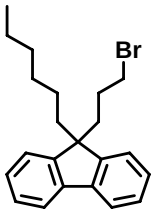

17

2-Bromo-9-(3-bromopropy)-9-hexyl-fluorene 17 *rwii15*: Fluorene (3.0 g, 28.2 mmol) was dissolved in 150 ml of anhydrous THF, cooled to -78 ^{o}C, and *n*-butyllithium (1.6 M, 11.3 ml, 18.1 mmol) was added dropwise over 20 min. The mixture was stirred at -78 ^{o}C for 60 min and then 1-bromohexane (3.0 g, 18.1 mmol) was added dropwise. The reaction was allowed to warm to RT and then cooled to -78 ^{o}C. *n*-Butyllitium (1.6 M, 13.6 ml, 21.7 mmol) was added dropwise over 20 min. After 60 min, 1,3-dibromopropane (18.3 g, 91 mmol) was added quickly. The reaction was allowed to warm to RT and the reaction was quenched with water. The aqueous layer was washed with hexane (2 x 50 ml) and the combined organic layers were washed with brine and dried over magnesium sulfate. The excess 1,3-dibromopropane was removed by vacuum distillation and the crude product was purified by column chromatography (silica gel, hexanes then 5% CH_2Cl_2 / hexanes as the eluent) to yield the product as a colorless oil (4.8 g, 72%). ^{1}H NMR (300 MHz, $CDCl_3$) δ 0.57 (b, 2 H), 0.63 (t, 2 H, J = 7.5 Hz), 1.0-1.3 (b, 8 H),1.97 (m, 2 H), 2.15 (m, 2 H), 3.01 (t, 2 H, J = 6.6 Hz) 7.26-7.40 (b, 6 H), 7.69 (b, 2 H). ^{13}C NMR (75 MHz, $CDCl_3$) δ 14.2, 22.7, 23.8, 27.5, 29.8, 31.7, 34.7, 38.9, 40.7, 54.7, 120.0, 123.0,

127.3, 127.5, 141.3, 150.0. MS (EI) *m/z* 372 ($M^{\cdot+}$) 285, 249. HRMS calcd for $C_{22}H_{27}Br$: 370.1296. Found 370.1280.

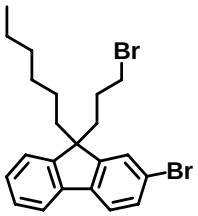

18

2-Bromo-9-(3-bromopropy)-9-hexyl-fluorene 18 *rwiii34*: 2-Bromo-9-(3-bromopropy)-9-hexyl-fluorene **17** (0.93 g, 2.5 mmol) was dissolved in 50 ml of $CHCl_3$ and bromine (0.40 g, 2.5 mmol) was added slowly. The reaction mixture was heated to reflux for 18 h and then quenched with a sodium thiosulfate solution. The aqueous layer was washed with $CHCl_3$ (2 x 25 ml) and the combined organics were dried over $MgSO_4$. The product was purified by column chromatography (silica gel, 5% in CH_2Cl_2 / hexanes as the eluent) to yield the product as a clear oil (0.85 g, 76%). ^{1}H NMR (300 MHz, $CDCl_3$) δ 0.60 (b, 2 H), 0.75 (t, 2 H, J = 7.5 Hz), 1.0-1.3 (b, 8 H), 1.97 (m, 2 H), 2.14 (m, 2 H), 3.10 (t, 2 H, J = 6.6 Hz) 7.33 (m, 5 H), 7.69 (m, 2 H). ^{13}C NMR (75 MHz, $CDCl_3$) δ 14.0, 22.6, 23.6, 27.2, 27.3, 29.6, 31.5, 34.6, 38.7, 40.5, 54.5, 119.8, 121.2, 122.8, 126.1, 127.1, 127.3, 127.8, 130.3, 141.1, 149.8. MS (EI) *m/z* 450 ($M^{\cdot+}$) 365, 285

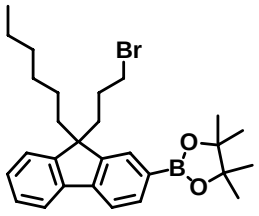

19

Boron pinacolate fluorene 19 *rwiii67*: 2-Bromo-9-(3-bromopropy)-9-hexyl-fluorene **18** (3.2 g, 7.1 mmol), bis(pinacolato) diboron (2.7 g, 10.7 mmol), $PdCl_2$dppf (0.29 g, 5 mol %), potassium acetate (2.8 g, 28 mmol), and 25 ml of 1,4-dioxane were added to a Schlenk flask and sparged

with N_2 for 20 minutes. After the reaction was heated to 70 ^oC for 24 h, water was added and the aqueous layer was washed with diethyl ether (3 x 50 ml). The combined organics were was washed with brine and dried over magnesium sulfate. The product was purified by column chromatography (silica gel, 10% CH_2Cl_2 / hexanes then 50% CH_2Cl_2 / hexanes as the eluent) to yield the product as a colorless oil (2.1 g, 60% yield). ^1H NMR (300 MHz, $CDCl_3$) δ 0.57 (b, 2 H), 0.73 (t, 2 H, J = 7.5 Hz), 1.0-1.3 (b, 8 H), 1.98 (m, 2 H), 2.15 (m, 2 H), 3.10 (t, 2 H, J = 6.6 Hz) 7.33 (m, 3 H), 7.68-7.83 (m, 4 H). ^{13}C NMR (75 MHz, $CDCl_3$) δ 14.0, 22.6, 23.6, 24.9, 25.0, 27.3, 29.6, 31.5, 34.5, 38.6, 40.3, 54.5, 83.8, 119.2, 120.3, 122.9, 127.1, 127.8, 128.8, 134.1, 140.9, 144.1, 149.0, 150.3. MS (EI) *m/z* 498 ($M^{\cdot+}$) 411, 375. HRMS calcd for $C_{28}H_{38}BO_2Br$: 496.2148. Found 496.2129.

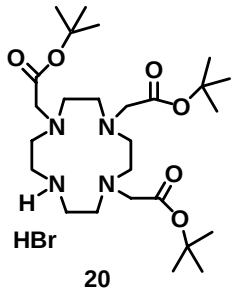

20

1,4,7-Tris(*tert*-butoxycarbonylmethyl)-1,4,7,10-tetraazacyclododecane, hydrobromide salt 20 *rwii103*: According to the method of Dabadhoy et al,[164] 1,4,7,10-tetraazacyclododecane (5.0 g, 29 mmol), $NaHCO_3$ (8.06 g, 96 mmol), and 100 ml of anhydrous acetonitrile were added to a round bottom flask and cooled to 0 ^oC. *tert*-Butyl bromoacetate (18.7 g, 96 mmol) was added dropwise over 20 min and then the reaction was allowed warm to RT. After 24 h, the solids were filtered and the solvent was removed from the filtrate. The solids was recrystallized twice from toluene to yield the product (5.0 g, 29%) as white solid. ^1H NMR (300 MHz, $CDCl_3$) δ 1.46 (s, 27 H), 2.9 (m, 12 H), 3.1 (m, 4 H), 3.26 (s, 2 H), 3.35 (s, 4 H), 10.01 (b, 2 H). ^{13}C NMR (75 MHz, $CDCl_3$) δ 28.2, 47.5, 48.9, 49.3, 51.3, 51.4, 58.2, 81.7, 81.8, 169.6, 170.5.

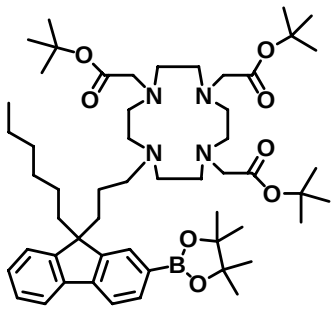

21

***t*-butyl-DOTA-B($O_2C_2Me_4$)-Fluorene 21** *rwiii69*: According to the method of Wilkinson et al,[202] **Boron pinacolate fluorene 19** (1.7 g, 3.4 mmol), 1,4,7-Tris(*tert*-butoxycarbonylmethyl)-1,4,7,10-tetraazacyclododecane, hydrobromide salt **20** (2.04 g, 3.4 mmol), cesium carbonate (3.32 g, 10.2 mmol), and 20 ml of acetonitrile were added to a round bottom flask and stirred at RT for 24 h. The solids were filtered and the solvent was removed under reduced pressure. The crude product was purified by column chromatography (silica gel, 5% CH_3OH / CH_2Cl_2 then 10% CH_3OH / CH_2Cl_2) to yield the product as a colorless oil (2.5 g, 79% yield). ^1H NMR (300 MHz, $CDCl_3$) δ 0.3-1.0 9 (m, 10) 1.3 (m, 40 H), 1.5-3.5 (b, 32 H), 7.1-7.3 (m, 3 H), 7.5-7.9 (m, 4 H). MS (TOF ES) *m/z* 932 HRMS calcd for $C_{54}H_{88}BN_4O_8$: 931.6739. Found 931.6695.

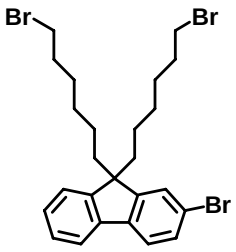

22

2-Bromo-9,9-bis-(6-bromo-hexyl)-fluorene 22 *rwii69*: 2-Bromofluorene (2.5 g, 10.2 mmol), 1,6-dibromohexane (20.0 g, 82 mmol), KOH (20 ml, 50 % in H_2O), TBABr (0.65 g, 2 mmol), and 20 ml of toluene were added to a Schlenk flask and heated to 80 ^oC under N_2. After 2 h the reaction was cooled to RT and water was added. The aqueous layer was washed with hexanes (2 x 100 ml) and the combined organic layers were washed with brine and dried over magnesium

sulfate. The excess 1,6-dibromohexane was removed under reduced pressure and the crude product was purified by column chromatography (silica gel, 5% CH_2Cl_2 / hexanes) to yield the product (3.5 g, 60%) as a colorless oil. ^{1}H NMR (300 MHz, $CDCl_3$) δ 0.58 (m, 4 H), 1.0-1.3 (m, 8 H), 1.65 (m, 4 H), 1.94 (m, 4 H), 3.26 (t, 4 H, J = 6.6 Hz) 7.31 (m, 3 H), 7.44 (m, 2 H), 7.55 (m, 1 H), 7.65 (m, 1 H). ^{13}C NMR (75 MHz, $CDCl_3$) δ 23.5, 27.8, 29.0, 32.6, 33.9, 40.1, 55.3, 119.8, 121.1, 122.8, 126.0, 127.1, 127.6, 130.1, 140.0. 140.2, 149.9, 152.6. MS (EI) *m/z* 570 (M^{+}) 407, 328. HRMS calcd for $C_{25}H_{31}Br_3$: 567.9976. Found 567.9973.

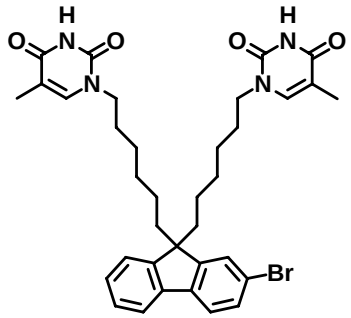

23

Bis(thymine)-2-bromo-fluorene 23 *rwii72*: 2-Bromo-9,9-bis-(6-bromo-hexyl)-fluorene **22** (1.32 g, 2.3 mmol), thymine (1.74 g, 13.9 mmol), K_2CO_3 (1.92 g, 13.9 mmol), KI (10 mg), and 25 ml of DMSO were added to a round bottom flask and stirred at RT for 24 h. Water was added and the aqueous was washed with ethyl acetate (4 x 50 ml). The combined organic layers were washed with water, then brine, and then dried over magnesium sulfate. The crude product was purified by column chromatography (silica gel, 10% CH_2Cl_2 / ethyl acetate) to yield the desired product (1.2 g, 80%) as a white solid. ^{1}H NMR (300 MHz, $CDCl_3$) δ 0.50 (b, 4 H), 0.98 (b, 8 H), 1.37 (b, 4 H), 1.73-1.86 (m, 8 H), 3.47 (t, 4 H, J = 6.6 Hz), 6.83 (s, 2 H), 7.36-7.60 (m, 7 H), 10.33 (s, 2 H). ^{13}C NMR (75 MHz, $CDCl_3$) δ 12.3, 23.4, 23.6, 25.9, 28.8, 29.3, 40.0, 48.3, 53.6, 55.2, 110.3, 120.9, 121.2. 121.5, 122.8, 127.0, 127.1, 127.6, 130.0, 139.0, 139.9, 140.6, 149.9,

151.2, 152.6, 164.9. MS (EI) *m/z* 662 ($M^{\cdot+}$) 581, 452. HRMS calcd for $C_{35}H_{41}N_4O_4Br$: 660.2311. Found 660.2305.

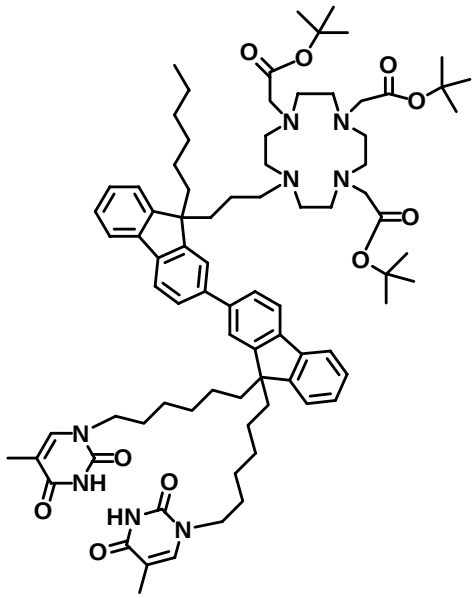

24

Bis(thymine)-t-butyl DOTA-bifluorene 24 *rwiii75*: Bis(thymine)-2-bromo-fluorene **23** (0.59 g, 0.90 mmol), *t*-butyl-DOTA-B($O_2C_2Me_4$)-fluorene **21** (0.70 g, 0.75 mmol), $PdCl_2$dppf (0.06 g, 0.1 equiv), Na_2CO_2 (0.40 g, 3.5 mmol), 15 ml of DMF, and 1 ml of water were added to a Schlenk flask. After heating to 90 ^oC for 24 h, water was added and the aqueous layer was washed with CH_2Cl_2 (3 x 50 ml). The combined organic layers were washed with brine and dried over magnesium sulfate. The crude product was purified by column chromatography (silica gel, 10% methanol / CH_2Cl_2 then on basic alumina oxide, 5% methanol / CH_2Cl_2) to yield the desired product (0.3 g, 29%) as a tan solid. ^1H NMR (300 MHz, D_6-DMSO, 360 K) δ 0.72 (b, 8 H), 1.08 (b, 16 H), 1.44 (s, 27 H), 1.75 (m, 4 H), 2.10 (b, 8 H), 2.65 (b, 8 H), 3.1 (b, 5 H), 3.69 (t, 4 H, J = 6.9 Hz) 7.20- 8.0 (m, 16 H), 10.5 (b, 2 H). ^{13}C NMR (75 MHz, CD_2Cl_2) δ 20.1, 22.5, 23.7, 23.8, 25.9, 27.6, 27.8, 28.0, 28.8, 29.5, 31.4, 36.5, 38.2, 39.4, 40.1, 48.2, 49.1, 49.7, 50.4, 81.5, 82.6, 82.9, 110.0, 119.7, 120.0, 120.3, 121.2, 121.3, 123.0, 125.9, 126.2, 126.6, 127.0, 127.1, 127.5, 140.2, 140.4, 140.7, 140.9, 149.8, 150.3, 150.4, 150.7, 151.1, 151.3, 151.5, 164.6,

169.8, 169.9, 172.6, 173.5. MS (TOF ES) *m/z* 1387. HRMS calcd for $C_{83}H_{117}N_8O_{10}$: 1385.8934. Found 1385.8893.

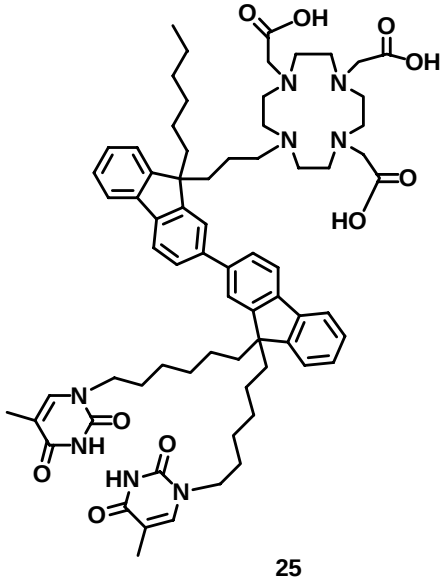

25

Bis(thymine)-DOTA-bifluorene 25 *rwiii74*: According to the method of Wilkinson et al,[202] Bis(thymine)-*t*-butyl DOTA-bifluorene **24** (0.25 g, 0.18 mmol), 3 ml of trifluoroacetic acid, and 2 ml of CH_2Cl_2 were to a round bottom flask and let stir at RT for 24 h. The trifluoroacetic acid and CH_2Cl_2 were removed under reduced pressure to yield the desired product **25** (0.22 g, 100%) as a tan viscous oil. HRMS calcd for $C_{71}H_{93}N_8O_{10}$: 1217.7015. Found 1217.7053.

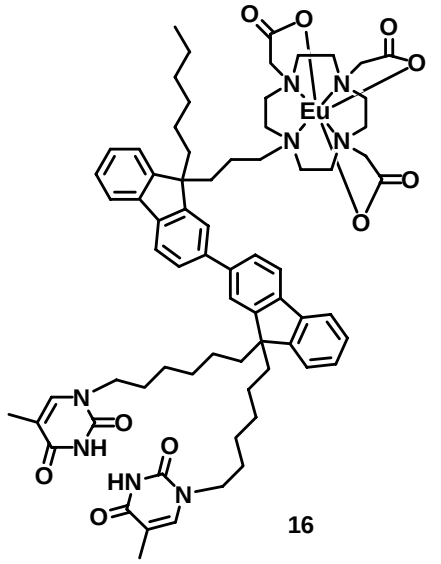

16

Bis(thymine)-DOTA-bifluorene-Eu-complex 16 *rwiii96*: Bis(thymine)-DOTA-bifluorene **25** (0.053 g, 0.04 mmol), $EuCl_3 \cdot (H_2O)_6$ (0.016 g, 0.04 mmol), K_2CO_3 (0.024 g, 0.17 mmol), and 3 ml of DMSO were added to a Schlenk flask and heated to 90 ^oC for 24 h. After cooling to RT, the crude product was purified by precipitation into water. The white solid was dried under vacuum for 24 h to yield the desired product **16** as a white solid (0.024 g, 44%). MS (TOF ES) *m/z* 1389 (Mass + Na) and 1411 (Mass + 2 Na).

APPENDIX A

SELECTED NMR SPECTRA

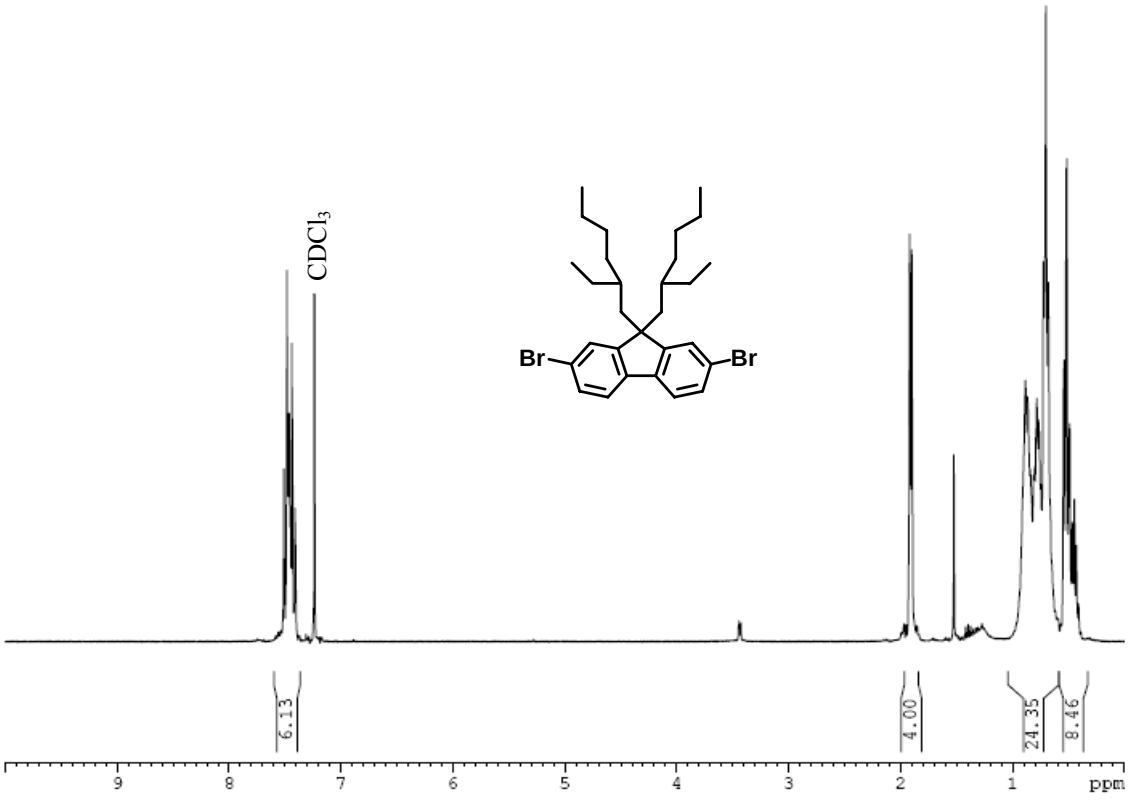

Figure A.1. ^{1}H NMR Spectrum of **Br-ehF-Br**.

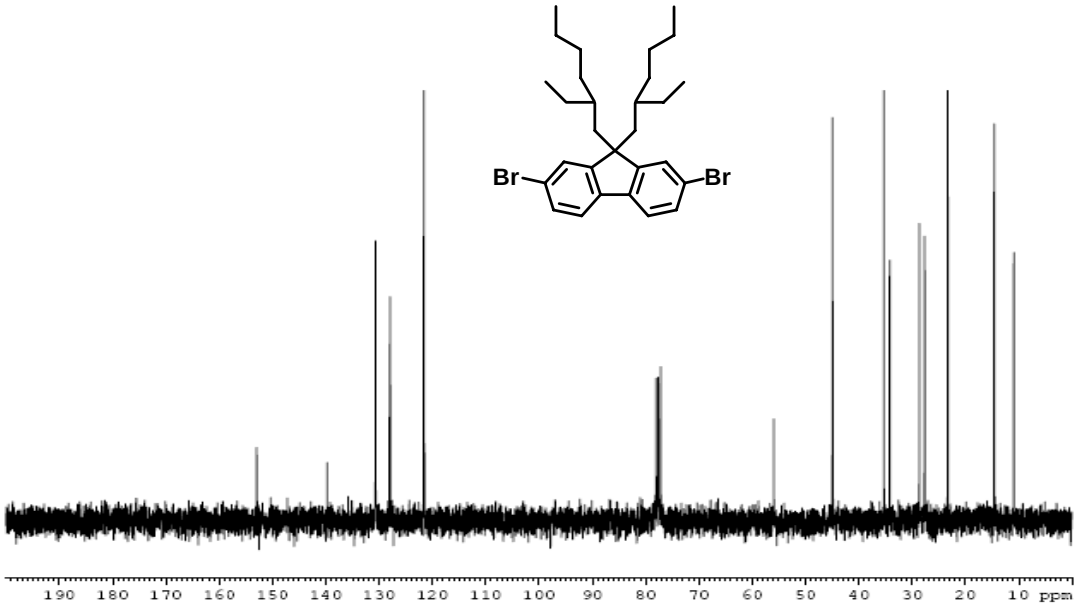

Figure A.2. ^{13}C NMR Spectrum of **Br-ehF-Br**.

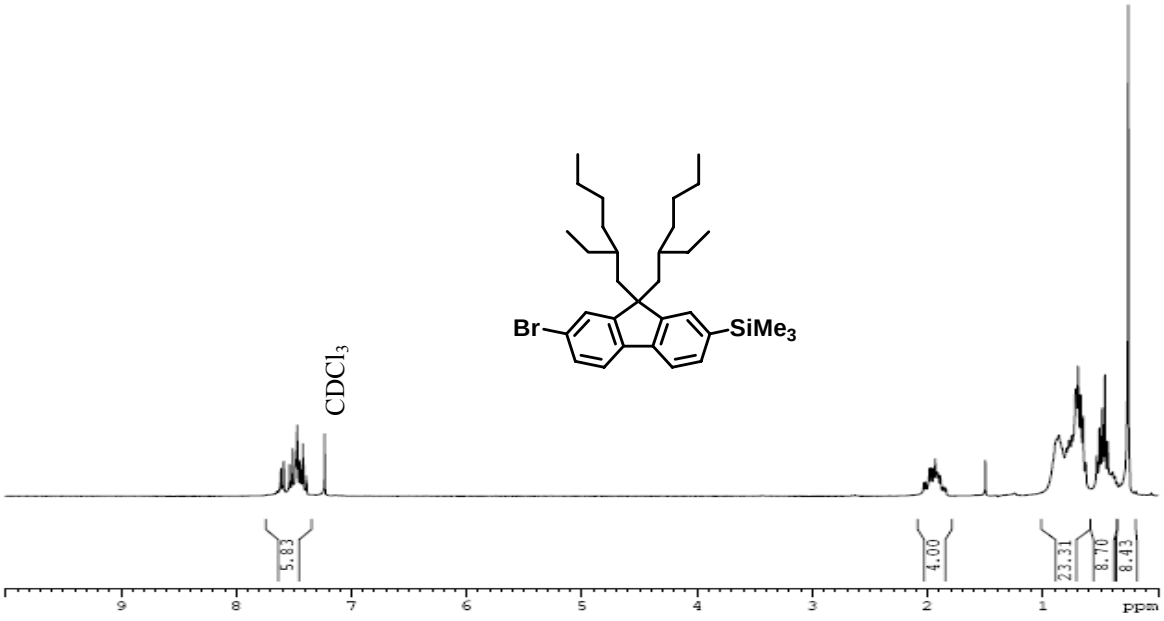

Figure A.3. ^{1}H NMR Spectrum of **Br-ehF-Si**.

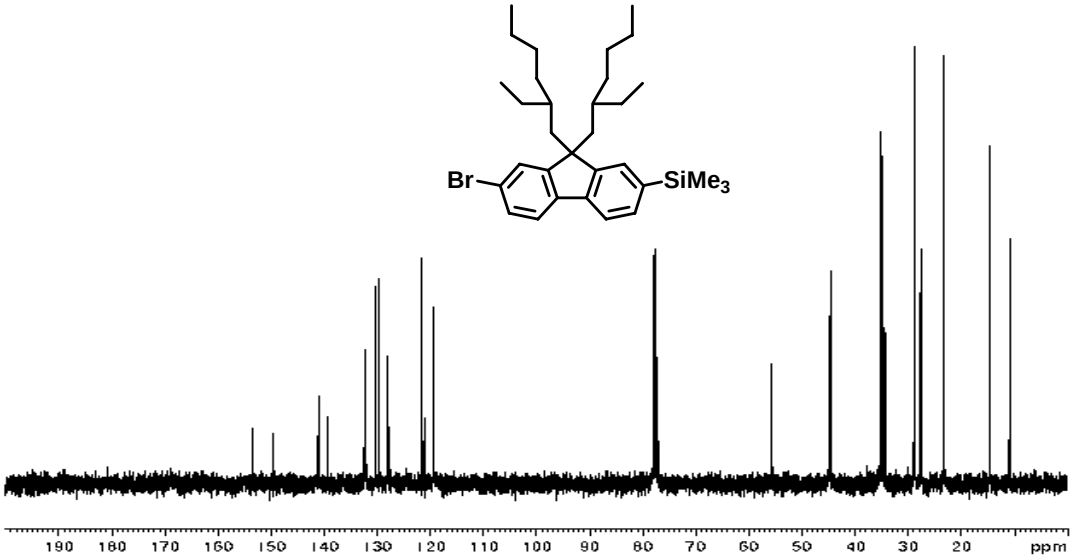

Figure A.4. ^{13}C NMR Spectrum of **Br-ehF-Si**.

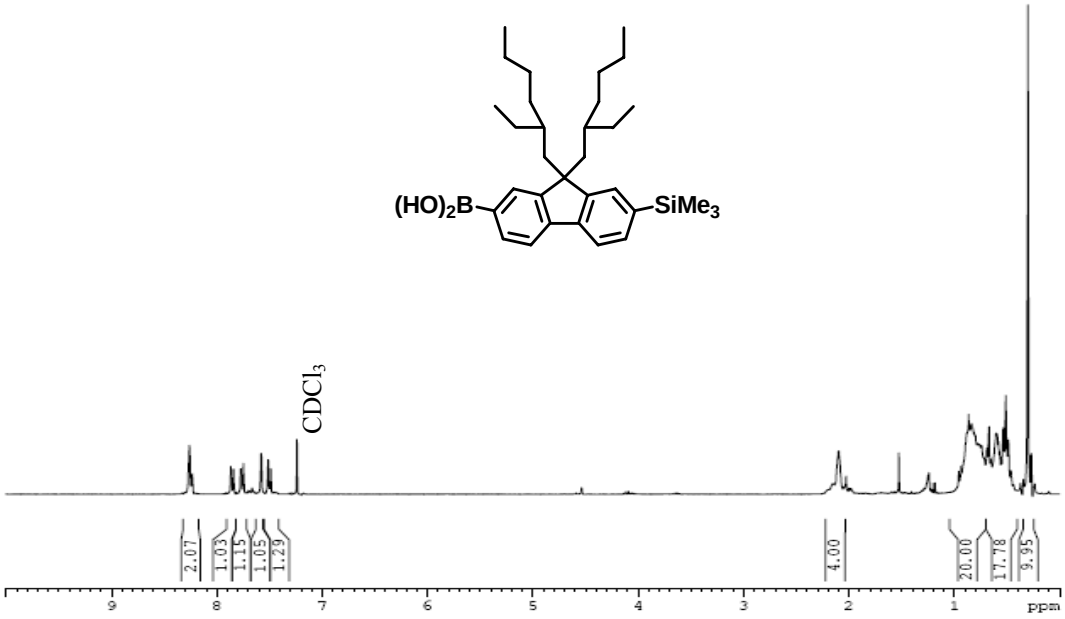

Figure A.5. ^{1}H NMR Spectrum of **B-ehF-Si**.

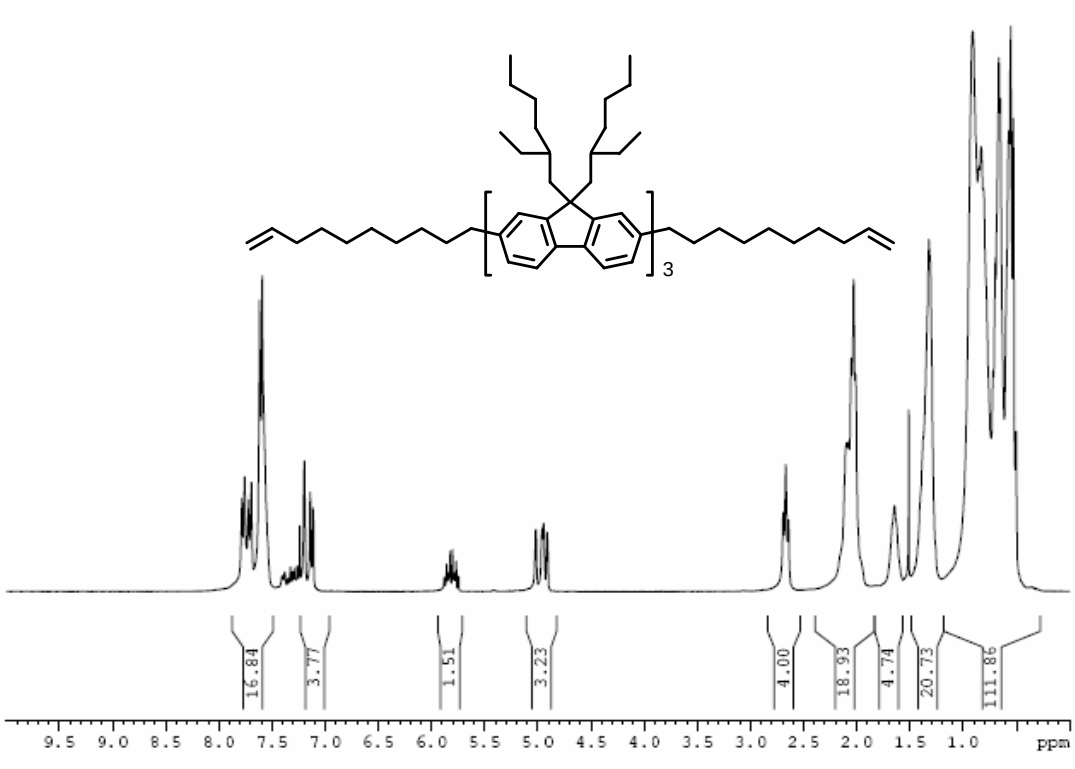

Figure A.6. ^{1}H NMR Spectrum of **s(ehF$_3$M$_{18}$)**.

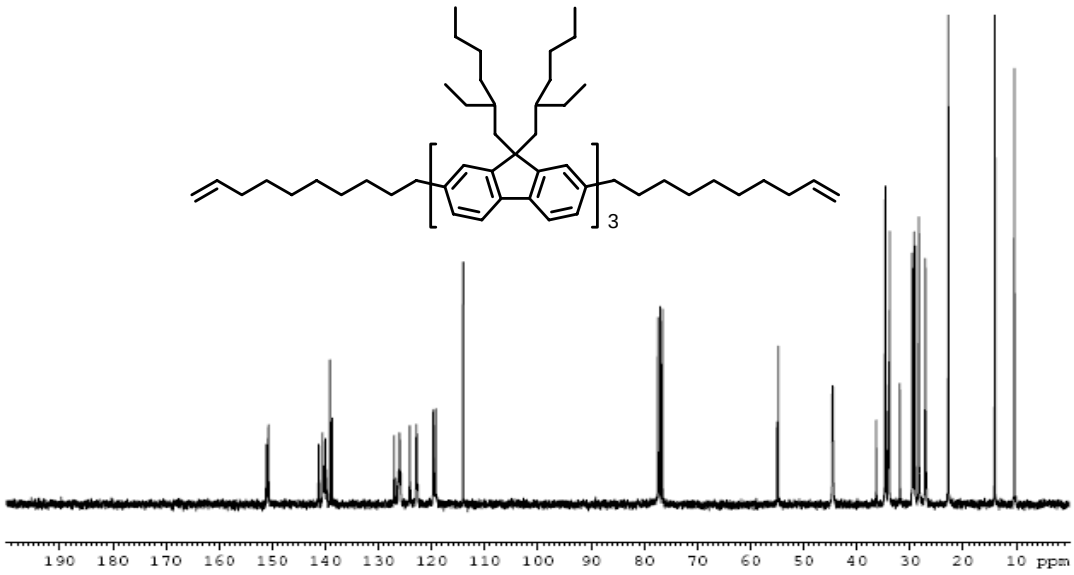

Figure A.7. ^{1}H NMR Spectrum of **s(ehF$_3$M$_{18}$)**.

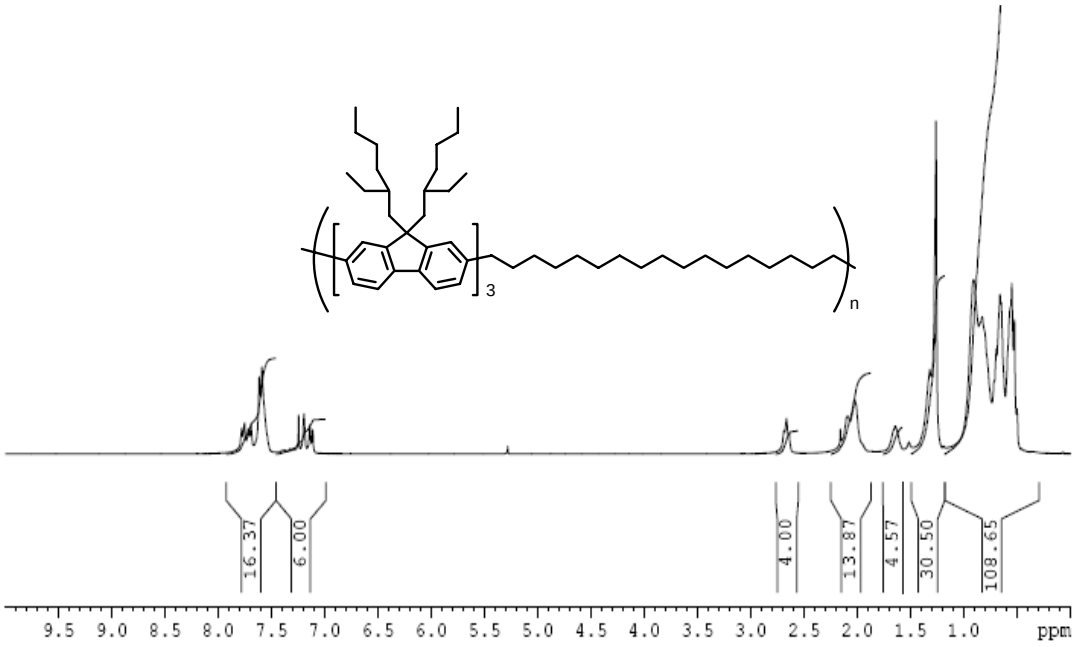

Figure A.8. ^{1}H NMR Spectrum of **p(ehF$_3$M$_{18}$)**.

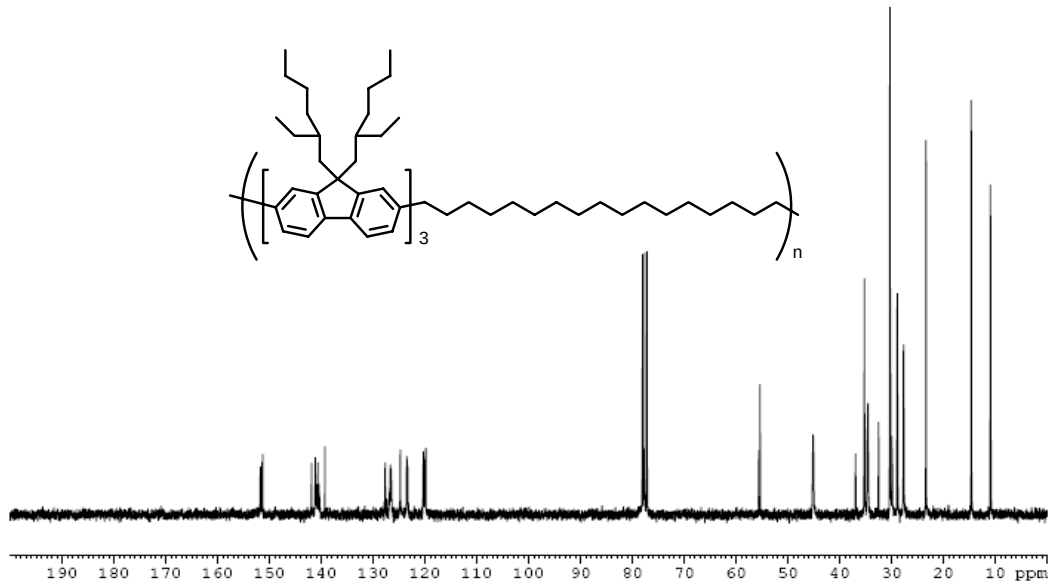

Figure A.9. ^{13}C NMR Spectrum of **p(ehF$_3$M$_{18}$).**

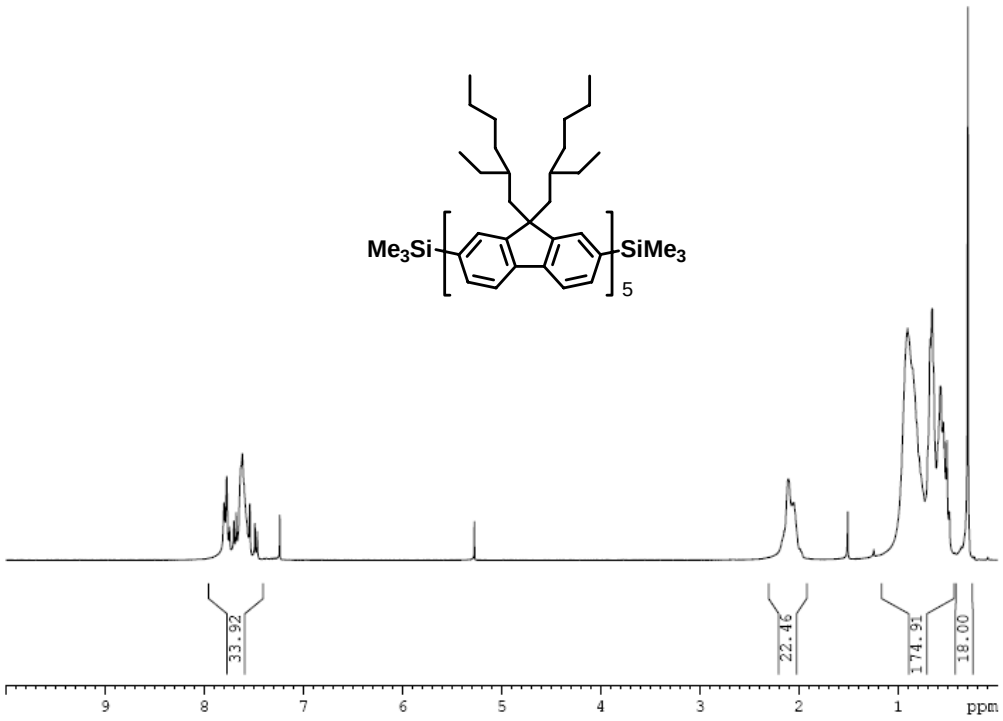

Figure A.10. ^{1}H NMR Spectrum **SI-ehF$_5$-Si**.

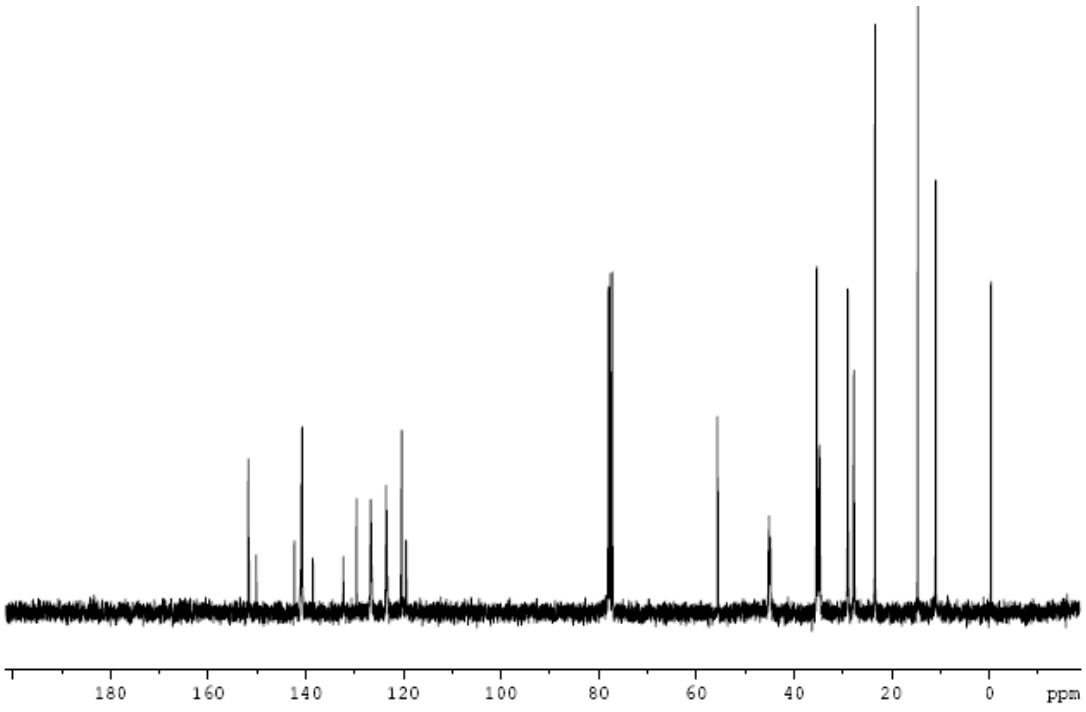

Figure A.11. ^{13}C NMR Spectrum **SI-ehF$_5$-Si**.

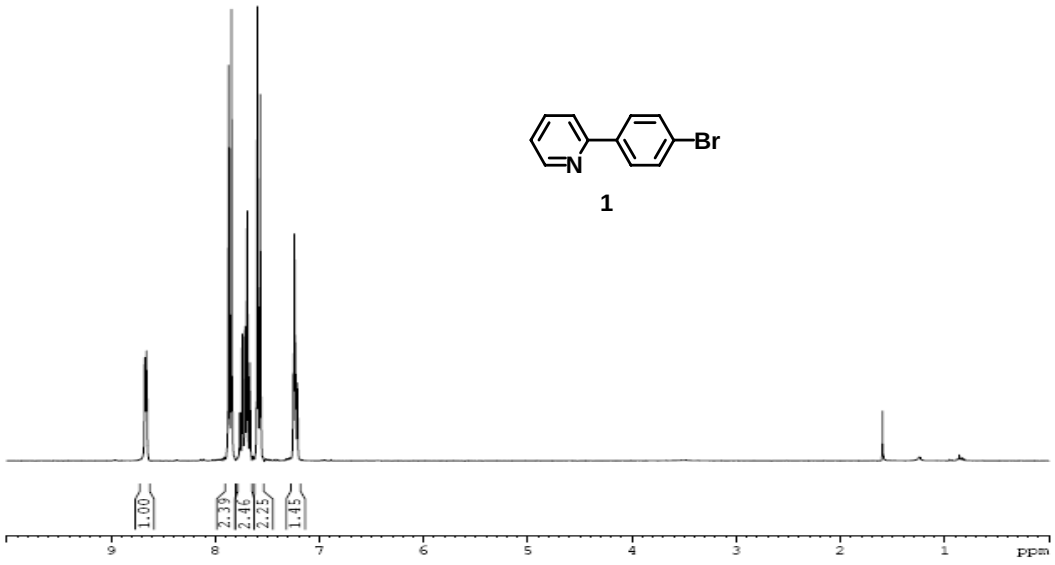

Figure A.12. ^{1}H NMR Spectrum of compound **1**.

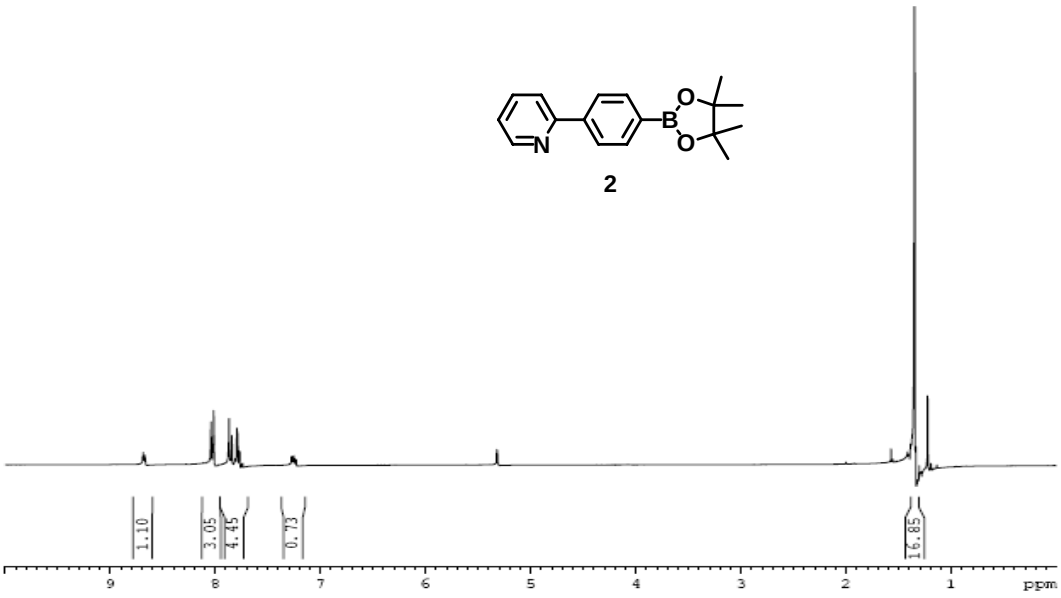

Figure A.13. ^{1}H NMR Spectrum of compound **2**.

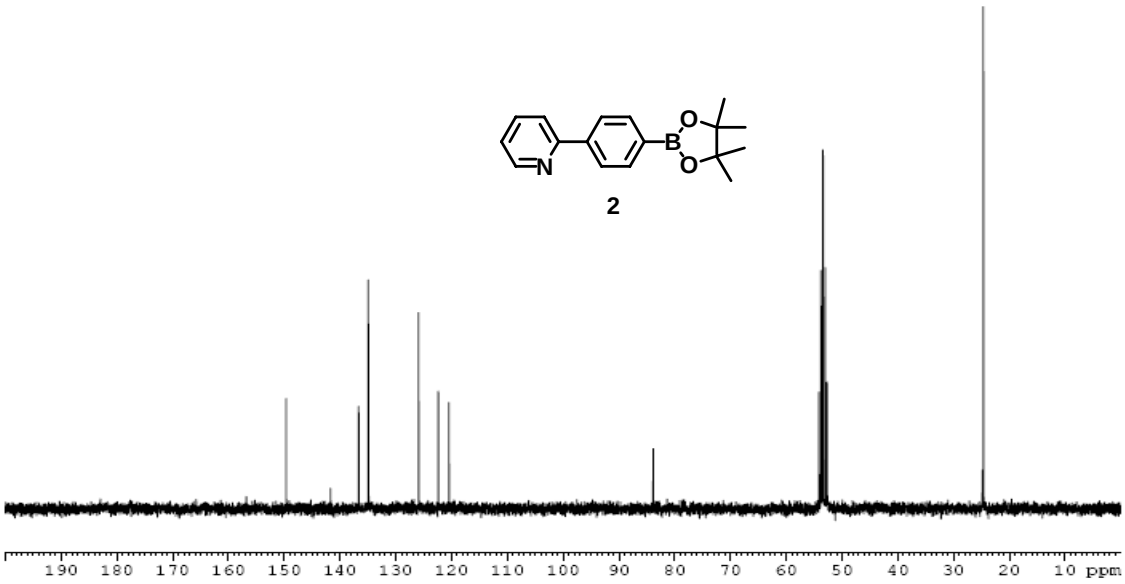

Figure A.14. ^{13}C NMR Spectrum of compound **2**.

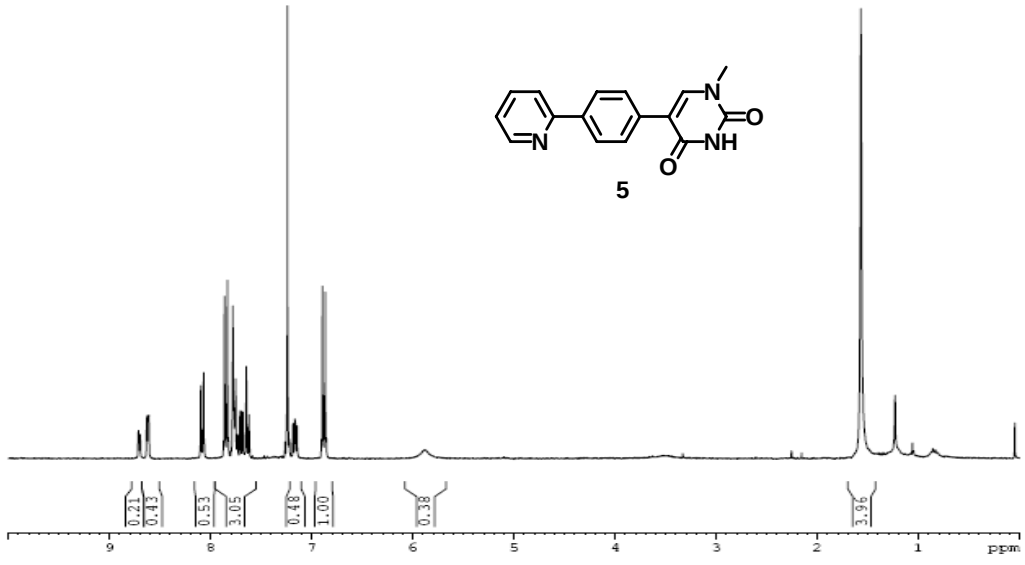

Figure A.15. ^{1}H NMR Spectrum of **uppy** (compound **5**).

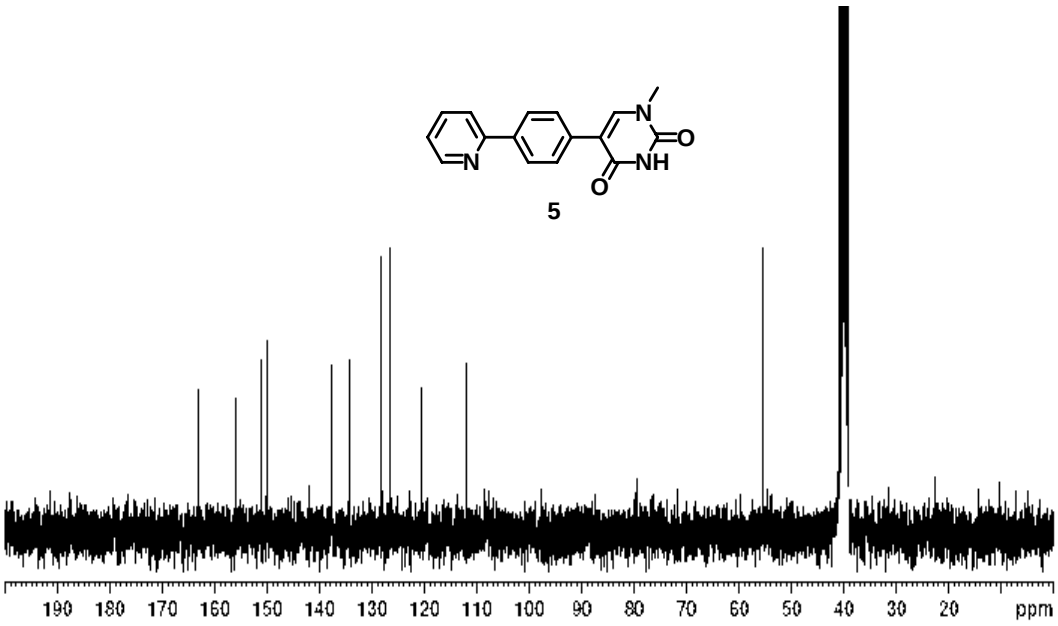

Figure A.16. ^{13}C NMR Spectrum of **uppy** (compound **5**).

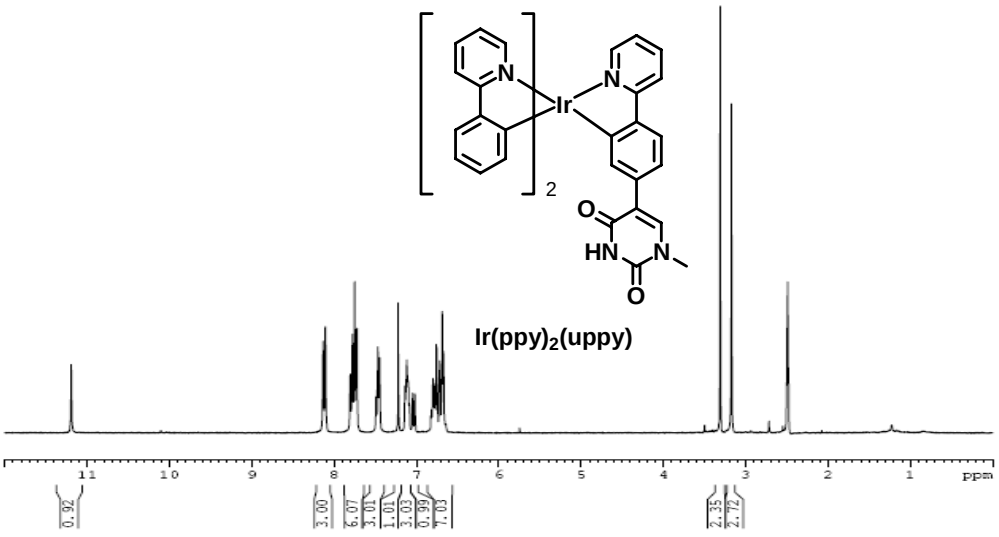

Figure A.17. ^{1}H NMR Spectrum of **Ir(ppy)$_2$(uppy)**.

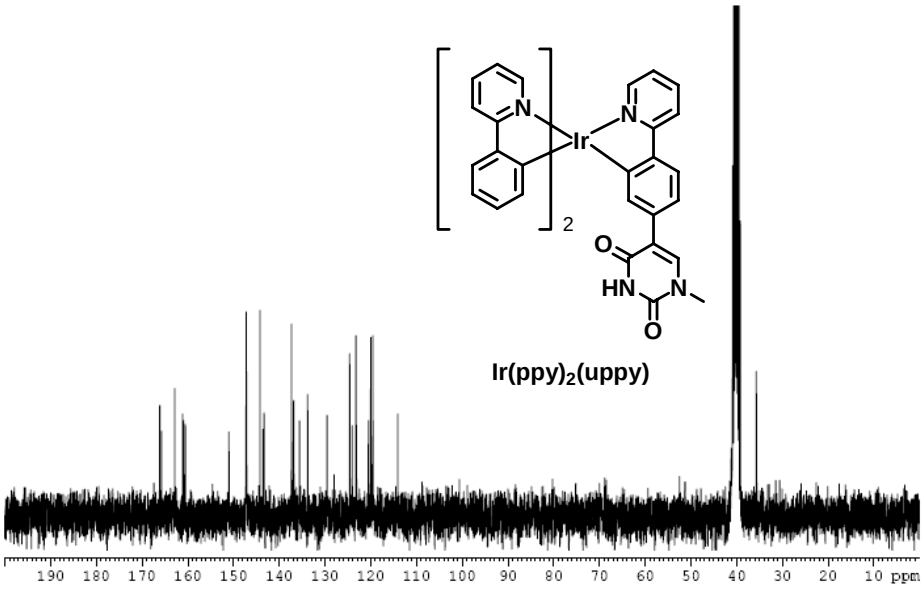

Figure A.18. [1]H NMR Spectrum of **Ir(ppy)$_2$(uppy).**

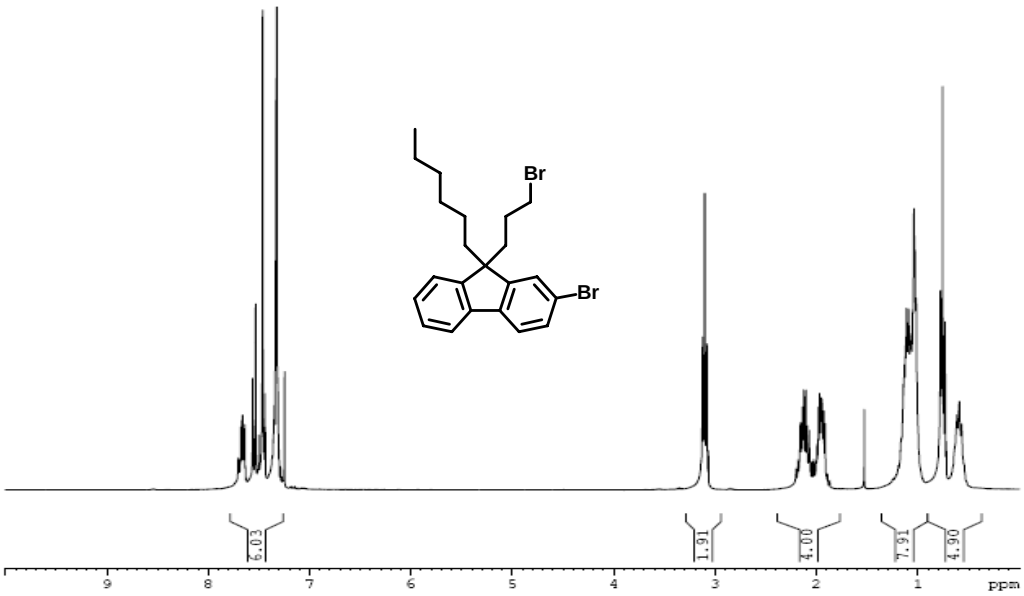

Figure A.19. [1]H NMR Spectrum of compound **17**.

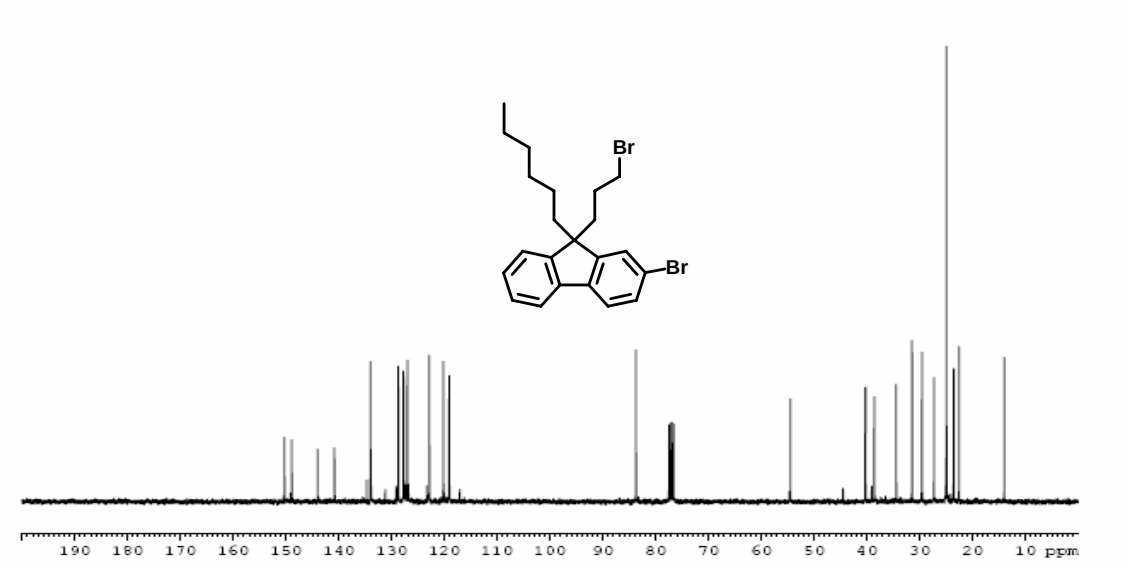

Figure A.20. [1]H NMR Spectrum of compound **17**.

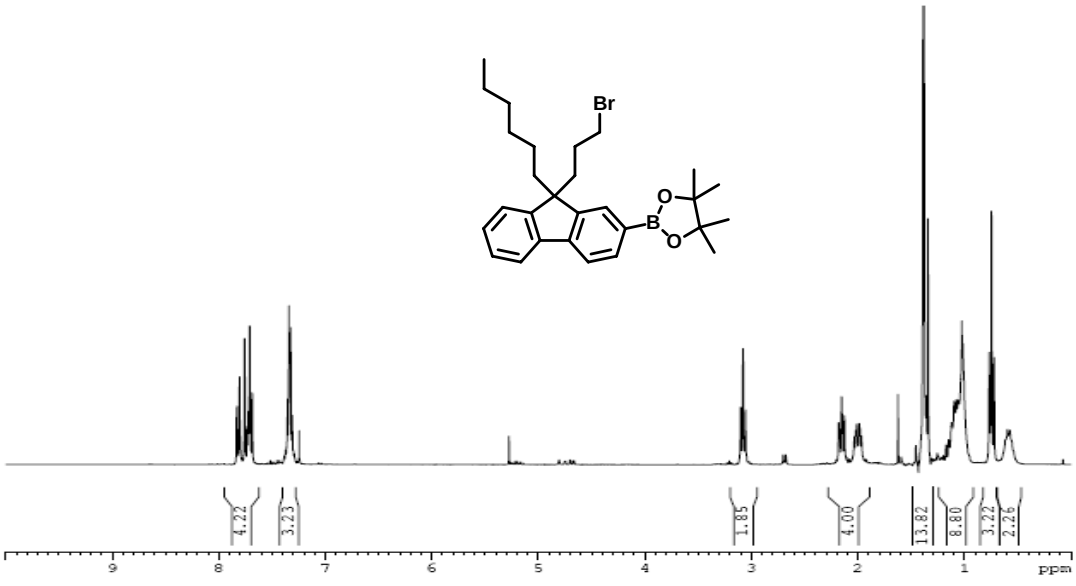

Figure A.21. [1]H NMR Spectrum of compound **19**.

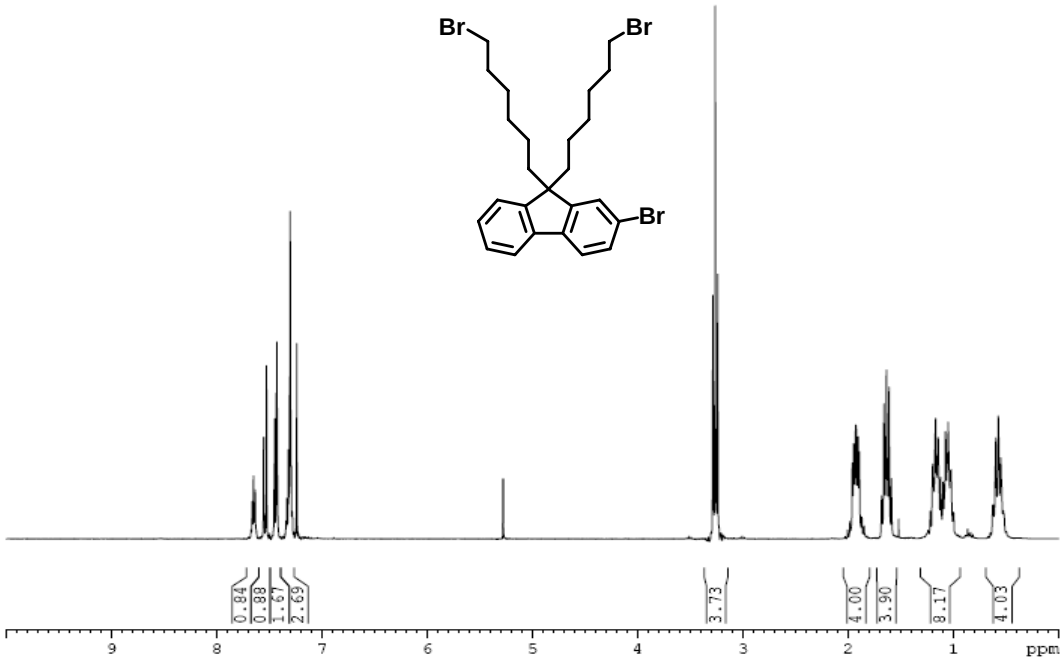

Figure A.22. ^{1}H NMR Spectrum of compound **22**.

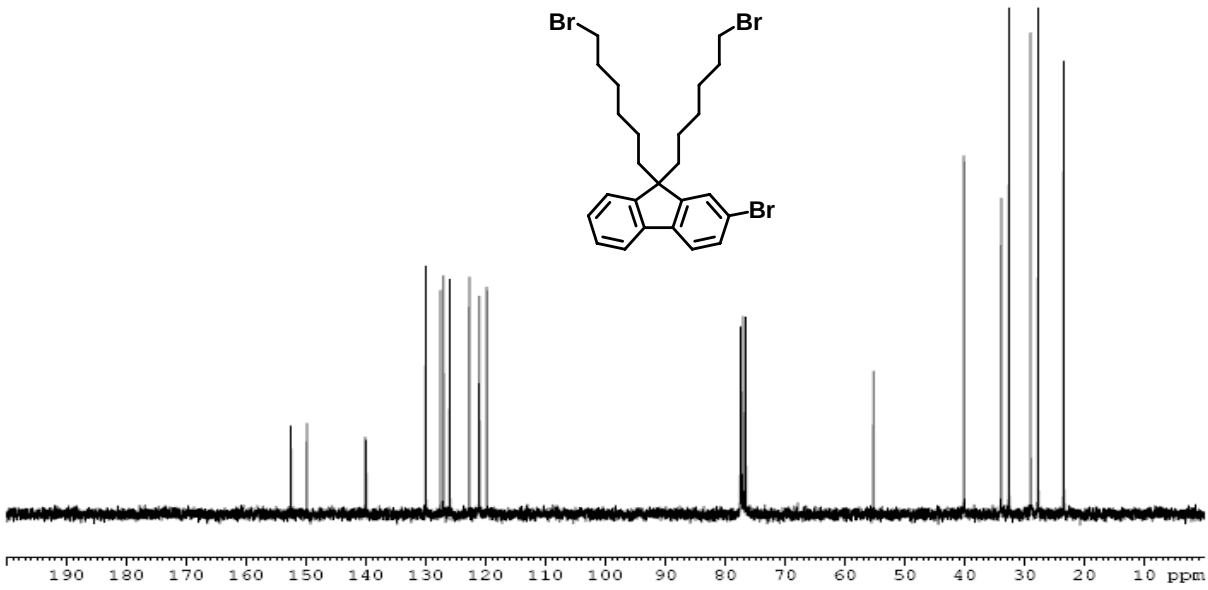

Figure A.23. ^{13}C NMR Spectrum of compound **22**.

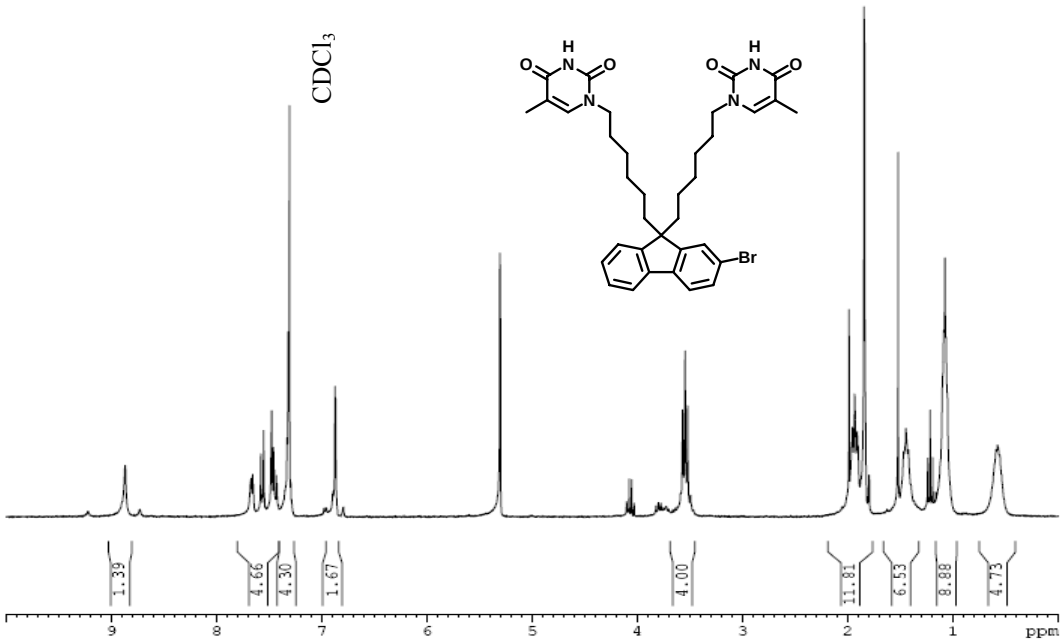

Figure A.24. ^{1}H NMR Spectrum of compound **23**.

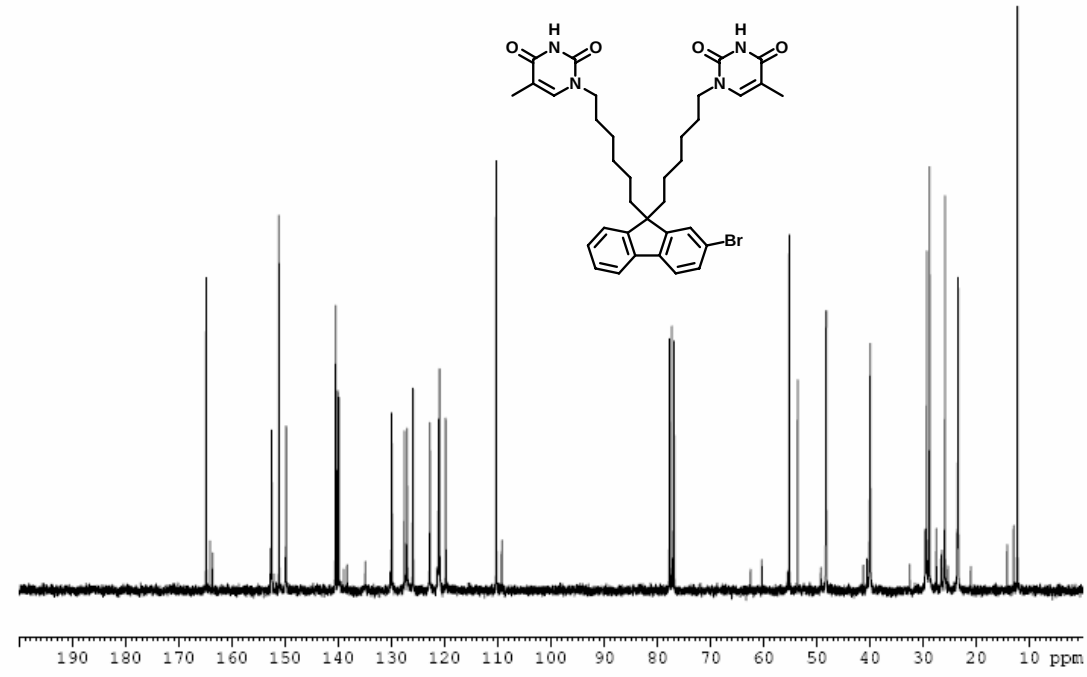

Figure A.25. ^{13}C NMR Spectrum of compound **23**.

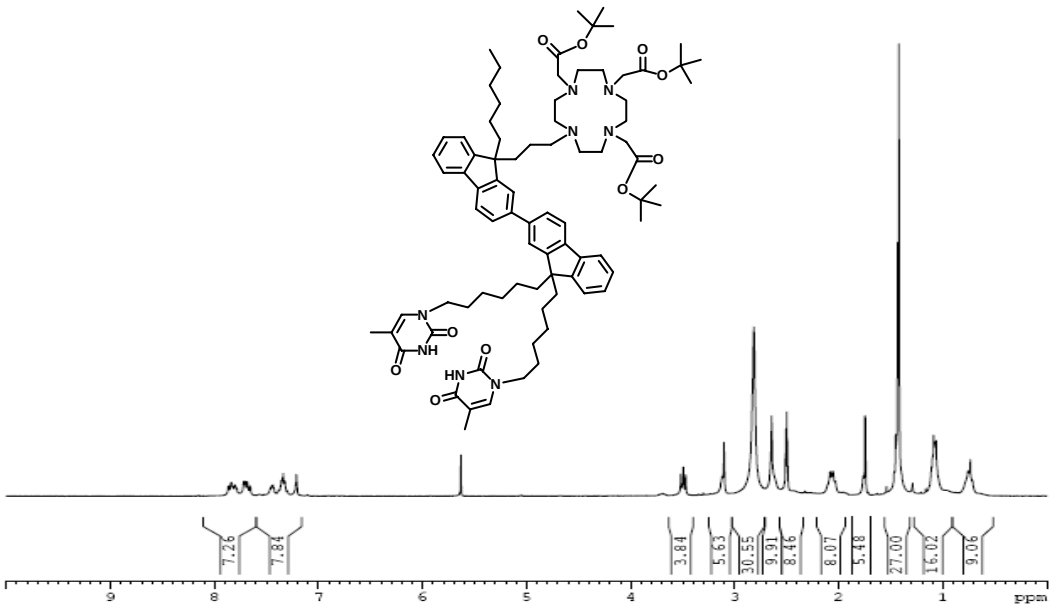

Figure A.26. ^{1}H NMR Spectrum of compound **24** at 360 K.

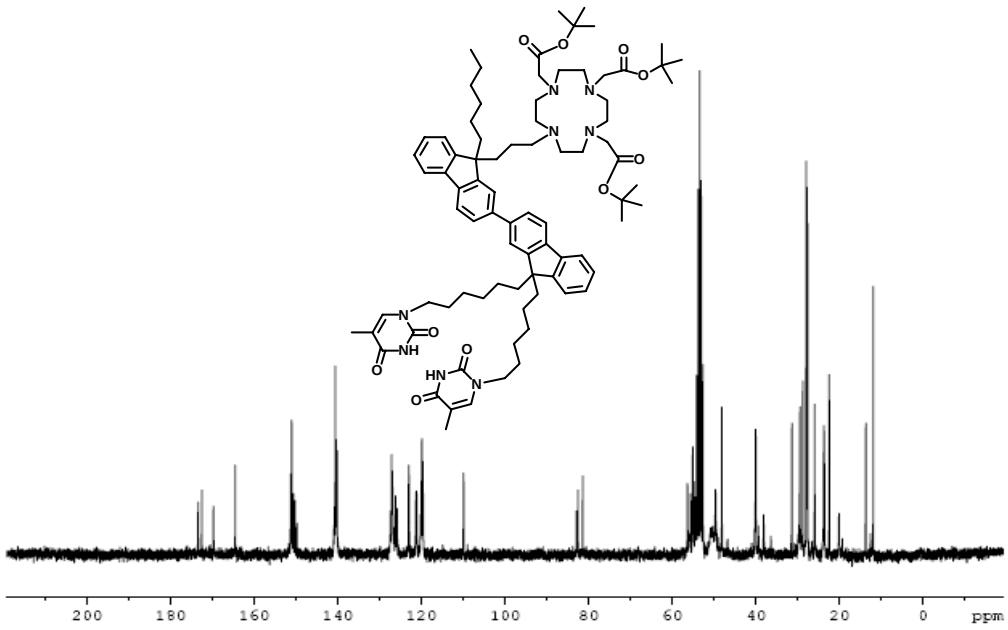

Figure A.27. ^{13}C NMR Spectrum of compound **24**.

APPENDIX B

GPC TRACES OF P(ehF_XM_Y)s

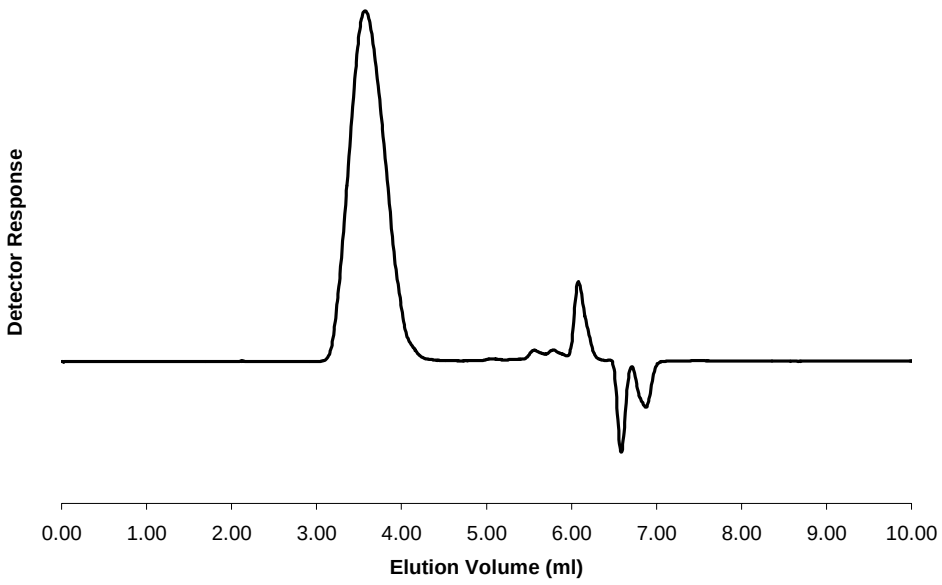

Figure B.1. GPC trace of **p(ehF_3M_{18})** in THF.

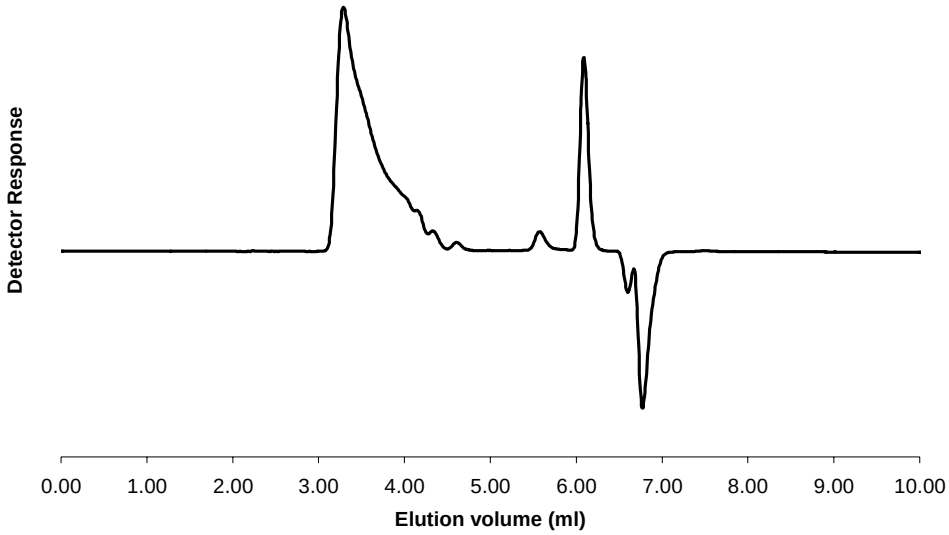

Figure B.2. GPC trace of **p(ehF$_3$M$_{10}$)** in THF.

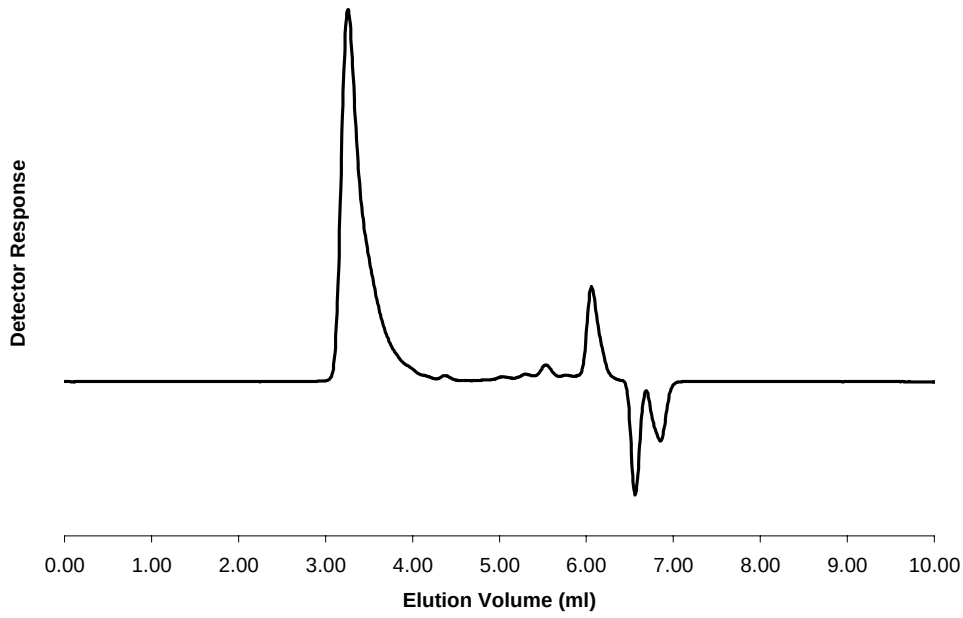

Figure B.3. GPC trace of **p(ehF$_4$M$_{18}$)** in THF.

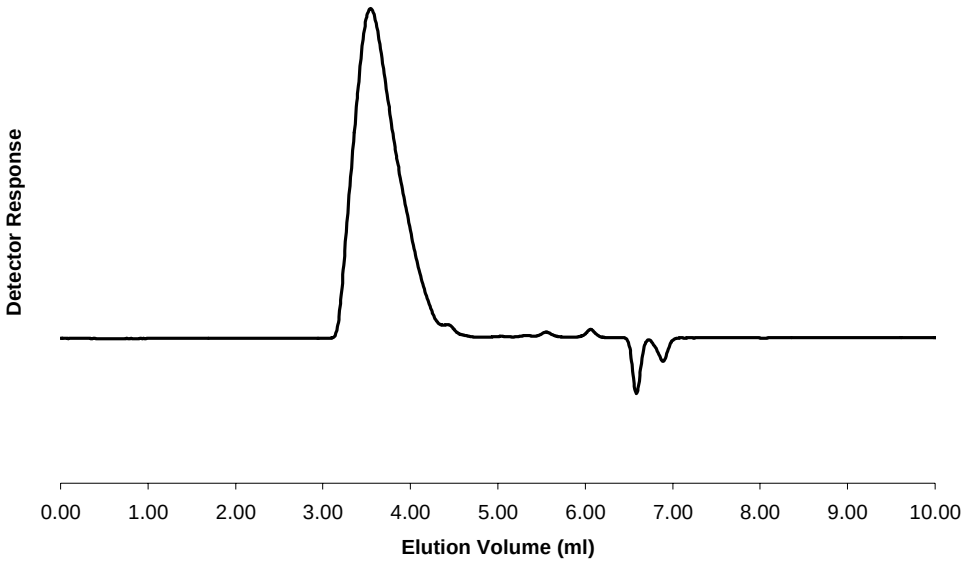

Figure B.4. GPC trace of **p(ehF$_4$M$_{10}$)** in THF.

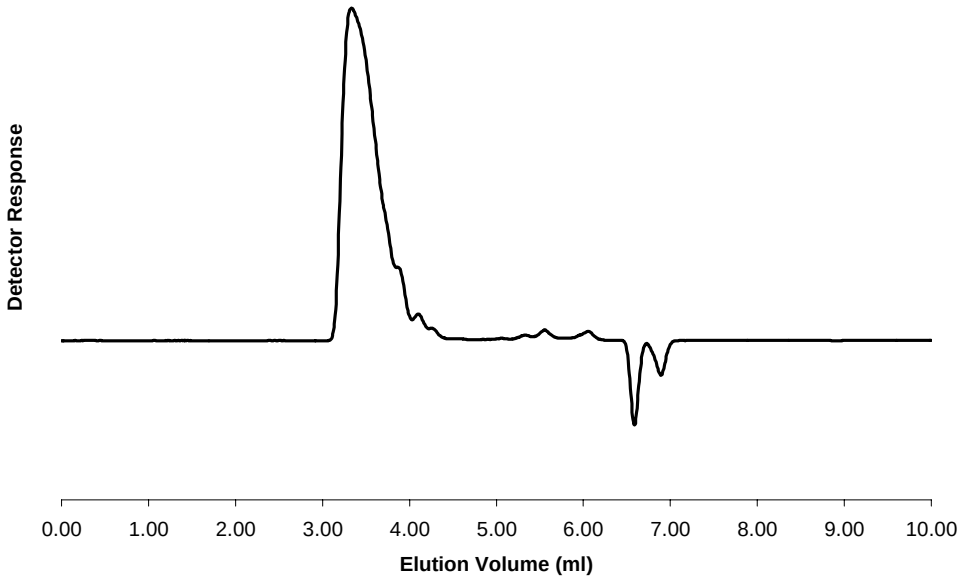

Figure B.5. GPC trace of **p(ehF$_5$M$_{18}$)** in THF.

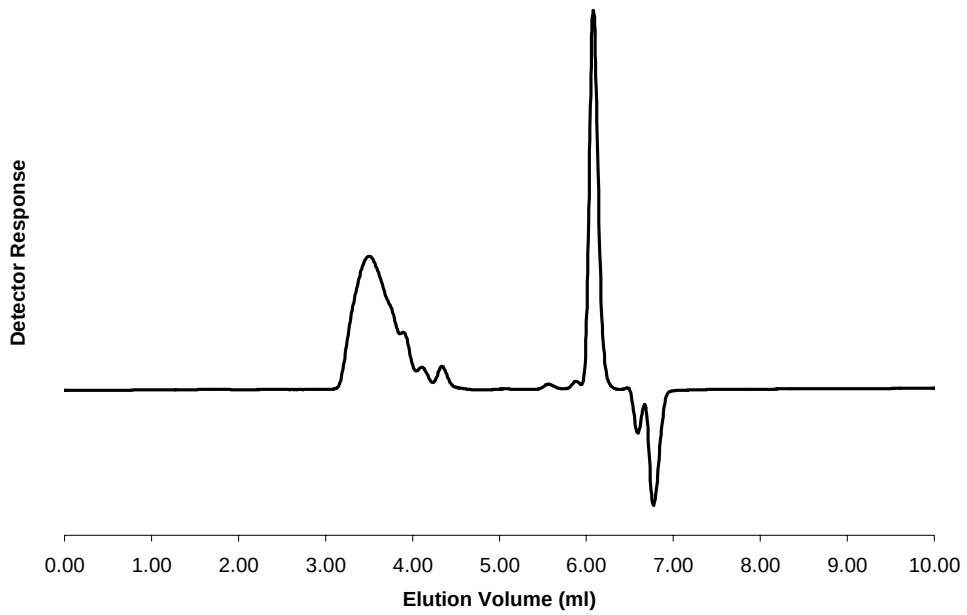

Figure B.6. GPC trace of **p(ehF$_5$M$_{10}$)** in THF.

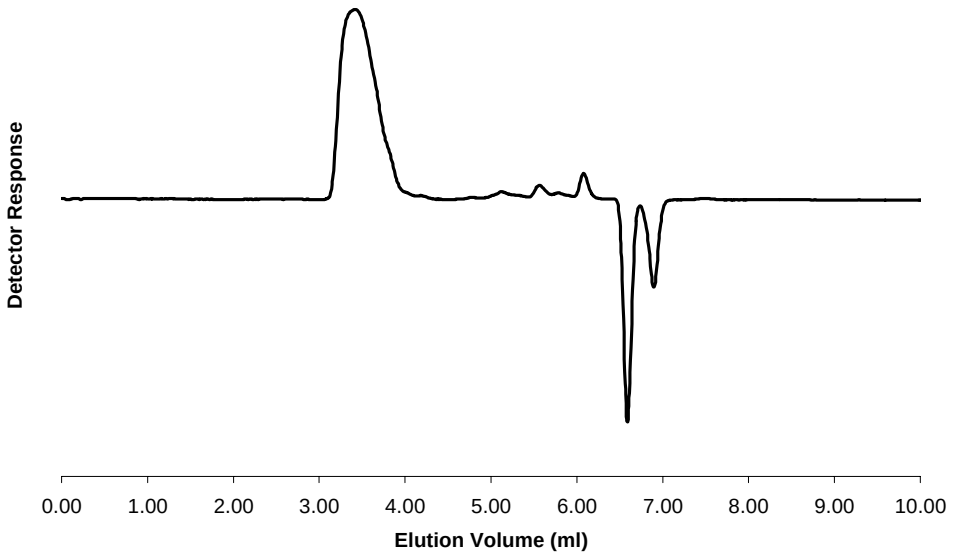

Figure B.7. GPC trace of **p(ehF$_6$M$_{18}$)** in THF.

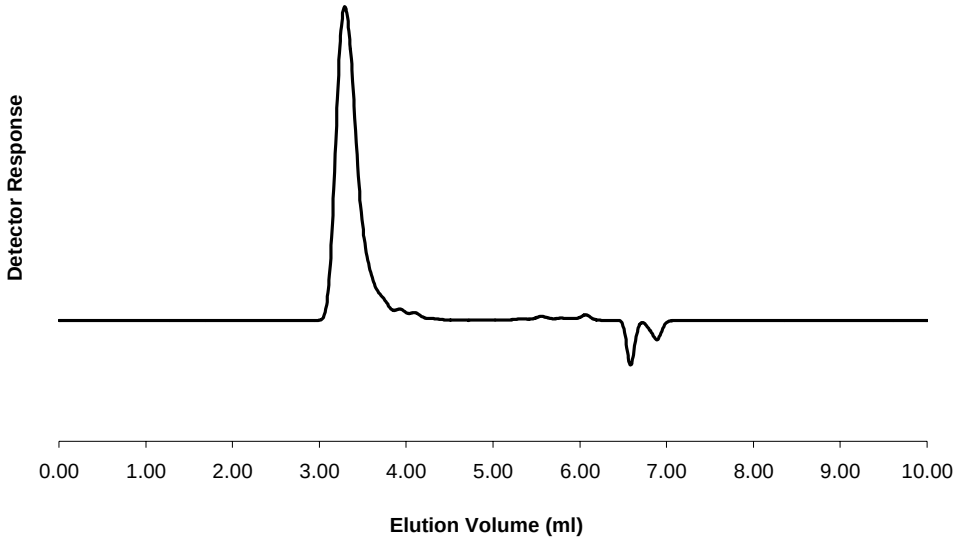

Figure B.8. GPC trace of **p(ehF$_7$M$_{18}$)** in THF.

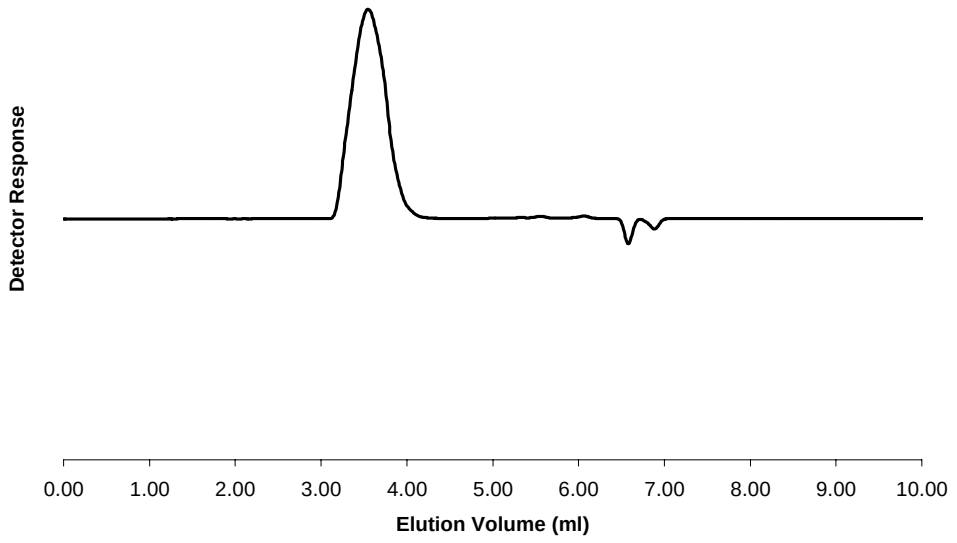

Figure B.9. GPC trace of **p(ehF$_8$M$_{18}$)** in THF.

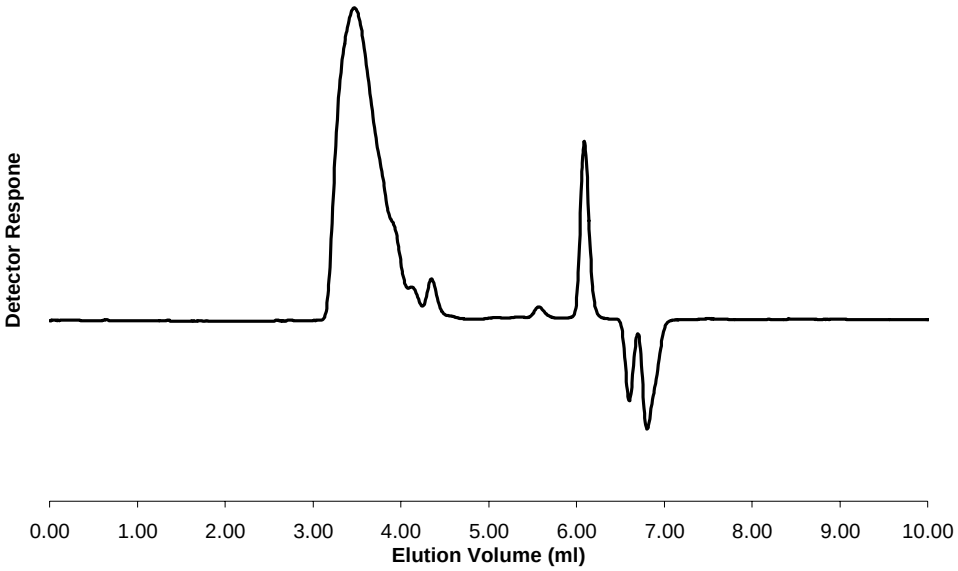

Figure B.10. GPC trace of **10% p(ehF$_3$M$_{10}$) : 90% 10% p(ehF$_3$M$_{10}$)** in THF.

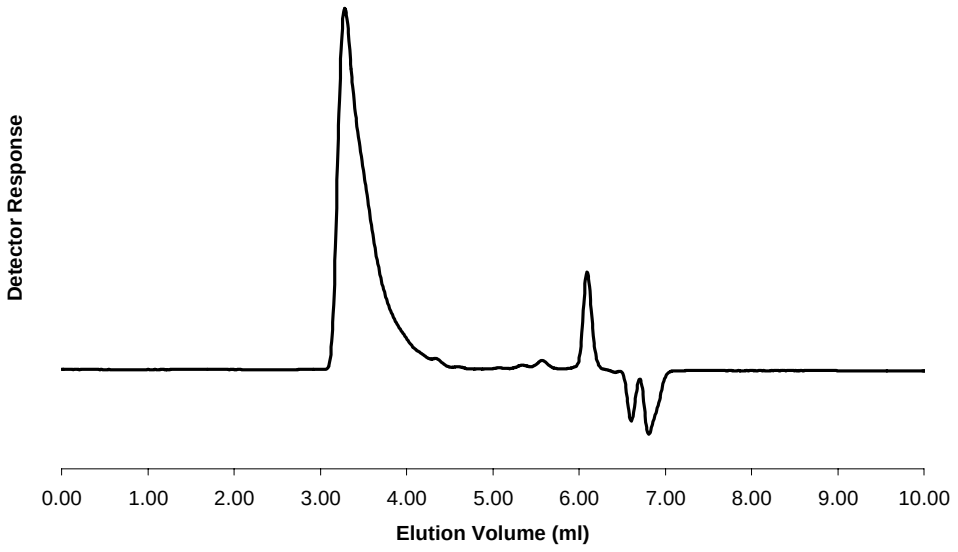

Figure B.11. GPC trace of **50% p(ehF$_3$M$_{10}$) : 50% 10% p(ehF$_3$M$_{10}$)** in THF.

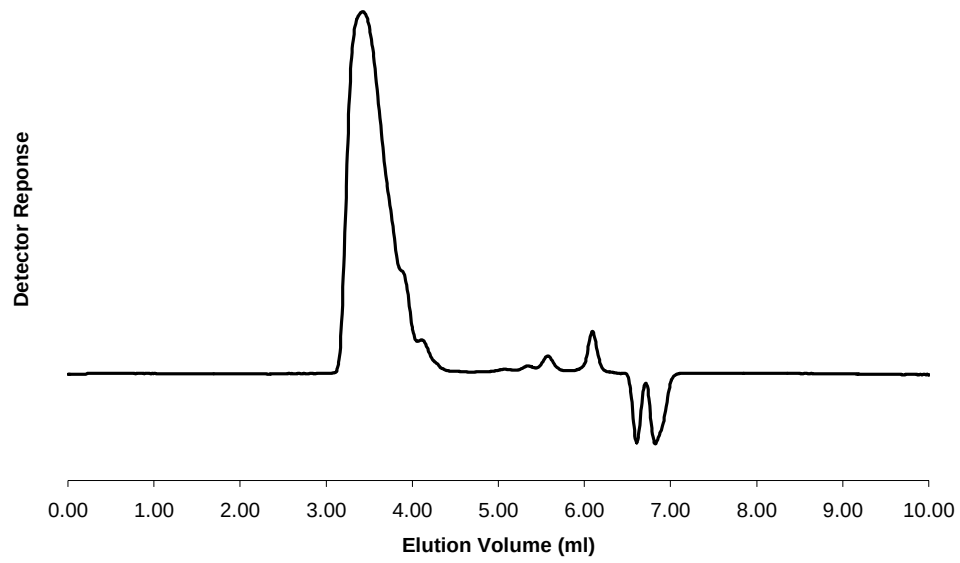

Figure B.12. GPC trace of **p(F_4M_{18}).**

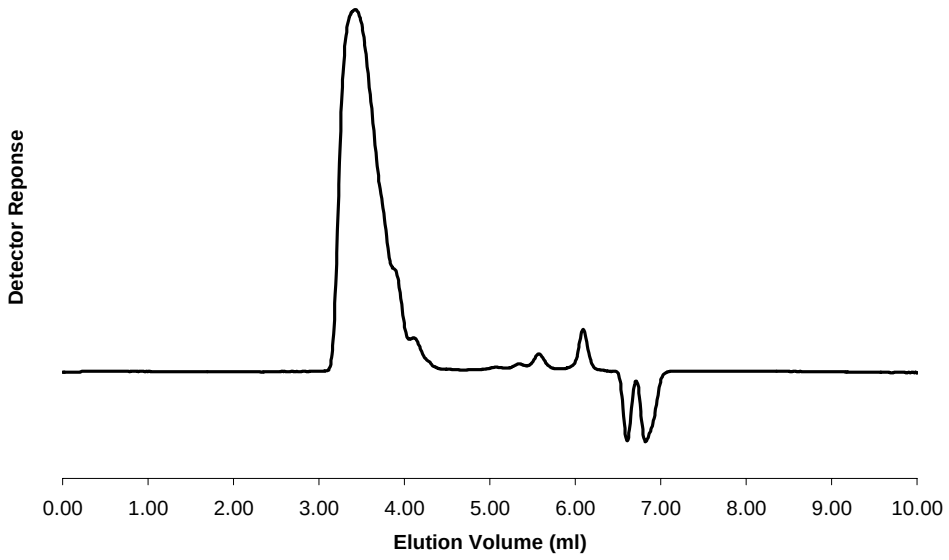

Figure B.13. GPC trace of **p(F_5M_{18})** in THF.

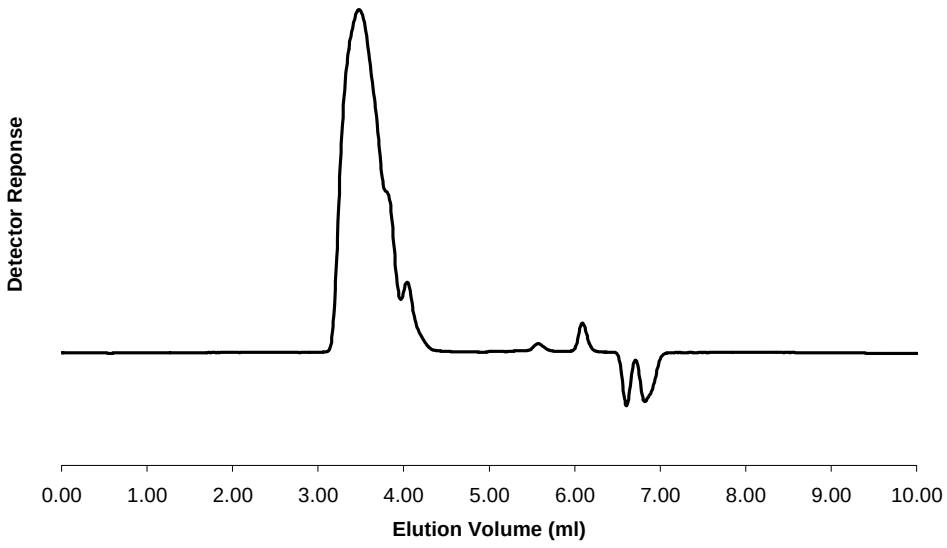

Figure B.14. GPC trace of **p(F_6M_{18})** in THF.

APPENDIX C

DIFFERENTIAL SCANNING CALORIMETRY (DSC) DATA

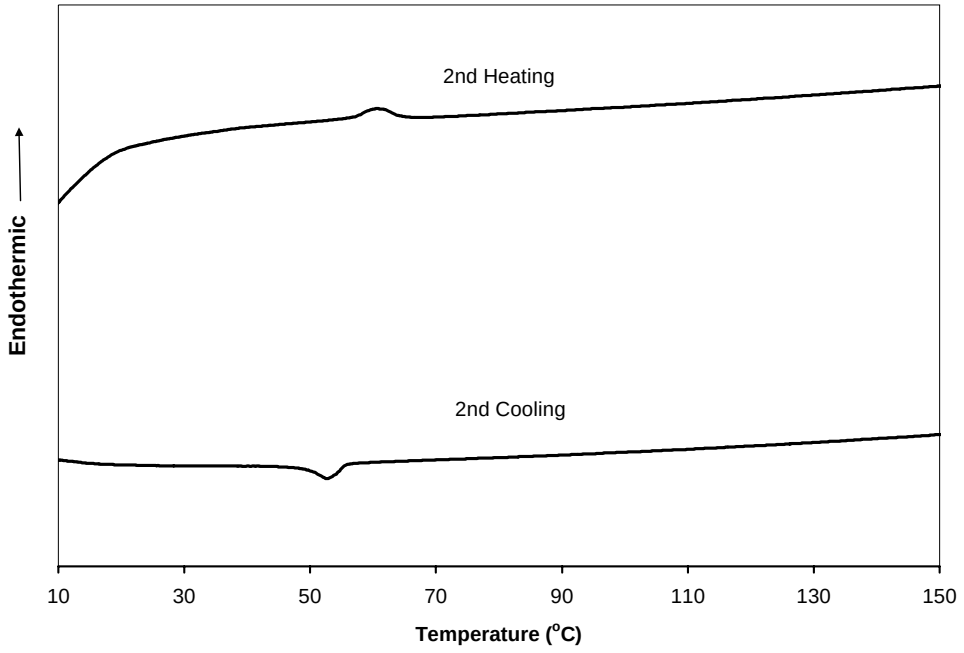

Figure C.1. DSC scan of **p(ehF$_3$M$_{18}$)** at 10 ^{0}C / min.

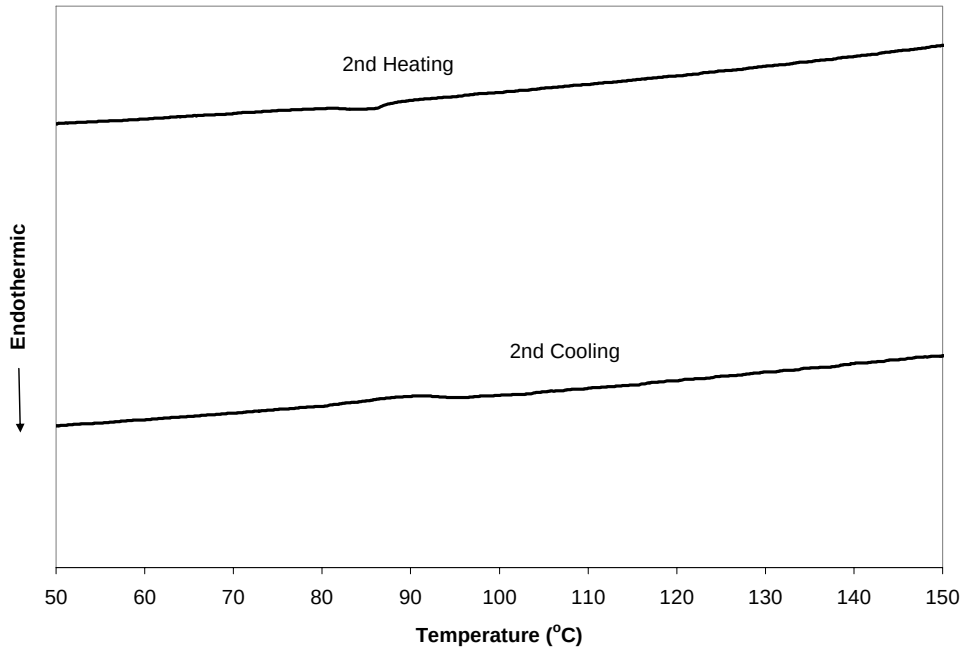

Figure C.2. DSC scan of **p(ehF$_3$M$_{10}$)** at 10 ^{0}C / min.

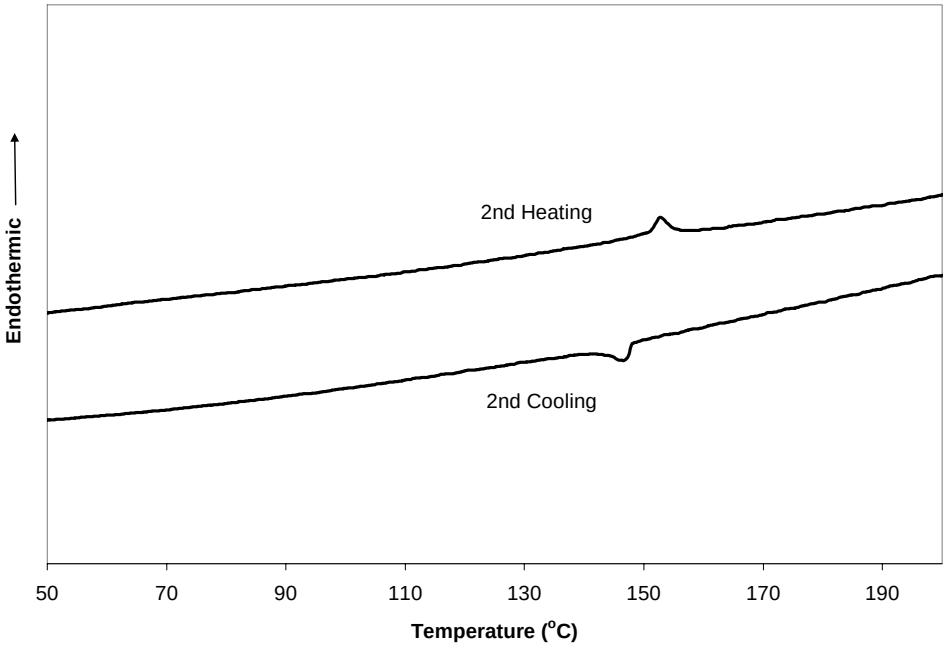

Figure C.3. DSC scan of **p(ehF$_4$M$_{18}$)** at 10 ^{0}C / min.

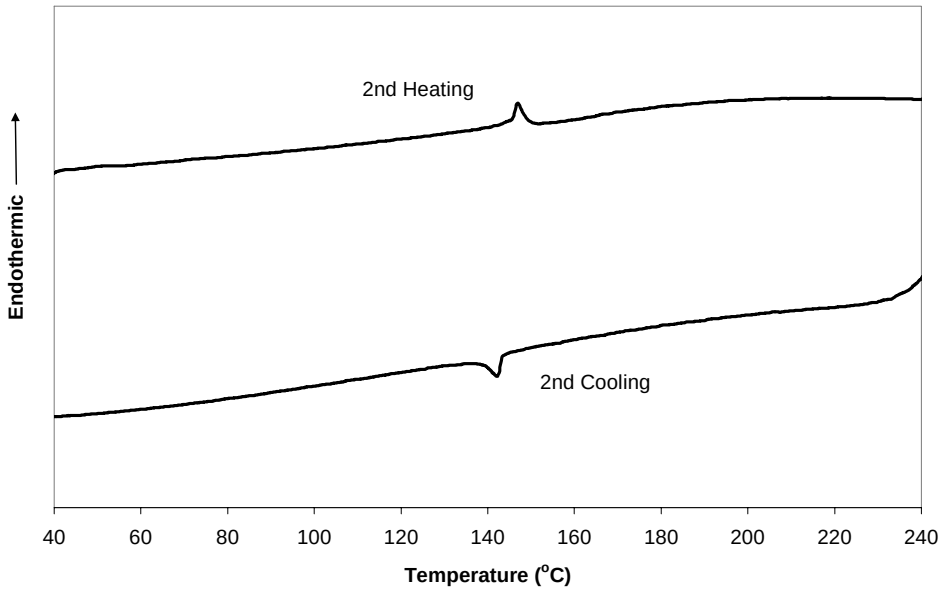

Figure C.3. DSC scan of **p(ehF$_4$M$_{10}$)** at 10 ^{0}C / min.

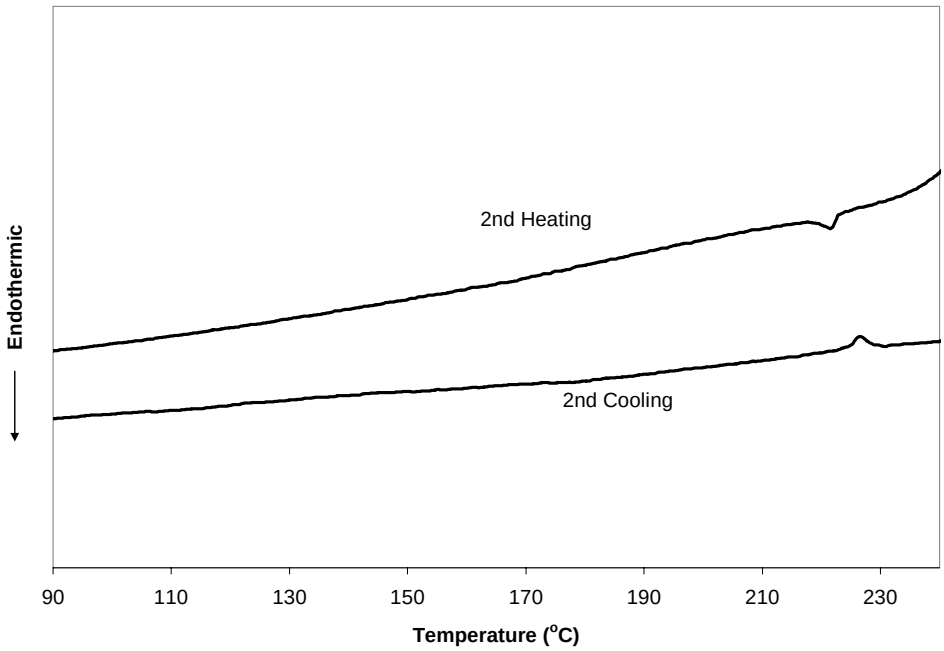

Figure C.5. DSC scan of **p(ehF$_5$M$_{18}$)** at 10 ^{0}C / min.

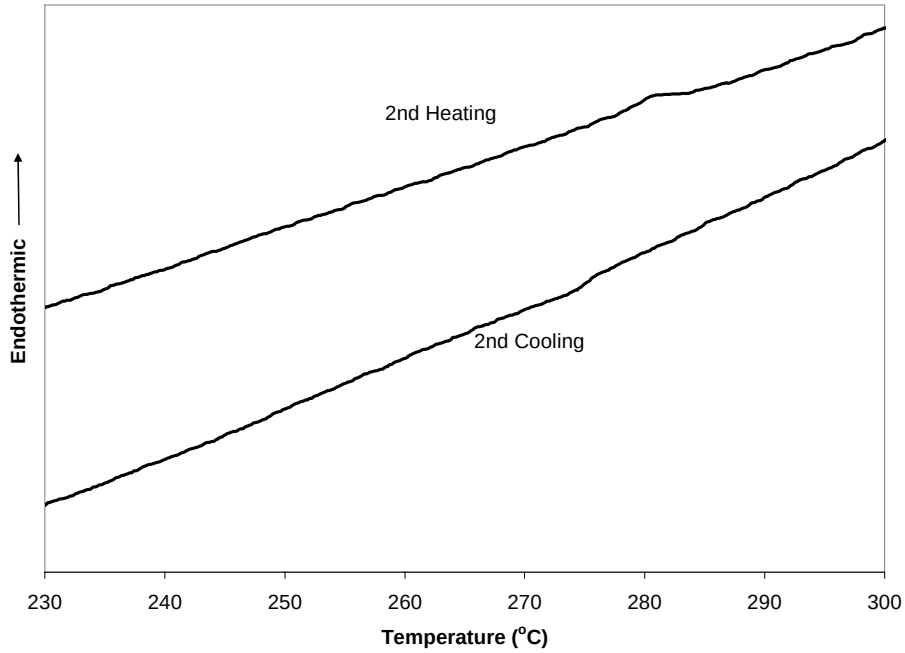

Figure C.6. DSC scan of **p(ehF$_6$M$_{18}$)** at 10 ^{0}C / min.

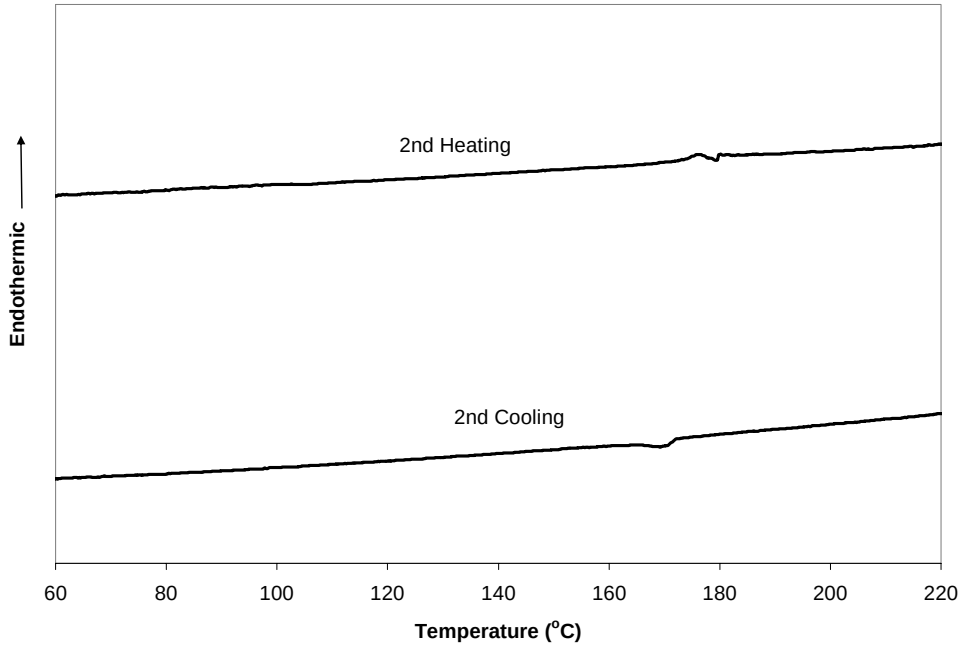

Figure C.7. DSC scan of **50% p(ehF$_3$M$_{10}$) : 50% p(ehF$_5$M$_{10}$)** at 10 ^{0}C / min.

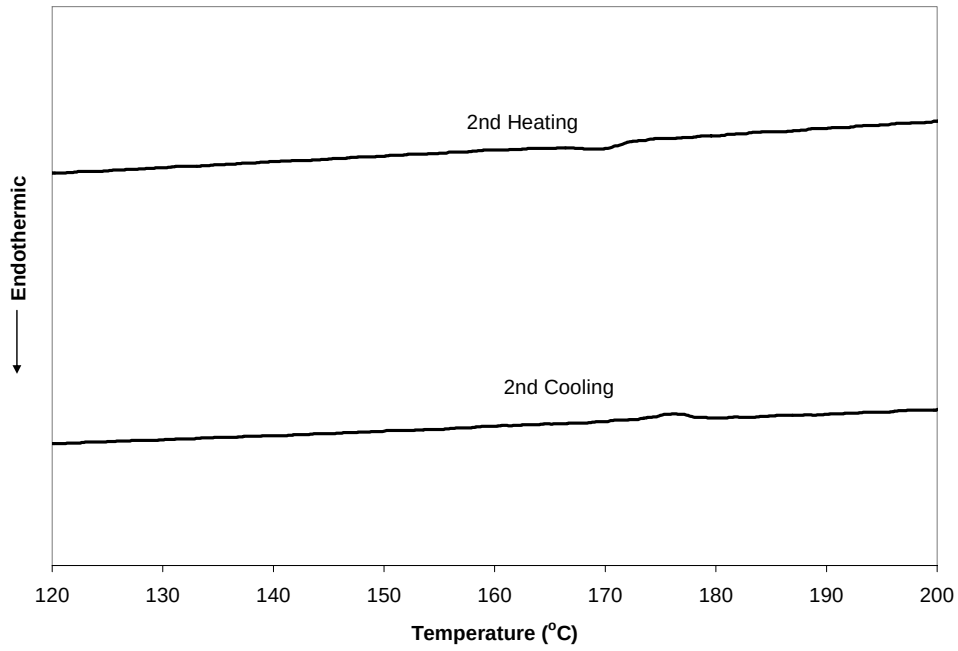

Figure C.8. DSC scan of **10% p(ehF$_3$M$_{10}$) : 90% p(ehF$_5$M$_{10}$)** at 10 ^{0}C / min.

APPENDIX D

X-RAY STRUCTURE REFINEMENT FOR $Ir(ppy)_2(uppy)$

Table D.1. Crystal data and structure refinement for **$Ir(ppy)_2uppy$**

Identification code	rwm1027s	
Empirical formula	C40 H32 Cl4 Ir N5 O4	
Formula weight	980.71	
Temperature	203(2) K	
Wavelength	0.71073 Å	
Crystal system	Monoclinic	
Space group	P2(1)/n	
Unit cell dimensions	a = 13.293(4) Å	α= 90°.
	b = 13.226(4) Å	β= 90.620(7)°.
	c = 23.259(7) Å	γ = 90°.
Volume	4089(2) $Å^3$	
Z	4	
Density (calculated)	1.593 Mg/m^3	
Absorption coefficient	3.573 mm^{-1}	
F(000)	1936	
Crystal size	0.16 x 0.16 x 0.26 mm^3	
Theta range for data collection	1.77 to 25.00°.	
Index ranges	-15<=h<=15, -15<=k<=15, -27<=l<=27	
Reflections collected	31544	
Independent reflections	7194 [R(int) = 0.1898]	
Completeness to theta = 25.00°	99.9 %	
Absorption correction	multi-scan	

Refinement method	Full-matrix least-squares on F^2
Data / restraints / parameters	7194 / 4 / 487
Goodness-of-fit on F^2	1.047
Final R indices [I>2sigma(I)]	R1 = 0.0872, wR2 = 0.1779
R indices (all data)	R1 = 0.1679, wR2 = 0.2040
Largest diff. peak and hole	1.380 and -1.878 e.$Å^{-3}$

Table D.2. Atomic coordinates (x 10^4) and equivalent isotropic displacement parameters ($Å^2$x 10^3) for rwm1027s. U(eq) is defined as one third of the trace of the orthogonalized U^{ij} tensor.

	x	y	z	U(eq)
Ir	5554(1)	3576(1)	8241(1)	47(1)
N(1)	6934(9)	3137(9)	8621(5)	45(3)
C(1)	7834(12)	3434(12)	8462(7)	54(4)
O(1)	2704(9)	840(12)	10336(6)	97(4)
O(2)	-107(9)	214(11)	9300(5)	89(4)
N(2)	1313(10)	516(11)	9810(6)	66(4)
C(2)	8716(15)	3140(15)	8724(9)	82(6)
N(3)	1233(10)	833(11)	8820(5)	63(4)
C(3)	8652(13)	2498(15)	9201(7)	75(5)
C(4)	7669(12)	2190(12)	9379(7)	60(4)
N(4)	4157(13)	4021(14)	7983(7)	97(5)
N(5)	6253(9)	4413(9)	7564(5)	48(3)
C(5)	6832(10)	2522(11)	9075(6)	46(4)
C(6)	5814(11)	2184(11)	9192(6)	45(4)
C(7)	5552(12)	1485(11)	9596(7)	57(4)
C(8)	4581(13)	1178(11)	9689(6)	57(4)
C(9)	3821(11)	1581(10)	9333(6)	44(4)
C(10)	4085(12)	2307(10)	8936(6)	51(4)
C(11)	5070(10)	2632(10)	8847(6)	42(4)
C(12)	2789(12)	1178(11)	9350(6)	53(4)
C(13)	2297(15)	861(16)	9857(7)	76(5)
C(14)	2213(12)	1106(11)	8870(7)	59(4)
C(15)	756(14)	476(13)	9309(8)	64(5)
C(16)	665(14)	853(18)	8271(8)	98(7)
C(17)	5385(13)	4808(12)	8798(6)	47(4)
C(18)	6008(19)	5124(14)	9212(9)	99(8)
C(19)	5880(30)	5933(19)	9571(11)	138(12)
C(20)	5010(30)	6400(30)	9524(13)	154(15)
C(21)	4320(30)	6170(20)	9102(13)	140(12)
C(22)	4520(20)	5321(15)	8726(10)	93(7)
C(23)	3823(16)	4950(15)	8293(8)	71(5)

C(24)	2930(20)	5360(30)	8128(13)	142(13)
C(25)	2320(20)	4890(30)	7731(15)	168(19)
C(26)	2596(16)	3990(30)	7469(11)	133(11)
C(27)	3509(13)	3568(18)	7589(8)	99(8)
C(28)	6505(11)	5375(12)	7583(7)	57(4)
C(29)	6997(13)	5834(14)	7162(8)	72(5)
C(30)	7235(12)	5301(15)	6687(8)	69(5)
C(31)	6951(12)	4283(14)	6638(7)	66(5)
C(32)	6481(11)	3841(11)	7112(6)	49(4)
C(33)	6193(11)	2768(12)	7136(6)	48(4)
C(34)	6383(12)	2082(16)	6699(6)	70(5)
C(35)	6058(15)	1067(15)	6740(9)	84(6)
C(36)	5546(13)	805(13)	7213(8)	67(5)
C(37)	5362(12)	1464(13)	7665(7)	64(4)
C(38)	5663(10)	2471(12)	7649(6)	47(4)
Cl(1)	4341(5)	9091(5)	8722(3)	122(2)
Cl(2)	5638(6)	7978(6)	8007(3)	155(3)
Cl(3)	3037(5)	3136(6)	5983(3)	136(2)
Cl(4)	4986(7)	2548(10)	5515(3)	226(5)
C(39)	5567(9)	8777(14)	8599(7)	107(8)
C(40)	4252(12)	2700(30)	6123(6)	195(17)
O(3)	8622(8)	6514(9)	10702(7)	106(5)
O(4)	8348(13)	4681(11)	10134(8)	156(8)

Table D.3. Bond lengths [Å] and angles [°] for rwm1027s.

Ir-C(11)	1.994(14)
Ir-C(38)	2.015(15)
Ir-N(4)	2.034(18)
Ir-C(17)	2.095(15)
Ir-N(1)	2.108(12)
Ir-N(5)	2.144(11)
N(1)-C(1)	1.315(17)
N(1)-C(5)	1.342(17)
C(1)-C(2)	1.37(2)
C(1)-H(1A)	0.9400
O(1)-C(13)	1.233(18)
O(2)-C(15)	1.199(18)
N(2)-C(15)	1.37(2)
N(2)-C(13)	1.39(2)
C(2)-C(3)	1.40(2)
C(2)-H(2A)	0.9400
N(3)-C(14)	1.356(19)
N(3)-C(15)	1.391(19)
N(3)-C(16)	1.48(2)
C(3)-C(4)	1.43(2)
C(3)-H(3A)	0.9400
C(4)-C(5)	1.38(2)
C(4)-H(4A)	0.9400
N(4)-C(27)	1.39(2)
N(4)-C(23)	1.49(2)
N(5)-C(28)	1.316(17)
N(5)-C(32)	1.334(17)
C(5)-C(6)	1.454(19)
C(6)-C(7)	1.366(19)
C(6)-C(11)	1.399(19)
C(7)-C(8)	1.37(2)
C(7)-H(7A)	0.9400
C(8)-C(9)	1.41(2)
C(8)-H(8A)	0.9400

C(9)-C(10)	1.380(18)
C(9)-C(12)	1.47(2)
C(10)-C(11)	1.395(19)
C(10)-H(10A)	0.9400
C(12)-C(14)	1.35(2)
C(12)-C(13)	1.42(2)
C(14)-H(14A)	0.9400
C(16)-H(16A)	0.9700
C(16)-H(16B)	0.9700
C(16)-H(16C)	0.9700
C(17)-C(18)	1.33(3)
C(17)-C(22)	1.35(3)
C(18)-C(19)	1.37(3)
C(18)-H(18A)	0.9400
C(19)-C(20)	1.31(4)
C(19)-H(19A)	0.9400
C(20)-C(21)	1.37(4)
C(20)-H(20A)	0.9400
C(21)-C(22)	1.45(3)
C(21)-H(21A)	0.9400
C(22)-C(23)	1.44(3)
C(23)-C(24)	1.36(3)
C(24)-C(25)	1.37(4)
C(24)-H(24A)	0.9400
C(25)-C(26)	1.39(4)
C(25)-H(25A)	0.9400
C(26)-C(27)	1.36(3)
C(26)-H(26A)	0.9400
C(27)-H(27A)	0.9800
C(27)-H(27B)	0.9800
C(28)-C(29)	1.33(2)
C(28)-H(28A)	0.9400
C(29)-C(30)	1.35(2)
C(29)-H(29A)	0.9400
C(30)-C(31)	1.40(2)
C(30)-H(30A)	0.9400

C(31)-C(32)	1.40(2)
C(31)-H(31A)	0.9400
C(32)-C(33)	1.47(2)
C(33)-C(34)	1.39(2)
C(33)-C(38)	1.445(18)
C(34)-C(35)	1.41(2)
C(34)-H(34A)	0.9400
C(35)-C(36)	1.35(2)
C(35)-H(35A)	0.9400
C(36)-C(37)	1.39(2)
C(36)-H(36A)	0.9400
C(37)-C(38)	1.39(2)
C(37)-H(37A)	0.9400
Cl(1)-C(39)	1.709(9)
Cl(2)-C(39)	1.740(9)
Cl(3)-C(40)	1.743(9)
Cl(4)-C(40)	1.738(9)
C(39)-H(39A)	0.9800
C(39)-H(39B)	0.9800
C(40)-H(40A)	0.9800
C(40)-H(40B)	0.9800

C(11)-Ir-C(38)	93.2(6)
C(11)-Ir-N(4)	95.1(6)
C(38)-Ir-N(4)	94.6(6)
C(11)-Ir-C(17)	90.8(5)
C(38)-Ir-C(17)	174.8(6)
N(4)-Ir-C(17)	81.6(7)
C(11)-Ir-N(1)	79.5(5)
C(38)-Ir-N(1)	91.0(5)
N(4)-Ir-N(1)	172.5(5)
C(17)-Ir-N(1)	93.1(6)
C(11)-Ir-N(5)	170.9(5)
C(38)-Ir-N(5)	80.6(5)
N(4)-Ir-N(5)	92.0(5)
C(17)-Ir-N(5)	95.9(5)

N(1)-Ir-N(5)	93.9(5)
C(1)-N(1)-C(5)	120.2(13)
C(1)-N(1)-Ir	126.2(11)
C(5)-N(1)-Ir	113.7(9)
N(1)-C(1)-C(2)	124.5(16)
N(1)-C(1)-H(1A)	117.8
C(2)-C(1)-H(1A)	117.8
C(15)-N(2)-C(13)	125.3(14)
C(1)-C(2)-C(3)	117.7(17)
C(1)-C(2)-H(2A)	121.2
C(3)-C(2)-H(2A)	121.2
C(14)-N(3)-C(15)	117.8(15)
C(14)-N(3)-C(16)	123.5(14)
C(15)-N(3)-C(16)	118.7(14)
C(2)-C(3)-C(4)	117.6(16)
C(2)-C(3)-H(3A)	121.2
C(4)-C(3)-H(3A)	121.2
C(5)-C(4)-C(3)	119.6(16)
C(5)-C(4)-H(4A)	120.2
C(3)-C(4)-H(4A)	120.2
C(27)-N(4)-C(23)	119.2(19)
C(27)-N(4)-Ir	129.0(16)
C(23)-N(4)-Ir	111.7(13)
C(28)-N(5)-C(32)	120.9(13)
C(28)-N(5)-Ir	126.0(11)
C(32)-N(5)-Ir	113.0(10)
N(1)-C(5)-C(4)	120.4(14)
N(1)-C(5)-C(6)	115.9(12)
C(4)-C(5)-C(6)	123.6(14)
C(7)-C(6)-C(11)	119.9(14)
C(7)-C(6)-C(5)	125.5(14)
C(11)-C(6)-C(5)	114.6(13)
C(6)-C(7)-C(8)	123.8(16)
C(6)-C(7)-H(7A)	118.1
C(8)-C(7)-H(7A)	118.1
C(7)-C(8)-C(9)	117.8(14)

C(7)-C(8)-H(8A)	121.1
C(9)-C(8)-H(8A)	121.1
C(10)-C(9)-C(8)	118.1(14)
C(10)-C(9)-C(12)	120.9(14)
C(8)-C(9)-C(12)	120.8(13)
C(9)-C(10)-C(11)	124.1(14)
C(9)-C(10)-H(10A)	118.0
C(11)-C(10)-H(10A)	118.0
C(10)-C(11)-C(6)	116.3(13)
C(10)-C(11)-Ir	127.5(11)
C(6)-C(11)-Ir	116.0(10)
C(14)-C(12)-C(13)	113.9(15)fina
C(14)-C(12)-C(9)	121.5(13)
C(13)-C(12)-C(9)	124.6(15)
O(1)-C(13)-N(2)	117.9(15)
O(1)-C(13)-C(12)	123.8(18)
N(2)-C(13)-C(12)	118.3(16)
C(12)-C(14)-N(3)	128.7(15)
C(12)-C(14)-H(14A)	115.7
N(3)-C(14)-H(14A)	115.7
O(2)-C(15)-N(2)	122.2(16)
O(2)-C(15)-N(3)	121.9(17)
N(2)-C(15)-N(3)	115.7(15)
N(3)-C(16)-H(16A)	109.5
N(3)-C(16)-H(16B)	109.5
H(16A)-C(16)-H(16B)	109.5
N(3)-C(16)-H(16C)	109.5
H(16A)-C(16)-H(16C)	109.5
H(16B)-C(16)-H(16C)	109.5
C(18)-C(17)-C(22)	117.2(19)
C(18)-C(17)-Ir	128.4(15)
C(22)-C(17)-Ir	114.4(14)
C(17)-C(18)-C(19)	127(3)
C(17)-C(18)-H(18A)	116.4
C(19)-C(18)-H(18A)	116.4
C(20)-C(19)-C(18)	116(3)

C(20)-C(19)-H(19A)	122.1
C(18)-C(19)-H(19A)	122.1
C(19)-C(20)-C(21)	122(3)
C(19)-C(20)-H(20A)	118.8
C(21)-C(20)-H(20A)	118.8
C(20)-C(21)-C(22)	119(3)
C(20)-C(21)-H(21A)	120.6
C(22)-C(21)-H(21A)	120.6
C(17)-C(22)-C(23)	117.0(17)
C(17)-C(22)-C(21)	118(3)
C(23)-C(22)-C(21)	125(3)
C(24)-C(23)-C(22)	128(2)
C(24)-C(23)-N(4)	117(2)
C(22)-C(23)-N(4)	115.2(17)
C(23)-C(24)-C(25)	121(3)
C(23)-C(24)-H(24A)	119.6
C(25)-C(24)-H(24A)	119.6
C(24)-C(25)-C(26)	122(3)
C(24)-C(25)-H(25A)	118.8
C(26)-C(25)-H(25A)	118.8
C(27)-C(26)-C(25)	120(3)
C(27)-C(26)-H(26A)	120.2
C(25)-C(26)-H(26A)	120.2
C(26)-C(27)-N(4)	121(3)
C(26)-C(27)-H(27A)	107.2
N(4)-C(27)-H(27A)	107.2
C(26)-C(27)-H(27B)	107.2
N(4)-C(27)-H(27B)	107.2
H(27A)-C(27)-H(27B)	106.8
N(5)-C(28)-C(29)	123.0(16)
N(5)-C(28)-H(28A)	118.5
C(29)-C(28)-H(28A)	118.5
C(28)-C(29)-C(30)	119.0(18)
C(28)-C(29)-H(29A)	120.5
C(30)-C(29)-H(29A)	120.5
C(29)-C(30)-C(31)	120.2(15)

C(29)-C(30)-H(30A)	119.9
C(31)-C(30)-H(30A)	119.9
C(32)-C(31)-C(30)	117.3(16)
C(32)-C(31)-H(31A)	121.4
C(30)-C(31)-H(31A)	121.4
N(5)-C(32)-C(31)	119.5(14)
N(5)-C(32)-C(33)	117.0(13)
C(31)-C(32)-C(33)	123.5(14)
C(34)-C(33)-C(38)	121.4(15)
C(34)-C(33)-C(32)	123.6(14)
C(38)-C(33)-C(32)	115.0(13)
C(33)-C(34)-C(35)	121.0(15)
C(33)-C(34)-H(34A)	119.5
C(35)-C(34)-H(34A)	119.5
C(36)-C(35)-C(34)	117.1(16)
C(36)-C(35)-H(35A)	121.4
C(34)-C(35)-H(35A)	121.4
C(35)-C(36)-C(37)	123.5(17)
C(35)-C(36)-H(36A)	118.3
C(37)-C(36)-H(36A)	118.3
C(36)-C(37)-C(38)	121.8(15)
C(36)-C(37)-H(37A)	119.1
C(38)-C(37)-H(37A)	119.1
C(37)-C(38)-C(33)	115.2(14)
C(37)-C(38)-Ir	130.8(11)
C(33)-C(38)-Ir	114.0(11)
Cl(1)-C(39)-Cl(2)	109.9(7)
Cl(1)-C(39)-H(39A)	109.7
Cl(2)-C(39)-H(39A)	109.7
Cl(1)-C(39)-H(39B)	109.7
Cl(2)-C(39)-H(39B)	109.7
H(39A)-C(39)-H(39B)	108.2
Cl(4)-C(40)-Cl(3)	114.4(9)
Cl(4)-C(40)-H(40A)	108.7
Cl(3)-C(40)-H(40A)	108.7
Cl(4)-C(40)-H(40B)	108.7

Cl(3)-C(40)-H(40B) 108.7

H(40A)-C(40)-H(40B) 107.6

Symmetry transformations used to generate equivalent atoms:

Table D.4. Anisotropic displacement parameters ($Å^2 x\ 10^3$) for rwm1027s. The anisotropic displacement factor exponent takes the form: $-2\pi^2[\ h^2\ a^{*2}U^{11} + ...\ + 2\ h\ k\ a^*\ b^*\ U^{12}\ ]$

	U^{11}	U^{22}	U^{33}	U^{23}	U^{13}	U^{12}
Ir	53(1)	46(1)	41(1)	0(1)	13(1)	-1(1)
N(1)	49(8)	47(7)	39(7)	-5(6)	8(6)	-3(6)
C(1)	47(9)	54(11)	63(10)	-5(9)	8(8)	-16(8)
O(1)	61(8)	165(14)	66(9)	21(9)	24(7)	-18(8)
O(2)	63(8)	133(12)	71(9)	28(8)	6(7)	-25(8)
N(2)	53(9)	90(11)	55(9)	12(8)	-1(7)	-20(8)
C(2)	81(15)	81(14)	83(15)	-14(12)	19(12)	-38(12)
N(3)	58(9)	79(10)	51(8)	4(8)	15(7)	-13(8)
C(3)	67(13)	101(16)	57(11)	-21(12)	-19(10)	6(11)
C(4)	61(11)	66(11)	53(10)	-6(9)	8(9)	-11(9)
N(4)	110(14)	122(15)	60(10)	23(10)	17(10)	-16(12)
N(5)	53(8)	41(8)	50(8)	0(7)	9(6)	-9(6)
C(5)	39(9)	54(10)	44(9)	-3(8)	-6(7)	-4(7)
C(6)	50(9)	46(9)	39(8)	-2(8)	10(7)	6(8)
C(7)	69(11)	43(9)	60(10)	5(9)	12(9)	-3(9)
C(8)	91(13)	45(10)	36(9)	5(7)	7(9)	-2(9)
C(9)	50(9)	38(9)	43(8)	1(7)	14(7)	-6(7)
C(10)	68(11)	40(9)	44(9)	7(8)	2(8)	1(8)
C(11)	37(8)	41(9)	47(9)	-19(7)	12(7)	-5(7)
C(12)	65(10)	56(11)	37(8)	14(8)	8(8)	0(8)
C(13)	81(14)	108(16)	38(10)	26(11)	-4(10)	-3(12)
C(14)	54(10)	65(12)	58(11)	0(9)	13(9)	-3(8)
C(15)	60(12)	68(12)	66(12)	14(10)	15(10)	-7(9)
C(16)	85(14)	140(19)	70(13)	13(14)	-13(11)	-30(14)
C(17)	74(11)	44(9)	22(8)	3(7)	5(8)	0(9)
C(18)	170(20)	58(13)	68(14)	-15(11)	50(15)	-10(14)
C(19)	220(30)	90(19)	100(20)	-55(16)	50(20)	10(20)
C(20)	230(40)	140(30)	90(20)	-40(20)	90(20)	10(30)
C(21)	210(30)	110(20)	100(20)	7(18)	80(20)	60(20)
C(22)	150(20)	59(13)	74(15)	-3(12)	57(15)	6(14)
C(23)	95(15)	71(13)	49(11)	11(10)	33(11)	39(12)

C(24)100(20)	200(30)	130(20)	60(20)	68(17)	90(20)
C(25)80(20)	290(50)	140(30)	80(30)	24(18)	100(30)
C(26)43(13)	260(40)	100(19)	30(20)	-1(12)	26(18)
C(27)51(11)	180(20)	65(12)	38(15)	-13(10)	-48(14)
C(28)56(10)	44(10)	71(12)	3(9)	8(9)	7(8)
C(29)79(13)	69(12)	67(12)	31(11)	16(11)	2(10)
C(30)61(11)	90(15)	57(11)	38(11)	19(9)	4(10)
C(31)75(12)	75(13)	48(10)	22(10)	5(9)	-15(10)
C(32)56(10)	51(10)	41(9)	6(8)	5(7)	18(7)
C(33)54(9)	66(11)	26(8)	10(8)	8(7)	13(8)
C(34)63(11)	127(18)	20(8)	-14(10)	22(7)	17(12)
C(35)94(15)	78(14)	82(15)	-39(12)	6(12)	-11(11)
C(36)81(13)	51(11)	69(12)	-9(10)	11(10)	8(9)
C(37)74(11)	51(10)	69(11)	1(10)	18(9)	-9(10)
C(38)34(8)	76(12)	32(8)	-5(8)	-1(7)	-5(8)
Cl(1)136(5)	128(5)	103(4)	-34(4)	-19(4)	37(4)
Cl(2)186(7)	111(5)	169(7)	-24(5)	78(6)	10(5)
Cl(3)133(6)	146(6)	129(6)	7(5)	-33(4)	-12(5)
Cl(4)176(8)	404(17)	96(6)	12(8)	9(5)	-24(10)
C(39)97(16)	130(20)	92(16)	25(15)	-9(13)	-14(14)
C(40)100(20)	350(50)	130(20)	130(30)	39(17)	60(20)
O(3)55(7)	64(8)	198(15)	-59(9)	30(8)	-4(6)
O(4)147(14)	105(12)	220(20)	-119(13)	-50(13)	21(10)

Table D.5. Hydrogen coordinates (x 10^4) and isotropic displacement parameters ($Å^2$x 10^3) for rwm1027s.

	x	y	z	U(eq)
H(1A)	7875	3878	8148	65
H(2A)	9342	3362	8588	98
H(3A)	9233	2276	9398	90
H(4A)	7595	1765	9699	72
H(7A)	6066	1198	9824	68
H(8A)	4430	714	9982	69
H(10A)	3570	2601	8712	61
H(14A)	2535	1266	8523	71
H(16A)	1088	1126	7971	148
H(16B)	73	1273	8312	148
H(16C)	462	171	8169	148
H(18A)	6604	4752	9263	118
H(19A)	6375	6140	9835	165
H(20A)	4853	6912	9790	185
H(21A)	3734	6562	9056	168
H(24A)	2728	5982	8287	170
H(25A)	1703	5179	7633	201
H(26A)	2152	3665	7210	160
H(27A)	3870	3514	7225	119
H(27B)	3389	2877	7723	119
H(28A)	6328	5754	7908	68
H(29A)	7176	6520	7195	86
H(30A)	7592	5613	6388	83
H(31A)	7072	3913	6300	79
H(34A)	6733	2295	6372	84
H(35A)	6194	596	6448	101
H(36A)	5300	140	7239	80
H(37A)	5025	1223	7990	77
H(39A)	5852	8438	8939	128
H(39B)	5960	9391	8529	128

H(40A)	4589	3175	6384	234
H(40B)	4208	2047	6322	234

BIBLIOGRAPHY

1. Copenhafer, J. E.; Walters, R. W.; Meyer, T. Y., Synthesis and Characterization of Repeating Sequence Copolymers of Fluorene and Methylene Monomers. *Macromolecules* **2008,** 41, (1), 31-35.

2. Di Lorenzo, M. L.; Pyda, M.; Wunderlich, B., Reversible melting in nanophase-separated poly (oligoamide-alt-oligoether)s and its dependence on sequence length, crystal perfection, and molecular mobility. *J. Polym. Sci., Part B: Polym. Phys.* **2001,** 39, (23), 2969-2981.

3. Versteegen, R. M.; Sijbesma, R. P.; Meijer, E. W., Synthesis and characterization of segmented copoly(ether urea)s with uniform hard segments. *Macromolecules* **2005,** 38, (8), 3176-3184.

4. Abhiraman, A. S.; Kim, Y. W.; Wagener, K. B., Evolution of structure and properties in fiber formation from a thermoplastic polyester-polyether segmented copolymer. *J. Polym. Sci., Part B: Polym. Phys.* **1987,** 25, (1), 205-28.

5. Seliger, H.; Bitar, M. B.; Nguyen, T. H.; Marx, A.; Roberts, R.; Krueger, J. K.; Unruh, H. G., Segmented block copolymer models of uniform chain length and defined structure, 1. Synthesis and characterization. *Makromol. Chem.* **1984,** 185, (7), 1335-60.

6. Chen, C.-C.; Chueh, J.-Y.; Tseng, H.; Huang, H.-M.; Lee, S.-Y., Preparation and characterization of biodegradable PLA polymeric blends. *Biomaterials* **2003,** 24, (7), 1167-1173.

7. Velankar, S.; Cooper, S. L., Microphase Separation and Rheological Properties of Polyurethane Melts. 1. Effect of Block Length. *Macromolecules* **1998,** 31, (26), 9181-9192.

8. Velankar, S.; Cooper, S. L., Microphase Separation and Rheological Properties of Polyurethane Melts. 2. Effect of Block Incompatibility on the Microstructure. *Macromolecules* **2000,** 33, (2), 382-394.

9. Velankar, S.; Cooper, S. L., Microphase Separation and Rheological Properties of Polyurethane Melts. 3. Effect of Block Incompatibility on the Viscoelastic Properties. *Macromolecules* **2000,** 33, (2), 395-403.

10. Antoun, S.; Lenz, R. W.; Jin, J. I., Liquid crystal polymers. IV. Thermotropic polyesters with flexible spacers in the main chain. *J. Polym. Sci., Part A: Polym. Chem.* **1981,** 19, (8), 1901-20.

11. Stayshich, R. M.; Meyer, T. Y., Preparation and microstructural analysis of poly(lactic-alt-glycolic acid). *J. Polym. Sci., Part A: Polym. Chem.* **2008,** 46, (14), 4704-4711.

12. Tetsuka, H.; Doi, Y.; Abe, H., Novel Periodic Copolymers Consisting of Ester and Amide Units with the Same Carbon Numbers: Effects of Comonomeric and Sequential Structures on Crystalline Structures and Physical Properties. *Macromolecules* **2006,** 39, (26), 9071-9079.

13. Abe, H.; Doi, Y., Novel biodegradable copolymers with a periodic sequence structure derived from succinate butane-1,4-diol, and butane-1,4-diamine. *Macromol. Rapid Commun.* **2004,** 25, (14), 1303-1308.

14. Wagener, K. B.; Valenti, D.; Watson, M., Precisely branched polyethylene and other very regular polymer structures via ADMET chemistry. *Polymer Preprints* **1998,** 39, (1), 719-720.

15. Smith, J. A.; Brzezinska, K. R.; Valenti, D. J.; Wagener, K. B., Precisely Controlled Methyl Branching in Polyethylene via Acyclic Diene Metathesis (ADMET) Polymerization. *Macromolecules* **2000,** 33, (10), 3781-3794.

16. Sworen, J. C.; Smith, J. A.; Berg, J. M.; Wagener, K. B., Modeling Branched Polyethylene: Copolymers Possessing Precisely Placed Ethyl Branches. *J. Am. Chem. Soc.* **2004,** 126, (36), 11238-11246.

17. Watson, M. D.; Wagener, K. B., Functionalized Polyethylene via Acyclic Diene Metathesis Polymerization: Effect of Precise Placement of Functional Groups. *Macromolecules* **2000,** 33, (24), 8963-8970.

18. Watson, M. D.; Wagener, K. B., Ethylene/Vinyl Acetate Copolymers via Acyclic Diene Metathesis Polymerization. Examining the Effect of \"Long\" Precise Ethylene Run Lengths. *Macromolecules* **2000,** 33, (15), 5411-5417.

19. Boz, E.; Wagener, K. B.; Ghosal, A.; Fu, R.; Alamo, R. G., Synthesis and Crystallization of Precision ADMET Polyolefins Containing Halogens. *Macromolecules* **2006,** 39, (13), 4437-4447.

20. Baughman, T. W.; Chan, C. D.; Winey, K. I.; Wagener, K. B., Synthesis and Morphology of Well-Defined Poly(ethylene-co-acrylic acid) Copolymers. *Macromolecules* **2007,** 40, (18), 6564-6571.

21. Sworen, J. C.; Smith, J. A.; Wagener, K. B.; Baugh, L. S.; Rucker, S. P., Modeling Random Methyl Branching in Ethylene/ Propylene Copolymers Using Metathesis Chemistry: Synthesis and Thermal Behavior. *J. Am. Chem. Soc.* **2003,** 125, (8), 2228-2240.

22. Wallace, J. U.; Chen, S. H., Fluorene-based conjugated oligomers for organic photonics and electronics. *Adv. Polym. Sci.* **2008,** 212, 145-186.

23. Forrest, S. R., The path to ubiquitous and low-cost organic electronic appliances on plastic. *Nature (London)* **2004,** 428, (6986), 911-918.

24. Friend, R. H.; Gymer, R. W.; Holmes, A. B.; Burroughes, J. H.; Marks, R. N.; Taliani, C.; Bradley, D. D. C.; Dos Santos, D. A.; Bredas, J. L.; Logdlund, M.; Salaneck, W. R., Electroluminescence in conjugated polymers. *Nature (London)* **1999,** 397, (6715), 121-128.

25. Shirota, Y., Organic materials for electronic and optoelectronic devices. *J. Mater. Chem.* **2000,** 10, (1), 1-25.

26. Shirota, Y., Photo- and electroactive amorphous molecular materials-molecular design, syntheses, reactions, properties, and applications. *J. Mater. Chem.* **2005,** 15, (1), 75-93.

27. Chiang, C. K.; Fincher, C. R., Jr.; Park, Y. W.; Heeger, A. J.; Shirakawa, H.; Louis, E. J.; Gau, S. C.; MacDiarmid, A. G., Electrical conductivity in doped polyacetylene. *Phys. Rev. Lett.* **1977,** 39, (17), 1098-101.

28. Groenendaal, L. B.; Jonas, F.; Freitag, D.; Pielartzik, H.; Reynolds, J. R., Poly(3,4-ethylenedioxythiophene) and its derivatives: past, present, and future. *Adv. Mater.* **2000,** 12, (7), 481-494.

29. MacDiarmid, A. G.; Epstein, A. J., Polyanilines: a novel class of conducting polymers. *Faraday Discuss. Chem. Soc.* **1989,** 88, 317-32.

30. Grazulevicius, J. V.; Strohriegl, P.; Pielichowski, J.; Pielichowski, K., Carbazole-containing polymers: synthesis, properties and applications. *Prog. Polym. Sci.* **2003,** 28, (9), 1297-1353.

31. Neher, D., Polyfluorene homopolymers: conjugated liquid-crystalline polymers for bright blue emission and polarized electroluminescence. *Macromol. Rapid Commun.* **2001,** 22, (17), 1365-1385.

32. Burroughes, J. H.; Bradley, D. D. C.; Brown, A. R.; Marks, R. N.; Mackay, K.; Friend, R. H.; Burns, P. L.; Holmes, A. B., Light-emitting diodes based on conjugated polymers. *Nature (London)* **1990,** 347, (6293), 539-41.

33. So, F.; Krummacher, B.; Mathai, M. K.; Poplavskyy, D.; Choulis, S. A.; Choong, V.-E., Recent progress in solution processable organic light emitting devices. *J. Appl. Phys.* **2007,** 102, (9), 091101/1-091101/21.

34. Liu, J.; Chen, L.; Shao, S.; Xie, Z.; Cheng, Y.; Geng, Y.; Wang, L.; Jing, X.; Wang, F., Highly efficient red electroluminescent polymers with dopant/host system and molecular dispersion feature: polyfluorene as the host and 2,1,3-benzothiadiazole derivatives as the red dopant. *J. Mater. Chem.* **2008,** 18, (3), 319-327.

35. Ma, W.; Iyer, P. K.; Gong, X.; Liu, B.; Moses, D.; Bazan, G. C.; Heeger, A. J., Water/methanol-soluble conjugated copolymer as an electron-transport layer in polymer light-emitting diodes. *Adv. Mater.* **2005,** 17, (3), 274-277.

36. Charas, A.; Morgado, J.; Alcacer, L.; Brogueira, P.; Cacialli, F., Synthesis and luminescence properties of a new polyfluorene copolymer with regulated solubility. *Synth. Met.* **2004,** 147, (1-3), 275-279.

37. Charas, A.; Morgado, J.; Martinho, J. M. G.; Alcacer, L.; Lim, S. F.; Friend, R. H.; Cacialli, F., Synthesis and luminescence properties of three novel polyfluorene copolymers. *Polymer* **2003,** 44, (6), 1843-1850.

38. Charas, A.; Morgado, J.; Martinho, J. M. G.; Fedorov, A.; Alcacer, L.; Cacialli, F., Excitation energy transfer and spatial exciton confinement in polyfluorene blends for application in light-emitting diodes. *J. Mater. Chem.* **2002,** 12, (12), 3523-3527.

39. Morgado, J.; Friend, R. H.; Cacialli, F., Improved efficiency of light-emitting diodes based on polyfluorene blends upon insertion of a poly(p-phenylene vinylene) electron confinement layer. *Appl. Phys. Lett.* **2002,** 80, (14), 2436-2438.

40. Craig, M. R.; de Kok, M. M.; Hofstraat, J. W.; Schenning, A. P. H. J.; Meijer, E. W., Improving color purity and stability in a blue emitting polyfluorene by monomer purification. *J. Mater. Chem.* **2003,** 13, (12), 2861-2862.

41. McFarlane, S. L.; Coumont, L. S.; Piercey, D. G.; McDonald, R.; Veinot, J. G. C., "One-Pot" Synthesis of a Thermally Stable Blue Emitter: Poly[spiro(fluorene-9,9'-(2'-phenoxy-xanthene)]. *Macromolecules* **2008,** 41, (21), 7780-7782.

42. He, B.; Li, J.; Bo, Z.; Huang, Y., Studies of green emission in polyfluorenes using a model polymer. *Polym. J.* **2007,** 39, (12), 1345-1350.

43. Wu, Y.-S.; Li, J.; Ai, X.-C.; Fu, L.-M.; Zhang, J.-P.; Fu, Y.-Q.; Zhou, J.-J.; Li, L.; Bo, Z.-S., Interplay between the Keto Defect and the Interchain Interaction on the Green Emission of Fluorene-Based Polymer. *J. Phys. Chem.* **2007,** 111, (45), 11473-11479.

44. Cho, S. Y.; Grimsdale, A. C.; Jones, D. J.; Watkins, S. E.; Holmes, A. B., Polyfluorenes without Monoalkylfluorene Defects. *J. Am. Chem. Soc.* **2007,** 129, (39), 11910-11911.

45. Grisorio, R.; Suranna, G. P.; Mastrorilli, P.; Nobile, C. F., Insight into the role of oxidation in the thermally induced green band in fluorene-based systems. *Adv. Funct. Mater.* **2007,** 17, (4), 538-548.

46. Liu, L.; Tang, S.; Liu, M.; Xie, Z.; Zhang, W.; Lu, P.; Hanif, M.; Ma, Y., Photodegradation of Polyfluorene and Fluorene Oligomers with Alkyl and Aromatic Disubstitutions. *J. Phys. Chem. B* **2006,** 110, (28), 13734-13740.

47. Chan, K. L.; McKiernan, M. J.; Towns, C. R.; Holmes, A. B., Enhanced color stability from poly(2,7-dibenzosilole). *Proc. SPIE-Int. Soc. Opt. Eng.* **2005,** 5937, 59372A/1-59372A/8.

48. Kulkarni, A. P.; Zhu, Y.; Jenekhe, S. A., Quinoxaline-Containing Polyfluorenes: Synthesis, Photophysics, and Stable Blue Electroluminescence. *Macromolecules* **2005,** 38, (5), 1553-1563.

49. Grell, M.; Bradley, D. D. C.; Inbasekaran, M.; Woo, E. P., A glass-forming conjugated main-chain liquid crystal polymer for polarized electroluminescence applications. *Adv. Mater.* **1997,** 9, (10), 798-802.

50. Klaerner, G.; Miller, R. D., Polyfluorene Derivatives: Effective Conjugation Lengths from Well-Defined Oligomers. *Macromolecules* **1998,** 31, (6), 2007-2009.

51. Lee, S. H.; Tsutsui, T., Molecular design of fluorene-based polymers and oligomers for organic light-emitting diodes. *Thin Solid Films* **2000,** 363, (1,2), 76-80.

52. Anemian, R.; Mulatier, J.-C.; Andraud, C.; Stephan, O.; Vial, J.-C., Monodisperse fluorene oligomers exhibiting strong dipolar coupling interactions. *Chem. Commun.* **2002**, (15), 1608-1609.

53. Geng, Y.; Trajkovska, A.; Katsis, D.; Ou, J. J.; Culligan, S. W.; Chen, S. H., Synthesis, Characterization, and Optical Properties of Monodisperse Chiral Oligofluorenes. *J. Am. Chem. Soc.* **2002,** 124, (28), 8337-8347.

54. Jo, J.; Chi, C.; Hoeger, S.; Wegner, G.; Yoon, D. Y., Synthesis and characterization of monodisperse oligofluorenes. *Chem.--Eur. J.* **2004,** 10, (11), 2681-2688.

55. Tirapattur, S.; Belletete, M.; Drolet, N.; Leclerc, M.; Durocher, G., Spectral and Photophysical Properties of Fluorene-Based Polyesters in Solution and in the Solid State. *Macromolecules* **2002,** 35, (23), 8889-8895.

56. Chochos, C. L.; Papakonstandopoulou, D.; Economopoulos, S. P.; Gregoriou, V. G.; Kallitsis, J. K., Synthesis and optical properties on a series of polyethers incorporating terfluorene segments and methylene spacers. *J. Macromol. Sci., Part A: Pure Appl. Chem.* **2006,** 43, (3), 419-431.

57. MacDonald, W. A., Thermotropic main chain liquid crystal polymers. *Liq. Cryst. Polym.* **1992**, 407-46.

58. Pavel, D.; Hibbs, D.; Shanks, R., Review of main chain liquid crystalline polymers. *Adv. Res. Polym. Sci.* **2006**, 65-84.

59. Hensel, V.; Schluter, A. D., A cyclotetraicosaphenylene. *Chem. --Eur. J.* **1999,** 5, (2), 421-429.

60. Liess, P.; Hensel, V.; Schlueter, A. D., Oligophenylene rods. A repetitive approach. *Liebigs Ann.* **1996**, (7), 1037-1040.

61. Miyaura, N.; Suzuki, A., Palladium-Catalyzed Cross-Coupling Reactions of Organoboron Compounds. *Chem. Rev.* **1995,** 95, (7), 2457-83.

62. Chung, T. C., Synthesis of polyalcohols via Ziegler-Natta polymerization. *Macromolecules* **1988,** 21, (4), 865-9.

63. Tindall, D.; Wagener, K. B., Acyclic Diene Metathesis (ADMET) Segmented Copolymers. *Macromolecules* **2004,** 37, (9), 3328-3336.

64. Schwendeman, J. E.; Church, A. C.; Wagener, K. B., Synthesis and catalyst issues associated with ADMET polymerization. *Adv. Synth. Catal.* **2002,** 344, (6+7), 597-613.

65. Watson, M. D.; Wagener, K. B., Ethylene/Vinyl Acetate Copolymers via Acyclic Diene Metathesis Polymerization. Examining the Effect of "Long" Precise Ethylene Run Lengths. *Macromolecules* **2000,** 33, (15), 5411-5417.

66. Watson, M. D.; Wagener, K. B., Tandem Homogeneous Metathesis/Heterogeneous Hydrogenation: Preparing Model Ethylene/CO2 and Ethylene/CO Copolymers. *Macromolecules* **2000,** 33, (9), 3196-3201.

67. Nguyen, T. P., Defects in organic electronic devices. *Phys. Status Solidi A* **2008,** 205, (1), 162-166.

68. Price, D. W.; Tour, J. M., Biphenyl- and fluorenyl-based potential molecular electronic devices. *Tetrahedron* **2003,** 59, (17), 3131-3156.

69. Weber, S. K.; Galbrecht, F.; Scherf, U., Preferential Oxidative Addition in Suzuki Cross-Coupling Reactions Across One Fluorene Unit. *Org. Lett.* **2006,** 8, (18), 4039-4041.

70. Walba, D. M.; Yang, H.; Shoemaker, R. K.; Keller, P.; Shao, R.; Coleman, D. A.; Jones, C. D.; Nakata, M.; Clark, N. A., Main-Chain Chiral Smectic Polymers Showing a Large Electroclinic Effect in the SmA Phase. *Chem. Mater.* **2006,** 18, (19), 4576-4584.

71. Jo, J.; Chi, C.; Hoeger, S.; Wegner, G.; Yoon, D. Y., Synthesis and characterization of monodisperse oligofluorenes. *Chem. --Eur. J.* **2004,** 10, (11), 2681-2688.

72. Fukuda, M.; Sawada, K.; Yoshino, K., Synthesis of fusible and soluble conducting polyfluorene derivatives and their characteristics. *J. Polym. Sci., Part A: Polym. Chem.* **1993,** 31, (10), 2465-71.

73. Tanto, B.; Guha, S.; Martin, C. M.; Scherf, U.; Winokur, M. J., Structural and Spectroscopic Investigations of Bulk Poly[bis(2-ethylhexyl)fluorene]. *Macromolecules* **2004,** 37, (25), 9438-9448.

74. Teetsov, J.; Fox, M. A., Photophysical characterization of dilute solutions and ordered thin films of alkyl-substituted polyfluorenes. *J. Mater. Chem.* **1999,** 9, (9), 2117-2122.

75. Banach, M. J.; Friend, R. H.; Sirringhaus, H., Influence of the Molecular Weight on the Thermotropic Alignment of Thin Liquid Crystalline Polyfluorene Copolymer Films. *Macromolecules* **2003,** 36, (8), 2838-2844.

76. Banach, M. J.; Friend, R. H.; Sirringhaus, H., Influence of the Casting Solvent on the Thermotropic Alignment of Thin Liquid Crystalline Polyfluorene Copolymer Films. *Macromolecules* **2004,** 37, (16), 6079-6085.

77. Somma, E.; Chi, C.; Loppinet, B.; Grinshtein, J.; Graf, R.; Fytas, G.; Spiess, H. W.; Wegner, G., Orientation dynamics in isotropic phases of model oligofluorenes: glass or liquid crystal. *J. Chem. Phys.* **2006,** 124, (20), 204910.

78. Scherf, U.; List, E. J. W., Semiconducting polyfluorenes - towards reliable structure-property relationships. *Adv. Mater.* **2002,** 14, (7), 477-487.

79. Chen, S. H.; Su, A. C.; Chen, S. A., Noncrystalline Phases in Poly(9,9-di-n-octyl-2,7-fluorene). *J. Phys. Chem. B* **2005,** 109, (20), 10067-10072.

80. Knaapila, M.; Stepanyan, R.; Lyons, B. P.; Torkkeli, M.; Monkman, A. P., Towards general guidelines for aligned, nanoscale assemblies of hairy-rod polyfluorene. *Adv. Funct. Mater.* **2006,** 16, (5), 599-609.

81. Knaapila, M.; Stepanyan, R.; Lyons, B. P.; Torkkeli, M.; Hase, T. P. A.; Serimaa, R.; Guentner, R.; Seeck, O. H.; Scherf, U.; Monkman, A. P., The Influence of the Molecular Weight on the Thermotropic Alignment and Self-Organized Structure Formation of Branched Side Chain Hairy-Rod Polyfluorene in Thin Films. *Macromolecules* **2005,** 38, (7), 2744-2753.

82. Knaapila, M.; Dias, F. B.; Garamus, V. M.; Almasy, L.; Torkkeli, M.; Leppaenen, K.; Galbrecht, F.; Preis, E.; Burrows, H. D.; Scherf, U.; Monkman, A. P., Influence of Side Chain Length on the Self-Assembly of Hairy-Rod Poly(9,9-dialkylfluorene)s in the Poor Solvent Methylcyclohexane. *Macromolecules* **2007,** 40, (26), 9398-9405.

83. Knaapila, M.; Garamus, V. M.; Dias, F. B.; Almasy, L.; Galbrecht, F.; Charas, A.; Morgado, J.; Burrows, H. D.; Scherf, U.; Monkman, A. P., Influence of Solvent Quality on the Self-Organization of Archetypical Hairy Rods-Branched and Linear Side Chain Polyfluorenes: Rodlike Chains versus "Beta-Sheets" in Solution. *Macromolecules* **2006,** 39, (19), 6505-6512.

84. Ranger, M.; Rondeau, D.; Leclerc, M., New Well-Defined Poly(2,7-fluorene) Derivatives: Photoluminescence and Base Doping. *Macromolecules* **1997,** 30, (25), 7686-7691.

85. Thiem, H.; Jandke, M.; Hanft, D.; Strohriegl, P., Synthesis and orientation of fluorene containing reactive mesogens. *Macromol. Chem. Phys.* **2006,** 207, (4), 370-381.

86. Galli, G.; Demel, S.; Slugovc, C.; Stelzer, F.; Weissflog, W.; Diele, S.; Fodor-Csorba, K., Novel liquid crystal ADMET polymers with banana main-chain mesogens. *Molecular Crystals and Liquid Crystals* **2005,** 439, 1909-1919.

87. EPA, Mercury Update: Impact of Fish Advisories. . *EPA Fact Sheet EPA 823-F-01-011* **2001**.

88. Boening, D. W., Ecological effects, transport, and fate of mercury: a general review. *Chemosphere* **2000,** 40, (12), 1335-1351.

89. Clarkson, T. W.; Magos, L.; Myers, G. J., The toxicology of mercury - current exposures and clinical manifestations. *N. Engl. J. Med.* **2003,** 349, (18), 1731-1737.

90. Yu, C.-J.; Tseng, W.-L., Colorimetric Detection of Mercury(II) in a High-Salinity Solution Using Gold Nanoparticles Capped with 3-Mercaptopropionate Acid and Adenosine Monophosphate. *Langmuir* **2008,** 24, (21), 12717-12722.

91. Shunmugam, R.; Gabriel, G. J.; Smith, C. E.; Aamer, K. A.; Tew, G. N., A highly selective colorimetric aqueous sensor for mercury. *Chem. --Eur. J.* **2008,** 14, (13), 3904-3907.

92. Hirayama, T.; Taki, M.; Kashiwagi, Y.; Nakamoto, M.; Kunishita, A.; Itoh, S.; Yamamoto, Y., Colorimetric response to mercury-induced abstraction of triethylene glycol ligands from a gold nanoparticle surface. *Dalton Trans.* **2008**, (35), 4705-4707.

93. Lee, J.-S.; Han, M. S.; Mirkin, C. A., Colorimetric detection of mercuric ion (Hg2+) in aqueous media using DNA-functionalized gold nanoparticles. *Agnew. Chem., Int. Ed.* **2007,** 46, (22), 4093-4096.

94. Huang, C.-C.; Chang, H.-T., Parameters for selective colorimetric sensing of mercury(II) in aqueous solutions using mercaptopropionic acid-modified gold nanoparticles. *Chem. Commun.* **2007**, (12), 1215-1217.

95. Che, Y.; Yang, X.; Zang, L., Ultraselective fluorescent sensing of Hg2+ through metal coordination-induced molecular aggregation. *Chem. Commun.* **2008**, (12), 1413-1415.

96. Yoon, S.; Miller, E. W.; He, Q.; Do, P. H.; Chang, C. J., A bright and specific fluorescent sensor for mercury in water, cells, and tissue. *Agnew. Chem., Int. Ed.* **2007,** 46, (35), 6658-6661.

97. Wang, H.; Chan, W.-H., Cholic acid-based fluorescent sensor for mercuric and methyl mercuric ion in aqueous solutions. *Tetrahedron* **2007,** 63, (36), 8825-8830.

98. Praveen, L.; Ganga, V. B.; Thirumalai, R.; Sreeja, T.; Reddy, M. L. P.; Varma, R. L., A New Hg2+-Selective Fluorescent Sensor Based on a 1,3-Alternate Thiacalix[4]arene Anchored with Four 8-Quinolinoloxy Groups. *Inorg. Chem.* **2007,** 46, (16), 6277-6282.

99. Nolan, E. M.; Lippard, S. J., Turn-On and Ratiometric Mercury Sensing in Water with a Red-Emitting Probe. *J. Am. Chem. Soc.* **2007,** 129, (18), 5910-5918.

100. Lee, M. H.; Wu, J.-S.; Lee, J. W.; Jung, J. H.; Kim, J. S., Highly Sensitive and Selective Chemosensor for Hg2+ Based on the Rhodamine Fluorophore. *Org. Lett.* **2007,** 9, (13), 2501-2504.

101. Huang, C.-c.; Yang, Z.; Lee, K.-H.; Chang, H.-T., Synthesis of highly fluorescent gold nanoparticles for sensing mercury(II). *Agnew. Chem., Int. Ed.* **2007,** 46, (36), 6824-6828.

102. Feng, L.; Chen, Z., Screening mercury(II) with selective fluorescent chemosensor. *Sensors and Actuators B* **2007,** B122, (2), 600-604.

103. Chen, J.; Zheng, A.; Chen, A.; Gao, Y.; He, C.; Kai, X.; Wu, G.; Chen, Y., A functionalized gold nanoparticles and Rhodamine 6G based fluorescent sensor for high sensitive and selective detection of mercury(II) in environmental water samples. *Anal. Chem. Acta* **2007,** 599, (1), 134-142.

104. Zhao, Y.; Lin, Z.; He, C.; Wu, H.; Duan, C., A \"Turn-On\" Fluorescent Sensor for Selective Hg(II) Detection in Aqueous Media Based on Metal-Induced Dye Formation. *Inorg. Chem.* **2006,** 45, (25), 10013-10015.

105. Tang, Y.; He, F.; Yu, M.; Feng, F.; An, L.; Sun, H.; Wang, S.; Li, Y.; Zhu, D., A reversible and highly selective fluorescent sensor for mercury(II) using poly(thiophene)s that contain thymine moieties. *Macromol. Rapid Commun.* **2006,** 27, (6), 389-392.

106. Nolan, E. M.; Lippard, S. J., A "Turn-On" Fluorescent Sensor for the Selective Detection of Mercuric Ion in Aqueous Media. *J. Am. Chem. Soc.* **2003,** 125, (47), 14270-14271.

107. Yuan, M.; Li, Y.; Li, J.; Li, C.; Liu, X.; Lv, J.; Xu, J.; Liu, H.; Wang, S.; Zhu, D., A Colorimetric and Fluorometric Dual-Model Assay for Mercury Ion by a Molecule. *Org. Lett.* **2007,** 9, (12), 2313-2316.

108. Nazeeruddin, M. K.; Di Censo, D.; Humphry-Baker, R.; Gratzel, M., Highly selective and reversible optical, colorimetric, and electrochemical detection of mercury(II) by amphiphilic ruthenium complexes anchored onto mesoporous oxide films. *Adv. Funct. Mater.* **2006,** 16, (2), 189-194.

109. Zhao, Q.; Cao, T.; Li, F.; Li, X.; Jing, H.; Yi, T.; Huang, C., A Highly Selective and Multisignaling Optical-Electrochemical Sensor for Hg2+ Based on a Phosphorescent Iridium(III) Complex. *Organometallics* **2007,** 26, (8), 2077-2081.

110. Zhao, Q.; Liu, S.; Li, F.; Yi, T.; Huang, C., Multisignaling detection of Hg2+ based on a phosphorescent iridium(III) complex. *Dalton Trans.* **2008**, (29), 3836-3840.

111. Nolan, E. M.; Lippard, S. J., Tools and Tactics for the Optical Detection of Mercuric Ion. *Chem. Rev.* **2008,** 108, (9), 3443-3480.

112. Coronado, E.; Galan-Mascaros, J. R.; Marti-Gastaldo, C.; Palomares, E.; Durrant, J. R.; Vilar, R.; Gratzel, M.; Nazeeruddin, M. K., Reversible Colorimetric Probes for Mercury Sensing. *J. Am. Chem. Soc.* **2005,** 127, (35), 12351-12356.

113. Palomares, E.; Vilar, R.; Durrant, J. R., Heterogeneous colorimetric sensor for mercuric salts. *Chem. Commun.* **2004**, (4), 362-363.

114. Baldo, M. A.; O'Brien, D. F.; You, Y.; Shoustikov, A.; Sibley, S.; Thompson, M. E.; Forrest, S. R., Highly efficient phosphorescent emission from organic electroluminescent devices. *Nature* **1998,** 395, (6698), 151-154.

115. Lamansky, S.; Djurovich, P.; Murphy, D.; Abdel-Razzaq, F.; Kwong, R.; Tsyba, I.; Bortz, M.; Mui, B.; Bau, R.; Thompson, M. E., Synthesis and Characterization of Phosphorescent Cyclometalated Iridium Complexes. *Inorg. Chem.* **2001,** 40, (7), 1704-1711.

116. Lamansky, S.; Djurovich, P.; Murphy, D.; Abdel-Razzaq, F.; Lee, H.-E.; Adachi, C.; Burrows, P. E.; Forrest, S. R.; Thompson, M. E., Highly Phosphorescent Bis-Cyclometalated Iridium Complexes: Synthesis, Photophysical Characterization, and Use in Organic Light Emitting Diodes. *J. Am. Chem. Soc.* **2001,** 123, (18), 4304-4312.

117. You, Y.; Park, S. Y., Phosphorescent iridium(iii) complexes: toward high phosphorescence quantum efficiency through ligand control. *Dalton Trans.* **2009**, (8), 1267-1282.

118. Williams, J. A. G.; Wilkinson, A. J.; Whittle, V. L., Light-emitting iridium complexes with tridentate ligands. *Dalton Trans.* **2008**, (16), 2081-2099.

119. Flamigni, L.; Barbieri, A.; Sabatini, C.; Ventura, B.; Barigelletti, F., Photochemistry and photophysics of coordination compounds: iridium. *Top. Curr. Chem.* **2007,** 281, (Photochemistry and Photophysics of Coordination Compounds II), 143-203.

120. You, Y.; Park, S. Y., A phosphorescent Ir(III) complex for selective fluoride ion sensing with a high signal-to-noise ratio. *Adv. Mater.* **2008,** 20, (20), 3820-3826.

121. DeRosa, M. C.; Hodgson, D. J.; Enright, G. D.; Dawson, B.; Evans, C. E. B.; Crutchley, R. J., Iridium Luminophore Complexes for Unimolecular Oxygen Sensors. *J. Am. Chem. Soc.* **2004,** 126, (24), 7619-7626.

122. DeRosa, M. C.; Mosher, P. J.; Evans, C. E. B.; Crutchley, R. J., Iridium(III) complexes as polymer bound oxygen sensors. *Macromol. Symp.* **2003,** 196, 235-248.

123. DeRosa, M. C.; Mosher, P. J.; Yap, G. P. A.; Focsaneanu, K. S.; Crutchley, R. J.; Evans, C. E. B., Synthesis, Characterization, and Evaluation of [Ir(ppy)2(vpy)Cl] as a Polymer-Bound Oxygen Sensor. *Inorg. Chem.* **2003,** 42, (16), 4864-4872.

124. Zhao, Q.; Li, F.; Liu, S.; Yu, M.; Liu, Z.; Yi, T.; Huang, C., Highly Selective Phosphorescent Chemosensor for Fluoride Based on an Iridium(III) Complex Containing Arylborane Units. *Inorg. Chem.* **2008,** 47, (20), 9256-9264.

125. Ho, M.-L.; Hwang, F.-M.; Chen, P.-N.; Hu, Y.-H.; Cheng, Y.-M.; Chen, K.-S.; Lee, G.-H.; Chi, Y.; Chou, P.-T., Design and synthesis of iridium(III) azacrown complex: application as a highly sensitive metal cation phosphorescence sensor. *Organic & Biomolecular Chemistry* **2006,** 4, (1), 98-103.

126. Chen, H.; Zhao, Q.; Wu, Y.; Li, F.; Yang, H.; Yi, T.; Huang, C., Selective phosphorescence chemosensor for homocysteine based on an iridium(III) complex. *Inorg. Chem.* **2007,** 46, (26), 11075-11081.

127. Ren, X.; Xu, Q.-H., Highly Sensitive and Selective Detection of Mercury Ions by Using Oligonucleotides, DNA Intercalators, and Conjugated Polymers. *Langmuir* **2009,** 25, (1), 29-31.

128. Liu, B., Highly sensitive oligonucleotide-based fluorometric detection of mercury(II) in aqueous media. *Biosens. Bioelectron.* **2008,** 24, (4), 756-760.

129. Chiang, C.-K.; Huang, C.-C.; Liu, C.-W.; Chang, H.-T., Oligonucleotide-Based Fluorescence Probe for Sensitive and Selective Detection of Mercury(II) in Aqueous Solution. *Anal. Chem.* **2008,** 80, (10), 3716-3721.

130. Xue, X.; Wang, F.; Liu, X., One-Step, Room Temperature, Colorimetric Detection of Mercury (Hg2+) Using DNA/Nanoparticle Conjugates. *J. Am. Chem. Soc.* **2008,** 130, (11), 3244-3245.

131. Liu, X.; Tang, Y.; Wang, L.; Zhang, J.; Song, S.; Fan, C.; Wang, S., Optical detection of mercury(II) in aqueous solutions by using conjugated polymers and label-free oligonucleotides. *Adv. Mater.* **2007,** 19, (11), 1471-1474.

132. Kosturko, L. D.; Folzer, C.; Stewart, R. F., The crystal and molecular structure of a 2:1 complex of 1-methylthymine-mercury (II). *Biochemistry* **1974,** 13, (19), 3949-52.

133. Park, G. Y.; Kim, Y.; Ha, Y., Iridium complexes containing three different ligands as white OLED dopants. *Mol. Cryst. Liq. Cryst.* **2007,** 462, 179-188.

134. Lee, Y. H.; Park, G. Y.; Kim, Y. S., White light emission using heteroleptic tris-cyclometalated iridium (III) complexes. *J. Korean Phys. Soc. FIELD Full Journal Title:Journal of the Korean Physical Society* **2007,** 50, (6), 1722-1728.

135. Park, Y. H.; Kim, Y. S., Heteroleptic tris-cyclometalated iridium(III) complexes with phenylpridine and diphenylquinoline derivative ligands. *Thin Solid Films FIELD Full Journal Title:Thin Solid Films* **2007,** 515, (12), 5084-5089.

136. Rho, H. H.; Park, G. Y.; Ha, Y.; Kim, Y. S., Synthesis and photophysical studies of iridium complexes having different ligands. *Jpn. J. Appl. Phys., Part 1* **2006,** 45, (1B), 568-573.

137. Holland, L.; Shen, W.-Z.; Micklitz, W.; Lippert, B., Tetrakis- and Tris(1-Methyluracil) Complexes of PtII: Formation and Properties of a Carbon-Bonded Nucleobase Species as Well as of Heteronuclear Derivatives. *Inorg. Chem.* **2007,** 46, (26), 11356-11365.

138. Ruiz, J.; Villa, M. D.; Rodriguez, V.; Cutillas, N.; Vicente, C.; Lopez, G.; Bautista, D., A Novel Metal-Binding Mode of Thymine Nucleobases: N(3) and O(4) Chelation. *Inorg. Chem.* **2007,** 46, (14), 5448-5449.

139. Rottlaender, M.; Knochel, P., Palladium-Catalyzed Cross-Coupling Reactions with Aryl Nonaflates: A Practical Alternative to Aryl Triflates. *J. Org. Chem.* **1998,** 63, (1), 203-208.

140. Prasad, A. S. B.; Stevenson, T. M.; Citineni, J. R.; Nyzam, V.; Knochel, P., Preparation and reactions of new zincated nitrogen-containing heterocycles. *Tetrahedron* **1997,** 53, (21), 7237-7254.

141. Tsuji, T.; Kataoka, T.; Yoshioka, M.; Sendo, Y.; Nishitani, Y.; Hirai, S.; Maeda, T.; Nagata, W., Synthetic studies on beta -lactam antibiotics. VII. Mild removal of the benzyl ester protecting group with aluminum trichloride. *Tetrahedron Lett.* **1979**, (30), 2793-6.

142. Hsu, R.-T.; Cheng, L.-M.; Chang, N.-C.; Tai, H.-M., Regioselective Reduction of 3-Sulfonyl Glutarimides to 3,4-Dihydro-5-sulfonylpyridin-2-ones. Formal Synthesis of the Indolizidine 8a-epi-Dendroprimine. *J. Org. Chem.* **2002,** 67, (14), 5044-5047.

143. Tamayo, A. B.; Alleyne, B. D.; Djurovich, P. I.; Lamansky, S.; Tsyba, I.; Ho, N. N.; Bau, R.; Thompson, M. E., Synthesis and Characterization of Facial and Meridional Tris-cyclometalated Iridium(III) Complexes. *J. Am. Chem. Soc.* **2003,** 125, (24), 7377-7387.

144. Breu, J.; Stoessel, P.; Schrader, S.; Starukhin, A.; Finkenzeller, W. J.; Yersin, H., Crystal Structure of fac-Ir(ppy)3 and Emission Properties under Ambient Conditions and at High Pressure. *Chem. Mater.* **2005,** 17, (7), 1745-1752.

145. Mao, C.-H.; Hong, J.-L.; Yeh, A.-C., Influence of aggregation on the phosphorescence of iridium complex in poly(methyl methacrylate) matrix. *J. Polym. Sci., Part B: Polym. Phys.* **2008,** 46, (6), 631-639.

146. Kalinowski, J.; Mezyk, J.; Meinardi, F.; Tubino, R.; Cocchi, M.; Virgili, D., Phosphorescence response to excitonic interactions in Ir organic complex-based electrophosphorescent emitters. *J. Appl. Phys.* **2005,** 98, (6), 063532/1-063532/9.

147. Namdas, E. B.; Ruseckas, A.; Samuel, I. D. W.; Lo, S.-C.; Burn, P. L., Photophysics of Fac-Tris(2-Phenylpyridine) Iridium(III) Cored Electroluminescent Dendrimers in Solution and Films. *J. Phys. Chem. B* **2004,** 108, (5), 1570-1577.

148. Xie, H. Z.; Liu, M. W.; Wang, O. Y.; Zhang, X. H.; Lee, C. S.; Hung, L. S.; Lee, S. T.; Teng, P. F.; Kwong, H. L.; Zheng, H.; Che, C. M., Reduction of self-quenching effect in organic electrophorescence emitting devices via the use of sterically hindered spacers in phosphorescence molecules. *Adv. Mater.* **2001,** 13, (16), 1245-1248.

149. Kawamura, Y.; Brooks, J.; Brown, J. J.; Sasabe, H.; Adachi, C., Intermolecular Interaction and a Concentration-Quenching Mechanism of Phosphorescent Ir(III) Complexes in a Solid Film. *Phys. Rev. Lett.* **2006,** 96, (1), 017404/1-017404/4.

150. Huang, S.-P.; Jen, T.-H.; Chen, Y.-C.; Hsiao, A.-E.; Yin, S.-H.; Chen, H.-Y.; Chen, S.-A., Effective Shielding of Triplet Energy Transfer to Conjugated Polymer by Its Dense Side Chains from Phosphor Dopant for Highly Efficient Electrophosphorescence. *J. Am. Chem. Soc.* **2008,** 130, (14), 4699-4707.

151. Holzer, W.; Penzkofer, A.; Tsuboi, T., Absorption and emission spectroscopic characterization of Ir(ppy)3. *Chem. Phys.* **2004,** 308, (1-2), 93-102.

152. Kawamura, Y.; Goushi, K.; Brooks, J.; Brown, J. J.; Sasabe, H.; Adachi, C., 100% phosphorescence quantum efficiency of Ir(III) complexes in organic semiconductor films. *Appl. Phys. Lett.* **2005,** 86, (7), 071104/1-071104/3.

153. Barrios, A. M.; Craik, C. S., Scanning the prime-Site substrate specificity of proteolytic enzymes: A novel assay based on ligand-Enhanced lanthanide ion fluorescence. *Bioorg. Med. Chem. Lett.* **2002,** 12, (24), 3619-3623.

154. Beeby, A.; Botchway, S. W.; Clarkson, I. M.; Faulkner, S.; Parker, A. W.; Parker, D.; Williams, J. A. G., Luminescence imaging microscopy and lifetime mapping using kinetically stable lanthanide(III) complexes. *J. Photochem. Photobiol., B* **2000,** 57, (2-3), 83-89.

155. Frias, J. C.; Bobba, G.; Cann, M. J.; Hutchison, C. J.; Parker, D., Luminescent nonacoordinate cationic lanthanide complexes as potential cellular imaging and reactive probes. *Org. Biomol. Chem.* **2003,** 1, (6), 905-907.

156. Karvinen, J.; Hurskainen, P.; Gopalakrishnan, S.; Burns, D.; Warrior, U.; Hemmila, I., Homogeneous time-resolved fluorescence quenching assay (LANCE) for caspase-3. *J. Biomol. Screening* **2002,** 7, (3), 223-231.

157. Lin, Z.; Wu, M.; Schaeferling, M.; Wolfbeis, O. S., Fluorescent imaging of citrate and other intermediates in the citric acid cycle. *Angew. Chem., Int. Ed.* **2004,** 43, (13), 1735-1738.

158. Matsumoto, K.; Nojima, T.; Sano, H.; Majima, K., Fluorescent lanthanide chelates for biological systems. *Macromol. Symp.* **2002,** 186, (IUPAC 9th International Symposium on Macromolecule-Metal Complexes, 2001), 117-121.

159. Preaudat, M.; Ouled-Diaf, J.; Alpha-Bazin, B.; Mathis, G.; Mitsugi, T.; Aono, Y.; Takahashi, K.; Takemoto, H., A homogeneous caspase-3 activity assay using HTRF technology. *J. Biomol. Screening* **2002,** 7, (3), 267-274.

160. Vereb, G.; Jares-Erijman, E.; Selvin, P. R.; Jovin, T. M., Temporally and spectrally resolved imaging microscopy of lanthanide chelates. *Biophys. J.* **1998,** 74, (5), 2210-2222.

161. Leonard, J. P.; Nolan, C. B.; Stomeo, F.; Gunnlaugsson, T., Photochemistry and photophysics of coordination compounds: lanthanides. *Top. Curr. Chem.* **2007,** 281, (Photochemistry and Photophysics of Coordination Compounds II), 1-43.

162. Bobba, G.; Frias, J. C.; Parker, D., Highly emissive, nine-coordinate enantiopure lanthanide complexes incorporating tetraazatriphenylenes as probes for DNA. *Chem. Commun.* **2002**, (8), 890-891.

163. Chen, F.-F.; Bian, Z.-Q.; Lou, B.; Ma, E.; Liu, Z.-W.; Nie, D.-B.; Chen, Z.-Q.; Bian, J.; Chen, Z.-N.; Huang, C.-H., Sensitised near-infrared emission from lanthanides using an iridium complex as a ligand in heteronuclear Ir2Ln arrays. *Dalton Trans.* **2008**, (41), 5577-5583.

164. Dadabhoy, A.; Faulkner, S.; Sammes, P. G., Long wavelength sensitizers for europium(III) luminescence based on acridone derivatives. *J. Chem. Soc., Perkin Trans. 2 2* **2002**, (2), 348-357.

165. Hebbink, G. A.; Grave, L.; Woldering, L. A.; Reinhoudt, D. N.; van Veggel, F. C. J. M., Unexpected Sensitization Efficiency of the Near-Infrared Nd3+, Er3+, and Yb3+ Emission by Fluorescein Compared to Eosin and Erythrosin. *J. Phys. Chem. A* **2003,** 107, (14), 2483-2491.

166. Latva, M.; Takalo, H.; Mukkala, V.-M.; Matachescu, C.; Rodriguez-Ubis, J. C.; Kankare, J., Correlation between the lowest triplet state energy level of the ligand and lanthanide(III) luminescence quantum yield. *J. Lumin.* **1997,** 75, (2), 149-169.

167. Parker, D.; Dickins, R. S.; Puschmann, H.; Crossland, C.; Howard, J. A. K., Being Excited by Lanthanide Coordination Complexes: Aqua Species, Chirality, Excited-State Chemistry, and Exchange Dynamics. *Chem. Rev.* **2002,** 102, (6), 1977-2010.

168. Pope, S. J. A., Dual-emissive complexes: Visible and near-infrared luminescence from bis-pyrenyl lanthanide(III) complexes. *Polyhedron* **2007,** 26, (17), 4818-4824.

169. Quici, S.; Marzanni, G.; Cavazzini, M.; Anelli, P. L.; Botta, M.; Gianolio, E.; Accorsi, G.; Armaroli, N.; Barigelletti, F., Highly Luminescent Eu3+ and Tb3+ Macrocyclic Complexes Bearing an Appended Phenanthroline Chromophore. *Inorg. Chem.* **2002,** 41, (10), 2777-2784.

170. Samuel, A. P. S.; Xu, J.; Raymond, K. N., Predicting Efficient Antenna Ligands for Tb(III) Emission. *Inorg. Chem.* **2009,** 48, (2), 687-698.

171. Zhang, J.; Badger, P. D.; Geib, S. J.; Petoud, S., Sensitization of near-infrared-emitting lanthanide cations in solution by tropolonate ligands. *Angew. Chem., Int. Ed.* **2005,** 44, (17), 2508-2512.

172. Parker, D., Luminescent lanthanide sensors for pH, pO2 and selected anions. *Coord. Chem. Rev.* **2000,** 205, 109-130.

173. Wing-Wah Yam, V.; Kam-Wing Lo, K., Recent advances in utilization of transition metal complexes and lanthanides as diagnostic tools. *Coord. Chem. Rev.* **1999,** 184, 157-240.

174. Gunnlaugsson, T.; Leonard, J. P., Responsive lanthanide luminescent cyclen complexes: from switching/sensing to supramolecular architectures. *Chem. Commun.* **2005**, (25), 3114-3131.

175. Parker, D.; Williams, J. A. G., Responsive luminescent lanthanide complexes. *Met. Ions Biol. Syst.* **2003,** 40, (Lanthanides and Their Interrelations with Biosystems), 233-280.

176. Gunnlaugsson, T.; Glynn, M.; Tocci, G. M.; Kruger, P. E.; Pfeffer, F. M., Anion recognition and sensing in organic and aqueous media using luminescent and colorimetric sensors. *Coord. Chem. Rev.* **2006,** 250, (23+24), 3094-3117.

177. Pandya, S.; Yu, J.; Parker, D., Engineering emissive europium and terbium complexes for molecular imaging and sensing. *Dalton Trans.* **2006**, (23), 2757-2766.

178. Gunnlaugsson, T.; Stomeo, F., Recent advances in the formation of luminescent lanthanide architectures and self-assemblies from structurally defined ligands. *Org. Biomol. Chem.* **2007,** 5, (13), 1999-2009.

179. Masaki, M. E.; Paul, D.; Nakamura, R.; Kataoka, Y.; Shinoda, S.; Tsukube, H., Chiral tripode approach toward multiple anion sensing with lanthanide complexes. *Tetrahedron* **2009,** 65, (12), 2525-2530.

180. Plush, S. E.; Gunnlaugsson, T., Solution studies of trimetallic lanthanide luminescent anion sensors: towards ratiometric sensing using an internal reference channel. *Dalton Trans.* **2008**, (29), 3801-3804.

181. Kataoka, Y.; Paul, D.; Miyake, H.; Yaita, T.; Miyoshi, E.; Mori, H.; Tsukamoto, S.; Tatewaki, H.; Shinoda, S.; Tsukube, H., Experimental and theoretical approaches toward anion-responsive tripod-lanthanide complexes: mixed-donor ligand effects on lanthanide complexation and luminescence sensing profiles. *Chem.--Eur. J.* **2008,** 14, (17), 5258-5266.

182. Massue, J.; Quinn, S. J.; Gunnlaugsson, T., Lanthanide luminescent displacement assays: the sensing of phosphate anions using Eu(III)-cyclen-conjugated gold nanoparticles in aqueous solution. *J. Am. Chem. Soc.* **2008,** 130, (22), 6900-6901.

183. dos Santos, C. M. G.; Fernandez, P. B.; Plush, S. E.; Leonard, J. P.; Gunnlaugsson, T., Lanthanide luminescent anion sensing: Evidence of multiple anion recognition through hydrogen bonding and metal ion coordination. *Chem. Commun.* **2007**, (32), 3389-3391.

184. Leonard, J. P.; dos Santos, C. M. G.; Plush, S. E.; McCabe, T.; Gunnlaugsson, T., pH driven self-assembly of a ternary lanthanide luminescence complex: the sensing of anions using a beta -diketonate-Eu(III) displacement assay. *Chem. Commun.* **2007**, (2), 129-131.

185. Tsukube, H.; Onimaru, A.; Shinoda, S., Naked eye detection of F- anion with luminescent europium complexes. *Chem. Sens.* **2004,** 20, (Suppl. B), 482-483.

186. Mahajan, R. K.; Kaur, I.; Kaur, R.; Uchida, S.; Onimaru, A.; Shinoda, S.; Tsukube, H., Anion receptor functions of lanthanide tris(beta -diketonate) complexes: naked eye detection and ion-selective electrode determination of Cl- anion. *Chem. Commun.* **2003**, (17), 2238-2239.

187. Montalti, M.; Prodi, L.; Zaccheroni, N.; Charbonniere, L.; Douce, L.; Ziessel, R., A Luminescent Anion Sensor Based on a Europium Hybrid Complex. *J. Am. Chem. Soc.* **2001,** 123, (50), 12694-12695.

188. de Silva, A. P.; Gunaratne, H. Q. N.; Rice, T. E., Proton-controlled switching of luminescence in lanthanide complexes in aqueous solution: pH sensors based on long-lived emission. *Angew. Chem., Int. Ed. Engl.* **1996,** 35, (18), 2116-2118.

189. McCoy, C. P.; Stomeo, F.; Plush, S. E.; Gunnlaugsson, T., Soft Matter pH Sensing: From Luminescent Lanthanide pH Switches in Solution to Sensing in Hydrogels. *Chem. Mater.* **2006,** 18, (18), 4336-4343.

190. Parker, D.; Senanayake, K.; Williams, J. A. G., Luminescent chemosensors for pH, halide and hydroxide ions based on kinetically stable, macrocyclic europium-phenanthridinium conjugates. *Chem. Commun.* **1997**, (18), 1777-1778.

191. Tsukube, H.; Yano, K.; Ishida, A.; Shinoda, S., Lanthanide complex strategy for detection and separation of histidine-tagged proteins. *Chem. Lett.* **2007,** 36, (4), 554-555.

192. Gunnlaugsson, T.; Leonard, J. P.; Senechal, K.; Harte, A. J., pH Responsive Eu(III)-Phenanthroline Supramolecular Conjugate: Novel "Off-On-Off" Luminescent Signaling in the Physiological pH Range. *J. Am. Chem. Soc.* **2003,** 125, (40), 12062-12063.

193. Song, X.-Q.; Dou, W.; Liu, W.-S.; Yao, J.-N.; Guo, Y.-L.; Tang, X.-L., Design, synthesis, crystal structure and photophysical studies of an emissive, terbium based sensor for zinc. *Inorg. Chem. Commun.* **2007,** 10, (9), 1058-1062.

194. Hanaoka, K.; Kikuchi, K.; Kojima, H.; Urano, Y.; Nagano, T., Development of a Zinc Ion-Selective Luminescent Lanthanide Chemosensor for Biological Applications. *J. Am. Chem. Soc.* **2004,** 126, (39), 12470-12476.

195. Gunnlaugsson, T.; Leonard, J. P.; Senechal, K.; Harte, A. J., Eu(III)-cyclen-phen conjugate as a luminescent copper sensor: the formation of mixed polymetallic macrocyclic complexes in water. *Chem. Commun.* **2004**, (7), 782-783.

196. Pope, S. J. A.; Laye, R. H., Design, synthesis and photophysical studies of an emissive, europium based, sensor for zinc. *Dalton Trans.* **2006**, (25), 3108-3113.

197. Oxley, D. S.; Walters, R. W.; Copenhafer, J. E.; Meyer, T. Y.; Petoud, S.; Edenborn, H. M., Mono- and Terfluorene Oligomers as Versatile Sensitizers for the Luminescent Eu3+ Cation. *Inorg. Chem.* **2009,** 48, (14), 6332-6334.

198. Petoud, S.; Cohen, S. M.; Buenzli, J.-C. G.; Raymond, K. N., Stable Lanthanide Luminescence Agents Highly Emissive in Aqueous Solution: Multidentate 2-Hydroxyisophthalamide Complexes of Sm3+, Eu3+, Tb3+, Dy3+. *J. Am. Chem. Soc.* **2003,** 125, (44), 13324-13325.

199. Parker, D., Excitement in f block: structure, dynamics and function of nine-coordinate chiral lanthanide complexes in aqueous media. *Chem. Soc. Rev.* **2004,** 33, (3), 156-165.

200. Beeby, A.; Faulkner, S.; Parker, D.; Williams, J. A. G., Sensitized luminescence from phenanthridine appended lanthanide complexes: analysis of triplet mediated energy transfer processes in terbium, europium and neodymium complexes. *J. Chem. Soc., Perkin Trans. 2* **2001**, (8), 1268-1273.

201. Liu, B.; Gaylord, B. S.; Wang, S.; Bazan, G. C., Effect of Chromophore-Charge Distance on the Energy Transfer Properties of Water-Soluble Conjugated Oligomers. *J. Am. Chem. Soc.* **2003,** 125, (22), 6705-6714.

202. Wilkinson, A. J.; Maffeo, D.; Beeby, A.; Foster, C. E.; Williams, J. A. G., Sensitization of europium(III) luminescence by benzophenone-containing ligands: regioisomers, rearrangements and chelate ring size, and their influence on quantum yields. *Inorg. Chem.* **2007,** 46, (22), 9438-9449.